SAPIENZA
UNIVERSITÀ DI ROMA

Sedimentary Petrography and Sequence Stratigraphy: the relationships between compositional signatures and sequence-stratigraphic framework of siliciclastic successions

Daniel Tentori

PhD Thesis in Earth Sciences

Academic Year 2018/2019

Cycle 32 - SSD GEO /02

Supervisor:

Prof. Salvatore Milli

Dipartimento di Scienze della Terra

Sapienza, Università di Roma

P.le Aldo Moro 5, 00185, Roma, Italia

Co-Supervisor:

Prof. Kathleen Marsaglia

Department of Geological Sciences

California State University, Northridge

18111 Nordhoff Street, Northridge, CA 91330

Table of Contents

PREFACE

The body of this thesis work is structured in three Chapters presented in the form of three manuscripts. Petrographic data collection, interpretation and manuscripts writing are my own work. The thesis greatly benefited from continuing discussion with co-authors, collaborators, and reviewers. **Chapter 2** and **3** were published on the Journal of Sedimentary Research whereas **Chapter 4** is currently subject to internal review. Here is a references list of the papers:

Tentori, D., *Marsaglia, K., Milli, S., 2016, Sand compositional changes as a support for sequence-stratigraphic interpretation: the middle upper Pleistocene to Holocene deposits of the Roman Basin (Rome, Italy). Journal of Sedimentary Research, v. 86, p. 1208-1227.*

Tentori, D., *Milli, S., Marsaglia, K., 2018, A source-to-sink compositional model of a present highstand: an example in the low-rank Tiber depositional sequence (Latium Tyrrhenian margin, Italy), Journal of Sedimentary Research, v. 88, p. 1-22.*

Tentori, D., *Amorosi, A., Milli, S., Marsaglia, K., 2019, Sand variability in the modern Po River system and sediment dispersal pathways in the Po coastal plain since the Last Glacial Maximum, in prep.*

ABSTRACT

The use of petrographic procedures to characterize compositional variations within sedimentary successions and across stratigraphic unconformities has been successfully applied in different provenance studies. However, the use of variation in sand composition to support sequence-stratigraphic interpretation is still in an early stage and requires more case studies to test its effectiveness. Sediment composition and texture are controlled by the same allogenic (e.g., eustatic, climatic and tectonic changes) and autogenic (e.g., sediment transport, hydraulic sorting and post depositional processes) factors that govern the sequence-stratigraphic architecture of a sedimentary succession. Allogenic processes act on a long temporal scale and controls the rate and composition of sediment supply, basin physiography, and accommodation space. Autogenic processes occur over shorter temporal scales but may have considerable influence on local sediment supply and have low correlation potential across the sedimentary basin.

This work investigates how sediment composition varies within the systems tracts forming depositional sequences in continental and marine siliciclastic sedimentary succession in response to autogenic and allogenic forcing. For this purpose, I examined the sand variability along the modern Tevere and Po River systems and within their associated sedimentary successions for which the sequence-stratigraphic framework was already defined. Compositional trends within high-rank and low-rank depositional sequences of the Pleistocene to Holocene Roman and Po basins suggests that major provenance changes occurred in response to allogenic processes that forced major paleogeographic rearrangement associated with cyclic changes in relative-sea level. Subtle and local petrographic changes with low correlation potential across the sedimentary basin reflect instead the sedimentary processes operating in each depositional environment and their understanding is possible through comparison with modern detrital signatures.

The Middle Pleistocene to Holocene succession of the Roman Basin records a close interaction among tectonic uplift, volcanism, climate, and glacio-eustasy. Such interaction is reflected in a complex stratal pattern and stratigraphic architecture where high-rank and low-rank depositional sequences are developed and where qualitative and quantitative changes in sand composition are recorded across the systems tracts of the higher-rank Ponte Galeria Depositional Sequence (PGS). Tectonic evolution in the Tiber River drainage basin following Pleistocene volcanic activity played a major role controlling provenance and magnitude of erosion and stream-network reorganization in the Tiber drainage basin, which in turn is reflected in sand composition. Relative sea-level changes reflect local tectonic effects (regional uplift and volcanism) which overrode glacio-eustatic sea-level

fluctuations and controlled the overall stacking pattern and composition of the low-rank sequences forming the PGS. In the modern Tiber River system, sand compositional trends reflect provenance mixing, anthropic intervention, and the effects of local autogenic factors in continental to marine depositional environments. Petrofacies trends are linked, and intimately controlled by physical processes (e.g., hydraulic sorting and hydrodynamic fractionation by grain-size) and sedimentary mixing within each depositional environment.

Provenance changes within the Upper Pleistocene to Holocene Po coastal plain deposits reflect the paleogeographic reorganization during the last glacial-interglacial cycle (~120 kyr). Compositional signatures of sand deposits record the effect of sea-level transgression in controlling sediment generation and dispersal paths throughout the Po low-rank sequence development. The transgressive surface, which separates the lowstand from the transgressive system tracts marks a major change in lithic fragment composition that documents a major paleodrainage rearrangement and reflects the abrupt transition from an alluvial to an estuarine depositional system. In contrast, no significant change at the maximum flooding surface is captured in the sand petrographic record. Secondary controls on sand composition include downstream hydrodynamic sorting by size and sedimentary mixing by alongshore currents.

Stratigraphic units deposited during specific phases of relative sea-level cycles (e.g., systems tracts) are associated with petrofacies that reflect paleogeographic rearrangement and changes in sediment dispersal paths. Although compositional changes across key boundaries surfaces and within depositional sequences help detecting major paleogeographic changes, the main controls mechanisms that govern changes in relative sea-level cannot always be disentangled when looking at sediment petrography alone. In particular, the superposition of multiple forcing mechanisms (e.g., tectonic vs. volcanic activity and tectonism vs. eustatic fluctuations) makes the interpretation of detrital modes very challenging. The analysis of compositional trends within the Po and Tevere sedimentary successions show that when key boundaries surfaces are not associated with major compositional changes (e.g. variability across low-rank sequences) it is very difficult to disentangle the superposed effects of intrinsic and local factors that add to the time-dependent forcing mechanism. The stacking pattern of low-rank and high-frequency late Quaternary sequences record short-term eustatic cyclicity and results in a vertical succession of facies which in turn controls the compositional trends of the deposits.

RIASSUNTO

L'uso di procedure petrografiche per caratterizzare le variazioni composizionali all'interno di successioni sedimentarie e in corrispondenza di discontinuità stratigrafiche è stato applicato con successo in diversi studi di provenienza. Tuttavia, l'analisi delle variazioni composizionali dei sedimenti come supporto all'interpretazione stratigrafico-sequenziale di una successione sedimentaria è ancora in una fase iniziale e richiede ulteriori casi di studio per verificarne l'efficacia. La composizione e la tessitura dei sedimenti sono controllate dagli stessi fattori allogenici (ad es. fluttuazioni eustatiche, climatiche e tettoniche) e autogenici (ad es. trasporto di sedimenti, selezione idraulica e processi post-deposizionali) che governano l'architettura stratigrafico-sequenziale di una successione sedimentaria. I processi allogenici agiscono su scale temporali prolungate e controllano i tassi di apporto sedimentario, la composizione di sedimenti, la fisiografia del bacino e lo spazio di accodamento. I processi autogenici si verificano su scale temporali più brevi ma possono avere una notevole influenza sulle variazioni locali dell'apporto sedimentario che si riflettono in variazioni composizionali con basso potenziale di correlazione all'interno del bacino sedimentario.

Questo lavoro indaga sulle modificazioni composizionali dei sedimenti all'interno dei systems tracts di sequenze deposizionali sviluppate in depositi terrigeni continentali e marini al fine di investigare gli effetti delle forzanti autogeniche e allogeniche sulla distribuzione e sulla composizione del sedimento. A tale scopo, è stata esaminata la variabilità composizionale, sia delle sabbie attuali nei sistemi fluviali del Tevere e del Po, sia dei loro depositi tardo-pleistocenici e olocenici per i quali è ben conosciuta l'architettura stratigrafico-sequenziale. Nel caso del Tevere sono stati anche esaminate i depositi delle unità più antiche le quali, complessivamente, definiscono quella che in letteratura è conosciuta come Sequenza Deposizionale di Ponte Galeria. I trend composizionali più evidenti si registrano nei passaggi tra i system tracts delle sequenze di alto e basso rango; essi riflettono cambiamenti di provenienza in risposta a cambiamenti relativi del livello del mare regolate per lo più da forzanti allogeniche. L'analisi delle variazioni petrografiche con più basso potenziale di correlazione all'interno di questi bacini sedimentario riflettono, al contrario, processi sedimentari locali che operano nei diversi ambienti deposizionali e la loro interpretazione è resa possibile dal confronto con le mode detritiche dei sistemi attuali.

La successione Medio Pleistocenica-Olocenica nel Bacino Romano rappresenta il prodotto di una stretta interazione tra tettonica, attività vulcanica, e fluttuazioni glacio-eustatiche. Tale interazione

si riflette in un modello stratificato complesso in cui vengono sviluppate sequenze deposizionali di alto (durata circa 1 milione di anni) e di basso rango (con durata da 30 a 120 ky), e dove vengono registrati cambiamenti qualitativi e quantitativi nella composizione dei sedimenti. L'evoluzione tettonica e vulcanica Pleistocenica del bacino idrografico del fiume Tevere ha svolto un ruolo importante nel controllare la riorganizzazione idrografica e la provenienza dei sedimenti, che a sua volta si riflette nella composizione degli stessi. Questi processi si sono sommati alle fluttuazioni glacio-eustatiche del livello del mare e insieme hanno controllato l'architettura stratigrafica e la composizione delle sabbie nella sequenza deposizionale di alto rango di Ponte Galeria. Nel sistema attuale del fiume Tevere, i trend composizionali delle sabbie registrano l'interazione tra cambiamenti di provenienza, attività antropica e gli effetti dei fattori autogenici locali negli ambienti deposizionali continentali e marini. Le petrofacies sono controllate da processi fisici (es. abrasione meccanica durante trasporto eolico, selezione idraulica e frazionamento idrodinamico per granulometria) e di mixing sedimentario all'interno di ciascun ambiente deposizionale.

Le variazioni di provenienza nei depositi del Pleistocene Superiore-Olocene del bacino del Po rispecchiano la riorganizzazione paleogeografica dell'area durante l'ultimo ciclo glaciale-interglaciale (~120 kyr) e, più in particolare durante la risalita olocenica del livello marino. In particolare, la superficie di trasgressione che separa il lowstand dal transgressive system tracts della sequenza di basso rango del Po registra un grande cambiamento nella composizione dei frammenti litici che riflettono una variazione nella direzione di dispersione di sedimenti durante la transizione da un sistema deposizionale da alluvionale a estuario. Al contrario, nessun cambiamento significativo viene registrato al di sopra della superficie di massima ingressione marina (maximum flooding surface) dal momento che non si registrano particolari cambiamenti di provenienza. I controlli secondari sulla composizione della sabbia includono la selezione idrodinamica per granulometria e il mixing sedimentario lungo la costa.

Sebbene le unità stratigrafiche deposte durante specifiche fasi di cicli relativi del livello del mare (e.g., systems tracts) sono spesso associate a petrofacies che riflettono cambiamenti paleogeografici e di provenienza dei sedimenti, i principali meccanismi di controllo autogenici e allogenici non sempre possono essere discriminati con la sola petrografia del sedimentario. In particolare, la sovrapposizione di molteplici forzanti (es., attività tettonica e vulcanica e attività tettonica e fluttuazioni eustatiche) rendono l'interpretazione delle mode detritiche molto complessa.

L'analisi dei trend composizionali all'interno delle successioni sedimentarie del Po e del Tevere mostra che, quando le superfici di discontinuità stratigrafica non sono associate a grandi

cambiamenti composizionali (ad es. variabilità composizionale tra sequenze di basso rango), gli effetti dei fattori autogenici locali e di quelli allogenici possono risultare difficili da essere distinti. Le sequenze tardo Quaternarie di basso rango registrano, infatti, variazioni eustatiche ad alta-frequenza che producono una elevata variabilità di facies che si traduce in variazioni composizionali con basso potenziale di correlazione e controllate dai processi che agiscono all'interno degli ambienti deposizionali.

CHAPTER 1: INTRODUCTION

1.1 Sedimentary petrography and sequence-stratigraphy

The classical sedimentary petrology approach has been largely applied to provenance studies for the reconstruction of ancient tectonic settings of source terranes (Dickinson, 1985) and to characterize compositional variations within the sedimentary succession and across stratigraphic unconformities in response to major paleogeographic reorganization. Although several studies indicate that compositional changes may occur across key-boundaries surface of different hierarchy and sequence stratigraphic significance (Garzanti, 1991; Ito, 1991; Amorosi, 1995; Zuffa et al., 1995; Marchesini et al., 2000; Arribas et al., 2003; Lawton et al., 2003; Basu et al., 2009; Seyrafian and Toraby, 2009; Garzanti et al. 2011), the use of variation in sand composition as a tool in sequence-stratigraphy is still in an early stage and requires more case studies to test its effectiveness (Zuffa et al., 1995; Amorosi and Zuffa, 2011). A multi-method approach that combine sand petrography and sequence stratigraphy can be employed to facilitate paleogeographic reconstructions and investigate the forcing mechanism regulating sediment supply and dispersal paths. The analysis of compositional trends can be used to define provenance changes and better characterize facies associations that develop within chronostratigraphic units such as the depositional sequences. Detecting compositional changes could help characterize the systems tracts of a depositional sequence and the forcing mechanisms regulating the type and amount of sediment supply in response to base-level fluctuations such as tectonic, eustatic and climatic factors (Amorosi and Zuffa, 2011). Thus, qualitative and quantitative sand compositional changes may support the sequence-stratigraphic methodology, which is by definition, based on the pragmatic observation of stratal stacking patterns, irrespective of the forcing mechanism which controls the stratigraphic architecture (Catuneanu and Zecchin, 2016). The sequence stratigraphic approach, in fact, mainly focusses on basin-fill geometries with the aim of predicting preserved elements away from the control points or with sparse data (Helland-Hansen et al., 2016) and is not necessarily linked, in the first instance, to the forcing mechanism regulating the sedimentary succession development (Catuneanu and Zecchin, 2016).

Several processes control the compositional variability and the stratigraphic architecture of arenite successions and exert a different influence over different timescales. Time-dependent processes such as long-period tectonic activity and climate fluctuations, may cause sediment compositional modification within high rank depositional sequences (millions of years) and across

high-rank surfaces (Zuffa et al. 1995; Cibin et al., 2001; Marchesini et al. 2000; Garzanti et al., 2003), whereas rapid changes in sources, sedimentary mixing, and hydraulic sorting within singles depositional systems, appear to more efficiently control sediment composition within low rank depositional sequences (hundreds of thousands years) and low-rank stratigraphic surfaces (Amorosi and Zuffa, 2011). Petrofacies changes are expected to appear across sequence and systems tract boundaries but they may not be necessarily produced. Moreover, different compositional changes across the same sequence boundary or transitional and gradual variation in sediment composition can occur (Amorosi and Zuffa, 2011). In order to disentangle the relationship among factors controlling basin sedimentation, identification of compositional (e.g., carbonate vs siliciclastic grains), spatial (e.g., intrabasinal vs extrabasinal grains) and time (coeval and non-coeval grains) relationships among detrital grains is crucial (Zuffa, 1980, 1985, 1987, 1991; Zuffa et al., 1995; Critelli et al. 2007).

The study of the interaction between allogenic and autogenic factors, which in turn determines compositional variations in the depositional sequences, can be better assessed within stratigraphic succession for which detailed sedimentological observations of the depositional environment and a chronologic control of facies architecture are available. In this regard, the sequence stratigraphic architecture is very well displayed in the Quaternary successions of continental margins were the relative sea-level cycles under the influence of orbitally driven glacial-interglacial climate change are well constrained (Allen, 2017). Quaternary successions represent ideal case studies and offer well-preserved archives where many variables that contribute to define the ultimate sedimentary record, such as sea-level, climate and tectonic changes, can be separately analyzed. In the Quaternary the sources for sediments, their geology, extension and relative positions are known, thus each compositional change can be confidently traduced in a certain type of drainage basin reorganization. This is not easy or possible, usually, for ancient cases of study. Thus, sand petrography applied to high-resolution sequence-stratigraphy of Quaternary sedimentary succession provides the opportunity to investigate the relative influence of the forcing mechanism that regulates both the stratigraphic architecture and sand compositional changes of siliciclastic sedimentary succession.

The complexity of investigating the ancient record may be facilitated by exploring the modern counterparts where each control on sediment composition can be identified and quantified. By comparison with the modern we can correct for the chemical and physical processes operating during the entire sedimentary cycle and avoid the superimposed effects of post-depositional

changes. Several sedimentological factors might, in fact, influence sediment compositional and textural properties during the entire sedimentary cycle from source-to-sink and distort the primary signals imparted by source-rock lithologies (Ibbeken and Schleyer, 1991; Johnsson, 1993; Weltje, 2012; Garzanti, 2015). The understanding of sedimentary processes affecting the sediment-routing system from source-to-sink, and the investigation of the driving mechanisms operating in the lithosphere, hydrosphere and atmosphere which regulate sediment production and transport and the final deposition in marginal marine and deep water systems, can be crucial to prepare for future scenarios in the context of the evolving Earth' climate (Walsh, et al. 2016; Garzanti, 2016).

1.2 Sediment compositional changes from a source-to-sink perspective

The source-to-sink approach allow to investigate processes controlling sediment generation, transport and temporary storage in terrestrial catchments and ultimate deposition in deep-sea sink (Covault et al., 2013). The delivery of sediment and its final, long-term deposition is regulated by variations in topography, source rocks and climate which are ultimately controlled by plate tectonics and earth's astronomic cycles (e.g., Milankovitch cycles) (Allen 2008). Provenance studies and sediment composition may provide valuable insights on where the sediment originated and how it was modified into the sediment routing, during transport and intermediate storage. As opposed to common mass balance approaches which treat sediment a simple volume of material, in sedimentary petrology several parameters can be used to evaluate qualitatively and quantitatively sourceland composition providing a powerful way of linking sources to sinks and capture sediment compositional and textural transformations that take place during weathering and transport (Di Giulio, 1999; Garzanti, 2016).

Catchments physiography, topographic reliefs, drainage area extent, and source rock lithology constitute the primary controls for sediment production in the hinterland and are intimately controlled by tectonic uplift and climate changes. Provenance analyses defines the contribution of parent rocks from detrital material composition and assess the paleogeology of the source areas (Basu, 1985; Di Giulio, 1999; Di Giulio et al., 2003) providing crucial information for source-to-sink reconstructions (Garzanti, 2016). The key information lies in the rock fragments compositions, but other indicators could help predicting the properties of sediment entering the routing system (e.g., Metamorphic Index, Garzanti and Vezzoli 2003; Sand Generation Index, Palomares et al., 1993; Vezzoli et al. 2004). Textural and compositional sediment modification are also known to be related to climate and weathering which may contribute to modify parent material at the beginning of a

sedimentary cycle (Basu, 1985). In fact, while bedrock composition is primarily controlled by plate tectonics, the genesis of sediment begins with regolith or soil formation on bedrocks and depend on rainfall rates, temperature and hill slope angles.

As sediment is transported and temporary stored in the transfer zones it undergoes a series of physical and chemical modifications which can be recorded by sediment compositional and textural changes. The primary signal imparted by source rock lithologies is modified in terms of sediment dilution (e.g., provenance mixing), weathering, mechanical breakdown, and hydraulic sorting (Young et al., 1975; Nesbitt and Young 1996; Johnsson and Made, 1990; Garzanti et al. 2013; Garzanti, 2016) and new sediment can be produced from remobilization of temporary stored material and further modified by reworking during transport (Romans et al. 2016). All these processes are intimately interlinked, and their understanding may provide valuable information about climate, vegetation, and fluvial system geometry controls on sediment flux (Johnsson, 1993; McBride and Picard, 1987; Weltje, 2012). Investigation of the physical and chemical modification occurring during the entire sedimentary cycle may restore noise and lags occurring before deposition (e.g., environmental bias) and provide information about local factors which overprint the provenance signals and contribute to control sediment flux (Romans et al. 2016).

Just like catchments and transfer zones, the position, extent and durability of accumulation zones, can vary significantly from system to system and is strictly dependent to basin physiography (Romans et al., 2016). Sediment sinks may include continental settings dominated by elevated subsidence (alluvial and coastal plains), or marginal marine (e.g., shorelines and deltas) and deep-water settings, depending on the temporal and spatial scale of observation. Along shorelines and delta fronts, waves, tides and longshore currents not only control the morphology and stratigraphic architecture of coastal bodies but also modify sediment composition and texture (Garzanti et al. 2014, 2015). Hydrodynamic fractionation and hydraulic sorting affect sediment composition and distribution along the depositional profile through suspension and size-density sorting (Garzanti et al. 2009). In coastal dunes settings, eolian reworking modify rounding of softer grains (e.g., carbonate and volcanic lithic fragments) (Resentini et al. 2018; Morrone et al. 2017). In marine and deepwater basins, with progressive decrease of riverine influence, siliciclastic units are likely associated with carbonate-rich layers and intrabasinal allochems. Here, spatial and temporal relationship of terrigenous sediment can be deciphered classifying grains into carbonate versus non carbonate and coeval versus non coeval (Zuffa 1980, 1985, 1987, 1991; Zuffa et al., 1995). Post depositional diagenetic dissolution and grain cementation can be also recorded by sediment

composition and texture. Precipitation of cement and authigenic material can considerably influence the mechanical and chemical properties of sediment during burial. Diagenetic effects on sediment composition and texture not only influence reservoir quality but also reduce predictability and provenance information in ancient sedimentary successions (McBride, 1985).

Several parameters can slip in large scale observation during depositional budgets computations, which are usually performed by reconstructing the stratigraphic architecture through seismic-reflection and well data. Sedimentary petrography may provide valuable insights on the control mechanisms that govern the ultimate properties of the final deposits such as tectonic setting, climate, transport history, final depositional environment and burial history. The best way to get a comprehensive understanding of the sediment routing system is to apply a wide range of methodologies and multiscale observations, including sedimentary petrography.

1.3 Objectives and thesis structure

The thesis goal is to investigate the relationships between sand compositional variability and the sequence-stratigraphic architecture of siliciclastic sedimentary succession and define the main forcing mechanisms regulating sediment generation and their dispersion within depositional sequences of different hierarchical order. Two case studies were selected to test the potential of sedimentary petrography in sequence stratigraphy: the Tevere and Po river systems and their associated Pleistocene and Holocene sedimentary successions. The study of the detrital trends along the two modern river systems allowed to create a model that constrains the relationships between provenance, facies-related compositional trend, and sequence stratigraphic architecture under the influence of allogenic and autogenic processes. By comparison with the modern river systems it was possible to decipher the superposed effects of weathering, recycling and hydraulic-sorting effects and increase the opportunity to make correct provenance diagnoses and speculate on the forcing mechanism regulating sediment dispersal changes through time.

The Tevere and Po river catchments include a high variability of parent rocks lithologies, which are very well defined in terms of ages, petrography and compositions, allowing for a good characterization from source-to-sink. The drainage basin physiography and the modern structural settings in the Po and Tevere river systems reflect the Meso-Cenozoic evolution of the Apennines and Alpine belts and Tertiary and Quaternary volcanism. The Tevere river flows in the back-arc side of the Apennines thrust and along the Tyrrhenian sea margin, which was dominated by Quaternary volcanism and extensional tectonic, whereas the Po river system, flows through the Alpine

retroforeland and Apennine foredeep into the Adriatic Sea, a semi-enclosed basin with a shallow continental shelf.

The two case studies presented in this thesis work not only provided the opportunity to analyze in detail their modern sediment routing system from source to sink, but also to investigate their associated middle Pleistocene to Holocene Roman basin and Late Pleistocene to Holocene Po basin sedimentary successions which are very well characterized in terms of facies architecture and for which the sequence-stratigraphic framework has been clearly defined (Milli et al., 2016; Amorosi et al. 2016). These successions represent valuable case studies to unravel the relationships between compositional changes and stratigraphic architecture and to investigate compositional changes across high- and low-rank stratigraphic surfaces. The sequence-stratigraphic analysis of the Roman and Po basins sedimentary successions revealed that glacio-eustasy exerted a major control on their marginal marine sedimentary successions and that the effects of tectonic forcing (e.g., tectonic uplift/subsidence and volcanism) and intrinsic autogenic factors may have acted differently (Amorosi and Milli, 2001). The definition of detrital compositional trends within the systems tracts of these sedimentary succession are used to investigate the relative contribution of each forcing mechanisms in controlling paleogeographic changes and type and amount of sediment supply and compare how these are differently recorded by their stratal patterns and stratigraphic architecture evolution.

The body of this thesis work is structured in the form of three manuscripts and organized as follows:

In **Chapters 2 and 3,** I examine sediment variability along the modern Tevere system and within its associated Middle Pleistocene to Holocene Roman Basin sedimentary successions whereas in **Chapter 4** data from the Po river system deposits and its associated late Pleistocene to Holocene sedimentary succession are presented and discussed. **Chapter 2** analyzes sediment compositional variability among fluvial, coastal, and deltaic deposits sourced by the paleoTevere river that compose a high-rank stratigraphic unit known in the literature as the Ponte Galeria Sequence (PGS). The latter has been subdivided into twelve low-rank depositional sequences whose stratigraphic relationships is related to the interaction between tectonic uplift of the Latium Tyrrhenian margin and eustatic sea-level changes (Milli 1997; Milli et al. 2008; 2013). **Chapter 3** investigates sand variability of the youngest low-rank sequence, known as the Tiber Depositional Sequence (TDS) (Milli et al., 2016), with particular focus on the modern highstand. **Chapter 4** defines compositional

trend along the modern Po river system and within the Late Pleistocene to Holocene Po depositional sequence and investigate provenance changes in a selected sector of the coastal plain in response to paleogeographic reorganization during the last glacial-interglacial cycle (Amorosi et al., 2016). In **Chapter 5** the main results from the two case studies are compared and analyzed in a more comprehensive approach to investigate the potential application of sedimentary petrography in sequence stratigraphy.

REFERENCES

ALLEN, P.A., 2008, From landscapes into geological history: Nature, v. 451, p. 274.

ALLEN, P.A., 2017, Sediment routing systems: The fate of sediment from source to sink: Cambridge University Press.

AMOROSI, A., 1995, Glaucony and sequence stratigraphy; a conceptual framework of distribution in siliciclastic sequences: Journal of Sedimentary Research, v. 65, p. 419–425.

AMOROSI, A. AND ZUFFA, G.G., 2011, Sand composition changes across key boundaries of siliciclastic and hybrid depositional sequences: Sedimentary Geology, v. 236, p.153-163.

ARRIBAS, J., ALONSO, A., MAS, R., TORTOSA, A., RODAS, M., BARRENECHEA, J.F., ALONSO-AZCÁRATE, J., AND ARTIGAS, R., 2003, Sandstone petrography of continental depositional sequences of an intraplate rift basin: Western Cameros Basin (North Spain): Journal of Sedimentary Research, v. 73, p. 309–327.

AMOROSI, A., MASELLI, V. AND TRINCARDI, F., 2016, Onshore to offshore anatomy of a late Quaternary source-to-sink system (Po Plain–Adriatic Sea, Italy): Earth-Science Reviews, v. 153, p.212-237.

BASU, A., 1985, Influence of climate and relief on compositions of sands released at source areas, *in* Provenance of arenites, Springer, Dordrecht, p. 1-18.

BASU, A., BICKFORD, M.E., PATRANABIS-DEB, S., AND DHANG, P.C., 2009, $^{207}Pb/^{206}Pb$ SHRIMP ages of detrital zircons in the Mesoproterozoic Chhattisgarh Basin, Central India, aid in identifying relative low-stand and high-stand sandstones: Geological Society of America, Annual Meeting, Portland, 18-21 October 2009.

CATUNEANU, O., GALLOWAY, W.E., KENDALL, C.G.S.C., MIALL, A.D., POSAMENTIER, H.W., STRASSER, A. AND TUCKER, M.E., 2011, Sequence stratigraphy: methodology and nomenclature: Newsletters on stratigraphy, v. 44, p.173-245.

CATUNEANU, O., AND ZECCHIN, M., 2016, Unique vs. non-unique stratal geometries: relevance to sequence stratigraphy: Marine and Petroleum Geology, v. 78, p. 184-195.

CIBIN, U., SPADAFORA, E., ZUFFA, G.G., AND CASTELLARIN, A., 2001, Continental collision history from Arenites of Episutural Basins in the northern Apennine, Italy: Geological Society of America Bullettin, v. 113, p. 4-19.

COVAULT, J.A., CRADDOCK, W.H., ROMANS, B.W., FILDANI, A. AND GOSAI, M., 2013, Spatial and temporal variations in landscape evolution: Historic and longer-term sediment flux through global catchments: The Journal of Geology, v. 121, p.35-56.

CRITELLI, S., LE PERA, E., GALLUZZO, F., MILLI, S., MOSCATELLI, M., PERROTTA, S., AND SANTANTONIO, M., 2007, Interpreting siliciclastic–carbonate detrital modes in foreland basin systems: an example from Upper Miocene arenites of the central Apennines, Italy: *in* Arribas, J., Critelli, S., Johnsson, M.J. (Eds.), Sedimentary Provenance and Petrogenesis: Perspectives from Petrography and Geochemistry: Geological Society of America Special Paper, v.420, p. 107–133.

DICKINSON, W.R., 1985, Interpreting provenance relations from detrital modes of sandstones: *in* Provenance of arenites, Springer, Dordrecht, p. 333-361.

DI GIULIO, A., 1999, Mass transfer from the Alps to the Apennines: volumetric constraints in the provenance study of the Macigno–Modino source–basin system, Chattian–Aquitanian, northwestern Italy: Sedimentary Geology, v. 124., p. 69-80.

DI GIULIO A., CERIANI A., GHIA E. AND ZUCCA F., 2003, Composition of modern stream sands derived from sedimentary source rocks in a temperate climate (northern Apennines, Italy): Sedimentary Geology, v. 158, p. 145–161.

GARZANTI, E., 1991, Non-carbonate intrabasinal grains in arenites; their recognition, significance and relationship to eustatic cycles and tectonic setting: Journal of Sedimentary Research, v. 61, p. 959–975.

GARZANTI, E., 2016. From static to dynamic provenance analysis—Sedimentary petrology upgraded: Sedimentary Geology, v. 336, p. 3-13.

GARZANTI, E. AND VEZZOLI, G., 2003, A classification of metamorphic grains in sands based on their composition and grade: Journal of Sedimentary Research, v. 73, p.830-837.

GARZANTI, E., ANDÒ, S., VEZZOLI, G., AND DELL'ERA, D., 2003, From rifted margins to foreland basins: investigating provenance and sediment dispersal across desert Arabia (Oman, U.A.E.): Journal of Sedimentary Research, v. 73, p. 572–588.

GARZANTI, E., ANDÒ, S. AND VEZZOLI, G., 2009, Grain-size dependence of sediment composition and environmental bias in provenance studies: Earth and Planetary Science Letters, v. 277, p.422-432.

GARZANTI, E., VEZZOLI, G. AND ANDÒ, S., 2011, Paleogeographic and paleodrainage changes during Pleistocene glaciations (Po Plain, northern Italy): Earth-Science Reviews, v. 105, p.25-48.

GARZANTI, E., PADOAN, M., ANDÒ, S., RESENTINI, A., VEZZOLI, G., LUSTRINO, M., 2013, Weathering and relative durability of detrital minerals in equatorial climate: sand petrology and geochemistry in the East African Rift: The Journal of Geology, v. 121, p. 547–580.

GARZANTI, E., VERMEESCH, P., ANDÒ, S., LUSTRINO, M., PADOAN, M. AND VEZZOLI, G., 2014, Ultra-long distance littoral transport of Orange sand and provenance of the Skeleton Coast Erg (Namibia): Marine Geology, 357, p.25-36.

GARZANTI, E., ANDÒ, S., PADOAN, M., VEZZOLI, G. AND EL KAMMAR, A., 2015, The modern Nile sediment system: Processes and products: Quaternary Science Reviews, v. 130, p. 9-56.

HELLAND-HANSEN, W., SØMME, T.O., MARTINSEN, O.J., LUNT, I. AND THURMOND, J., 2016, Deciphering Earth's natural hourglasses: perspectives on source-to-sink analysis: Journal of Sedimentary Research, v. 86, p. 1008-1033.

IBBEKEN, H., AND SCHLEYER, R., 1991, Source and Sediment: A Case Study of Provenance and Mass Balance at an Active Plate Margin (Calabria, Southern Italy). Berlin: Springer-Verlag.

ITO, M., 1991, Compositional variation in depositional sequences of the upper part of the Kasuza Group, a middle Pleistocene forearc basin fill in the Boso Peninsula, Japan: Sedimentary Geology, v. 88, p. 219-230.

JOHNSSON, M.J., 1993, The system controlling the composition of clastic sediments, *in* Johnsson, M.J., Basu, A. (Eds.), Processes Controlling the Composition of Clastic Sediments: Geological Sociecty of America Special Paper, v. 284, p. 1–19.

JOHNSSON, M. J., AND MEADE, R. H. 1990, Chemical weathering of fluvial sediments during alluvial storage: the Macuapanim Island point bar, Solimo˜ es River, Brasil: Journal of Sedimentary Petrology, v. 60, p. 827–842.

LAWTON, T.F., POLLOCK, S.L., AND ROBINSON, R.A.J., 2003, Integrating sandstone petrology and nonmarine sequence stratigraphy: application to the Late Cretaceous fluvial systems of Southwestern Utah, U.S.A.: Journal of Sedimentary Research, v. 73, p. 389–406.

MARCHESINI, L., AMOROSI, A., CIBIN, U., SPADAFORA, E., ZUFFA, G.G., AND PRETI, D., 2000, Detrital supply versus facies architecture in the Late Quaternary deposits of the south- Eastern Po Plain (Italy): Journal of Sedimentary Research, v. 70, p. 829–838.

MCBRIDE, E.F., 1985, Diagenetic processes that effect provenance determination in sandstone, *in* Zuffa, G.G., ed., Provenance of Arenites: Dordecht, Reidel, p. 95–114.

MCBRIDE, E.F. AND PICARD, M.D., 1987, Downstream changes in sand composition, roundness, and gravel size in a short-headed, high-gradient stream, northwestern Italy: Journal of Sedimentary Research, v. 57, p. 1018-1026.

MILLI, S., 1997, Depositional setting and high-frequency sequence stratigraphy of the middle-upper Pleistocene to Holocene deposits of the Roman basin: Geologica Romana, v. 33, p. 99–136.

MILLI, S., MOSCATELLI, M., PALOMBO, M.R., PARLAGRECO, L. AND PACIUCCI, M., 2008, Incised valleys, their filling and mammal fossil record: a case study from Middle-Upper Pleistocene deposits of the Roman Basin (Latium, Italy), *in* Advances in Application of Sequence Stratigraphy in Italy (Eds A. Amorosi, B.U. Haq and L. Sabato): GeoActa Special Publication, v. 1, p. 67–87.

MILLI, S., D'AMBROGI, C., BELLOTTI, P., CALDERONI, G., CARBONI, M.G., CELANT, A., DI BELLA, L., DI RITA, F., FREZZA, V., MAGRI, D., PICHEZZI, R.M. AND RICCI, V., 2013, The transition from wave-dominated estuary to wave- dominated delta: the Late Quaternary stratigraphic architecture of Tiber deltaic succession (Italy): Sedimentary Geology, v. 284–285, p. 159–180.

MILLI, S., MANCINI, M., MOSCATELLI, M., STIGLIANO, F., MARINI, M., AND CAVINATO, G.P., 2016, From river to shelf, anatomy of a high-frequency depositional sequence: The Late Pleistocene to Holocene Tiber depositional sequence: Sedimentology, v. 63, p. 1886-1928.

MORRONE C., DE ROSA, R., LE PERA, E., AND MARSAGLIA, K.M., 2017, Provenance of volcaniclastic beach sand in a magmatic-arc setting: an example from Lipari island (Aeolian archipelago, Tyrrhenian Sea): Geological Magazine, v. 154, p. 804–828.

NESBITT, H.W. AND YOUNG, G.M., 1989, Formation and diagenesis of weathering profiles: The Journal of Geology, v. 97, p. 129-147.

PALOMARES, M., ARRIBAS, J., JOHNSSON, M.J. AND BASU, A., 1993, Modern stream sands from compound crystalline sources: composition and sand generation index: Geological Society of America Special Papers, p. 313-313.

POSAMENTIER, H.W., AND ALLEN, G.P., 1999, Siliciclastic sequence stratigraphy: concepts and applications: SEPM, Society for Sedimentary Geology ed., Tulsa, Oklahoma, v. 7, 210 p.

RESENTINI, A., ANDÒ, S. AND GARZANTI, E., 2018, Quantifying roundness of detrital minerals by image analysis: Sediment transport, shape effects, and provenance implications: Journal of Sedimentary Research, v. 88, p. 276-289.

ROMANS, B.W., CASTELLTORT, S., COVAULT, J. A., FILDANI, A., AND WALSH, J.P., 2016, Environmental signal propagation in sedimentary systems across timescales: Earth-Science Reviews, v. 153, p. 7-29.

SEYRAFIAN, A., AND TORABY, H., 2009, Petrofacies and sequence stratigraphy of the Qom Formation (Late Oligocene-Early Miocene?), north of Nain, southern trend of central Iranian Basin: Carbonates Evaporites, v. 20, p. 82–90.

SYVITSKI, J.P. AND MILLIMAN, J.D., 2007, Geology, geography, and humans battle for dominance over the delivery of fluvial sediment to the coastal ocean: The Journal of Geology, v. 115, p. 1-19.

VEZZOLI, G., GARZANTI, E., AND MONGUZZI, S., 2004, Erosion in the western Alps (Dora Baltea basin): 1. Quantifying sediment provenance: Sedimentary Geology, v. 171, p. 227-246.

WALSH, J.P., WIBERG, P.L., AALTO, R., NITTROUER, C.A. AND KUEHL, S.A., 2016, Source-to-sink research: economy of the Earth's surface and its strata: Earth-Science Reviews, v. 153, p.1.

WELTJE, G.J., 2012, Quantitative models of sediment generation and provenance: state of the art and future developments: Sedimentary Geology, v. 280, p. 4-20.

YOUNG, S. W., BASU, A., MACK, G., DARNELL, H., AND SUTTNER, L. J., 1975, Use of size-composition trends in Holocene soil and fluvial sand for paleoclimatic interpretation: Proceedings IXth International Congress of Sedimentology, Nice, France, p. 28-36.

ZUFFA, G.G., 1980, Hybrid arenites: their composition and classification: Journal of Sedimentary Petrology, v. 50, p. 21–29.

ZUFFA, G.G., 1985, Optical analyses of arenites: influence of methodology on compositional results: *in* Zuffa, G.G. (Ed.), Provenance of Arenites. NATO-ASI, Reidel Publications, Dordrecht, p. 165–189.

ZUFFA, G.G., 1987, Unravelling hinterland and offshore palaeo-geography from deep-water arenite: *in* Leggett, J.K., Zuffa, G.G. (Eds.), Marine Clastic Sedimentology, Models and Case Studies, Graham and Trotman, London, p. 39–61.

ZUFFA, G.G., 1991, On the use of turbidite arenites in provenance studies - critical remarks: *in* Morton, A.C., Todd, S.P., Haughton, P.D.W. (Eds.), Developments in Sedimentary Provenance Studies: Geological Society of London Special Publication, v. 57, p. 21–28.

ZUFFA, G.G., CIBIN, U., AND DI GIULIO, A., 1995, Arenite petrography in sequence stratigraphy: Journal of Geology, v.103, p. 451–459.

CHAPTER 2: SAND COMPOSITIONAL CHANGES AS A SUPPORT FOR SEQUENCE-STRATIGRAPHIC INTERPRETATION: THE MIDDLE UPPER PLEISTOCENE TO HOLOCENE DEPOSITS OF THE ROMAN BASIN (ROME, ITALY)

DANIEL TENTORI,[1] KATHLEEN M. MARSAGLIA[2], AND SALVATORE MILLI[1]

[1]Dipartimento di Scienze della Terra, SAPIENZA Università di Roma, Piazzale Aldo Moro 5, 00185 Roma, Italy

[2]Department of Geological Sciences, California State University Northridge, 18111 Nordhoff Street, Northridge, California, U.S.A.

Published in *Journal of Sedimentary Research (2016)*, v. 86, p. 1238-1259

ABSTRACT: Sand composition is one of the factors of a stratigraphic succession that best records the interaction between allogenic and autogenic processes. This is particularly true for the Quaternary successions where the effects of this processes are better recognized and differentiated. The Quaternary succession of the Roman Basin and, in particular, the one developed during the late early Pleistocene to Holocene, records a close interaction among tectonic uplift, volcanism, climate, and glacio-eustasy. Such interaction is reflected in a complex stratal pattern and stratigraphic architecture where high-rank and low-rank depositional sequences are developed and where qualitative and quantitative changes in sand composition are recorded in the same systems tracts. The analyzed succession corresponding to the high-rank Ponte Galeria sequence (PGS) was supplied by the Tiber River and its tributaries, which developed along the Latium Tyrrhenian margin; such deposits include sediment derived from carbonate to siliciclastic Meso-Cenozoic rocks and from Pleistocene volcanic complexes of the Roman Magmatic Province. We defined three main sand petrofacies (A, B, C) that have a good correspondence with lowstand (LST), transgressive (TST), and highstand (HST) systems tracts of PGS, which reflect changes in sand composition and sand provenance under the effects of tectonism, volcaniclastic input, sedimentary processes, and relative sea-level variations. Petrofacies A is feldspatho-litho-quartzose to feldspatho-quartzo-lithic in composition. It records the erosion and influx of siliciclastic and carbonate rock detritus without volcanic input into the LST fluvial and coastal sands of the PGS. Petrofacies B is characterized by a modal composition varying from feldspathic to litho-feldspathic and feldspatho-quartzo-lithic. It

characterizes the TST of the PGS and reflects the abrupt and rapid introduction of volcaniclastic sediment into the system. Petrofacies C is feldspatho-quartzo-lithic in composition. This petrofacies characterizes the HST of PGS and, with respect to the other two petrofacies, better records the effects of downstream transport and river-mouth sedimentary processes. Sand samples collected from ancient deposits are similar in composition to the modern Tiber River, suggesting provenance from a similar river system. Results show that tectonism during middle–upper Pleistocene volcanic activity in the Sabatini, Cimini, and Vulsini volcanic complexes played a major role controlling stream-network reorganization in the Tiber drainage basin and resulted in enhanced volcaniclastic input from ash fall and recycling of pyroclastic flows. Volcanic input (volcanic lithics and associated phenocrysts) and postdepositional alteration during paleosol development define pre-, syn-, and post-volcanic compositions in the high-rank Ponte Galeria depositional sequence. In low-rank depositional sequences, several processes produced variable quartz/feldspar and quartz/lithic ratios, as well as textural changes; these include hydraulic sorting during fluvial and coastal transport and postdepositional in situ weathering processes. Weathering and pedogenic processes in the source area (catchment) potentially remove provenance information, reducing correlation potential of petrographic signatures of proximal successions in the Tiber River sedimentary basin. This work tests the effectiveness of using variation in sand composition as a tool in sequence stratigraphy.

2.1 INTRODUCTION

Climate, eustasy, tectonics (subsidence, uplift), and sediment supply, with their multiple facets, are the main processes controlling sand composition in sedimentary basins. However, sand composition, starting from when it is liberated from source-rock lithologies, is also influenced by many physical and chemical processes that contribute to the final composition of sandy sediment in a basin. While the physical effects on particles (e.g., transport processes) can be understood and corrected (see, e.g., McBride and Picard 1987; Garzanti et al. 2009, 2015a), the chemical processes are more complex because the effects related to the climate before and during deposition (chemical weathering) tell us what is preserved, but not what has been destroyed (Nesbitt and Young 1996; Potter et al. 2001; Garzanti et al. 2003; Velbel 2007; Ando` et al. 2012; Garzanti et al. 2013; Garzanti 2016). Lastly, the effects of post-burial diagenesis (McBride 1985; Morton and Hallsworth 2007) may locally modify the composition of sand in a basin through grain dissolution and alteration.

Despite these problematic issues some questions arise with regard to application of sedimentary petrology, specifically sand detrital modes, to sequence stratigraphy: 1) Can sand composition be used to better characterize the sequence stratigraphic framework of a sedimentary succession? and 2) At what physical and temporal scales of depositional sequences might sand composition provide a significant contribution to the sequence-stratigraphic interpretation?

Generally, sand composition has been applied to provenance and paleogeographic studies but rarely to sequence stratigraphy (e.g., Amorosi and Zuffa 2011). However, several studies show that variation of sand composition among stratigraphic units bounded by unconformities occurs (see Garzanti 1991; Ito 1994; Amorosi 1995; Zuffa et al. 1995; Marchesini et al. 2000; Lawton et al. 2003; Critelli et al. 2007; Seyrafian and Toraby 2009). In this respect, understanding how sand composition can vary under the effects of the allogenic and autogenic factors represents a very difficult challenge. Defining the influence of climate, tectonism, and sea-level change on sand composition and sequence development is very complex, and this is particularly true in continental and coastal environments, where the interactions between fluvial and shallow marine processes affect sand distribution at various spatial and temporal scales (Critelli et al. 2003).

Studies indicate that sand composition is, in fact, an excellent tracer of sediment production and transport through modern source-to-sink systems (e.g., the Waipaoa Sedimentary System of New Zealand: Marsaglia et al. 2010; Parra et al. 2012; the Po Sedimentary System in Northern Italy: Marchesini et al. 2000; Amorosi and Zuffa 2011; Garzanti et al. 2011a). Actualistic models of modern stream and coastal sediment composition have been determined in several modern river systems elsewhere in Italy (e.g., McBride and Picard 1987; Ibbeken and Schleyer 1991; Le Pera and Critelli 1997; Critelli and Le Pera 2002; Garzanti et al. 2002; Di Giulio et al. 2003; Picard and McBride 2007), but these have not been linked to associated stratigraphic successions in a sequence framework. One exception is the work by Garzanti et al. (2011b) in the Po basin, in which petrographic composition and heavy-mineral suites of Pleistocene sediments were linked with paleodrainage changes in a detailed sequence-stratigraphic framework.

Continental and coastal to marine Quaternary successions constitute, in this respect, important case studies to test sand composition changes within a sequence stratigraphic context. Such successions, being more recent and in several cases better preserved with respect to other and older sedimentary successions, can allow better discrimination of the influence of allogenic and autogenic factors on sequence development. When accurate chronologic control of facies distribution is available, it is possible to characterize sand composition among individual systems

tracts and within a single systems tract (see, e.g., Marchesini et al. 2000; Amorosi and Zuffa 2011), showing that arenite petrography can be a useful tool to unravel paleogeographic evolution and changes in provenance associated with cyclic changes in sea level.

With this in mind, this paper provides an example of the application of petrographic methods to the high-resolution sequence stratigraphy of the middle–upper Pleistocene to Holocene succession of the Roman Basin of central Italy (Fig. 2.1), a stratigraphic unit known in the literature as the Ponte Galeria Sequence (Milli 1997; Milli et al. 2008; 2013; Milli and Palombo 2011). Facies analysis and sequence-stratigraphic interpretation of this succession has, in fact, produced a robust stratigraphic database that can be used for a combined sequence-stratigraphic and sand detrital-mode approach. At present only limited qualitative gravel and sand petrology (Bellotti et al. 1993b) and cursory compositional analysis of sand in the modern Tiber River and coastal system (Garzanti et al. 2002) have been conducted. Our study constitutes the first attempt to interpret these deposits in terms of both composition and provenance in order to provide insights on the environmental and stratigraphic evolution of the middle to late Quaternary deposits of the central Latium area. To do this we define the compositional trends of the ancient Tiber middle–upper Pleistocene deposits and of the modern Tiber River, river mouth, and coast. This allows us to create a model that constrains the relationships between provenance, sand composition, and sequence stratigraphic architecture.

2.2 GEOLOGICAL AND SEQUENCE-STRATIGRAPHIC SETTING

The Roman Basin is located in the central sector of Latium Tyrrhenian margin and extends north and south of Tiber River for about 135 km (Fig. 2.1A). Basin development started in the late Pliocene, along an extensional continental margin. Extension started during the late Miocene in connection with the opening of the back-arc Tyrrhenian Basin, which, in turn, was related to west-directed Apennine subduction (Patacca et al. 1990; Malinverno and Ryan 1986; Doglioni et al. 2004 and references therein). The Roman Basin is one of the half-graben basins, mainly oriented NNW–SSE/NW–SE, and subordinately NE–SW, which were filled with syn-rift and post-rift clastic sediments (Funiciello et al. 1976; Mariani and Prato 1988; Barberi et al. 1994 and references therein). These sediments were transported and deposited by a Pliocene to Pleistocene fluvial system similar to the modern Tiber River and its tributaries (Fig. 2.1B). Basin development was accompanied by continuous regional tectonic uplift (Milli 1997; Bordoni and Valensise 1998; Giordano et al. 2003) and intense volcanic activity, reaching its climax in the middle–upper Pleistocene, when the volcanic complexes of the Roman Magmatic Province developed (Locardi et

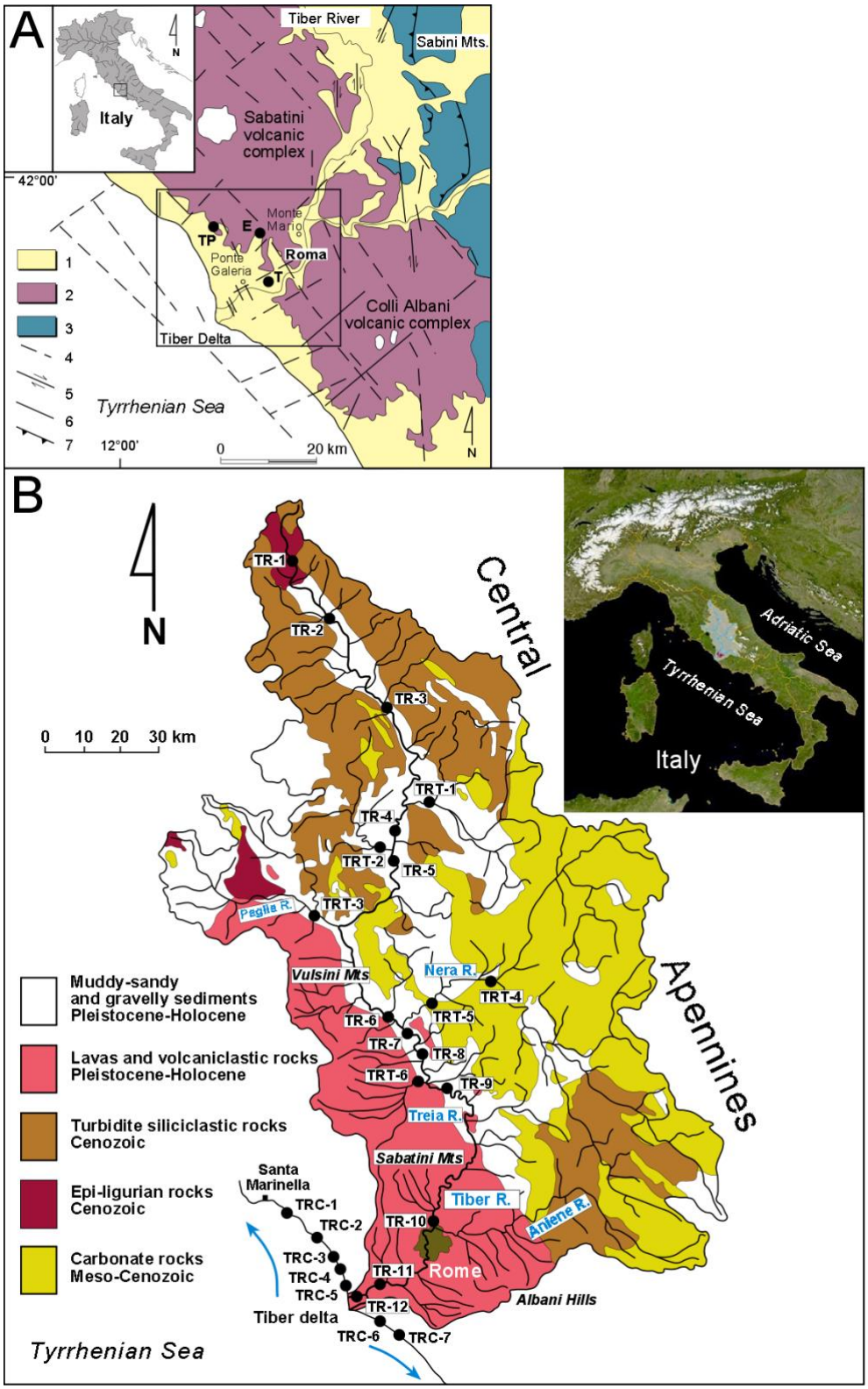

FIG. 2.1—A) Geological sketch of the Tyrrhenian margin of central Italy. Legend: 1) Messinian–Holocene sedimentary deposits, 2) Pliocene–Pleistocene lavas and volcaniclastic deposits, 3) Cenozoic sedimentary deposits, 4) main buried faults, 5) strike-slip faults, 6) normal faults, 7) major thrusts (barbs on hanging wall). TP, E, T indicate the locations of the Torre in Pietra, ESI quarry, and Tiberi quarry sections, respectively. Black square indicates the Roman Basin. B) Tiber River drainage basin and main geologic units that crop out there. Tiber River (TR), Tiber River tributary (TRT) and Tiber delta beach (TRC) sample locations correspond to numbered filled circles. Geology and general and local directions of littoral transport are from Bellotti et al. (1994).

al. 1976; Cioni et al. 1993; De Rita et al. 1993, 1995; Karner et al. 2001; Peccerillo 2005). The Sabatini volcanic complex in the study area was characterized by K-rich magmas that fed explosive eruptions (Conticelli et al. 1997; Sottili et al. 2004, 2010). Volcaniclastic rock fragments derived, essentially, from ash clouds and unconsolidated and welded pyroclastic flow deposits, and exhibit a glassy matrix with microlitic (~ 70%) and lathwork (, 10%) textures. Phenocrysts include quartz, K-feldspar, and pyroxene.

The stratigraphic setting of the Roman Basin is the result of the close interaction between tectonic uplift, volcanic activity, and glacio-eustatic sea-level fluctuations related to the Quaternary changes in climate (Cavinato et al. 1992; De Rita et al. 1994, 2002; Milli 1994, 1997; Giordano et al. 2003; Mancini and Cavinato 2005; Milli et al. 2008 and references therein). The stratal architecture of the basin is characterized by several depositional units constituting low-rank (high-frequency) depositional sequences (sensu Mitchum and Van Wagoner 1991; Catuneanu et al. 2009, 2011) with variable duration, from 30,000 yr to 120,000 yr, stacked to form two composite high-rank sequences: the Monte Mario Sequence (MMS; lower Pleistocene) and the Ponte Galeria Sequence (PGS; late lower Pleistocene–Holocene), respectively (Milli 1997; Milli et al. 2013 and references therein) (Figs. 2.2, 2.3). The MMS deposits are essentially known through the stratigraphy of several wells and outcrops of limited extent. These deposits are coastal and transition-shelf depositional systems, developed during the late lowstand and transgressive systems tracts of the MMS. The PGS strata contain fluvial, fluvio-lacustrine, barrier-island–lagoon, and transition- shelf facies, organized into the lowstand (LST), transgressive (TST), and highstand (HST) systems tracts of the PGS (Fig. 2.2). Well-dated volcaniclastic deposits belonging to the Albani and Sabatini volcanic complexes were used to constrain the age and duration of the low-rank depositional sequences in which they occur (Sottili et al. 2010; Marra et al. 2011; Marra et al. 2014 and references therein). Previous workers have shown the PGS to range from 10 to 110 m thick in the study area and to lie above shelfal mud of the MMS at a polygenic erosional surface formed during the sea-level fall between marine isotope stages 31 and 20 (Figs. 2.2, 2.3). This composite sequence consists of twelve low-rank sequences from 5 to 80 m thick, the boundaries of which are expressed by sharp erosional surfaces recording basin and downward shifts of facies, and subaerial exposure and paleosols in the interfluvial areas. The low-rank sequences (from PG01 to part of PG3) stack to form the LST of PGS. Sequences from PG4 to part of PG8 are referable to the TST, while the sequence PG9 (the Tiber Depositional Sequence, TDS) developed entirely during the HST of PGS (Figs. 2.2, 2.3) (Milli et al. 2016). The PGS shows a general seaward stacking of the low-rank depositional sequences (Fig. 2.3). This trend is

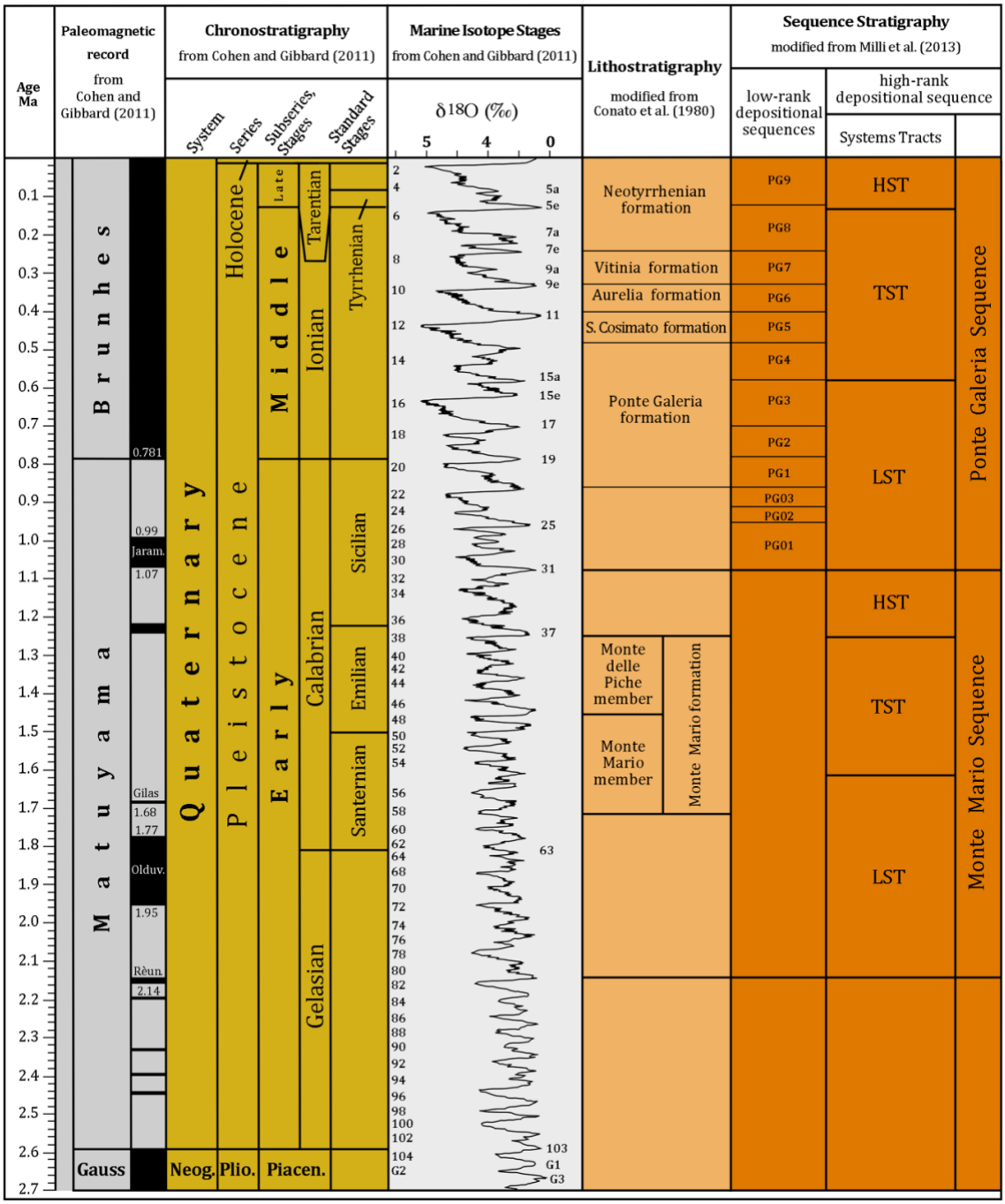

FIG. 2.2 —Chronostratigraphic and sequence-stratigraphic scheme of the Quaternary deposits of the Roman Basin (modified after Milli et al. 2013). HST: highstand systems tract; TST: transgressive systems tract; LST: lowstand systems tract; ELST: Early Lowstand Systems Tract; LLST: Late Lowstand Systems Tract. PG01–PG9 are the Ponte Galeria low-rank sequences. Neog.: Neogene; Plio.: Pliocene; Piacen.: Piacentian.

opposite to the trend that the PGS would have displayed if controlled by glacioeustasy alone. Consequently, the present setting of the PGS is thought to have been controlled by the interaction between eustatic sea-level changes and regional tectonic uplift; the latter forced the seaward migration of the low-rank sequence equilibrium points, thus helping to define the final stacking pattern of PGS (see more details and discussion in Milli 1997; Milli et al. 2008).

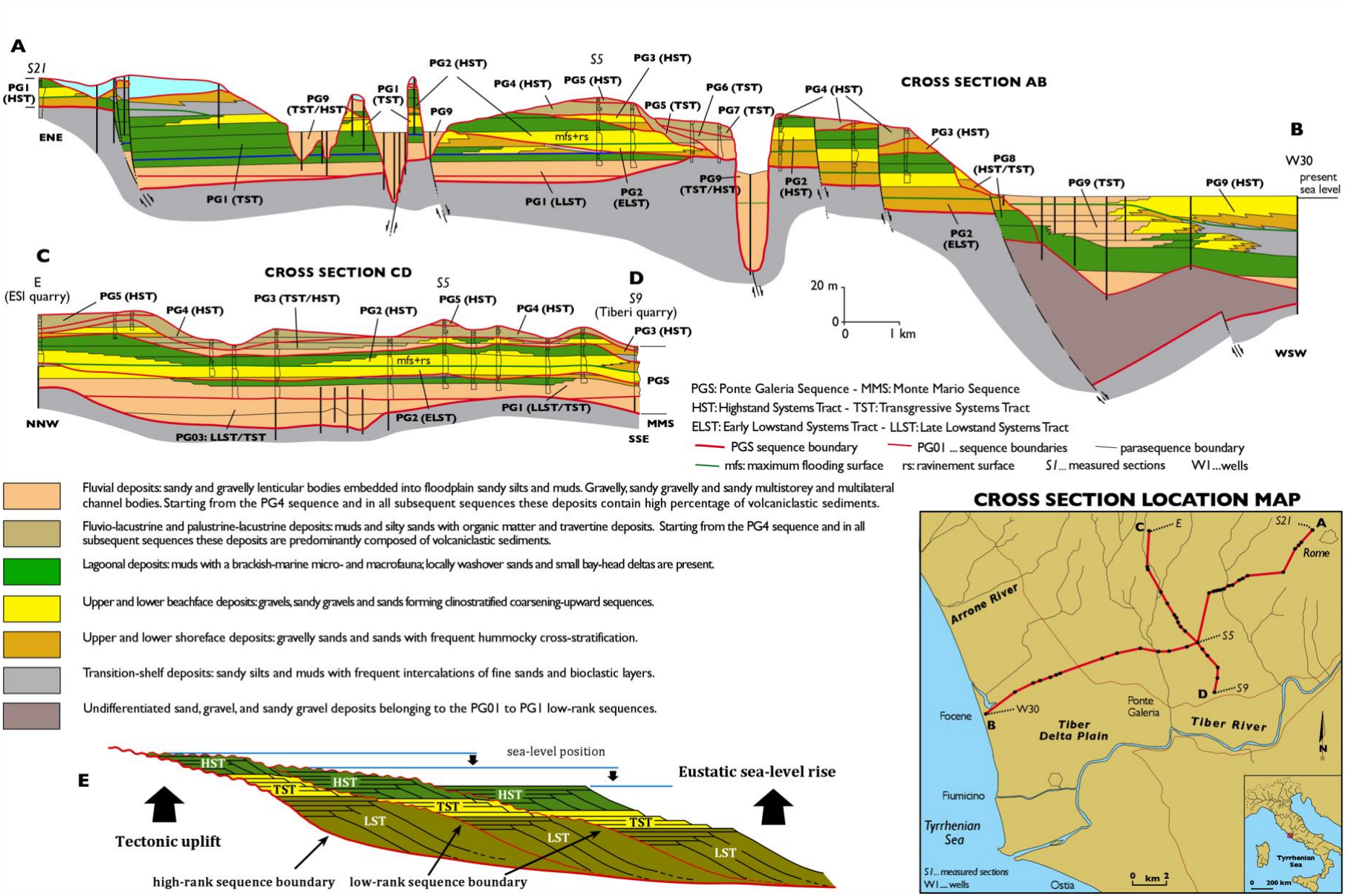

FIG. 2.3.—A–B, C–D) Stratigraphic cross sections showing the depositional architecture of the composite high-rank Ponte Galeria Sequence (modified after Milli 1997). E) Conceptual sketch showing the stratigraphic relationships among the low-rank sequences in the Roman basin related to the interaction between tectonic uplift of the Latium Tyrrhenian margin and eustatic sea-level changes during the development of the high-rank Ponte Galeria Sequence. Note the downward and seaward migration of the sequences due to the tectonic uplift of the continental margin.

2.3 SOURCE AND PROVENANCE OF PGS DEPOSITS

The ancient fluvial equivalent of the Tiber River system is thought to have been the main source of PGS deposits during the Quaternary. The Tiber River originates in the Apennine Mountains of Emilia Romagna and flows for 406 kilometers through Umbria and Lazio to the Tyrrhenian Sea (Fig. 2.1B). The drainage basin, 17,375 km2 in area, comprises a large portion of the central Apennines in which carbonate, siliciclastic, and volcanic rocks, varying in age from Mesozoic to Quaternary, are present. The Apennine belt includes ophiolitic sequences and continental-margin successions consisting largely of Meso-Cenozoic pelagic to platform carbonate deposits associated with synorogenic turbiditic sediments deposited during the Oligocene– Miocene in foreland-basin systems. The sandy turbidite compositions range from feldspatho-quartzose to litho-feldspatho-quartzose with common metamorphic, plutonic, sedimentary, and volcanic lithic fragments (Gandolfi et al. 1983; Gandolfi et al. 2007; Valloni and Zuffa 1984; Gandolfi and Paganelli 1993; Amendola et al. 2016). In more detail, the catchment basin of the Tiber River and its tributaries lies in the Latium–Campania Superprovince (Garzanti et al. 2002), and the composition of Tiber River sand reflects the recycling of Miocene turbidite detritus, the widespread exposure of Mesozoic carbonates, and the more recent Quaternary potassic and ultrapotassic volcanism of the Roman magmatic province. Data from Garzanti et al. (2002) indicate that the present Tiber River and delta contain: quartz, feldspars, and minor terrigenous lithic fragments from foredeep turbidites; limestone and chert from the Umbria pelagic succession; and subordinate volcanic detritus including rare volcanic lithic fragments, and leucite and sanidine crystals. These main components are those that, in different percentages, we have recognized in our analysis of basinal deposits and described and contextualized in the sequence stratigraphic framework of the Ponte Galeria Sequence.

2.4 METHODS

Methods used in this study include fieldwork and laboratory analyses. Fieldwork in the Roman basin deposits focused on the low-rank depositional sequences forming the PGS and included facies analysis and sample collection from new and previously measured sections in the Tiberi and ESI quarries and an outcrop at Torre in Pietra (Milli 1997; Milli and Moscatelli 2001; Tentori 2015). A total of twenty-nine samples was collected from the Tiberi quarry (TQ1–TQ15), ESI quarry (EQ1–EQ11), and Torre in Pietra outcrops (TO1–TO3), where early to middle Pleistocene deposits of the low-rank depositional sequences (from PG1 to PG7) are exposed (Figs. 2.4, 2.5, 2.6, 2.7).

In order to investigate the role of autogenic (e.g., sedimentary processes, provenance mixing, hydraulic sorting) vs. allogenic (e.g., tectonism, eustasy, volcanism) processes in controlling compositional trends in the stratigraphic succession, the samples were analyzed in the context of their depositional environment and their position in the sequence-stratigraphic framework. In particular, sampling focused across sequence boundaries and in facies associations related to the various systems tracts of the low- rank sequences in order to detect changes in composition due to evolving paleogeography and time-dependent factors. Of the last and most recent low-rank sequence forming the PGS, the Tiber Depositional Sequence (PG9) (Milli et al. 2013, in press) was sampled with greater detail, the HST both in the hinterland and along the coast. Eighteen stream-sand samples were collected from the modern Tiber River (TR1–TR12) and its major tributary streams (TRT1–TRT6) in order to evaluate downstream changes in sediment composition. Sand samples were collected at ~ 30 km intervals, from the headwaters to lower reaches, and in tributaries just upstream of their intersection with the main river (Fig. 2.1B). The sand samples collected along the coast derive from the swash zone of seven beaches north and south of the Tiber River mouth (TRC1–TRC7). They were analyzed to evaluate the influence of littoral transport and wave and current reworking on sand composition along the coastline, and to compare the HST coastal deposits of older low-rank sequences with those of the PG9 sequence.

Sixty-seven standard petrographic thin sections were made and stained for potassium and calcium feldspar using the method described by Marsaglia and Tazaki (1992). A total of 400 points was counted per slide using the Gazzi-Dickinson method (Ingersoll et al. 1984). Lithic, monomineralic, and biogenic grains were differentiated using categories by Zuffa (1980, 1985, 1987, 1991), Marsaglia (1992), and Marsaglia et al. (1999) (Tables A1, A2, and A3 in Appendix A), whereas volcanic lithic fragments were texturally differentiated into categories defined by Critelli et al. (2002) and Marsaglia et al. (2016). Examples of some of these grain types are displayed in Figure 2.8. Detrital modes were plotted on a QFL ternary classification diagram proposed by Garzanti (2016) with nomenclature introduced by Crook (1960) and endorsed by Dickinson (1970) and Weltje (2006) (Fig. 2.9). Modal compositions were also plotted using various lithic proportions in order to better define source areas (see also Zuffa 1980, 1987, 1991) (Fig. 2.10). Medium-sand fractions were chosen for analysis to be consistent with previous studies (e.g., McBride and Picard 1987), and seven samples (TR11; TQ4–TQ7–TQ12–TQ15; EQ2–EQ5) were selected to detect potential grain-size dependence of composition by also counting fine and very fine grain-size fractions. A resulting

model of compositional trends along the modern Tiber River and river mouth was compared to detrital modes determined for the sand specimens sampled from the two measured sections.

Changes in grain roundness were assessed along the modern Tiber River, the coastal area along the Tyrrhenian coast, and in the Pleistocene deposits of the Tiber River succession to evaluate grain resistance to transport (stream and wave abrasion; see Fig. 2.11 and Table A3 in Appendix A). Variations in mean roundness were determined on medium-sand-size monocrystalline quartz and carbonate (Lsc(cry) þ Lsc(mic)) lithic fragments following the techniques of McBride and Picard (1987) and Arribas et al. (2000). A numerical value was assigned to the first 30 grains encountered during point counting: very angular (1), angular (2), subangular (3), subrounded (4), rounded (5), and well-rounded (6) grains. Mean roundness values were then calculated for each sample for comparison.

2.5 RESULTS

The composition of the PGS sand samples analyzed in this study varies broadly in terms of quartz, lithic, and feldspar proportions, with quartz and/or lithic components generally dominating over feldspar except in a few instances (Fig. 2.9). In general, modal sand composition ranges from feldspatho-quartzo-lithic to feldspatho-lithic-quartzose with some samples showing feldspatho-quartzose, litho-quartzose, quartzo-lithic, litho-feldspathic, feldspathic, and lithic composition. For the purpose of combining compositional variations within the sequence stratigraphic organization of the PGS, ancient and modern samples were plotted separately by systems tract on various ternary plots (QFL and LmLvLs percentages, proportions of noncarbonate extrabasinal (NCE), carbonate extrabasinal (CE), and carbonate intrabasinal (CI) clasts) (Zuffa 1980) to see if they formed distinct petrofacies (Figs. 2.10, 2.12). The systems tracts cannot be clearly discriminated on the QFL, LmLvLs, or NCECECI ternary plots (Fig. 2.10), where there is significant overlap among the LST, TST, and HST compositions, particularly the Tiberi Quarry LST coastal-marine facies. Tiber petrofacies are more clearly defined on a plot of parameters and ratios that Ito (1994) used to discriminate systems tracts in forearc facies in the Bozo Peninsula of Japan. Discrimination is apparent in Figure 2.12, where the TST samples are particularly distinct and the HST samples form somewhat of a continuum from the TST cluster and slight overlap at low Lv/Lt values with the LST samples. Our results are more robust than Ito's, with better separation that allowed us to roughly distinguish sand from lowstand, transgressive, and highstand systems tracts of the PGS as petrofacies A, B, and C, respectively.

Quartz is abundant in Petrofacies A with significant feldspar and generally minor carbonate and

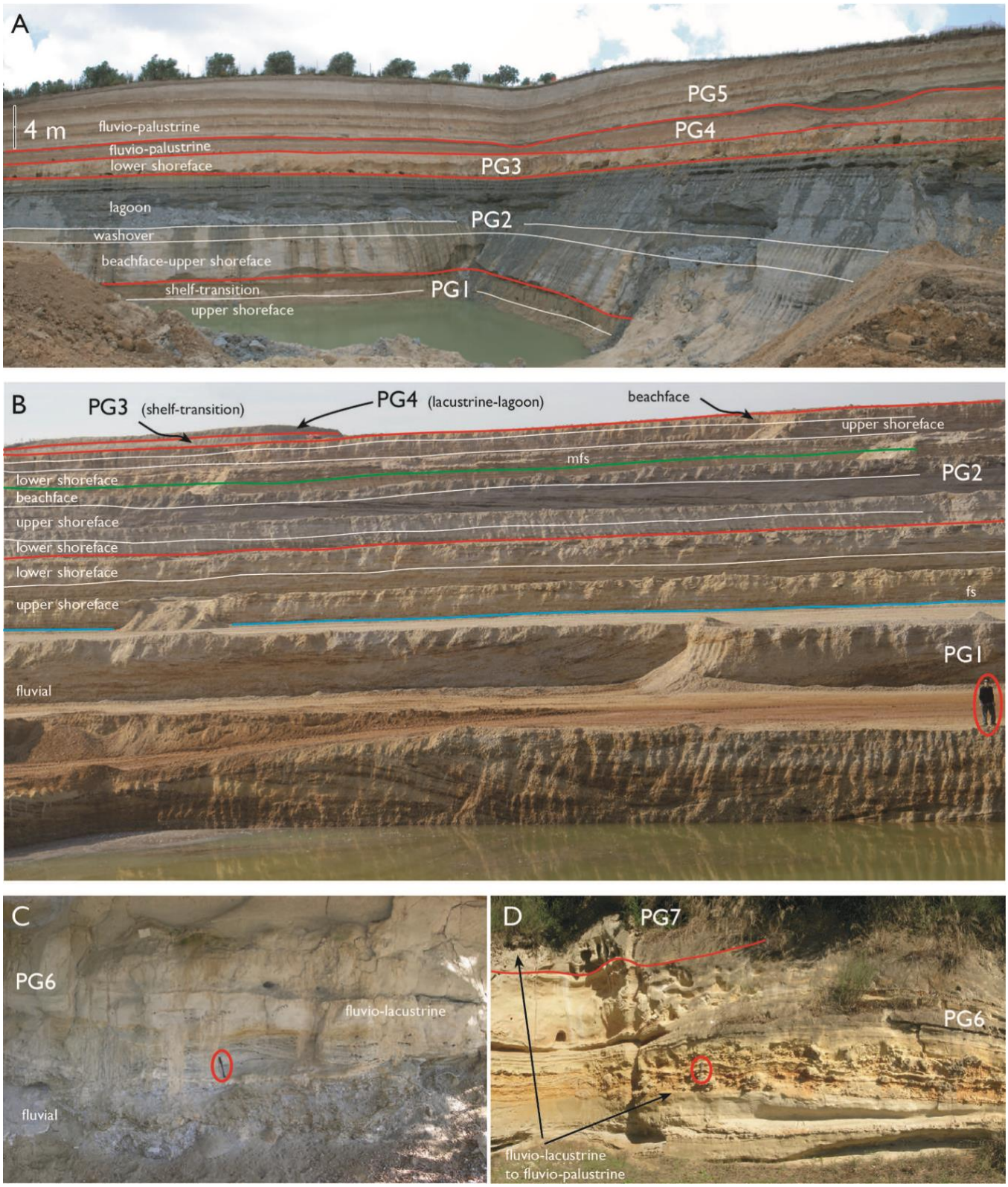

FIG. 2.4 —Field photographs of the A) ESI and B) Tiberi quarries and C, D) Torre in Pietra outcrop with related environmental and sequence-stratigraphic interpretations. In Part B, man for scale; in Part C, pencil for scale; in Part D, hammer for scale.

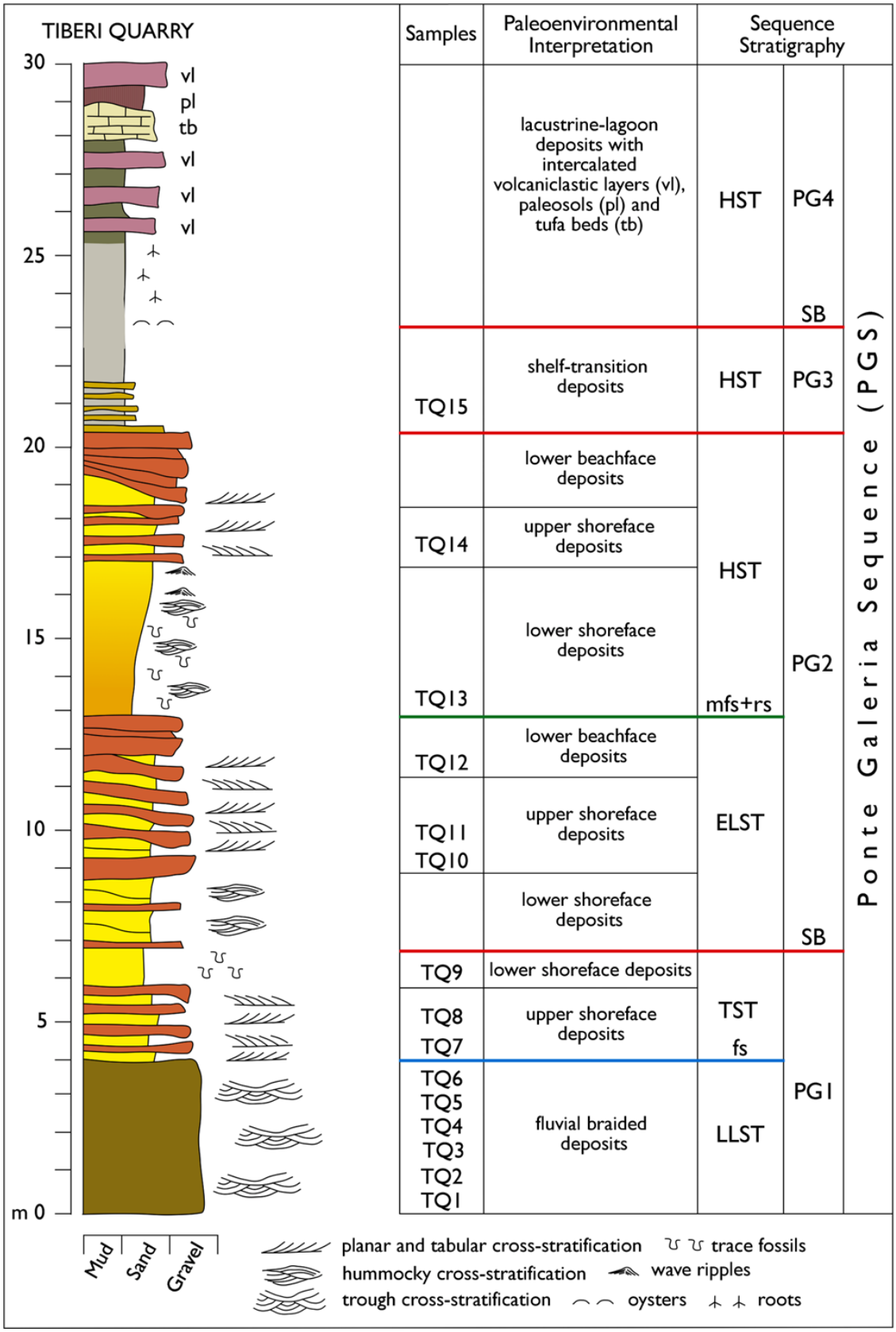

FIG. 2.5 —Stratigraphic column of Tiberi quarry showing the sampled intervals (TQ), the inferred depositional environment, and the sequence- stratigraphic interpretation.

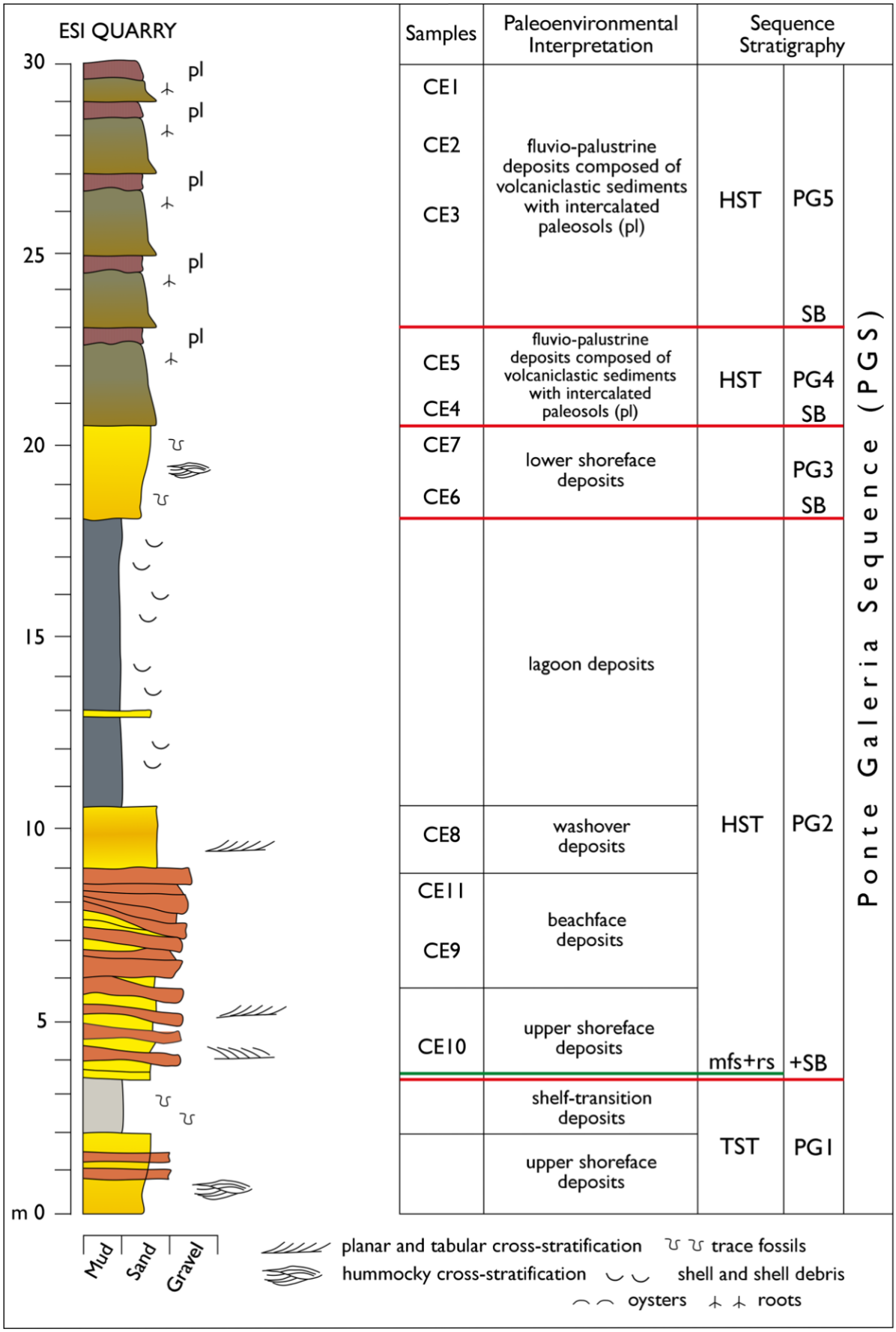

FIG. 2.6 —Stratigraphic column of ESI quarry showing the sampled intervals (EQ), the inferred depositional environment, and the sequence- stratigraphic interpretation.

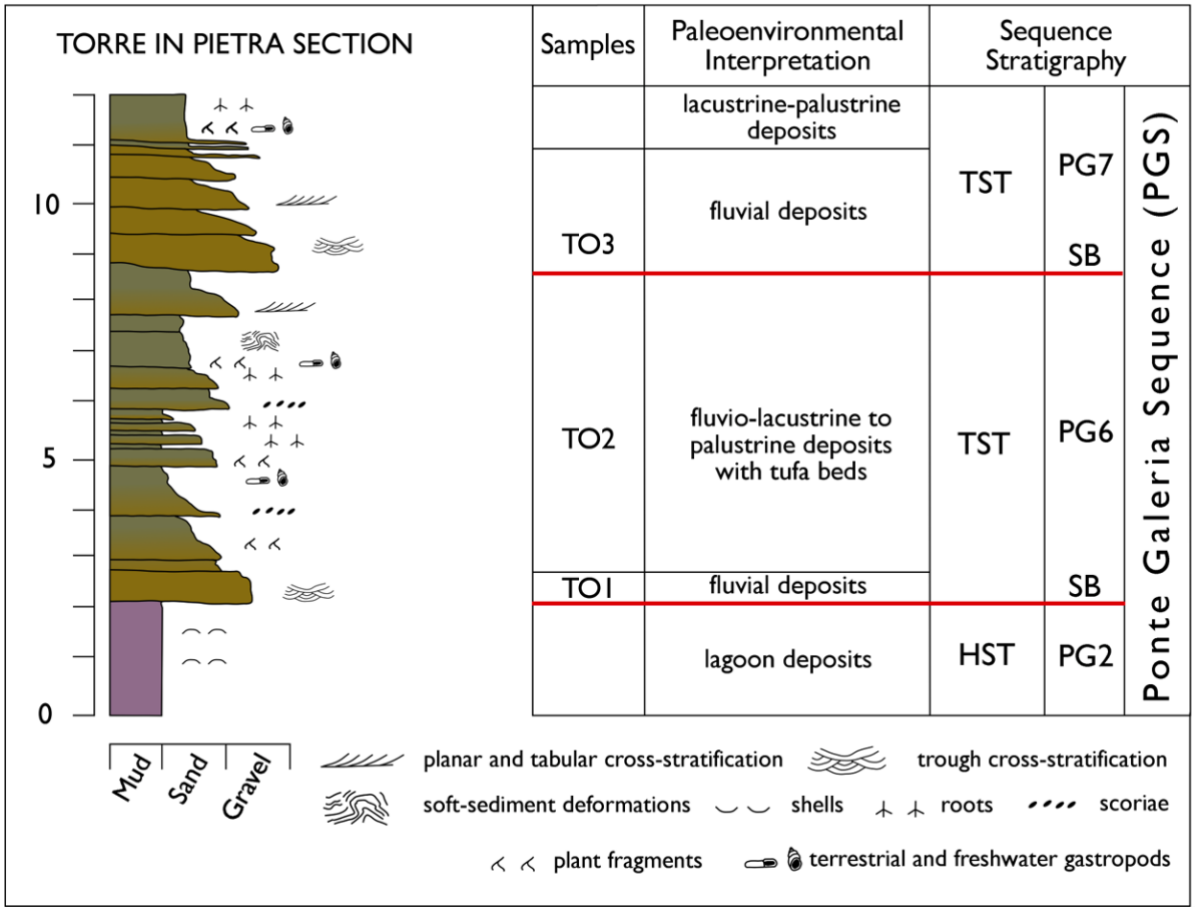

FIG. 2.7 —Stratigraphic column of Torre in Pietra outcrop showing the sampled intervals (TO), the inferred depositional environment, and the sequence-stratigraphic interpretation.

metamorphic lithic fragments (Fig. 2.10). This petrofacies includes few samples rich in volcanic lithic fragments. Samples are composed almost entirely of noncarbonate extrabasinal grains with only few samples with carbonate-extrabasinal components (mean = $NCE_{91}CE_8CI_1$) (Fig. 2.10).

Feldspar grains are abundant in Petrofacies B, with significant amounts of volcanic lithic fragments and minor quartz (Fig. 2.10). Volcanic glassy groundmass in the volcanic lithic fragments is highly altered, and most of the sand-sized grains in the PG5 samples are disaggregated soil bits, and feldspar (. 50) and pyroxene grains. These samples show a strong noncarbonate extrabasinal grain signature (mean = $NCE_{98}CE_2CI_0$) (Fig. 2.10).

Samples of Petrofacies C include abundant volcanic-lithic and siliciclastic sedimentary fragments and significant extrabasinal carbonate grains (mean = $NCE_{74}CE_{26}CI0$) (Fig. 2.10). Pyroxenes are abundant in the coastal deposits.

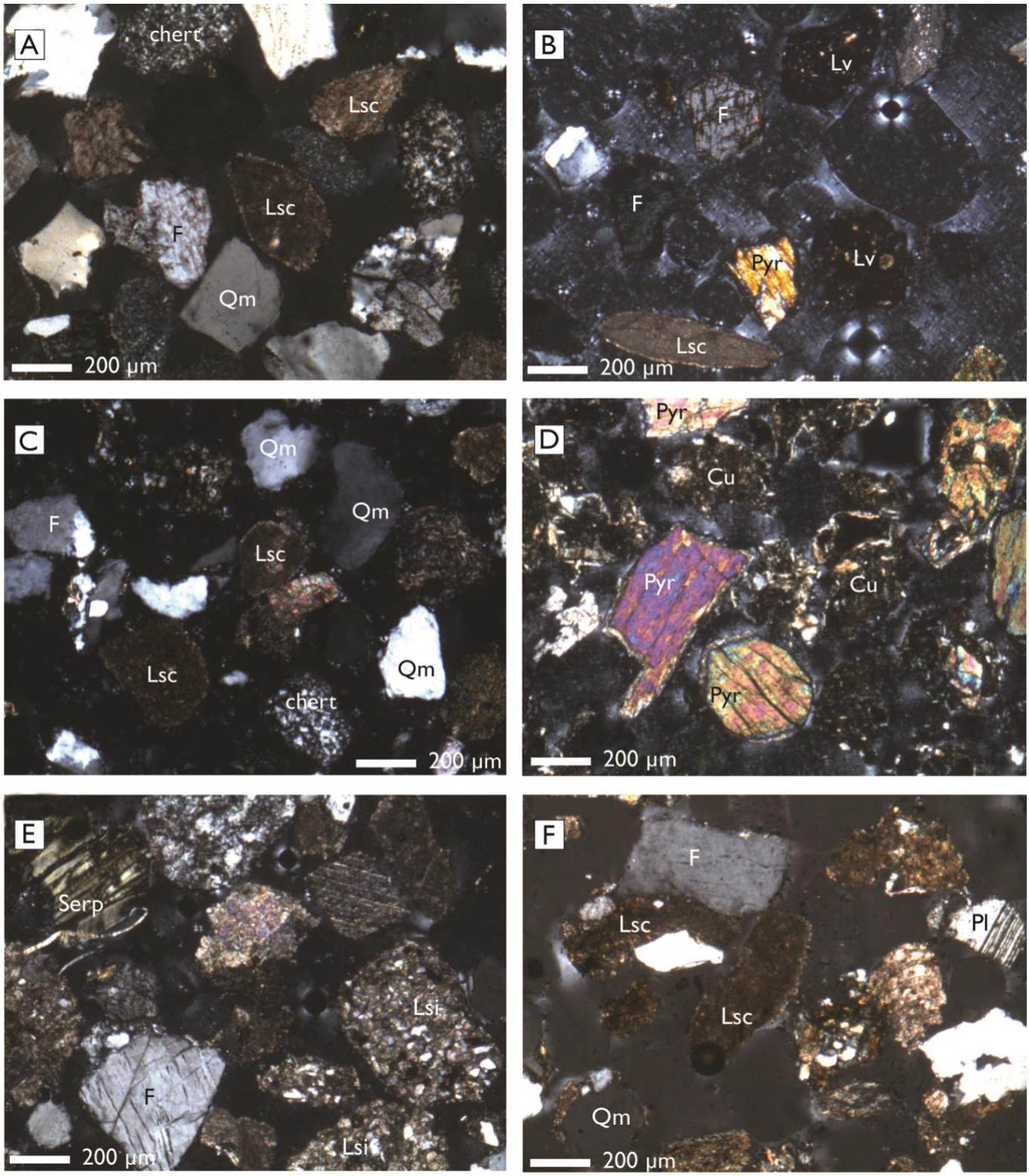

FIG. 2.8 —Photomicrographs of the A, B) Tiberi and C, D) ESI quarries, and E, F) modern Tiber River sands respectively, highlighting some key grain types. A) lower- shoreface sample TQ9 showing feldspar (F), monocrystalline quartz (Qm), and micritic carbonate lithic fragments (Lsc); B) upper-shoreface sample TQ10 showing feldspar (F) and pyroxene (Pyr) grains, volcanic (Lv) and micritic carbonate (Lsc) lithic fragments; C) beachface sample EQ1 showing few carbonate lithic fragments (Lsc), quartz (Qm), and feldspar (F) grains; D) fluvio-palustrine sample EQ10 showing pyroxene (Pyr) grains and cutan fragments (Cu) derived as a product of soil alteration; E) sample TR3 showing serpentine (Serp) and feldspar (F) grains and siltstone lithic fragments (Lsi); F) sample TR5 showing quartz (Qm) and feldspar (F þ Pl) grains and micritic carbonate lithic fragments (Lsc).

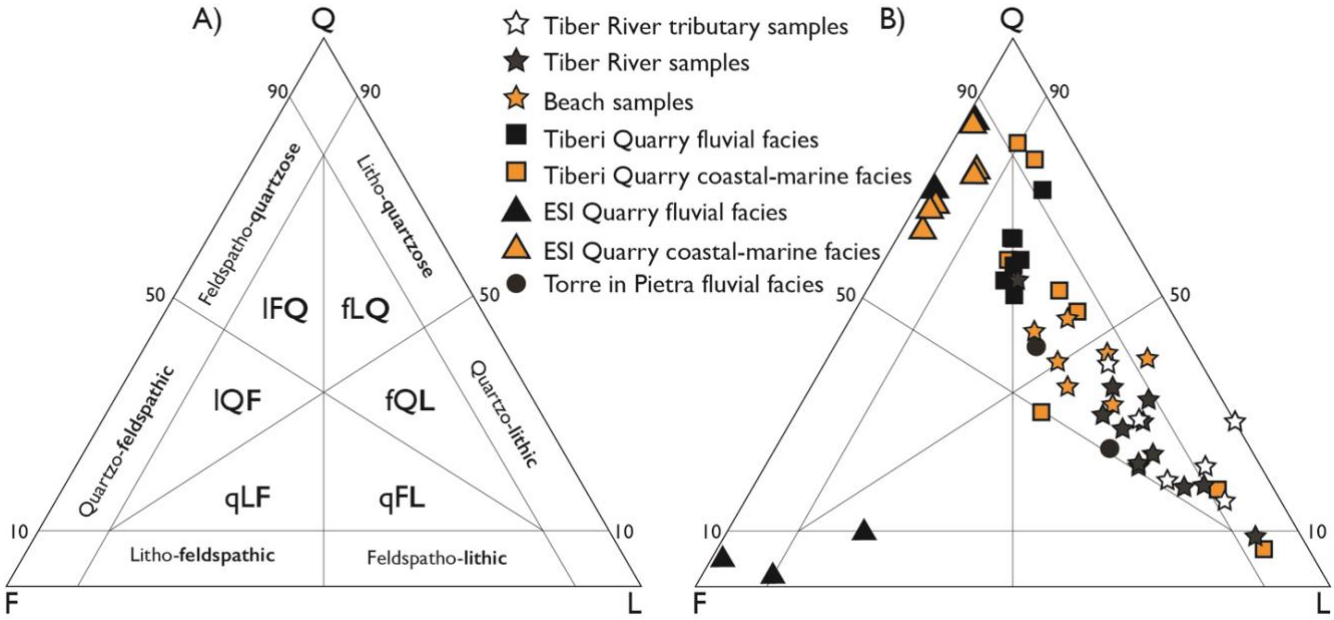

FIG. 2.9 —Ternary plots (A, B) used for the petrographic classification of the studied sand samples. Scheme (A) is from Garzanti (2016) and based on the nomenclature introduced by Crook (1960) and Dickinson (1970) and endorsed by Ingersoll (1983) and Weltje (2006). Q, quartzose; F, feldspathic; L, lithic; lFQ, litho-feldspatho-quartzose; fLQ, feldspatho-litho-quartzose; lQF, litho-quartzose-feldspathic; fQL, feldspatho-quartzo-lithic; qLF, quartzo-lithic-feldspathic; qFL, quartzo-feldspatho-lithic.

2.6 DISCUSSION

2.6.1 Interpretation of Petrofacies

Petrofacies A resulted from erosion of siliciclastic turbidites that crop out in restricted areas of the upper drainage basin, whereas carbonate lithic fragments were derived from erosion of limestone units in the middle and lower drainage basin, similar to the modern river. This petrofacies contains volcanic lithic fragments derived from the initial and sporadic explosive eruptions of the Sabatini complex. This petrofacies characterizes the LST fluvial and coastal sands of the PGS. In particular, the beachface sand deposits show a very close compositional and textural relationship with the fluvial deposits, thus indicating a direct influence from the paleo–fluvial system. In the modern coastal system compositional maturity increases alongshore by the effect of coastal reworking, a process that has been active from the middle Pleistocene to Present.

Petrofacies B includes the TST fluvial and fluvio-lacustrine deposits of PGS, since outcrops of marine deposits are absent in the investigated area. This petrofacies is very rich in volcanic lithic fragments with very little sedimentary lithic components. It records the rapid introduction into the system of volcanic supplies related to explosive eruptions of Sabatini volcanoes. It also shows the effects of pedogenic processes (see, e.g., Nesbitt and Young 1996) on volcanics-rich units, in that

they exhibit high concentrations of K-feldspar and pyroxene crystals and/or grains liberated from altered vitric volcanic clasts.

Petrofacies C samples are interpreted as part of the HST fluvial and coastal deposits of the PGS. Beach-sand composition reflects the reworking of altered volcanics-rich deposits and the effects of prolonged and constant coastal reworking and preferential abrasion and/or dissolution of volcanic glass in lithics, liberating their phenocryst phases (e.g., pyroxene grains). Also, carbonate extrabasinal fragments are generally less common in beach samples owing to coastal reworking with respect to modern river samples, which reflects direct input from tributaries draining carbonate successions (Fig. 2.10).

2.6.2 Compositional Characteristics of the High-Rank Ponte Galeria Sequence (PGS)

As highlighted above, the three petrofacies record, essentially, the effects of the interaction among tectonic uplift, volcanic activity, and glacio- eustatic sea-level fluctuations. In particular, tectonic uplift is thought to be responsible for the compositional changes related to the modification of source-rock types and the proportion of terrigenous detritus delivered to the basin in all systems tracts of the PGS. Extensive volcanic input dominates in the TST of PGS, during a phase that otherwise would have been characterized by a reduction of sediment supply owing to relative sea-level rise. Eustasy controlled base-level fluctuations and stream erosion capacity in all the PGS systems tracts influencing sediment supply (Milli 1997; Milli et al. 2008), but perhaps not sediment composition. Eustatic signals may be more pronounced in coastal and shelf facies, where shore-parallel currents during highstands influence sediment distribution.

Fluvial supply controlled the overall composition of the lowstand system tract reflecting high terrigenous sediment supply and a close source-to- basin relationship. Accommodation rates were minimal during lowstand and terrigenous sediment bypass into the basin. This might explain the large compositional range of the deposits, with compositional variation dictated by the nuances of relative rainfall and/or discharge in the paleo- Tiber subcatchments as seen today (e.g., Leombruni et al. 2009). The higher Qm/(Qm þ Lt) ratio compared to the highstand sands might be explained by taking into consideration the major areal extent of volcaniclastic and sedimentary formations in the Tiber River drainage during the PGS highstand (Fig. 2.12).

During the TST, volcanic input was at its highest and favored the presence of volcanic lithics and crystals in the continental deposits. This volcanic debris was essentially derived from fall events and pyroclastic density currents and only subordinately from erosion of lavas (Fig. 2.12). Syndepositional

and postdepositional weathering likely affected these volcanic mineral and vitric components to varying degrees (see, e.g., Castorina et al. 2015). Because of the high volcaniclastic influx during the TST, the relative proportion of carbonate sedimentary lithics decreased.

During highstand (HST), sedimentary processes controlled the compo- sitional variance of these units. The result was that the volcanic lithic proportions decreased owing to weathering and prolonged and constant reworking in a marginal marine environment, producing a feldspathic to lithic-arenite petrofacies. Highstand sand shows values of Lv/Lt and Qm/ (Qm þ Lt) similar to sand of the LST (Fig. 2.12). Modal compositions also denote a decrease of lithic fragments (particularly carbonate extrabasinal fragments) and an increase of quartz grains moving from Tiber fluvial to beach sands where the sediments are further reworked by wave and eolian coastal processes (Fig. 2.10).

2.6.3 Compositional Characteristics of Low-Rank Sequences Forming the PGS

Definition of the same petrofacies trends recognized in the PGS in the low-rank sequences is more complex due to the short time spans covered by individual sequences, the lack of preservation of all systems tracts, and the high variability of facies that reflect the concomitant action of autogenic (see, e.g., Ethridge 1977; Mack 1978; Suttner et al. 1981; Winn et al. 1984; Garzanti 1986) and allogenic factors (Marchesini et al. 2000; Amorosi and Zuffa 2011), as well as the effect of chemical weathering as introduced above.

However, analysis of sand compositional variations in the low-rank sequences suggests the following:

1) The low-rank depositional sequences PG1, PG2, and PG3 were formed before the major explosive activity of the Monti Sabatini volcanic district and contain only sparse tephra layers. Sand in these sequences exhibits higher proportions of monomineralic quartz grains with respect to lithic fragments, and a slightly higher proportion of NCE with respect to CE at the transition from the LLST (late lowstand systems tract) to the TST of each sequence. This can be explained by reduced fluvial sediment supply to the coast during the relative sea-level rise phases. The lithic fragments, mainly extrabasinal carbonate grains, supplied along the coast were further abraded by eolian and wave processes, as well as longshore and rip currents, potentially virtually removing all of the softer extrabasinal carbonate grains whereas quartz grains survived abrasion. During the HST of the low-

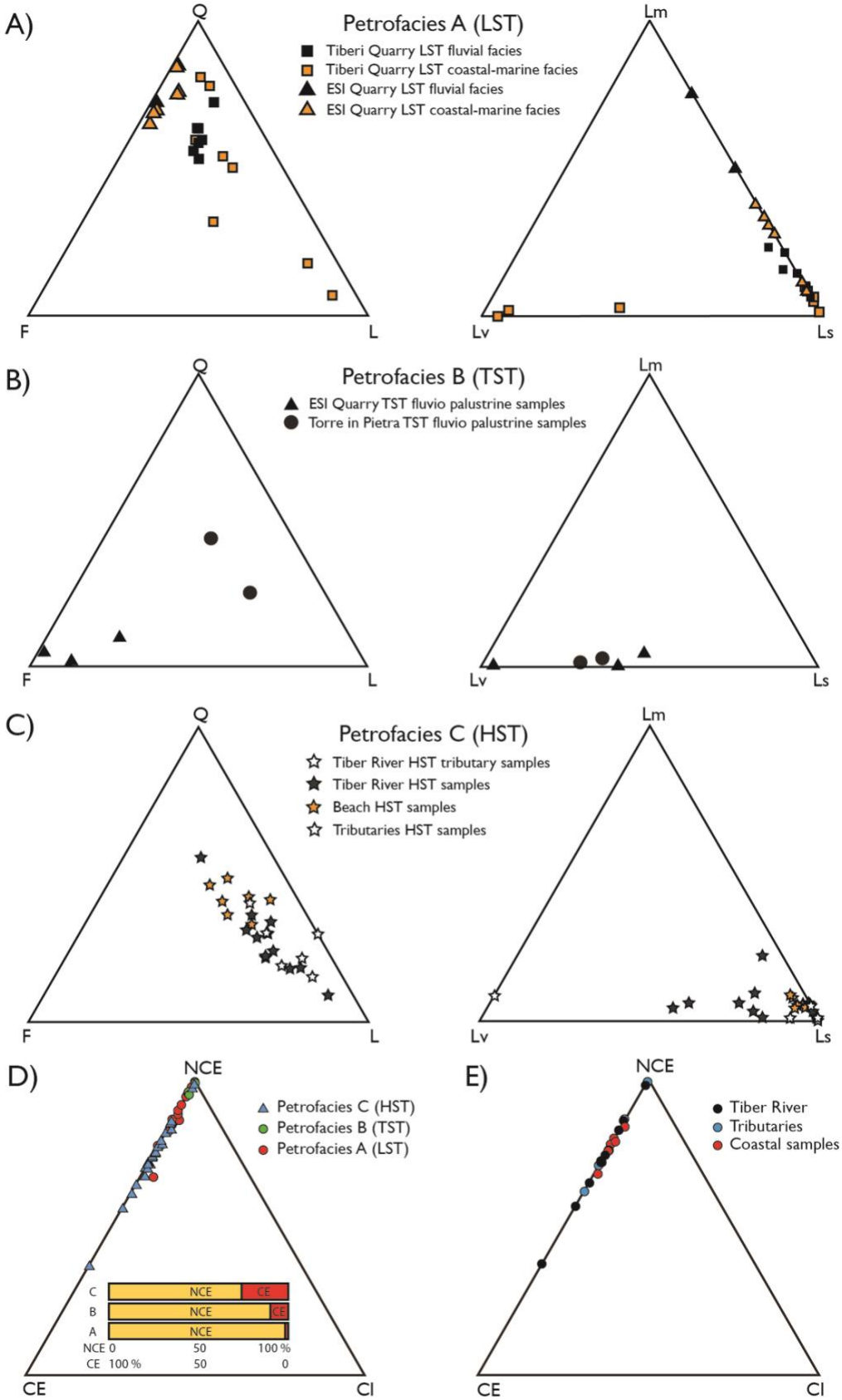

FIG. 2.10 —A, B, C) Quartz (Q), Feldspar (F), Lithic (L), metamorphic (Lm), volcanic (Lv), and sedimentary (Ls) lithic ternary plots for the PGS petrofacies associated with HST, TST, and LST deposits; D) NCE-CE-CI ternary plot for the PGS petrofacies; histograms relative percentages of NCE vs CE. CI values are minimal (, 1%) and not considered in the histograms; E) NCE-CE-CI ternary plot for the PGS highstand-systems-tract samples by depositional environment.

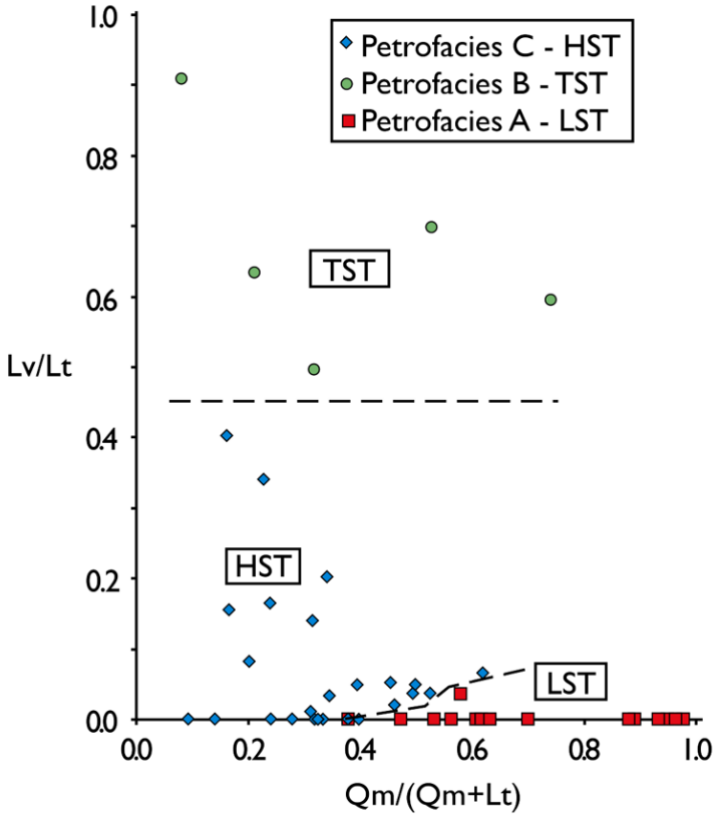

FIG. 2.12 —Compositional variation of PGS petrofacies based on parameters and ratios, after Ito (1994).

rank sequences NCE/CE and Q/L ratios are similar to those of the LLST, suggesting a return to similar depositional conditions. In general, the PG1 to PG3 sequences show some compositional variability among sequences and facies associations reflecting tectonic and paleo-geographic evolution in Pleistocene time and the effects of coastal reworking at the river mouth. Volcanic lithic fragments and phenocrysts increase up-section, reflecting the volcaniclastic input in the paleo–Tiber River drainage basin in Pleistocene time. Shoreface samples are generally more mature than fluvial samples in that they show higher quartz and lower feldspar and carbonate lithic proportions. Viewed in this light, the modifications of such ratios can be viewed as an expression of their changes both in time and space under the control of allogenic and autogenic factors.

2) The low-rank sequences formed during the major volcanic activity of the Sabatini volcanic complex (PG4, PG5, PG6, PG7, and PG8) record input of volcanic material derived from large explosive eruptions. As mentioned above, such sequences are stacked seaward due to the interaction among sea-level change, tectonic uplift, and volcanism, and mainly comprise fluvial and palustrine and/or lacustrine deposits that often filled incised valleys.

In contrast to the pre-volcanic sequences, which record a direct flux of sediments transported by the Tiber and its tributaries to the coastline, the evolution of the syn-volcanic sequences reflects a double provenance: 1) volcanic material derived from the explosive eruptions and 2) local sedimentary material derived from the erosion and cannibalization of the older pre-volcanic deposits, the latter being a result of concomitant sea- level change and tectonic uplift. This is reflected in modal compositions that show low sedimentary and high volcanic lithic fragment content.

3) The PG9 sequence is the only sequence formed post-volcanic activity; it is represented by Modern sand samples from the Tiber fluvial to coastal system. Being the most recent sequence, it best records the relationships between the inner and middle sectors of the Tiber drainage basin and the downstream sectors where fluvial and coastal processes interact at the Tiber River mouth. Monocrystalline quartz and feldspar grains are ubiquitous, whereas proportions of lithic fragments vary as a function of the different lithic contributions from tributaries draining diverse formations (Fig. 2.12).

In the upstream sectors sand composition reflects input from small tributaries draining Jurassic ophiolite, Jurassic to Oligocene limestone and siliciclastic units, and Miocene arenaceous, calcareous, clay-rich, and volcaniclastic foreland turbidites. Miocene turbidite units are the most likely sources for monomineralic and polymineralic quartz, potassium feldspar, plagioclase, dense minerals such as pyroxene, and siliciclastic and metamorphic lithic fragments. Carbonate lithic fragments and recycled carbonate bioclasts come from Jurassic to Oligocene limestone strata. Detrital serpentine grains with both foliated (serpentine schist) and cellular textures occur, suggesting derivation from erosion of the Jurassic ophiolites and/or from recycling of detrital-serpentine-bearing Oligo-Miocene turbidite strata (e.g., Garzanti et al. 2002; Amendola et al. 2016).

Samples from the middle sectors of the drainage basin show quartz/ feldspar ratios and percentages of pyroxene and dense-mineral proportions similar to the upper stream samples, but serpentine grains are notably absent. Monomineralic grains and metamorphic lithic fragments (Lma + Lmt) are likely reworked and recycled from Miocene foredeep sandy turbidites, while common carbonate lithics (Lsc(mic) + Lsc(cry)) were derived from limestone of the Umbria–Marche domain. Farther down-stream, samples show QFL and dense-mineral proportions similar to the middle sectors with feldspars, pyroxene, and feldspathoids, which are significant components found as monomineralic grains and phenocrysts in volcanic lithic fragments (Fig. 2.12). K-feldspar increases downstream with respect to plagioclase because of the high-K signature of the Roman Magmatic

volcanic rocks. Where the Tiber River drains mainly Mesozoic to Cenozoic sedimentary rocks there is a higher proportion of monomineralic quartz grains and limestone rock fragments, but carbonate lithic grains decrease rapidly in abundance downstream, likely through abrasion and dilution (see also McBride and Picard 1987). The increased effects of abrasion are documented in Figure 2.11 where the analyzed samples reach the highest rounding values (further discussed below).

The lower sectors of the Tiber drainage basin are characterized by volcaniclastic deposits and subordinate lavas, which are likely a major local sand source for samples collected in the city of Rome, which show significant amounts of feldspar and pyroxene grains present as detrital grains and as phenocryst phases in volcanic lithic fragments. The latter are very sensitive to dilution and abrasion (e.g., Cameron and Blatt 1971; Critelli et al. 1997), and their proportion in the downstream Tiber River drainage basin varies as a result of sediment input from tributaries draining volcaniclastics-rich lithologies, river transport, and weathering processes (see below). Lithic fragments include a significant quantity of volcanic and minor sedimentary and metamorphic lithic varieties. The presence of these grains reflects upstream input.

The composition of beach sand along the Lazio coast reflects sediment input from the Tiber River as well as reworking of sediment from the delta and associated coastal area. The beach samples are generally richer in quartz than the river samples (Fig. 2.12). They trend towards subequal amounts of quartz and lithic fragments. Pyroxenes are also significant and become dominant components in samples north of the Tiber River mouth, where small rivers draining volcanic rock outcrops feed the coast. Vitric volcanic lithic fragments are labile and weathered preferentially in the outcrop (see, for example, the PG5 deposits) releasing single pyroxene grains. Siliciclastic lithic fragments (Lsa þ Lsi) common in the coastal samples north of the Tiber River mouth could be derived from erosion of metamorphic-lithics-bearing turbiditic sandstone cropping out along the coast. This implies that the sediment was essentially carried south by longshore currents (Fig. 2.1B; see also Bellotti et al. 1993a). Bioclasts occurring along the present beach include modern fauna and recycled fossils.

2.6.4 Compositional Variability of Fluvial Sand in the PGS

The petrofacies change from LST to TST and finally to HST in the PGS reflects the evolution of the Tiber fluvial system through time, showing a trend of enrichment in lithic (volcaniclastic) debris, which highlights the importance of tectonic and volcanic control on PGS development (see QFL ternary diagram of Fig. 2.13A). Starting from the PG1 sequence (~ 860 ka) and during the LST, monomineralic and lithic compositions of fluvial samples suggest that the paleo–Tiber River was

draining carbonate and siliciclastic sedimentary rocks of the central and northern Apennines. From ~ 600 ka, at the beginning of the volcanic activity and during the TST, the river network abruptly changed; a morphological change of the Tiber River drainage basin occurred as a result of inland tectonic uplift and volcaniclastic input. The sedimentary lithic fraction was considerably diluted, and proportions of monomineralic quartz as well as volcanic lithic content increased (Fig. 2.13A, B), suggesting stream-network reorganization and/or a major erosion of the rapidly deposited pyroclastic material. From ~ 400 ka, volcanism was at its climax and supplied with its materials the Tiber River basin. The associated sand is rich in volcanic lithic fragments and pyroxene grains, suggesting that the tephra (both fall deposits and pyroclastic flows) that covered the landscape was easily eroded, producing a large volume of volcanic material subsequently transported downstream. This is particularly evident for the pyroxene grains, whose concentration increased due to either weathering of lavas and pyroclastic rocks or abrasive liberation during fluvial transport of glassy pyroclastic fragments. Although compositionally similar, there are differences between the TST and HST fluvial samples reflecting this increase of volcanic input and reworking of tephra deposits (Fig. 2.13B).

2.6.5 Other Controls on Composition and Texture of Tiber System Sand

Component Loss Owing to Weathering.—Carbonate and volcanic rocks (including volcaniclastics) that crop out in the Tiber drainage basin, as well as detritus derived from these sources, are susceptible to chemical weathering and pedogenic processes that reduce their percentages as lithic components through dissolution and alteration in outcrop and in soil horizons (McBride 1985). The low percentages of carbonate lithic fragments in the ancient Tiber River succession could be explained by such postdepositional weathering. To demonstrate the potential effects of dissolution of carbonate lithic, QFL percentages were calculated without including carbonate lithic fragments (QFL-c; Fig. 2.14A). On this plot, detrital modes show similar Q/F ratios with the only variance in composition attributable to possible volcanic input (Fig. 2.14B). Thus chemical dissolution could have been a major factor responsible for the lack of carbonate lithics in these sequences.

The effects of weathering on volcanoclastics-rich deposits (fall and pyroclastic flow deposits) is evaluated considering the types and percentages of volcanic lithic fragments and phenocryst phases in synvolcanic and postvolcanic deposits. Chemical weathering on poly-mineralic grains (e.g.,

volcanic lithic fragments) may cause, in fact, a rapid physical breakdown of that grain and thus make rock fragments more prone to chemical weathering (Grantham and Velbel 1988).

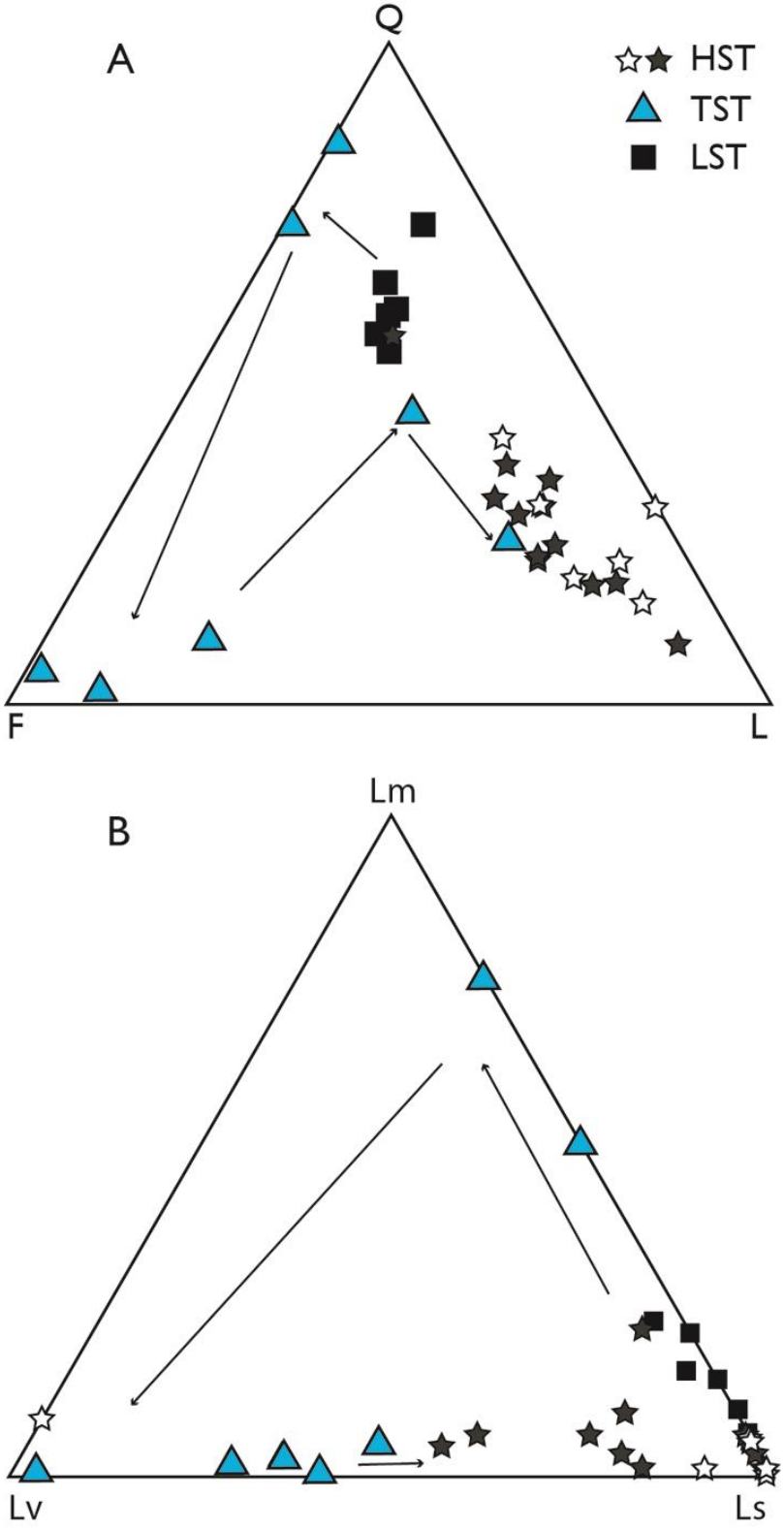

FIG. 2.13 —A) QFL and B) LmLvLs ternary plots showing the evolution of fluvial sand composition through time (late early Pleistocene to Holocene) in the Tiber Delta region.

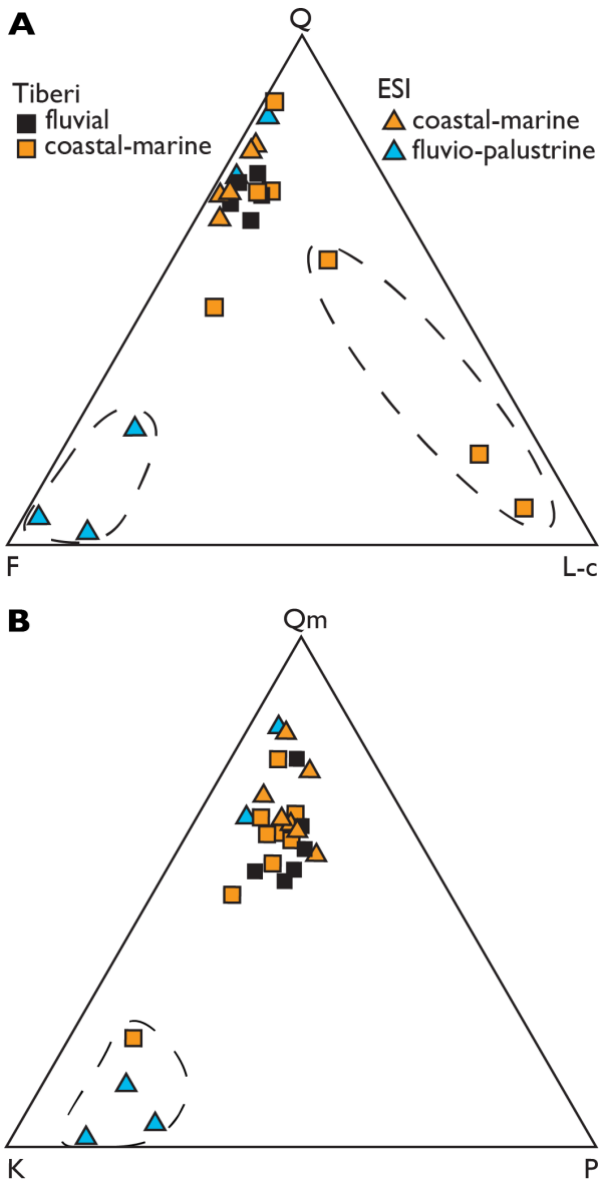

FIG. 2.14 —A) QFL-Lc and B) QmKP ternary plots of samples from the Tiberi and ESI quarry samples. Note that considering only the monomineralic fraction all the samples plot together except for the volcaniclastics-rich deposits (dotted circles).

The modal compositions of sequences formed during the major Sabatini volcanic activity (PG4 to PG8 sequences) are characterized by high percentages of glassy volcanic debris which is highly altered in paleosol intervals, leaving high concentrations of K-feldspar and pyroxene grains in a clay-rich soil horizon; in these soils plagioclase is mostly altered (see also Nesbitt and Young 1996; Borrelli et al. 2012) and the bulk geochemistry differs from equivalent intervals of reworked tephra (see also Castorina et al. 2015). In this respect, a distinction can be made between reworked and pedogenized pyroclastic rocks.

Both chemical weathering and mechanical abrasion are well recorded in postvolcanic modern beach samples that show a higher concentration of phenocryst phases with respect to volcanic lithic fragments. Modern beach samples show a high concentration of pyroxene grains and low volcanic

lithic proportions, suggesting either that the Tiber River and small rivers that feed the coast currently drain weathered volcanic rocks that produce less volcanic lithic fragments and more phenocryst phases, or that coastal reworking has preferentially concentrated these mineral phases (e.g., pyroxenes) in the foreshore and backshore subenvironments (see next section on hydraulic sorting).

Grain-Size Variations Owing to Hydraulic Sorting.—Hydraulic sorting is a process that can dramatically affect sediment composition, particularly with respect to the dense-mineral and micaceous fractions (e.g., Garzanti et al. 2009), which is why they are not used in sand classification schemes. Recent studies have documented relationships between grain size and sediment composition (e.g., Garzanti et al. 2015b), particularly in sediment derived from tectonically active landscapes such as that of the Tiber catchment, where sediment sources are dominated by young sedimentary rocks with volcanic input (James et al. 2007; Marsaglia et al. 2010). So representative samples were chosen from the Tiberi and ESI quarries and the modern Tiber River for modal analysis of the very fine to coarse sand fractions to explore. All of these show similar trends in composition (see Appendix A Fig. A1): decrease in quartz and an increase in feldspar and lithic content in the fine and very fine sand fractions; increase in K-feldspar with respect to plagioclase in the fine sand; and higher plagioclase in the very fine sand fractions.

Lithic fragments show different trends of enrichment in the finer grain-size fractions (see Appendix A Fig. A1). In the Tiberi quarry proportions of sedimentary lithic fragments generally increase in the fine and very fine sand fractions, although volcanic lithic fragments can be locally dominant components in the very fine sand fraction where the deposits record a sharp volcanic input (tephra events) related to an explosive phase of the Sabatini Volcanic District. In contrast, the samples from the ESI quarry show an increase in the metamorphic lithic fraction in the fine sand and similar lithic composition in the medium and very fine sand fractions. These differences might have resulted from mixing of two or more populations with distinct provenance and grain size derived from eastern and the northern sectors of the Tiber drainage basin (Fig. 2.1B), or from hydraulic sorting during fluvial sediment transport (see also Garcon et al. 2014 and Garzanti et al. 2015b).

Component Loss Owing to Abrasion.—Another means of component loss is through abrasion, which is manifested in the degree of grain rounding. Very few studies have measured sand-grain rounding along river systems, from the headwaters to the coastal zones (e.g., McBride and Picard 1987; Picard and McBride 2007). Downstream changes in roundness for quartz and carbonate lithic fragments (Lsc(cry) + Lsc(mic)) from samples collected from the Tiber River are shown in Figure 2.15.

Mean roundness of quartz and carbonate grains increases from subangular to subrounded from the headwaters to the lower reaches, likely due to the effects of sediment transport, with softer carbonate grains (micrite and sparite fragments) generally more rounded than quartz grains, and micrite more rounded than sparitic carbonate (Fig. 2.15). The parallel downstream trends in carbonate and quartz rounding reinforce the notion that this is indeed documentation of abrasion effects. These findings are similar to results from a short-headed, high-gradient stream in northwestern Italy where McBride and Picard (1987) found that limestone grains showed a downstream increase in roundness.

Mean roundness of beach samples (Qtz = 3.3; Carb = 4.1) is slightly higher than the more downstream river samples (Qtz = 2.9; Carb = 3.4); in particular quartz roundness of beach samples ranges from 2.8 to 3.7, values that are greater than those reported in McMaster et al. (2010) and Picard and McBride (1993). This might reflect a more extensive history of reworking of these grains related both to coastal eolian and wave transport (see Bellotti et al. 1993a, and also Dott 2003; Garzanti et al. 2015b).

Carbonate rock fragments also survive wave abrasion, in agreement with the observations of McBride and Picard (1987). There are greater differences between minimum and maximum carbonate roundness values than quartz roundness along the coast, suggesting that wave abrasion might be more effective on softer carbonate lithic fragments. These values range from 3.3 to 4.9 and are similar to roundness of beach sands from Elba Island, Italy (Picard and McBride 1993), including the observation that micrite carbonate grains are more rounded than sparite carbonate grains. However, beach sand likely includes nonrecycled bioclastic debris produced in the marine environment that may alter carbonate content and roundness values.

This study provides an opportunity to see downstream trends and changes to coastal environments as well as evaluate rounding trends in ancient sequences of similar provenance. Mean roundness of quartz and carbonate grains from the paleo-Tiber fluvial samples are very close to those of modern and ancient beach sand, suggesting that reworking in the coastal environment might have occurred or potentially facies have been misinterpreted as fluvial or have experienced eolian reworking. The analysis of mean roundness of quartz and carbonate grains in modern and ancient deposits defines a new approach to integrate to field observations for investigations and interpretation of fluvial to coastal deposits. Future work might provide a more detailed, statistically robust data set which along with grain-size distribution and sorting would help to clarify the

relationship between facies and sediment texture using the approach of Cameron and Blatt (1971), McBride and Picard (1987), and McMaster et al. (2010).

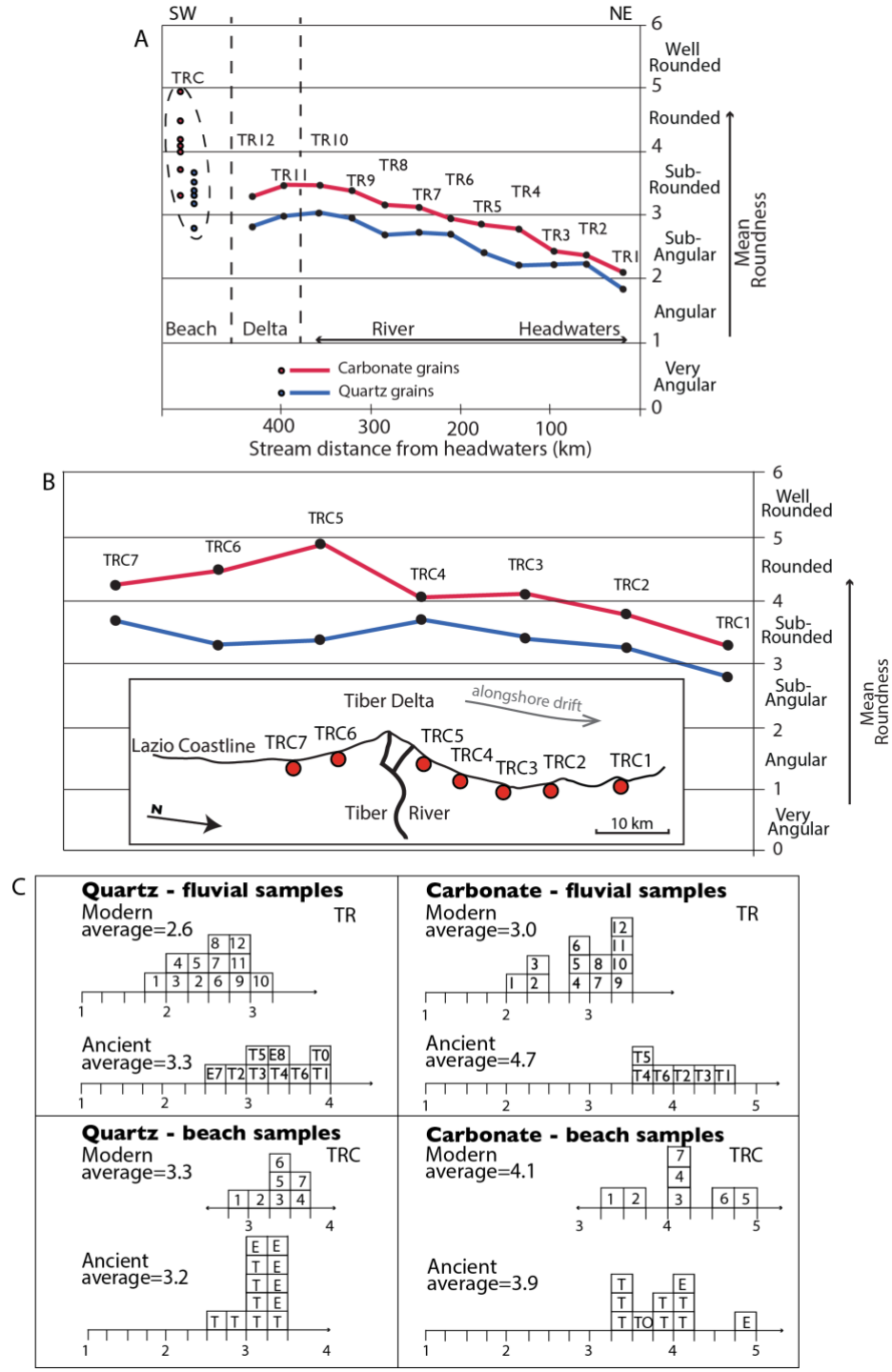

FIG. 2.15 — A) Changes in mean roundness of Tiber River fluvial sand from the headwaters to the lower reaches. Note that grain roundness of fluvial samples increases downstream for both quartz and carbonate grains. Range of TRC beach sample data (detailed in Part B below) are shown for comparison. B) Roundness of beach samples collected along Lazio coast. Note that beach samples are well rounded, particularly near the river mouth (TRC5), where wave reworking is likely more intense. Grey arrow shows the main direction of along shore drift (after Bellotti et al., 1994). C) Histogram of mean roundness for fluvial quartz and carbonate grains and beach quartz and carbonate grains from ancient and modern deposits. Note in Part C that quartz roundness from ancient deposits is greater than the modern quartz grains. Roundness of ancient fluvial carbonates is always greater than the modern fluvial carbonate grains. Note that ranges and average quartz roundness is similar for modern and ancient beach samples. Beach-carbonate roundness range is wider than beach-quartz roundness.

2.7 CONCLUSIONS

Tectonism, volcaniclastic input, and sea-level variations played a major role in the sequence-stratigraphic evolution of the Latium Tyrrhenian extensional margin, and their effects are recorded by sand compositional variations in the high-rank PGS and in the low-rank depositional sequences developed along the margin. Nevertheless, sediment mixing and reworking associated with depositional processes operating in the different sedimentary environments makes the interpretation of compositional trends very challenging. The high facies variability and the short time span covered by the succession allow the interpretation of petrofacies trends in the high- rank PGS, but a clear interpretation of the same petrofacies in the low-rank sequences is significantly more difficult, owing to the role of autogenic depositional processes that add to the effects of the allogenic ones. In the analysis of the PGS deposits, sediment generation not only is seen as a product of physical and chemical weathering but also takes also into account the penecontemporaneous volcanic activity and chemical–biogenic processes. Volcanic activity, in particular, played an important role in the PGS development resulting in a tripartite division of the entire succession: before, during, and after volcanic activity. Volcanism, through explosive phases, introduced a huge volume of material into the various environments that substantially modified sand composition of the low-rank sequences forming the PGS.

Tectonic evolution in the Tiber River drainage basin following Pleistocene volcanic activity played a major role controlling provenance and magnitude of erosion and stream-network reorganization in the Tiber drainage basin, which in turn is reflected in sand composition. Tectonic effects (regional uplift) overrode glacio-eustatic sea-level fluctuations and volcanism (throughout most of the succession), and controlled the overall composition of the PGS.

This study illustrates the complexity of interpreting compositional signatures applied to sequence stratigraphic interpretation. While compositional signals are clearer when analyzing stratigraphic units developed on a long temporal scale (high-rank sequences, about one million years), the interpretation of compositional trends is more complex when considering stratigraphic units developed on short temporal scales (low-rank sequences, 100 ka or less). However, comparing detrital signatures in the low-rank sequences helps define provenance, paleogeographic evolution, and the role of postdepositional weathering in the PGS succession. The detailed interpretation of the most recent and most complete low-rank sequence (the PG9 sequence) and compositional changes from upper to lower portion of the Tiber drainage basin and along the coastal system allows

the use of a model for the interpretation of ancient deposits. So the important implication of our study is that the Quaternary succession, being more complete and with a major control on facies, stacking pattern, and chronology of the stratigraphic units (low-rank and high-rank sequences), may allow a better understanding of the genetic factors responsible for petrographic changes that characterize the depositional sequences developed at various spatial and temporal scales along continental margins.

ACKNOWLEDGMENTS

This research was funded through grants to D. Tentori from the Geological Society of America, the California State University Northridge (Hannah Research Grant), and the Gene and Sue Fritsche Scholarship. Thanks to Richard Heermance for comments on a preliminary version of this manuscript. We also thank John Southard for his thorough copy editing and the AE of JSR (R. Ingersoll) and the reviewers S. Critelli and E. Garzanti for their constructive and detailed revision, which has led to significant improvements in the quality and clarity of this manuscript.

SUPPLEMENTARY MATERIAL - See Appendix A -

REFERENCES

AMENDOLA, U., PERRI, F., CRITELLI, S., MONACO, P., CIRILLI, S., TRECCI, T., AND RETTORI, R., 2016, Composition and provenance of the Macigno Formation (Late Oligocene–Early Miocene) in the Trasimeno Lake area (Northern Apennines): Marine and Petroleum Geology, v. 69, p. 146–167.

AMOROSI, A., 1995, Glaucony and sequence stratigraphy: a conceptual framework of distribution in siliciclastic sequences: Journal of Sedimentary Research, v. 65, p. 419– 425.

AMOROSI, A., AND ZUFFA, G.G., 2011, Sand composition changes across key boundaries of siliciclastic and hybrid depositional sequences: Sedimentary Geology, v. 236, p. 153– 163.

ANDO`, S., GARZANTI, E., PADOAN, M., AND LIMONTA, M., 2012, Corrosion of heavy minerals during weathering and diagenesis: a catalogue for optical analysis: Sedimentary Geology, v. 280, p. 165–178.

ARRIBAS, J., CRITELLI, S., LE PERA, E., AND TORTOSA, A., 2000, Composition of modern stream sand derived from a mixture of sedimentary and metamorphic rocks (Henares River, central Spain): Sedimentary Geology, v. 133, p. 27–48.

BARBERI, F., BUANASORTE, G., CIONI, R., FIORDELISI, A., FORESI, L., IACCARINO, S., LAURENZI, M.A., SBRANA, A., VERNIA, L., AND VILLA, I.M., 1994, Plio-Pleistocene geological evolution of the geothermal area of Tuscany and Lazio: Memorie Descrittive della Carta Geologica d'Italia, v. 49, p. 77–134.

BELLOTTI, P., CHIOCCI, F.L., MILLI, S., AND TORTORA, P., 1993a, Variabilita` nel tempo della distribuzione granulometrica sui fondali del delta del Tevere: Societa` Geologica Italiana, Bollettino, v. 112, p. 143–153.

BELLOTTI, P., CHIOCCHINI, U., CIPRIANI, N., AND MILLI, S., 1993b, I sistemi deposizionali nei sedimenti clastici pleistocenici affioranti nei dintorni di Ponte Galeria (SW di Roma): Societa` Geologica Italiana, Bollettino, v. 112, p. 923–941.

BELLOTTI, P., CHIOCCI, F.L., MILLI, S., TORTORA, P., AND VALERI, P., 1994, Sequence stratigraphy and depositional setting of the Tiber delta: integration of high resolution seismics, welllogs and archaeological data: Journal of Sedimentary Research, v. 64, p. 416–432.

BORDONI, P., AND VALENSISE, G., 1998, Deformation of the 125 ka marine terrace in Italy: tectonic implications, in Stewart, I.S., and Finzi, C.V., eds., Coastal Tectonics: Geological Society of London, Special Publication 146, p. 71–110.

BORRELLI, L., PERRI, F., CRITELLI, S., AND GULLA` G., 2012, Minero-petrographical features of weathering profiles in Calabria, southern Italy: Catena, v. 92, p. 196–207.

CAMERON, K.L., AND BLATT, H., 1971, Durabilities of sand size schist and ''volcanic'' rock fragments during fluvial transport, Elk Creek, Black Hills, South Dakota: Journal of Sedimentary Petrology, v. 41, p. 565–576.

CASTORINA, F., MASI, U., MILLI, S., ANZIDEI, A.P., AND BULGARELLI, G.M., 2015, Geochemical and Sr-Nd isotopic characterization of Middle Pleistocene sediments from the paleontological site of La Polledrara di Cecanibbio (Sabatini Volcanic District, central Italy): Quaternary International, v. 357, p. 253–263.

CATUNEANU, O., ABREU, V., BHATTACHARYA, J.P., BLUM, M.D., DALRYMPLE, R.W., ERIKSSON, P.G., FIELDING, C.R., FISHER W.L., GALLOWAY, W.E., GIBLING, M.R., GILES, K.A., HOLBROOK, J.M., JORDAN, R., KENDALL, C.G.ST.C., MACURDA, B., MARTINSEN, O.J., MIALL, A.D., NEAL, J.E., NUMMEDAL, D., POMAR, L., POSAMENTIER, H.W., PRATT, B.R., SARG, J.F., SHANLEY, K.W., STEEL, R.J., STRASSER, A., TUCKER, M.E., AND WINKER, C., 2009, Towards the standardization of Sequence Stratigraphy: Earth-Science Reviews, v. 92, p. 1–33.

CATUNEANU, O., GALLOWAY, W.E., KENDALL, C.G.ST.C., MIALL A.D., POSAMENTIER, H.W., STRASSER, A., AND TUCKER, M.E., 2011, Sequence stratigraphy: methodology and nomenclature: Newsletters on Stratigraphy, v. 44, p. 173–245.

CAVINATO, G., DE RITA, D., MILLI., S., AND ZARLENGA, F., 1992, Correlazione tra i principali eventi tettonici, sedimentari, vulcanici ed eustatici che hanno interessato l'entroterra (conche intrappenniniche) ed il margine costiero tirrenico laziale durante il Pliocene superiore ed il Pleistocene: Studi Geologici Camerti, Volume Speciale 1, p. 109–114.

CIONI, R., LAURENZI, M.A., SBRANA, A., AND VILLA, I.M., 1993, 40Ar/39Ar chronostratig- raphy of the initial activity in the Sabatini Volcanic Complex (Italy): Societa` Geologica Italiana, Bollettino, v. 112, p. 251–263.

COHEN, K.M., AND GIBBARD, P., 2011, Global chronostratigraphical correlation table for the last 2.7 million years: Cambridge, U.K., International Commission on Stratigraphy, Subcommission on Quaternary Stratigraphy.

CONATO, V., ESU, D., MALATESTA, A., AND ZARLENGA, F., 1980, New data on the Pleistocene of Rome: Quaternaria, v. 22, p. 131–176.

CONTICELLI, S., FRANCALIANCI, L., MANETTI, P., CIONI, R., AND SBRANA, A., 1997, Petrology and geochemistry of the ultrapotassic rocks from the Sabatini volcanic district, central Italy: the role of evolutionary process in the genesis of variably enriched alkaline magmas: Journal of Volcanology and Geothermal Research, v. 5, p. 107–136.

CRITELLI, S., AND LE PERA, E., 2002, Provenance relations and modern sand petrofacies in an uplifted thrust-belt, northern Calabria, Italy: Memorie Descrittive della Carta Geologica d'Italia, v. 61, p. 25–38.

CRITELLI, S., LE PERA, E., AND INGERSOLL, R.V., 1997, The effects of source lithology, transport, deposition and sampling scale on the composition of southern California sand: Sedimentology, v. 44, p. 653–671.

CRITELLI, S., MARSAGLIA, K.M., AND BUSBY, C.J., 2002, Tectonic history of a Jurassic backarc basin sequence (the Gran Can˜on Formation) based on compositional modes of tuffaceous deposits: Geological Society of America, Bulletin, v. 114, p. 515–527.

CRITELLI, S., ARRIBAS, J., LE PERA, E., TORTOSA, A., MARSAGLIA, K.M., AND LATTER, K.K., 2003, The recycled orogenic sand provenance from an uplifted thrust-belt, Betic Cordillera, southern Spain: Journal of Sedimentary Research, v. 73, p. 72–81.

CRITELLI, S., LE PERA, E., GALLUZZO, F., MILLI, S., MOSCATELLI, M., PERROTTA, S., AND SANTANTONIO, M., 2007, Interpreting siliciclastic–carbonate detrital modes in foreland basin systems: an example from upper Miocene arenites of the Central Apennines, Italy, in Arribas, J., Critelli, S., and Johnsson, M., eds., Sedimentary Provenance: Petrographic and Geochemical Perspectives: Geological Society of America, Special Paper 420, p. 107–133.

CROOK, K.A.W., 1960, Classification of arenites: American Journal of Science, v. 258, p. 419–428.

DE RITA, D., FUNICIELLO, R., CORDA, L., SPOSATO, A., AND ROSSI, U., 1993, Volcanic Units, in Di Filippo, M., ed., Sabatini Volcanic Complex: Consiglio Nazionale Delle Ricerche, Progetto Finalizzato ‘‘Geodinamica,’’ Monografie Finali 11, p. 33–79.

DE RITA, D., MILLI, S., ROSA, C., ZARLENGA, F., AND CAVINATO, G.P., 1994, Catastrophic eruptions and eustatic cycles: example of Lazio volcanoes: Atti dei Convegni Lincei, v. 112, p. 135–142.

DE RITA, D., FACCENNA, C., FUNICIELLO, R., AND ROSA, C., 1995, Stratigraphy and volcano- tectonics, in Trigila, R., The Volcano of the Albani Hills: Tipografia S.G.S., p. 33–71. DE RITA, D., FABBRI, M., MAZZINI, I., PACCARA, P., SPOSATO, A., AND TRIGARI, A., 2002,

Volcaniclastic sedimentation in coastal environments: the interplay between volcanism and Quaternary sea level changes (central Italy): Quaternary International, v. 95–96, p. 141–154.

DICKINSON, W.R., 1970, Interpreting detrital modes of graywacke and arkose: Journal of Sedimentary Petrology, v. 40, p. 695–707.

DI GIULIO, A., CERIANI A., GHIA, E., AND ZUCCA, F., 2003, Composition of modern stream sands Derived from sedimentary source rocks in a temperate climate (northern Apennines, Italy): Sedimentary Geology, v. 158, p. 145–161.

DOGLIONI, C., INNOCENTI, F., MORELLATO, C., PROCACCIANTI, D., AND SCROCCA, D., 2004, On the Tyrrhenian sea opening: Memorie Descrittive Carta Geologica Italiana, v. 44, p. 147– 164.

DOTT, R.H., 2003, The importance of eolian abrasion in supermature quartz sandstones and the paradox of weathering on vegetation free-landscapes: The Journal of Geology, v. 111, p. 387–405.

ETHRIDGE, F.G., 1977, Petrology, transport, and environment in isochronous upper Devonian sandstone and siltstone units, New York: Journal of Sedimentary Petrology, v. 47, p. 53–65.

FUNICIELLO, R., LOCARDI, E., AND PAROTTO, M., 1976, Lineamenti geologici dell’area sabatina orientale: Bollettino Societa` Geologica Italiana, v. 95, p. 831–849.

GANDOLFI, G., AND PAGANELLI, L., 1993, Le torbiditi arenacee Oligo-Mioceniche dell'Apennino settentrionale fra la Spezia ed Arezzo-Studio petrografico ed implicazioni paleogeografiche: Giornale di Geologia, v. 55, p. 93–102.

GANDOLFI, G., PAGANELLI, L., AND ZUFFA, G.G., 1983, Petrology and dispersal pattern in the Marnoso Arenacea Formation (Miocene, Northern Apennines): Journal of Sedimentary Petrology, v. 53, p. 493–507.

GANDOLFI, G., PAGANELLI, L., AND CAVAZZA, W., 2007, Heavy-mineral associations as tracers of limited compositional mixing during turbiditic sedimentation of the Marnoso- Arenacea Formation (Miocene, Northern Apennines, Italy): Amsterdam, Elsevier, Developments in Sedimentology, v. 58, p. 621–645.

GARCON, M., CHAUVEL, C., FRANCE-LANORD, C., LIMONTA, M., AND GARZANTI, E., 2014, Which minerals control the Nd–Hf–Sr–Pb isotopic compositions of river sediments?: Chemical Geology, v. 364, p. 42–55.

GARZANTI, E., 1986, Source rock versus sedimentary control on the mineralogy of deltaic volcanic arenites (Upper Triassic, Northern Italy): Journal of Sedimentary Petrology, v. 56, p. 267–275.

GARZANTI, E., 1991, Non-carbonate intrabasinal grains in arenites; their recognition, significance and relationship to eustatic cycles and tectonic setting: Journal of Sedimentary Petrology, v. 61, p. 959–975.

GARZANTI, E., 2016, From static to dynamic provenance analysis: sedimentary petrology upgraded: Sedimentary Geology, v. 336, p. 3–13.

GARZANTI, E., CANCLINI, S., FOGGIA, F.M., AND PETRELLA, N., 2002, Unraveling magmatic and orogenic provenance in modern sand: the back-arc side of the Apennine thrust belt, Italy: Journal of Sedimentary Research, v. 72, p. 2–17.

GARZANTI, E., ANDO`, S., VEZZOLI, G., AND DELL'ERA, D., 2003, From rifted margins to foreland basins: investigating provenance and sediment dispersal across desert Arabia (Oman, UAE): Journal of Sedimentary Research, v. 73, p. 572–588.

GARZANTI, E., ANDO`, S., AND VEZZOLI, G., 2009, Grain-size dependence of sediment composition and environmental bias in provenance studies: Earth and Planetary Science Letters, v. 277, p. 422–432.

GARZANTI, E., ANDO`, S., FRANCE-LANORD, C., GALY, V., CENSI, P., AND VIGNOLA, P., 2011a, Mineralogical and chemical variability of fluvial sediments. 2. Suspended-load silt (Ganga Brahmaputra, Bangladesh): Earth and Planetary Science Letters, v. 302, p. 107– 120.

GARZANTI, E., VEZZOLI, G., AND ANDO`, S., 2011b, Paleogeographic and paleodrainage changes during Pleistocene glaciations (Po Plain, northern Italy): Earth-Science Reviews, v. 105, p. 25–48.

GARZANTI, E., PADOAN, M., ANDO`, S., RESENTINI, A., VEZZOLI, G., AND LUSTRINO, M., 2013, Weathering and relative durability of detrital minerals in equatorial climate: sand petrology and geochemistry in the East African Rift: The Journal of Geology, v. 121, p. 547–580.

GARZANTI, E., RESENTINI, A., ANDO`, S., VEZZOLI, G., AND VERMEESCH, P., 2015a, Physical controls on sand composition and relative durability of detrital minerals during long- distance littoral and eolian transport (coastal Namibia): Sedimentology, v. 62, p. 971– 996.

GARZANTI, E., ANDO`, S., PADOAN, M., VEZZOLI, G., AND EL KAMMAR, A., 2015b, The Nile sediment system: processes and products: Quaternary Science Reviews, v. 130, p. 9–56. GIORDANO, G., ESPOSITO, A., DE RITA, D., FABBRI, M., MAZZINI, I., TRIGARI, A., ROSA, C., AND FUNICIELLO, R., 2003, The sedimentation along the roman coast between middle and upper Pleistocene: the interplay of eustatism, tectonics and volcanism new data and review: Il Quaternario, v. 16, p. 121–129.

GRANTHAM, J.H., AND VELBEL, M.A., 1988, The influence of climate and topography on rock-fragment abundance in modern fluvial sands of the southern Blue Ridge Mountains, North Carolina: Journal of Sedimentary Petrology, v. 58, p. 219–227.

IBBEKEN, H., AND SCHLEYER, R., 1991, Source and Sediment: A Case study of Provenance and Mass Balance at an Active Plate Margin (Calabria, Southern Italy): Berlin,Heidelberg, Springer-Verlag, 286 p.

INGERSOLL, R.V., 1983, Petrofacies and provenance of late Mesozoic forearc basin, northern and central California: American Association of Petroleum Geologists, Bulletin, v. 67, p. 1125–1142.

INGERSOLL, R.V., BULLARD, T.F., FORD, R.L., GRIMM, J.P., PIKLE, J.D., AND SARES, S.W., 1984, The effect of grain size on detrital modes: a test of the Gazzi-Dickinson point counting method: Journal Sedimentary Petrology, v. 54, p. 103–116.

ITO, M., 1994, Compositional variation in depositional sequences of the upper part of the Kasuza Group, a middle Pleistocene forearc basin fill in the Boso Peninsula, Japan: Sedimentary Geology, v. 88, p. 219–230.

JAMES, D.E., DEVAUGHN, A.M., AND MARSAGLIA, K.M., 2007, Sand and gravel provenance in the Waipaoa River System: sedimentary recycling in an actively deforming forearc basin, North Island, New Zealand, in Arribas J., Critelli, S., and Johnsson, M., eds., Sedimentary Provenance:

Petrographic and Geochemical Perspectives: Geological Society of America, Special Paper 420, p. 253–276.

KARNER, D.B., MARRA, F., AND RENNE, P.R., 2001, The history of the Monti Sabatini and Alban Hills volcanoes: groundwork for assessing volcanic–tectonic hazards for Rome: Journal of Volcanology and Geothermal Research, v. 107, p. 185–219.

LAWTON, T.F., POLLOCK, S.L., AND ROBINSON, R.A.J., 2003, Integrating sandstone petrology and nonmarine sequence stratigraphy: application to the Late Cretaceous fluvial systems of southwestern Utah, U.S.A: Journal of Sedimentary Research, v. 73, p. 389–406.

LE PERA, E., AND CRITELLI, S., 1997, Sourceland controls on the composition of beach and fluvial sand of the Tyrrhenian coast of Calabria, Italy: implications for actualistic petrofacies: Sedimentary Geology, v. 110, p. 81–97.

LEOMBRUNI, A., BLOIS, L., AND MANCINI, M., 2009, First evaluation of soil erosion and sediment delivery in the high part of the Tevere watershed: Electronic Journal of Geotechnical Engineering, v. 14, p. 1–26.

LOCARDI, E., LOMBARDI, G., FUNICIELLO, R., AND PAROTTO, M., 1976, The main volcanic group of Lazio (Italy): relations between structural evolution and petrogenesis: Geologica Romana, v. 15, p. 279–300.

MALINVERNO, A., AND RYAN, W.B.F., 1986, Extension in the Tyrrhenian Sea and shortening in the Apennines as result of arc migration driven by sinking of the lithosphere: Tectonics, v. 5, p. 227–245.

MACK, G.H., 1978, The survivability of labile light mineral grains in fluvial, eolian, and littoral environments: the Permian Cutler–Cedar Mesa formations, Utah: Sedimentology, v. 25, p. 587–604.

MANCINI, M., AND CAVINATO, G.P., 2005, The Middle Valley of the Tiber River, central Italy: Plio-Pleistocene fluvial and coastal sedimentation, extensional tectonics and volcanism, in Blum, M., Marriot, S., and Leclair, S., eds., Fluvial Sedimentology VII: International Association of Sedimentologists, Special Publication 35, p. 373–396.

MARCHESINI, L., AMOROSI, A., CIBIN, U., SPADAFORA, E., ZUFFA, G.G., AND PRETI, D., 2000, Detrital supply versus facies architecture in the late Quaternary deposits of the south- eastern Po Plain (Italy): Journal of Sedimentary Research, v. 70, p. 829–838.

MARIANI, M., AND PRATO, R., 1988, I bacini Neogenici costieri del margine tirrenico: approccio sismico-stratigrafico: Societa` Geologica Italiana, Memorie, v. 41, p. 519–531. MARRA, F.,

DEOCAMPO, D., JACKSON, M.D., AND VENTURA, G., 2011, The Alban Hills and Monti Sabatini volcanic products used in ancient Roman masonry (Italy): an integrated stratigraphic, archeological, environmental and geochemical approach: Earth-Science Reviews, v. 108, p. 115–136.

MARRA, F., SOTTILI, G., GAETA, M., GIACCIO, B., JICHA, B., MASOTTA, M., PALLADINO, D.M., AND DEOCAMPO, D.M., 2014, Major explosive activity in the Monti Sabatini Volcanic District (central Italy) over the 800–390 ka interval: geochronological–geochemical overview and tephrostratigraphic implications: Quaternary Science Reviews, v. 94, p. 74–101.

MARSAGLIA, K.M., 1992, Petrography and provenance of volcaniclastic sands recovered from the Izu–Bonin Arc, Leg 126: Proceedings of the Ocean Drilling Program, Scientific Results, v. 126, p. 139–154.

MARSAGLIA, K.M., AND TAZAKI, K., 1992, Diagenetic trends in ODP Leg 126 sandstone: Proceedings of the Ocean Drilling Program, Scientific Results, v. 126, p. 125–138.

MARSAGLIA K.M., LATTER, K.K., AND CLINE, V., 1999, Sand provenance in the Alborian and Tyrrhenian basins: Proceedings of the Ocean Drilling Program, Scientific Results, v. 161, p. 37–56.

MARSAGLIA, K.M., DEVAUGHN, A.M., JAMES, D.E., AND MARDEN, M., 2010, Provenance of fluvial terrace sediments within the Waipaoa sedimentary system and their importance to New Zealand source-to-sink studies: Marine Geology, v. 270, p. 84–93.

MARSAGLIA K.M., BARONE M., CRITELLI S., BUSBY C., AND FACKLER-ADAMS, B., 2016, Petrography of volcaniclastic rocks in intra-arc volcano-bounded to fault-bounded basins of the Rosario segment of the Lower Cretaceous Alisitos oceanic arc, Baja California, Mexico: Sedimentary Geology, v. 336, p. 138–146.

MCBRIDE, E.F., 1985, Diagenetic processes that effect provenance determination in sandstone, in Zuffa, G.G., ed., Provenance of Arenites: Dordecht, Reidel, p. 95–114. MCBRIDE, E.F., AND PICARD, M.D., 1987, Downstream changes in sand composition, roundness, and gravel size in a short-headed high-gradient stream, north-western Italy: Journal of Sedimentary Petrography, v. 57, p. 1018–1026.

MCMASTER, K., WHITMORE, J.H., AND STROM, R., 2010, A comparison of beach and dune sands along the southern Oregon coast, USA: Geological Society of America, Abstracts with Programs, v. 42, p. 311–322.

MILLI, S., 1994, High-frequency sequence stratigraphy of the middle–late Pleistocene to Holocene deposits of the Roman Basin (Rome, Italy): relationships among high frequency eustatic cycles,

tectonics and volcanism, in Posamentier, H.W., and Mutti, E., eds., Second High-Resolution Sequence Stratigraphy Conference: Tremp, Spain, p. 20– 27.

MILLI, S., 1997, Depositional setting and high-frequency sequence stratigraphy of the middle–upper Pleistocene to Holocene deposits of the Roman Basin: Geologica Romana, v. 33, p. 99–136.

MILLI, S., AND MOSCATELLI, M., 2001, The Torre in Pietra section: sedimentology and physical stratigraphy: Poster session, 1st International Congress, The World of Elephants, Rome, 16–20 October.

MILLI, S., AND PALOMBO, M.R., 2011, Stratigrafia fisica e assetto deposizionale della successione del tardo Pleistocene inferiore/Olocene del Bacino Romano, in Milli, S., Palombo, M.R., and Anzidei, A.P., eds., I depositi pleistocenici di Ponte Galeria e la Polledrara di Cecanibbio: Congresso Aiqua Roma, 2011, Il Quaternario Italiano, Conoscenze e prospettive, Guida all'Escursione Post-congresso Roma 26 Febbraio, p. 2– 27.

MILLI, S., MOSCATELLI, M., PALOMBO, M.R., PARLAGRECO, L., AND PACIUCCI, M., 2008, Incised-valleys, their filling and mammal fossil record: a case study from Middle-Upper Pleistocene deposits of the Roman Basin (Latium, Italy): GeoActa, Special Publication, v. 1, p. 67–88.

MILLI, S., D'AMBROGI, C., BELLOTTI, P., CALDERONI, G., CARBONI, M.G., CELANT, A., DI BELLA, L., DI RITA, F., FREZZA, V., MAGRI, D., PICHEZZI, R.M., AND RICCI, V., 2013, The transition from wave-dominated estuary to wave-dominated delta: the Late Quaternary stratigraphic architecture of Tiber River deltaic succession (Italy): Sedimentary Geology, v. 284–285, p. 159–180.

MILLI, S., MANCINI, M., MOSCATELLI, M., STIGLIANO, F., MARINI, M., AND CAVINATO, G.P., 2016, From river to shelf, anatomy of a high-frequency depositional sequence: the late Pleistocene–Holocene Tiber depositional sequence: Sedimentology, v. 63, p. 1886-1928.

MITCHUM, R.M., JR., AND VAN WAGONER, J.C., 1991, High-frequency sequences and their stacking pattern: sequence stratigraphy evidence of high-frequency eustatic cycles: Sedimentary Geology, v. 70, p. 131–170.

MORTON, A.C., AND HALLSWORTH, C., 2007, Stability of detrital heavy minerals during burial diagenesis, in Mange, M.A., and Wright, D.T., eds., Heavy Minerals in Use: Amsterdam, Elsevier, Developments in Sedimentology, v. 58, p. 215–245.

NESBITT, H.W., AND YOUNG, G.M., 1996, Petrogenesis of sediments in the absence of chemical weathering: effects of abrasion and sorting on bulk composition and mineralogy: Sedimentology, v. 42, p. 341–358.

PARRA, J.G., MARSAGLIA, K.M., RIVERA, K.S., DAWSON, S.T., AND WALSH, J.P., 2012, Provenance of sand on the Poverty Bay shelf, the link between source and sink sectors of the Waipaoa River sedimentary system: Sedimentary Geology, v. 280, p. 208–233.

PATACCA, E., SARTORI R., AND SCANDONE P., 1990, Tyrrenian basin and Apenninic arc: kinematic relations since late Tortonian times: Societa` Geologica Italiana, Memorie, v. 45, p. 425–451.

PECCERILLO, A., 2005, Plio-Quaternary Volcanism in Italy: Petrology, Geochemistry, Geodynamics: Heidelberg, Springer, 365 p.

PICARD, M.D., AND MCBRIDE, E.F., 1993, Beach sands of Elba Island, Tuscany, Italy: Roundness study and evidence of provenance, in Johnsson, M.J., and Basu, A., eds., Processes Controlling the Composition of Clastic Sediments: Geological Sociey of America, Special Paper 284, p. 235–246.

PICARD, M.D., AND MCBRIDE, E.F., 2007, Comparison of river and beach sand composition with source rocks, Dolomite Alps and drainage basin, northeastern Italy, in Arribas, J., Critelli, S., and Johnsson, M.J., eds., Sedimentary Provenance and Petrogenesis: Perspectives from Petrography and Geochemistry: Geological Society of America, Special Paper 420, p. 1–12.

POTTER, P.E., HUH, Y., AND EDMOND, J.M., 2001, Deep-freeze petrology of Lena River sand, Siberia: Geology, v. 29, p. 999–1002.

SEYRAFIAN, A., AND TORABY, H., 2009, Petrofacies and sequence stratigraphy of the Qom Formation (Late Oligocene–Early Miocene?), north of Nain, southern trend of central Iranian Basin: Carbonates and Evaporites, v. 20, p. 82–90.

SOTTILI, G., PALLADINO, D.M., AND ZANON, V., 2004, Plinian activity during the early eruptive history of the Sabatini Volcanic District, Central Italy: Journal of Volcanology and Geothermal Research, v. 135, p. 361–379.

SOTTILI, G., PALLADINO, D.M., MARRA F., JICHA B., KARNER, D.B., AND RENNE, P., 2010, Geochronology of the most recent activity in the Sabatini Volcanic District, Roman Province, central Italy: Journal of Volcanology and Geothermal Research, v. 196, p. 20– 30.

SUTTNER, L.J., BASU, A., AND MACK, G.H., 1981, Climate and the origin of quartzarenites: Journal of Sedimentary Petrology, v. 51, p. 1235–1246.

TENTORI, D., 2015, Sand compositional changes as a key for sequence-stratigraphic interpretation: the Pleistocene Tiber River deltaic succession (Italy) [Master's Thesis]: California State University, Northridge, 88 p.

VALLONI, V., AND ZUFFA, G.G., 1984, Provenance changes for arenaceous formations of the northern Apennines, Italy: Geological Society of America, Bulletin, v. 95, p. 1035–1039. VELBEL,

M.A., 2007, Surface textures and dissolution processes of heavy minerals in the sedimentary cycle: examples from pyroxenes and amphiboles, in Mange, M.A., and Wright, D.T., eds., Heavy Minerals in Use: Amsterndam, Elsevier, Developments in Sedimentology, v. 58, p. 112–150.

WELTJE, G.J., 2006, Ternary sandstone composition and provenance: an evaluation of the ‘‘Dickinson model,’’ in Buccianti, A., Mateu-Figueras, G., and Pawlowsky-Glahn, V., eds., Compositional Data Analysis: From Theory to Practice: Geological Society of London, Special Publication 264, p. 611–627.

WINN, R.D., JR., STONECIPHER, S.A., AND BISHOP, M.G., 1984, Sorting and wave abrasion: controls on composition and diagenesis in lower Frontier Sandstones, southwestern Wyoming: American Association of Petroleum Geologists, Bulletin, v. 68, p. 268–284.

ZUFFA, G.G., 1980, Hybrid arenites, their composition and classification: Journal of Sedimentary Petrology, v. 50, p. 21–29.

ZUFFA, G.G., 1985, Optical analyses of arenites: influence of methodology on compositional results, in Zuffa, G.G., ed., Provenance of Arenites: NATO-ASI, Dordrecht, Reidel, p. 165–189.

ZUFFA, G.G., 1987, Unravelling hinterland and offshore palaeo-geography from deepwater arenites, in Leggett, J.K., and Zuffa, G.G., eds., Marine Clastic Sedimentology, Models and Case Studies: London, Graham and Trotman, p. 39–61.

ZUFFA, G.G., 1991, On the use of turbidite arenites in provenance studies: critical remarks, in Morton, A.C., Todd, S.P., and Haughton, P.D.W., eds., Developments in Sedimentary Provenance Studies: Geological Society of London, Special Publication 57, p. 21–28.

ZUFFA, G.G., CIBIN, U., AND DI GIULIO, A., 1995, Arenite petrography in sequence stratigraphy: Journal of Geology, v. 103, p. 451–459.

CHAPTER 3: A SOURCE-TO-SINK COMPOSITIONAL MODEL OF A PRESENT HIGHSTAND: AN EXAMPLE IN THE LOW-RANK TIBER DEPOSITIONAL SEQUENCE (LATIUM TYRRHENIAN MARGIN, ITALY)

DANIEL TENTORI[1], SALVATORE MILLI[1], AND KATHLEEN M. MARSAGLIA[2]

[1]Dipartimento di Scienze della Terra, SAPIENZA Università di Roma, Piazzale Aldo Moro 5, 00185 Roma, Italy

[2]Department of Geological Sciences, California State University Northridge, 18111 Nordhoff Street, Northridge, California, U.S.A.

Published in *Journal of Sedimentary Research (2018)*, v. 88, no. 10, 1238-1259

ABSTRACT: Our source-to-sink compositional model of sediment distribution in the present highstand of the Tiber Depositional Sequence has important implications for sediment source lithology, generation, transport, and deposition. In the Tiber River system, sand compositional trends reflect provenance mixing, anthropic intervention, and the effects of local autogenic factors in continental to marine depositional environments. Fluvial feldspatho- quartzo-lithic sand results from the contribution of the major tributaries of the Tiber drainage basin, which can be divided into two sub-basins separated by the Corbara dam built in the 1950s. Upstream-drainage-basin sand has a siliciclastic sedimentary lithic signature, whereas carbonate and volcanic lithic fragments dominate downstream- drainage-basin sand. Downstream sand is further modified in the coastal environment by hydraulic sorting, and mixed with detritus derived from the recycling of coastal dune sand and altered volcaniclastic paleosols. The latter are associated with lower-course floodplain and channel deposits, which produce a quartzo-feldspatho-lithic sand. Sediment grain-size zonation in the marine environment is influenced by coastal hydrodynamics, which, in turn, produce two detrital populations with distinct compositional signatures and hydraulic behavior. Coarser minerals (essentially pyroxene phenocrysts) and finer feldspar grains are progressively concentrated in higher-energy and lower-energy environments, respectively. Biogenic continental shelf and slope deposits off the Tiber River mouth show very little riverine influence. This study of the last highstand system tract in the Tiber Depositional Sequence clarifies the effects of hydraulic sorting, grain-size dependence, and sediment reworking in controlling the final composition of

modern sand. This knowledge can be used to better understand detrital modes of ancient sedimentary successions.

3.1 INTRODUCTION

The source-to-sink concept has been applied to modern and ancient sedimentary systems to characterize their various components from source areas to basin sinks (e.g., Carter et al. 2002, 2010; Critelli et al. 2003; Marsaglia et al. 2010; Parra et al. 2012; Garzanti et al. 2015; Anderson et al. 2016; Bentley et al. 2016; Kuehl et al. 2016) and to quantitatively assess the sediment flux from inland to the coastal zone and into the deep basin (sediment budgets) (e.g., Brommer et al. 2009; Covault et al. 2011; Weltje and Brommer 2011; Guillocheau et al. 2012; Amorosi et al. 2016). Allogenic processes such as tectonics, climate, and sea-level or base-level changes are among the main factors controlling the genesis, transport, and degree of preservation of sediments. However, further compositional modifications occur during inland and marine transport (e.g., reworking and hydraulic sorting) and after deposition in different depositional systems in response to autogenic forcing (McBride 1985; Garzanti 1986; Le Pera and Critelli 1997; Critelli et al. 1997; McBride and Picard 1997; Critelli et al. 2003; Marsaglia et al. 2007; Garzanti et al. 2015). Consequently, reconstructing sediment transfer from source area to the final sink, from basinal sequence stratigraphic units of different rank and age, is complex. In particular, the influence of allogenic and autogenic factors is differently recorded in each sequence-stratigraphic unit and often impossible to separate, especially in ancient sedimentary successions. On the contrary, Quaternary successions, particularly late Pleistocene to Holocene successions can offer well-preserved archives, where many variables can be described and quantified, and relationships among stratigraphic architecture and sea-level, climate, and tectonic forcing can be better constrained (Blum et al. 2013).

In the Mediterranean area, modern continental and marine sediments have been investigated to show relationships among sediment provenance, composition, and depositional environments (e.g., Critelli and Le Pera 1994, 2002; Critelli et al. 2003; Zaghloul et al. 2009; Garzanti et al. 2009, 2015; Perri et al. 2012; Reddad et al. 2016). These studies demonstrate that autogenic vs. allogenic controls (sedimentary differentiation versus provenance and time-dependent effects) can be estimated through several compositional parameters (e.g., Q/F, Q/L, dense-mineral concentrations, MI 1⁄4 mineralogical maturity index). However, very few studies have analyzed how physical and chemical weathering processes act on composition during an entire sedimentary route from source

to sink (e.g., Le Pera and Critelli 1997; Marchesini et al. 2000; Critelli et al. 2003; Le Pera and Arribas 2004; Garzanti et al. 2011, 2015; Ando` et al. 2012). Consequently, the analysis of modern fluvial and beach, as well as shelf and deep-marine sand composition, is a useful tool to capture provenance information and to correct for physical and chemical weathering processes acting during onland, shoreface, and offshore sediment transport.

Study of the modern Tiber provenance from source to sink may provide better understanding of development of axial drainage and deltaic environments in response to tectonic extension, volcanic input, and glacio- eustatic changes from the early Pleistocene to the Holocene. The Quaternary succession of the Roman basin, which includes Pleistocene to Holocene fluvial, coastal, and deltaic deposits associated with the Tiber River, has recently been analyzed by comparing data derived from provenance, composition, and sequence-stratigraphy (Garzanti et al. 2002; Milli et al. 2016; Tentori et al. 2016; with references therein). However, compositional data from the modern Tiber River system comprising the last 6 kyr (the present highstand phase) are limited to continental and subaerial parts of the fluvio-delta system. In this study, we integrate new data collected from cores from the submarine delta-front and prodelta settings with quantitative sand petrology from the modern Tiber River for a detailed compositional analysis from source to sink. Analysis of sediment distribution along the Tyrrhenian coasts provides information about entry points of detritus and dispersal patterns of deep-sea sediments (cf. Garzanti et al. 2002). Also, detailed examination of the Tiber River coast, beach, and shelf sand clarifies the effects of hydraulic sorting, grain size, and sediment transport on the composition of modern sand. Analysis of grain-size distribution in depositional environments is crucial to interpreting facies- related detrital modes (cf. Garzanti et al. 2009). The purpose of this study is to define compositional trends along the modern Tiber River, river mouth, coast, and shelf sectors, creating a source-to-sink model to constrain relationships among provenance, sand composition, depositional environment, and stratigraphic architecture of the Tiber wave-dominated deltaic succession in the context of Holocene climatic variability.

Results from this study are also compared with sand detrital modes from deep-marine cores recovered at Ocean Drilling Program (ODP) Site 974 (Tyrrhenian basin) on ODP Leg 161, as these sediments were previously interpreted as being sourced by the Tiber River (e.g., Marsaglia et al. 1999). Data collected in this study could potentially test this hypothesis.

3.2 TIBER SEDIMENTARY SYSTEM

The Tiber River is located in the west-central region of the Italian Peninsula. It originates in the Apennine Mountains and flows 406 km through Umbria and Latium to the Tyrrhenian Sea, a sector of central Italy with a complex tectonic evolution, resulting in highly variable structural, magmatic, and stratigraphic signatures (Fig. 3.1). The 17,000 km^2 Tiber River drainage basin includes part of the northern-central Apennines, where siliciclastic, carbonate, and volcaniclastic rocks crop out (Fig. 3.2). The siliciclastic and carbonate highlands of the northern-central Apennines are the watershed separating the Adriatic and the Tyrrhenian river domains. The Tiber Delta has developed along the Tyrrhenian Sea, a margin affected by extensional tectonics since the late Miocene, in connection with opening of the back-arc Tyrrhenian Basin, in turn related to eastward migration of west-directed Apennines subduction (Malinverno and Ryan 1986; Patacca et al. 1990; Doglioni et al. 2004, with references therein). Extensional tectonics during the middle Pleistocene was coeval with intense volcanic activity of the Roman Magmatic Province (De Rita et al. 1993, 1994; Peccerillo 2005), which dominates the southwestern part of the Tiber drainage basin. Along the Tyrrhenian margin, northwest– southeast normal faulting and northeast–southwest transverse systems generated clastic basins during Pliocene and Pleistocene time (Mariani and Prato 1988; Barberi et al. 1994, with references therein). The Roman Basin is one of these basins (Fig. 3.1); it extends north and south of the Tiber Delta for about 135 km and was mainly filled with sediment provided by the Tiber River. Evolution of this basin was accompanied by continuous regional uplift (Milli 1997; Bordoni and Valensise 1998; Giordano et al. 2003) and by intense volcanic activity, reaching its climax in the middle– late Pleistocene (Locardi et al. 1976; Cioni et al. 1993; De Rita et al. 1993, 1995; Karner et al. 2001; Peccerillo 2005). Consequently, the stratigraphic framework of the Roman Basin represents the close interaction among tectonic uplift, volcanic activity, and Quaternary glacio-eustatic sea-level fluctuations (Cavinato et al. 1992; De Rita et al. 1994, 2002; Milli 1994, 1997; Giordano et al. 2003; Mancini and Cavinato 2005; Milli et al. 2008, and references therein). All this gave rise to accumulation of several low- rank depositional sequences (sensu Mitchum and Van Wagoner 1991; Catuneanu et al. 2009, 2011), with durations from 30 to 120 kyr, that are stacked to form two high-rank composite sequences known as the Monte Mario Sequence (MMS: lower Pleistocene) and the Ponte Galeria Sequence (PGS: upper lower Pleistocene to Holocene)(Milli 1997; Milli et al. 2013, 2016 and references therein) (Fig. 3.3).

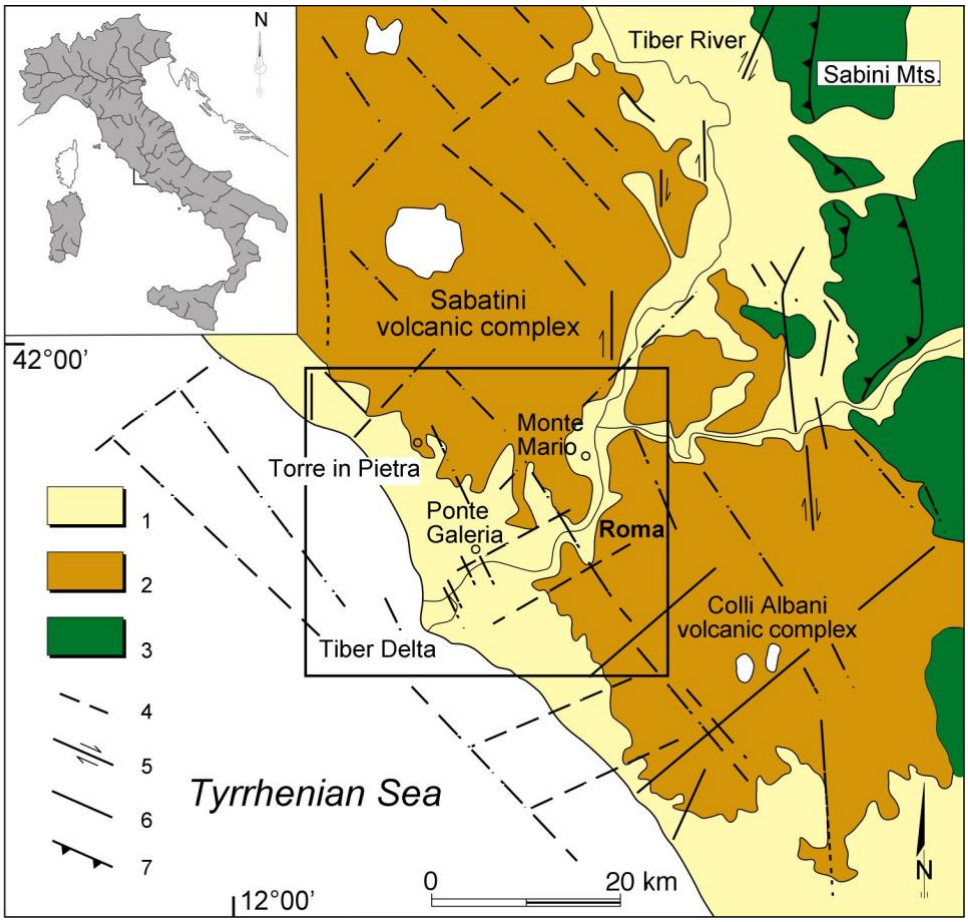

FIG. 3.1 —Geological sketch of the central Tyrrhenian margin of Italy. (1) Messinian–Holo- cene sedimentary deposits; (2) Pliocene–Pleisto- cene lavas and volcaniclastic deposits; (3) Mesozoic–Cenozoic sedimentary deposits; (4) main buried faults; (5) strike-slip faults; (6) normal faults; (7) major thrusts. The black square indicates the fluvial downstream and marine study area (modified from Milli et al. 2016).

The MMS, having limited outcrops in the study area, has been studied through subsurface data and the stratigraphy of numerous wells. The most complete PGS, which crops out between the city of Rome and the Tyrrhenian Sea, ranges in thickness from 10 to 110 meters, including fluvial, fluvio-palustrine-lacustrine, barrier-island lagoon, and transitional- shelf depositional systems intercalated with volcaniclastic products from the Albani and Sabatini volcanic complexes. The PGS is a composite sequence formed by twelve low-rank sequences organized to constitute lowstand (LST), transgressive (TST), and highstand (HST) system tracts. The six oldest low-rank sequences (from PG01 to PG3) stack to form the Late LST (Milli et al. 2016). Sequences from PG4 to part of PG8 constitute the TST, whereas the PG9 sequence (the Tiber Depositional Sequence, TDS) developed entirely during the HST of the PGS (Milli et al. 2016) (Fig. 3.3).

The goal of this paper is to analyze sand compositional variability of the HST related to the Tiber Depositional Sequence in order to verify the influence of allogenic and autogenic processes in this source-to-sink system.

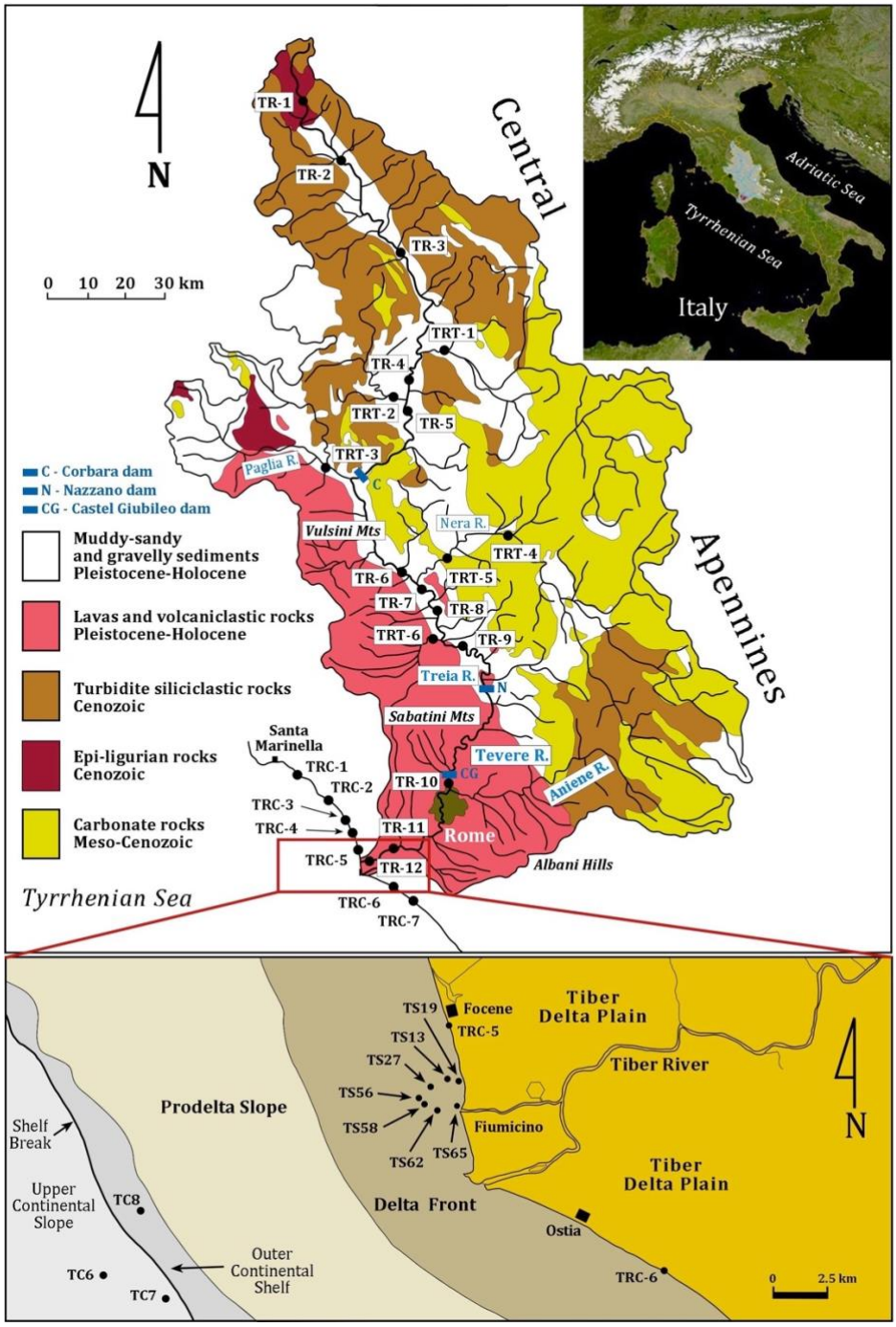

FIG. 3.2 —Tiber River and main geologic units that crop out within the catchment. Tiber River (TR), Tiber River tributary (TRT), Tiber foreshore (TRC), Tiber shoreface (TS), and Tiber continental shelf (TC) sample locations correspond to numbered filled circles (modified from Tentori et al. 2016). Geology is from Bellotti et al. (1994).

3.3 THE TIBER DEPOSITIONAL SEQUENCE

The TDS is one of the most complete low-rank depositional sequences developed in the Mediterranean area during the last glacial–interglacial cycle of post-Tyrrhenian age (last 120 kyr) (Figs. 3.3, 3.4). The lower boundary of the TDS is an erosional surface formed during the sea-level

fall following the last highstand phase correlated to MIS 5.5. The TDS succession ranges from , 1 m to 80 m and documents the transition from a wave-dominated estuary to a wave-dominated delta. The upper TDS boundary is represented by the modern depositional surface (see more details in Milli et al. 2013, 2016). A stratal stacking pattern characterized by forestepping-downstepping, forestepping-upstepping, backstepping, and upstepping-forestepping allow for the recognition in the TDS of the LST (early and late), TST, and HST systems tracts (Fig. 3.4). During LST, falling, stillstand, and initial sea-level rise allowed development of the Tiber-incised valley and subsequent deposition of fluvial, lagoonal, and beach deposits. With sea-level rise during the TST, the Tiber-incised valley evolved into a wave-dominated estuary. The TST represents the most developed systems tract of the TDS, showing a facies architecture characterized by a retrogradational stacking pattern of a sinuous fluvial system, a few bayhead deltas, a coastal-barrier-lagoon system, and a shelf depositional system. During the HST, as the rate of sea-level rise decreased, a prograding wave-dominated cuspate delta developed (Fig. 3.5). High-resolution seismic profiles illustrate prograding clinoforms down- lapping onto the present outer shelf (Bellotti et al. 1994; Milli et al. 2016) (Fig. 3.4). The HST documents a very complex paleoenvironmental evolution of the Tiber River, owing to the marked climatic variability of the Holocene in the Mediterranean area. During early Holocene (8000 to 6000 cal yr BP) northern Italy was characterized by humid winters and dry summers, whereas southern Italy had humid winters and summers. This pattern reversed after the mid-Holocene (4000 to 2000 cal yr BP), with drier conditions in the south and wetter conditions in the north (Peyron et al. 2013). However, according to Sadori et al. (2013), the Mediterranean area experienced an overall increasing dryness due to climate oscillations and human impact from the mid-Holocene to the present, which has also been responsible for decreasing river discharge today.

In the Tiber area during the first phase of the HST (6000–2700 yr BP) (Fig. 3.5A), the paleo–Tiber Delta prograded at a rate of 1 m/yr and beach ridges developed along the coast; during the same period the sedimentation rate in the outer-shelf sector was approximately 0.45 mm/yr. For the second phase (2700–1900 yr BP) (Fig. 3.5B), foraminiferal assemblages, oxygen and carbon isotopic values, and variations in sediment discharges provide evidence for two cool and warm periods (Di Bella et al. 2013). The most important event characterizing this period was shifting of the Tiber River mouth about 3 km southward. This event corresponded with a cold phase in the Mediterranean area (Incarbona et al. 2010) that should be coincident with the Bond cycle B2 (Bond et al. 1997). The Tiber Delta prograded at a rate of 5–6 m/yr, allowing for development of the entire deltaic system (Fig. 3.5B). Also during this period, and after 2350–2400 yr BP, delta growth was interrupted, and

an important erosive phase occurred about 1650 yr BP, in connection with decrease of Tiber floods (Bellotti et al. 2011; Giraudi 2011). This process was amplified by the impact of human activities (i.e., construction of Claudio and Traiano harbors), which were particularly severe during Roman Imperial times. Major changes have occurred also during the last 2000 yr due to anthropogenic influence, coastal erosion, and major river floods shaping the present cuspate delta (Fig. 3.5C).

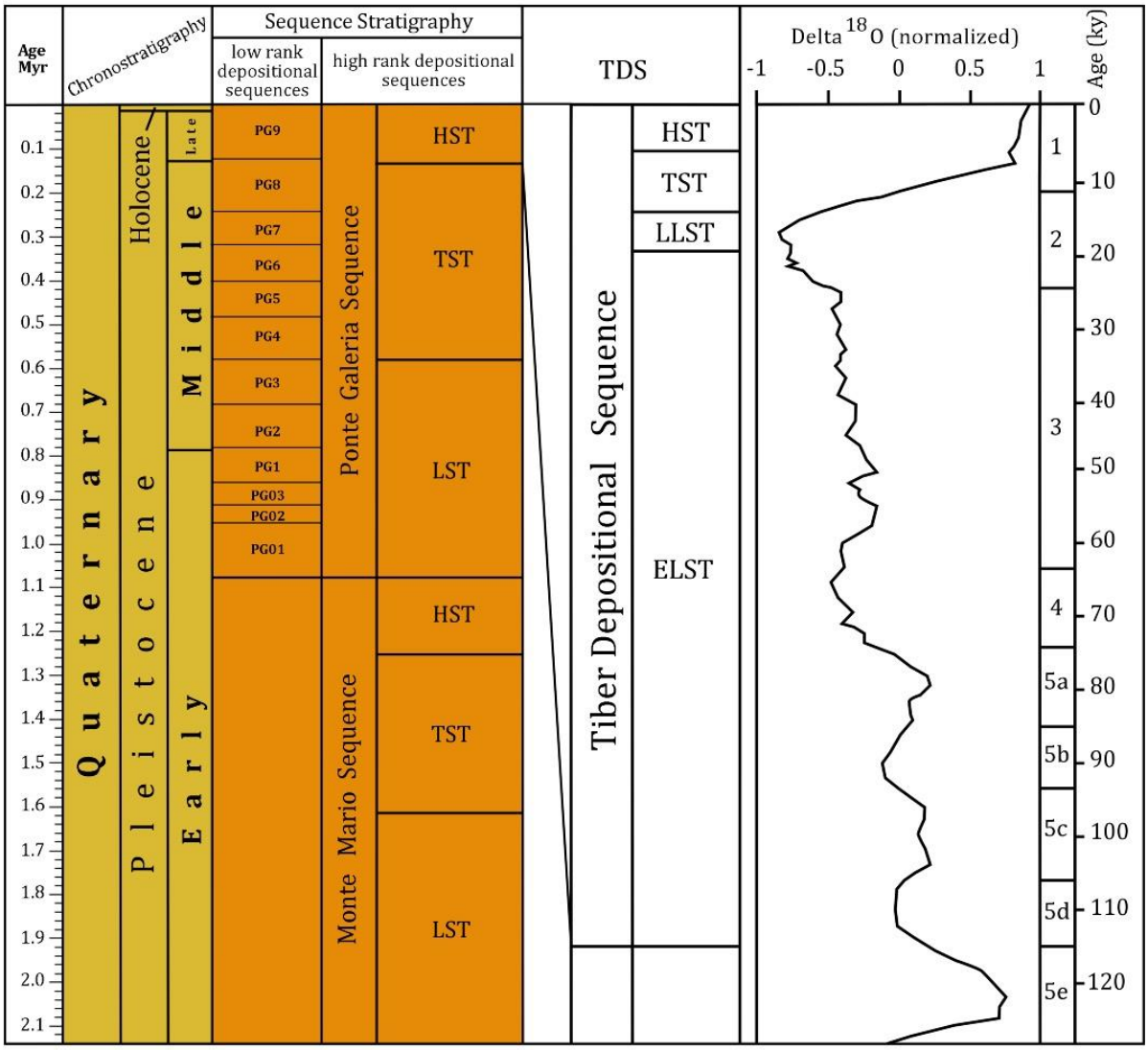

FIG. 3.3 —Chronostratigraphic and sequence- stratigraphic scheme of the Quaternary deposits of the Roman Basin modified after Milli et al. (2013). Abbreviations are as follows: HST, high- stand systems tract; TST, transgressive systems tract; LST, lowstand systems tract; ELST, early lowstand systems tract; LLST, late lowstand systems tract.

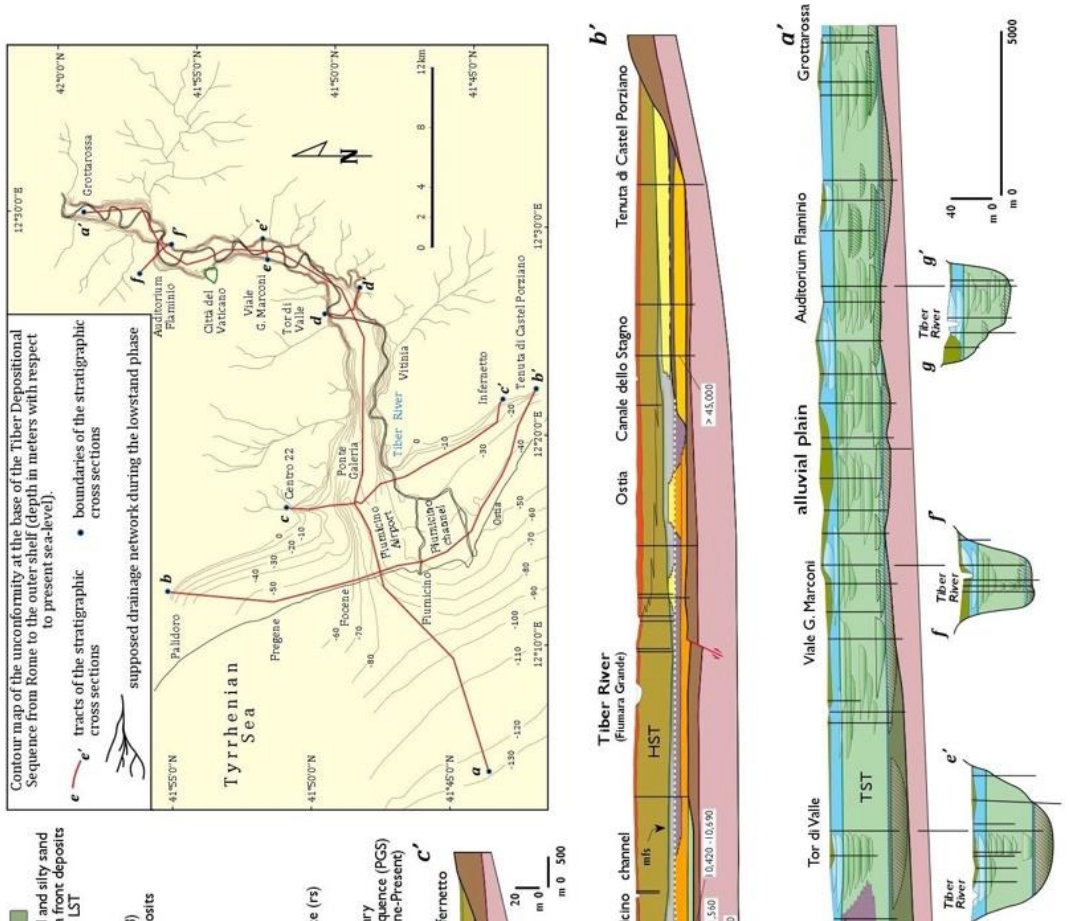

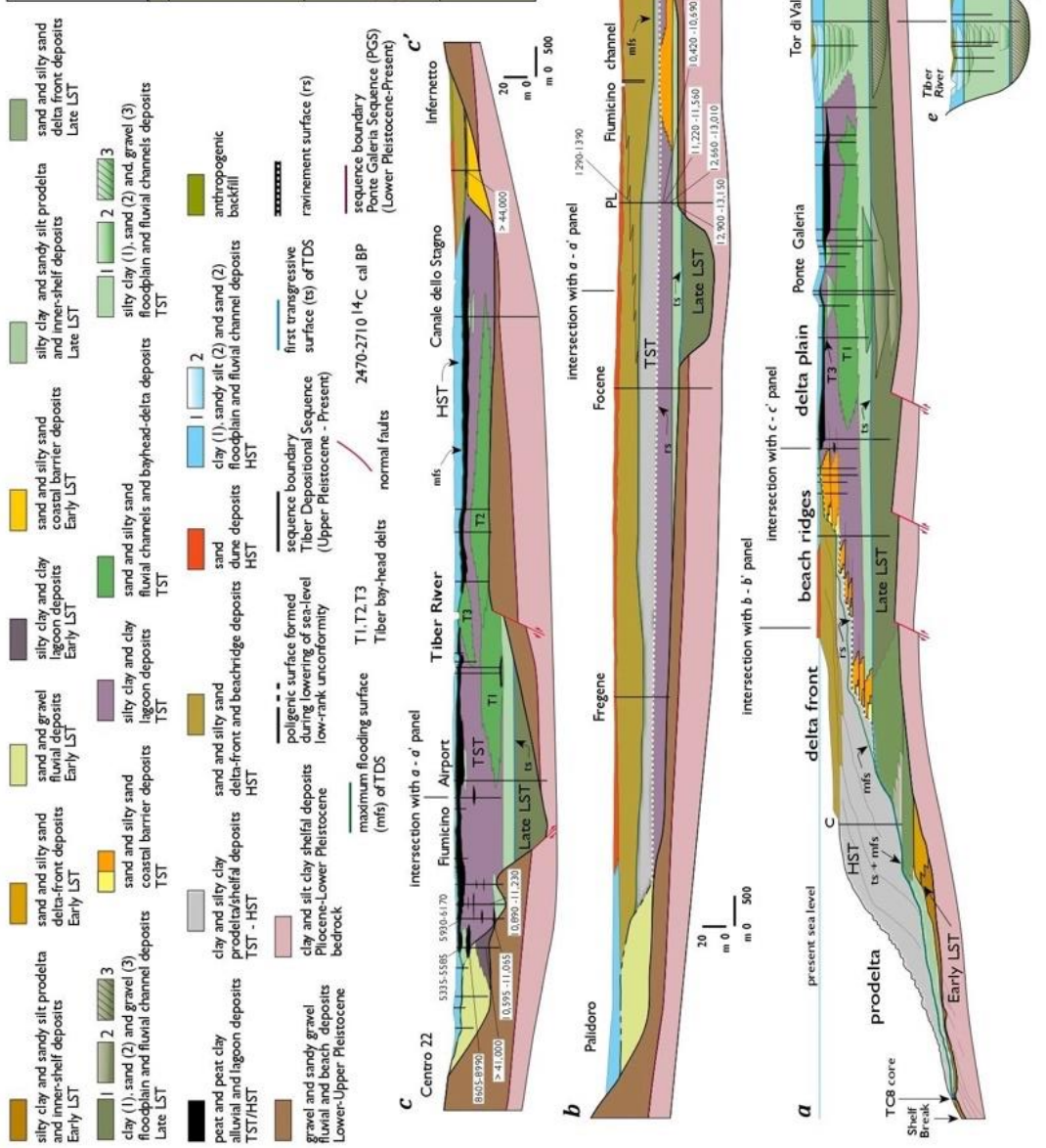

FIG. 3.4.—Stratigraphic cross sections showing the depositional architecture of the Tiber Depositional Sequence (modified after Milli et al. 2016).

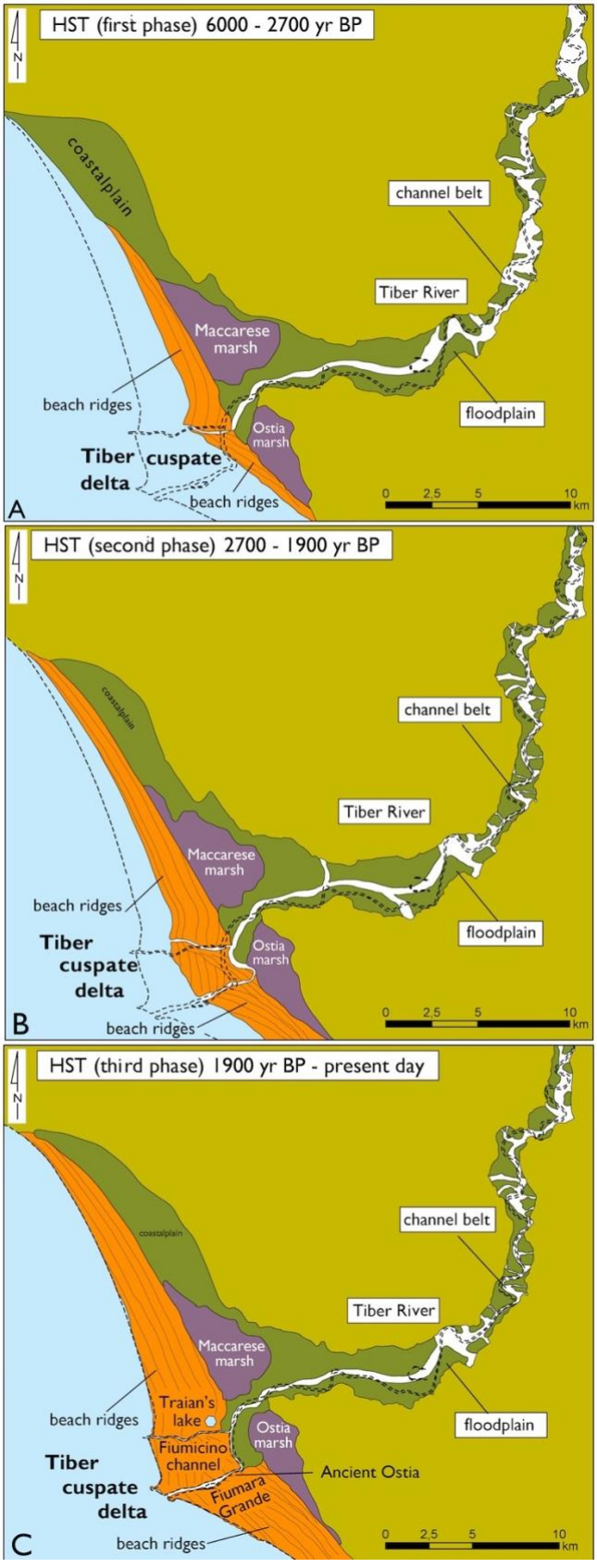

FIG. 3.5 —Paleogeographical sketches showing evolution of the Tiber River during the last 6000 years. The colors in the figures reflect the different depositional environments as labeled.

3.4 STUDY AREA

3.4.1 Tiber Drainage Basin

The modern Tiber river drainage basin (Fig. 3.2) can be subdivided into two main sub-basins: the upstream Tiber drainage basin up to the confluence with the Paglia River, and the downstream drainage basin and its main tributaries (Paglia, Nera, Treia, and Aniene) (see also Bersani and Bencivenga 2001). Oligocene to Miocene siliciclastic turbidite successions are exposed in the upstream Tiber river drainage basin, which has an area of 6077 km2. The downstream Tiber drainage basin, with area 5343 km2, exposes Oligocene to Pliocene fine-grained marine sediments, Jurassic to Miocene carbonate successions, and Plio-Pleistocene volcanic units of the Vulsini, Vico, Sabatini, and Colli Albani volcanic centers (Fig. 3.2). The Tiber River flow rate increases below the Nera, Treia, and Aniene river confluence (downstream tributaries), whereas the Chiascio and Nestore rivers (upstream tributaries) provide smaller contributions, which are almost entirely limited to the winter season (Boni et al. 1993). The Tiber River average flow rate is 230 m3/s, with highest peaks reaching 3000 m3/s. Sediment discharge underwent drastic changes in the 1960s, varying from 12 3 109 kg/yr to 1 3 109 kg/yr owing to construction of the Corbara dam a few kilometers upstream of the Paglia confluence with the Tiber River. Recent studies documenting the pluviometric regime in 1990 (Bencivenga et al. 1995) record maximum average annual precipitation rate during fall (October–November) and minimum rates during summer (July–August). Highest peaks in precipitation are correlated with the main historical Tiber River flood events (Bencivenga et al. 1995; Bersani and Bencivenga 2001).

3.4.2 Morphodynamics of the Tiber Delta

The Tiber delta extends along the Tyrrhenian coast for about 35 km inland and ~ 10–15 km offshore, reaching a maximum water depth of 110 m. Main wave directions are from south, west, and southwest. According to Bortoluzzi et al. (1982), storm waves are able to mobilize sediments to a depth of 30 m. It is classified as a wave-dominated delta with microtidal regime (tidal range 0.4–0.6 m). The Tiber delta is affected by a general northwestward longshore current (velocity 0.10 and 0.25 m/s; Lechi and Todisco 1980), which deflects the river plume contributing to asymmetrical growth of the delta (Belfiore et al. 1987; Bellotti et al. 1994; Chiocci and La Monica 1996) (Fig. 3.6). Estimates of the longshore potential solid transport are about 120,000 m3/year northward and 100,000 m3/year southward, respectively (Noli et al. 1996). A saltwater plume intrudes the Tiber River for tens of kilometers upstream (Mikhailova et al. 1999).

The Tiber delta can be subdivided into four morphodynamic zones (Bellotti et al. 1994; Tortora 1995; Bellotti and Tortora 1996): the upper and the lower delta plain, the delta front, and the prodelta slope (Fig. 3.6). The upper delta plain consists of alluvial fine-grained muddy sediments related to floods of the Tiber River; it is also characterized by the presence of two marshy ponds (Stagno di Ponente and Stagno di Levante), which were reclaimed in 1884. Present sedimentary processes are entirely confined within the two main channels (Fiumicino and Fiumara Grande), which supply sediment to the coast. The lower delta plain consists of ancient sandy beach ridges, with dune and interdune ponds marking the recent progradation phase of the delta (the last 5700 yr). The delta front can be subdivided into upper and lower parts. The former includes beach and upper and lower shoreface, up to 10 m depth. The latter forms a gentle submarine slope (about 0.38) extending for about 4–6 km to 20–25 m depth. In the delta front, wave processes are very intense, allowing the formation of littoral cells and associated rip currents that are particularly active during storm events (Noli et al. 1996). Sediment is reworked along shore by persistent longshore currents with average speed of littoral drift of about 25–120 cm/s to the NW (Lechi and Todisco 1980; Caputo et al. 1987).

The prodelta slope of muddy deposits can be subdivided into upper and lower parts. The upper part, extending down to 70 m water depth, has a convex-up profile, a slope of about 18, and a step-like morphology due to synsedimentary creep (Tommasi et al. 1998). The lower part extends down to water depth of 115 m, has a gradient of about 0.88, and shows a smooth morphology that merges with the outer continental shelf (gradient of about 0.58). The latter, partially fed by the Tiber delta, is covered by mud and hosts the heads of 15 gullies near the shelf break at about 150 m depth that extend down the continental slope to a maximum depth of 400 m.

3.4.3 Grain-Size Distribution across the Tiber Delta and Coastal Dynamics

Grain-size distribution of the emerged and submerged sectors of the Tiber delta reflects the action of several erosional and depositional processes that are active in the drainage basin, at the Tiber mouth and surrounding beaches. During flood events, the Tiber River transports sandy and muddy sediments essentially as bedload and suspended load, respectively, whereas during normal flow conditions, most of the transported sediment is represented by mud (Bersani and Bencivenga 2001). Sediment load of the Tiber River has been strongly reduced since the 1950s due to construction of the Corbara, Nazzano, and Castel Giubileo dams in the lower and middle courses of

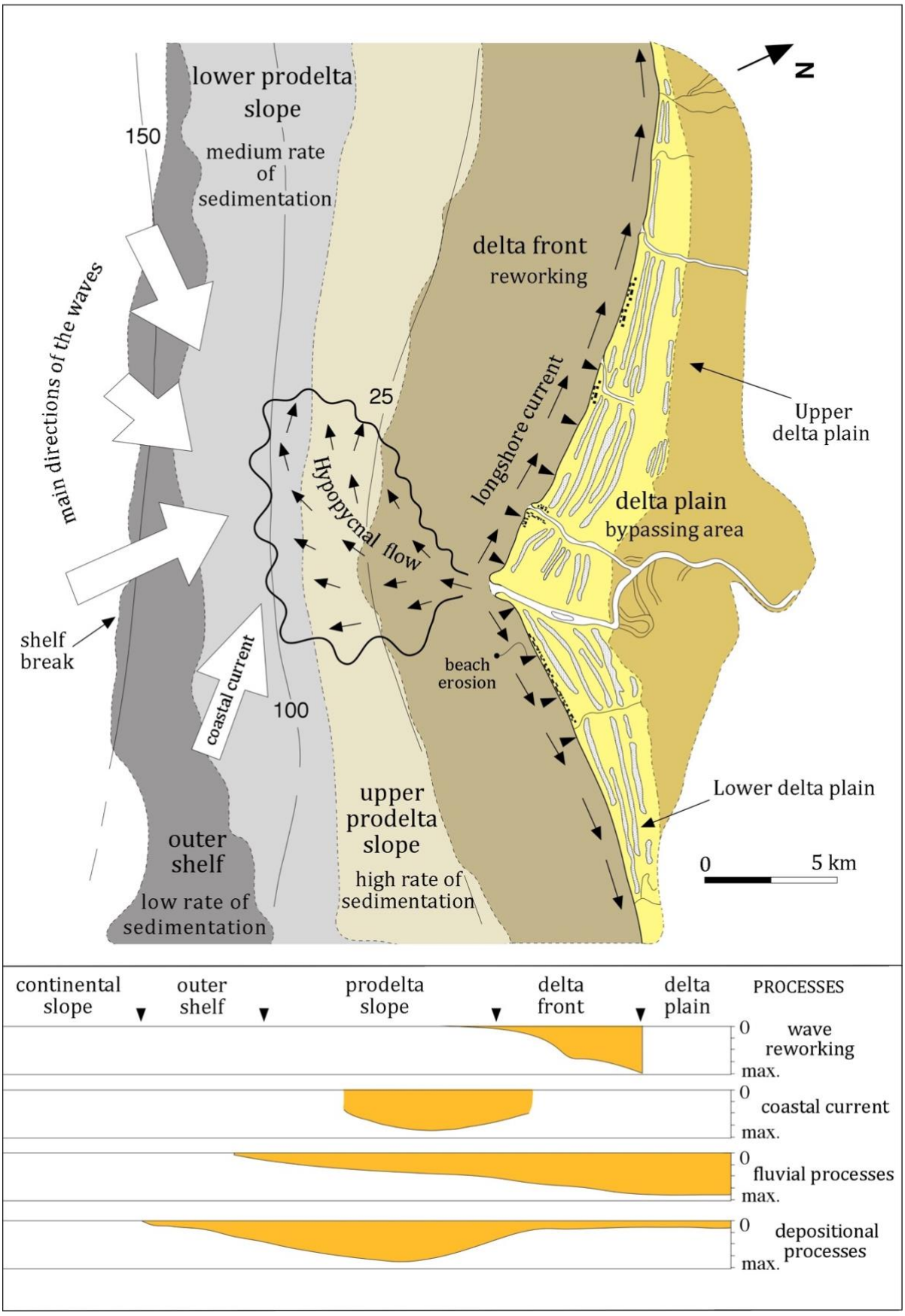

FIG. 3.6 —Main erosional and depositional processes occurring off the Tiber River mouth. Modified after Bellotti et al. (1994).

the Tiber River (Fig. 3.2). This has reduced the sediment to beaches close to the river mouth, which have since been affected by strong erosion. At present, the beaches are artificially nourished and protected by shore defenses (Ferrante et al. 1993; Hanson et al. 2002).

Grain-size distribution along the beaches north and south of the Tiber River mouth varies in response to fluvial and wave dynamics (Bellotti et al. 1993; Bellotti and Tortora 1996; Tortora 1999). Most sediments are medium-to-coarse quartzose sand with high concentrations of heavy minerals (Belfiore et al. 1987). The beaches farther from the river mouth are composed of fine to medium sand with lower percentages of heavy minerals (Belfiore et al. 1987).

In the submerged part of the Tiber delta, the pattern of grain-size distribution varies along the depositional profile (Bellotti et al. 1993; Bellotti and Tortora 1996). Sand and silty sand dominate the upper delta front, whereas the lower delta front is characterized by sandy silt. The upper prodelta slope is essentially sandy silt and sandy mud, whereas the lower prodelta slope consists of mud to clay. Previous studies show that the major textural variations along the delta depositional profile occur on the delta front (between –10 and –20 m), where fluvial and marine processes interact with different intensities over time. Seaward, beyond delta-front depths, textural variations are very low, especially on the deeper seafloor, being characterized by monotonous muddy sedimentation. Tortora (1995) and Bellotti and Tortora (1996) recognized, in particular, two sediment dispersal systems. In the first, fluvial sediment is redistributed along the proximal delta front by wave action. As a result, waves select the finer fraction (< 0.125 mm), carrying it alongshore and/or depositing it on the prodelta sector. In the second dispersal system, the Tiber River plume carries fine-grained sediment offshore through hypopycnal flows. In such case, fine-grained sediment bypasses the delta front and is deposited in the prodelta area. Both dispersal systems ultimately discharge sediment on the upper prodelta slope, which constitutes the main depocenter of the submarine system, whereas the delta front represents a bypassing area, where the sediment is only temporarily stored (Fig. 3.6).

3.5 METHODS

Methods used in this study include fieldwork and laboratory analysis. A survey of modern and recent highstand deposits of the Tiber Depositional Sequence was carried along the delta front and prodelta settings (Fig. 3.2). Twenty-one sand samples were collected from gravity cores in the Tiber delta front at various core intervals (Figs. 3.2, 3.7). This allowed detailed stratigraphic and grain-size analyses and evaluation of compositional changes through time (see Milli et al. 2016, with

references therein). An additional 21 sand samples were collected from three gravity cores (TC6/ TC7/TC8) (~ 4 m length) collected on the submerged sector of the Tiber delta off the river mouth (Figs. 2, 8). According to Di Bella et al. (2013), the TC6 core was drilled in an incised gully cutting the continental slope (240 m water depth); the TC7 and TC8 cores were located on the continental shelf near the shelf break (water depth of 155 m and 126 m, respectively) (Fig. 3.2).

Fifty-two thin sections were stained for potassium and plagioclase following methods illustrated by Marsaglia and Tazaki (1992). Point-count data were collected with an automated point-counting stepper stage using the Gazzi-Dickinson method (Ingersoll et al. 1984). Four hundred points were counted per slide; grains were differentiated using categories and parameters defined by Marsaglia (1992) and Marsaglia et al. (1999), and grouped based on Zuffa (1980) to differentiate noncarbonate extrabasinal (NCE), carbonate extrabasinal (CE), and carbonate intrabasinal (CI) grains (see Table B1 and Tables B2 and B3 in Appendix B). Examples of some grain types are shown in Figure 9. Medium-sand fractions from the complete sample suite and 15 fine-grained sand fractions selected from delta-front and prodelta sand were point counted to maximize sample coverage and investigate grain-size dependence. Modal compositions were defined by plotting the data on ternary diagrams and compositional biplots, after Zuffa (1980, 1985), McBride and Picard (1987), Garzanti (2016), and Veermesch et al. (2016). These data sets were merged with those reported in Tentori et al. (2016). Tentori et al. (2016) collected eighteen fluvial sand samples from the Tiber River (TR1–TR12) and its tributaries (TRT1– TRT6) at ~ 30 km intervals from the headwaters to the lower reaches. Tributaries were sampled just upstream of their intersection with the Tiber River. An additional seven sand samples were collected by Tentori et al. (2016) along the coast from beach swash zones (foreshore), north and south of the river mouth (TRC1–TRC7) (Fig. 3.2). Our data were compared to those of the Ocean Drilling Program from Marsaglia et al. (1999).

3.6 RESULTS

Compositional data for the modern tributaries (TRT1 to TRT7), Tiber River (TR-1 to TR-12) and foreshore sand are displayed in Table B2 and summarized in Table B3 (see Appendix B). For a detailed description of the modern tributaries, Tiber River, and foreshore sand signatures refer to Tentori et al. (2016).

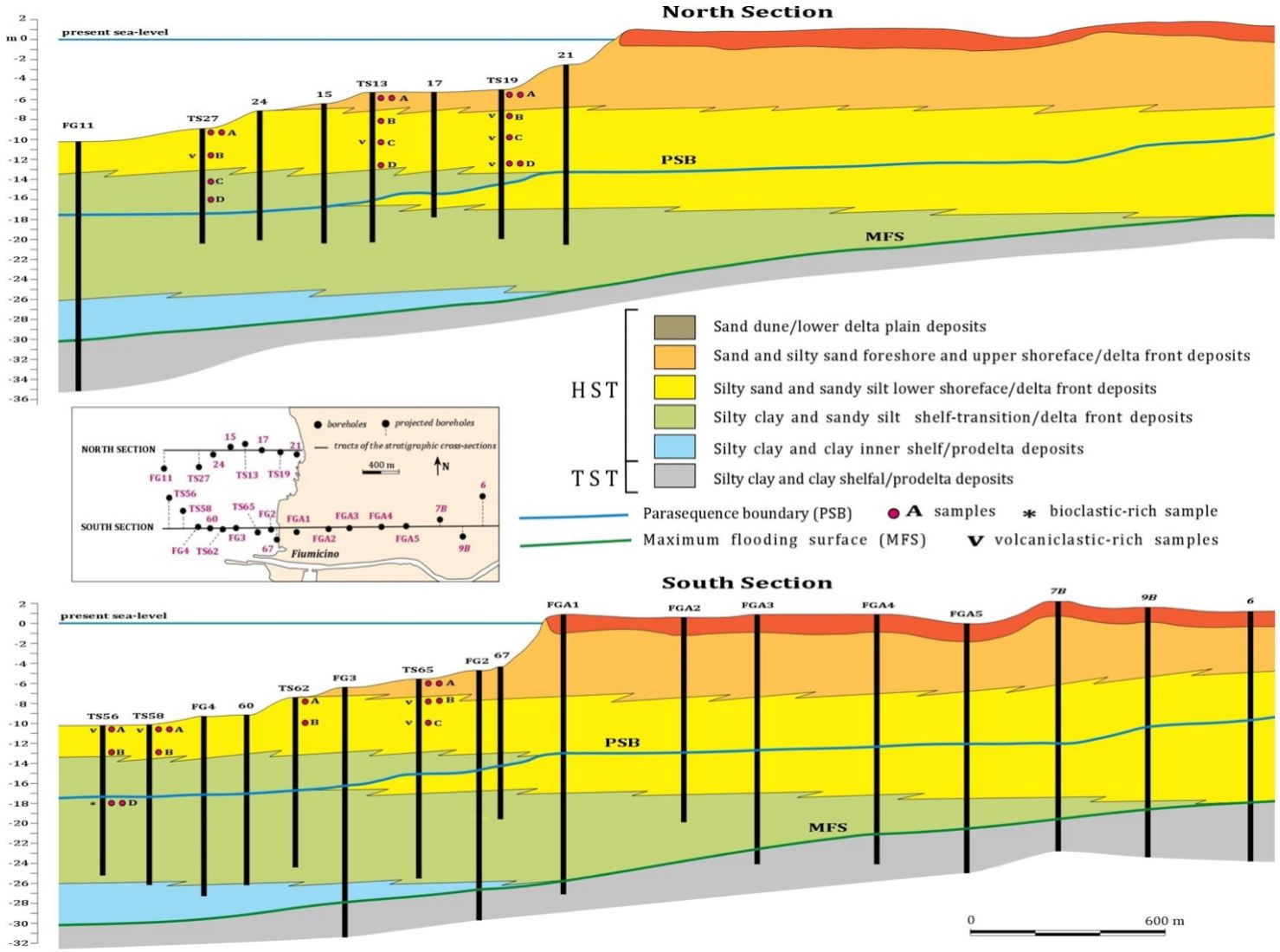

FIG. 3.7 —Stratigraphic sections and shoreface cores location in the A) northern and B) southern sectors off the Tiber river mouth. Red dots represents medium-grained sand and black dots fine-grained sand sampled from the cores TS13, TS19, TS27, TS56, TS58, TS62, TS65, and intervals A, B, C, and D. Note that all the volcanic-rich samples are located in the yellow lower shoreface facies and that bioclastic rich sample is below the parasequence boundary.

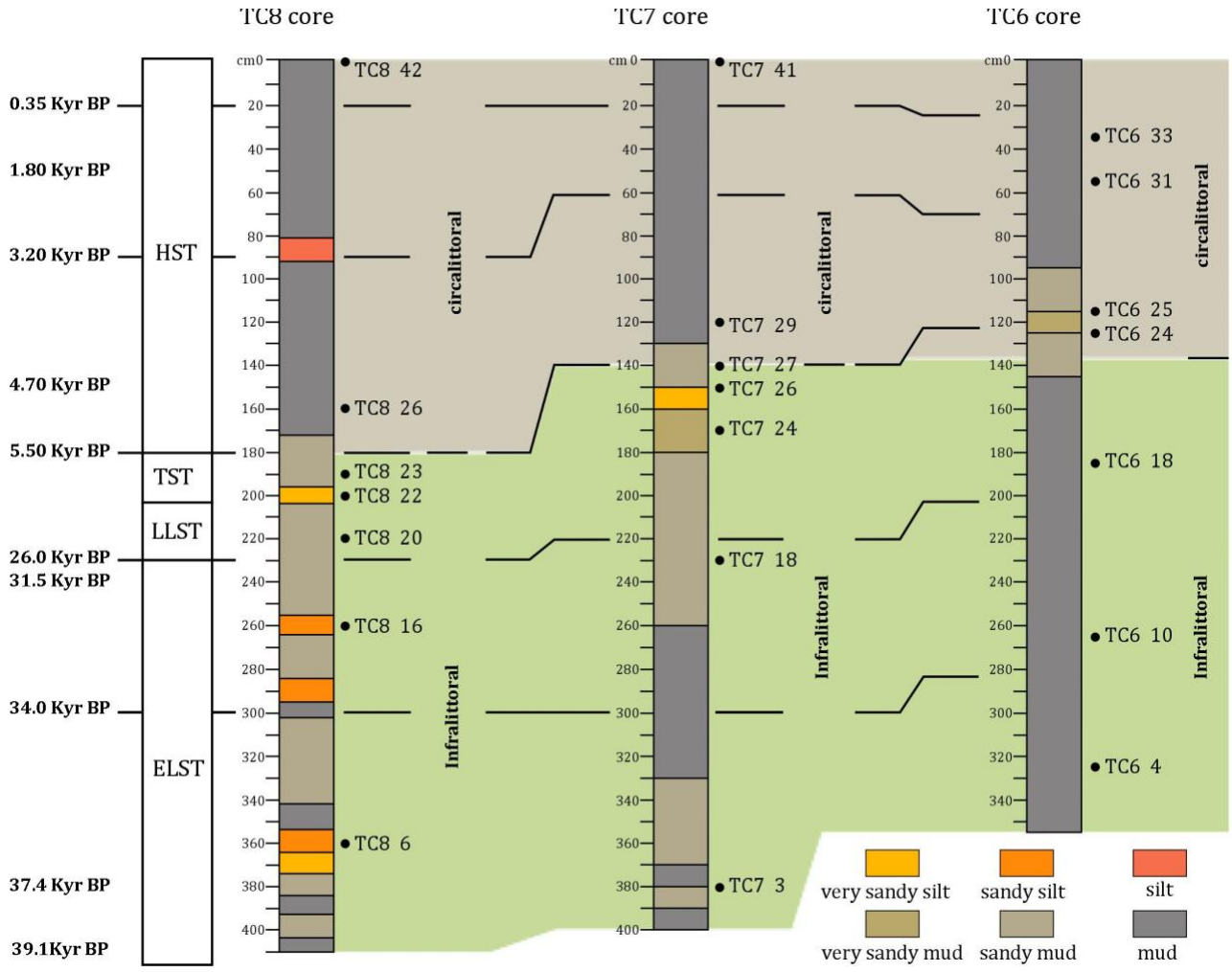

FIG. 3.8 —Lithology and sequence stratigraphic interpretation and sample locations in the TC6–TC7–TC8 continental shelf cores. See Figure 3.2 for core locations. Modified from Di Bella et al. (2013).

3.6.1 Tiber Delta-Front Samples

Samples from this sector comprise those belonging to the upper delta front, which include foreshore (Tentori et al. 2016) and upper and lower shoreface (this study). In the upper- and lower-shoreface samples, the dominant components are monomineralic grains of quartz and feldspar, and sedimentary lithic fragments. Common components are grains of pyroxene and micas (biotite, muscovite, and chlorite). Other minor monomineralic grains include opaque and non-opaque dense minerals, serpentine grains, and alterites. Alterites are opaque to semi-opaque finely crystalline masses created during weathering, for which identification of the original grain is impossible as they do not show internal structure (sensu Johnsson 1990). They potentially include altered monomineralic grains, and sedimentary and volcanic lithic fragments. Minor polycrystal- line grains include polycrystalline quartz and chert grains. Carbonate bioclasts are common (significant in core

samples 56 and 58) and include intrabasinal (mainly foraminifera) and extrabasinal clasts. Siliciclastic sedimentary lithic fragments include feldspathic and lithic siltstone, and minor mudstone lithic fragments. Sparitic and micritic carbonate lithic fragments are common, whereas siliciclastic sedimentary, volcanic, and low-grade metamorphic fragments are less represented. Volcaniclastic rock fragments exhibit felsitic, vitric, and lathwork textures, with pumice, colorless, black, brown, and altered glass, and tuff fragments. Phenocrysts in volcanic lithic fragments include feldspar and pyroxene.

In general, pyroxene grains are common (~ 20%) in medium-grained samples off the river mouth (cores TS62, TS58, and TS27) and in proximity of the coast (core TS19), and decrease in finer sand (< 5%). Biotite, muscovite, and chlorite grains are minor components in medium- grained samples proximal to the river mouth (< 5%) and tend to increase (~ 10%) in the more distal and fine-grained sand samples (TS58A, TS58B, TS56A, TS56D).

Volcanic lithic fragments are significant components in medium-grained samples of cored intervals TS65B, TS65C, TS58A, TS19C, TS13C and fine-grained samples TS56A, TS56D, and TS27D.

3.6.2 Continental Shelf and Slope Samples

The samples of the three gravity cores TC6, TC7, and TC8 (Figs. 3.8, 3.10) are mainly composed of intrabasinal carbonate bioclasts (50–100%) (see also Di Bella et al. 2013), with the exception of a few samples from the TC6 core, which show common (~ 20–40%) monomineralic quartz and feldspar grains, and minor micas (muscovite, biotite, chlorite), pyroxene, amphibole, and dense opaque and non-opaque minerals. Bioclasts include mollusks, echinoderms, red algae, bryozoa, and foraminifera, commonly diagenetically altered to siderite and/or unknown minerals. Polycrystalline grains include quartz with and without tectonite fabric and chert grains. Lithic fragments are minor components and include sparitic and micritic carbonate (limestone), siliciclastic, altered volcanic, and low- and medium- grade metamorphic varieties.

3.7 DISCUSSION

Detrital modes from Tiber River sediments cover a broad range of compositions (Fig. 3.10). Quartz, feldspar, and lithic-fragment proportions define distinct petrofacies (R,C,S) from source to sink for sand samples showing significant riverine influence. In particular, fluvial, deltaic, and coastal sand show characteristic petrofacies signatures on a QFL diagram (Fig. 3.10), whereas shelfal sand can be easily differentiated based on the presence of carbonate lithics (NCE,CE,CI) and the high ratio

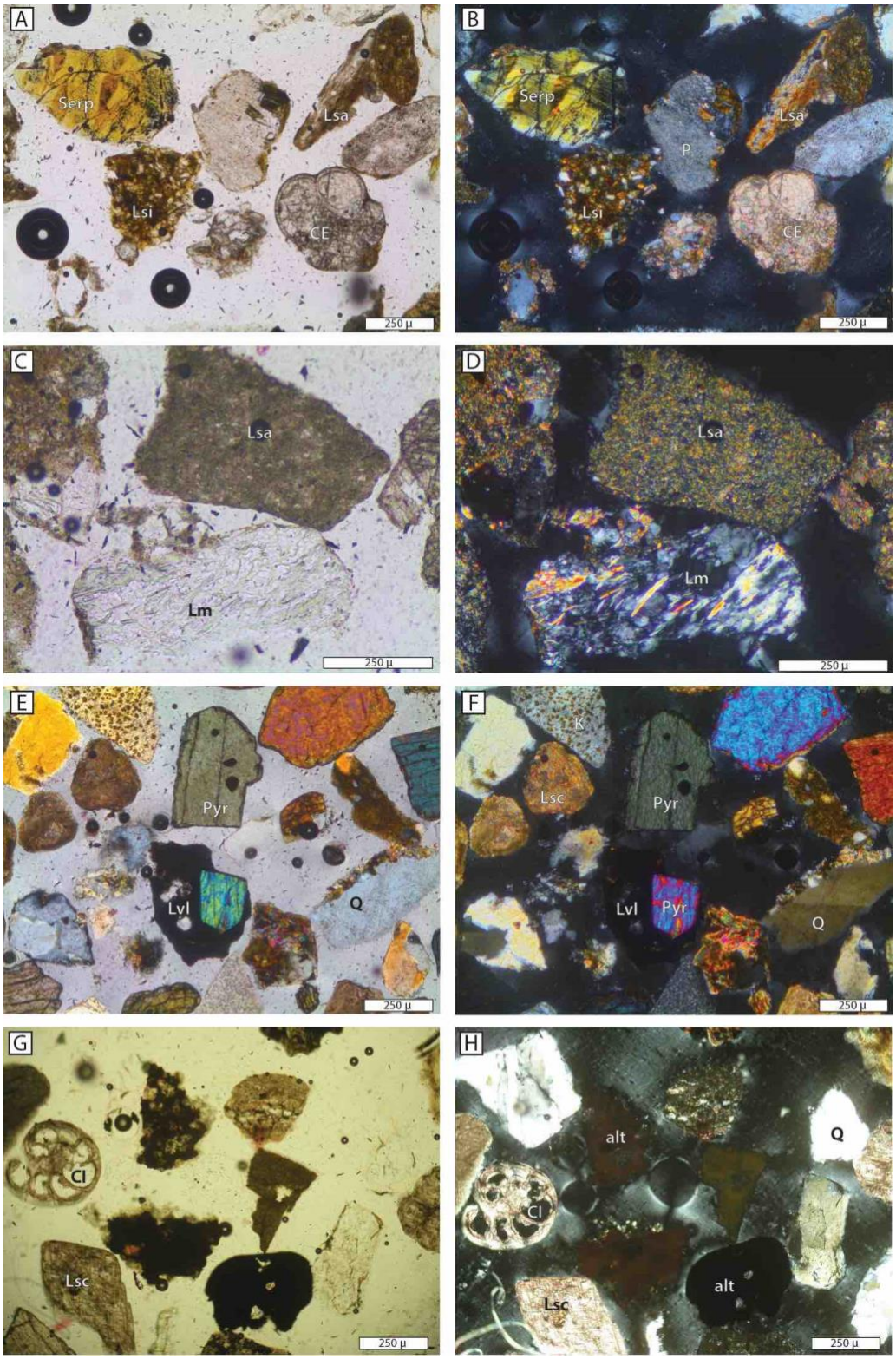

FIG. 3.9 —Photomicrographs of Tiber System sand showing the main grain types. A) Plane-polarized-light and B) cross-polarized-light views of the upstream Tiber drainage basin sand showing serpentine (Serp), plagioclase (P), and extrabasinal carbonate bioclast (CE) grains, and claystone (Lsa) and siltstone (Lsi) lithic fragments. C) Plane- polarized-light and D) cross-polarized-light views of the middle Tiber drainage basin sand showing claystone (Lsa) and metamorphic (Lm) lithic fragments. E) Plane- polarized-light and F) cross-polarized-light views of the lower Tiber drainage basin sand showing quartz (Q), pyroxene (Pyr) and k-feldspar (K) grains, and carbonate (Lsc) and volcanic lithic

(Lvl) fragments. G) Plane-polarized-light and H) cross-polarized-light views of the coastal sand off the Tiber River mouth showing intrabasinal carbonate bioclast (Cl), alterites (alt) grains, and carbonate lithic fragments.

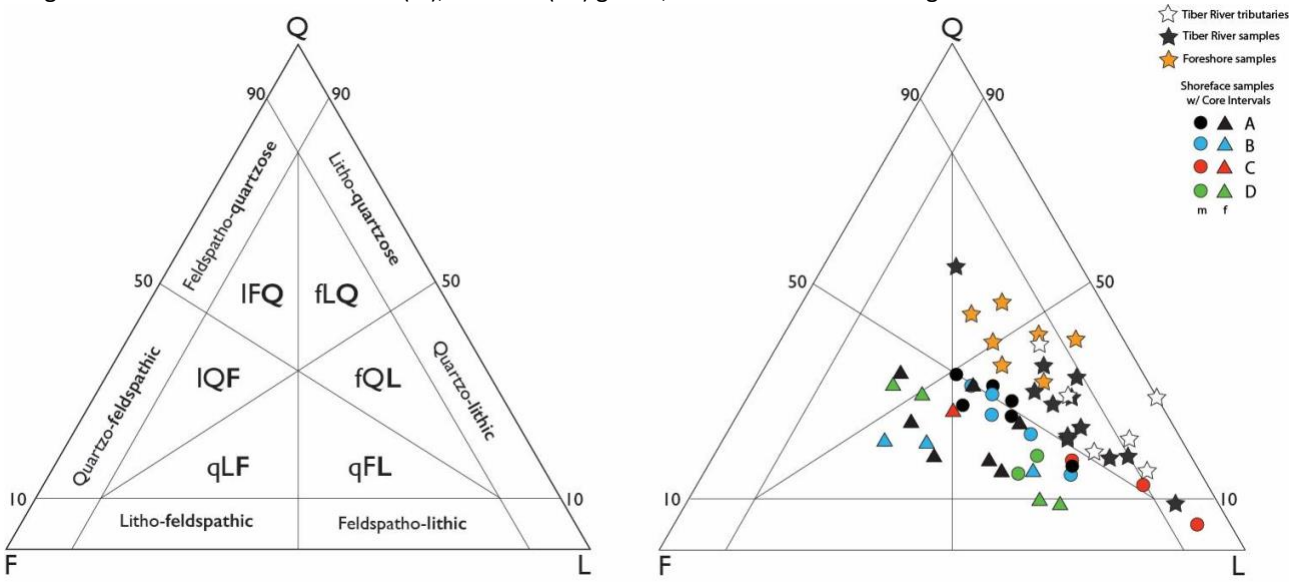

FIG. 3.10 —A, B) Ternary plots used for the petrographic classification of the studied sand samples. Scheme (A) is from Garzanti (2016) and based on the nomenclature introduced by Crook (1960) and Dickinson (1970) and endorsed by Weltje (2006). Q, quartzose; F, feldspathic; L, lithic; lFQ, litho-feldspatho-quartzose; fLQ, feldspatho- litho-quartzose; lQF, litho-quartzose-feldspathic; fQL, feldspatho-quartzo-lithic; qLF, quartzo-lithic feldspathic; qFL, quartzo-feldspatho-lithic.

of intrabasinal vs. extrabasinal (almost 100% bioclastic sand) (Fig. 3.11). Riverine sand ranges from lithic to fedspatho-litho-quartzose (petrofacies R); foreshore sand plots mainly into the feldspatho-quartzo-lithic field, and shoreface sand ranges from feldspatho-lithic to litho-quartzo-feldspathic (upper and lower delta front) (petrofacies C) (Fig. 3.9). Shelfal and slope sand (petrofacies S) shows a very small percentage of extrabasinal detrital grains and cannot be classified using the scheme based on Garzanti (2016). The compositional variability from inland to offshore is summarized in Figures 3.12, 3.13, and 3.14. The complex interaction between autogenic and allogenic factors, which controls sediment composition in the Tiber River system, are investigated in detail from fluvial to shelfal deposits in the following sections.

3.7.1 Fluvial-Sand Petrofacies (R)

Fluvial-sand petrofacies (petrofacies R) is discussed in detail in Tentori et al. (2016). However, results from this study more clearly highlight the control of source-area lithology on tributary sediment contributions and clarify the effects of anthropic impact in the Tiber River drainage basin. Turbidite successions are the main source of the Tiber River sand (~ 50– 70%) with significant contribution from carbonate (~ 10–30%), and volcanic source-rocks (~ 15%), in agreement with results from Tyrrhenian river and beach sand reported in Garzanti et al. (2002). In more detail, the

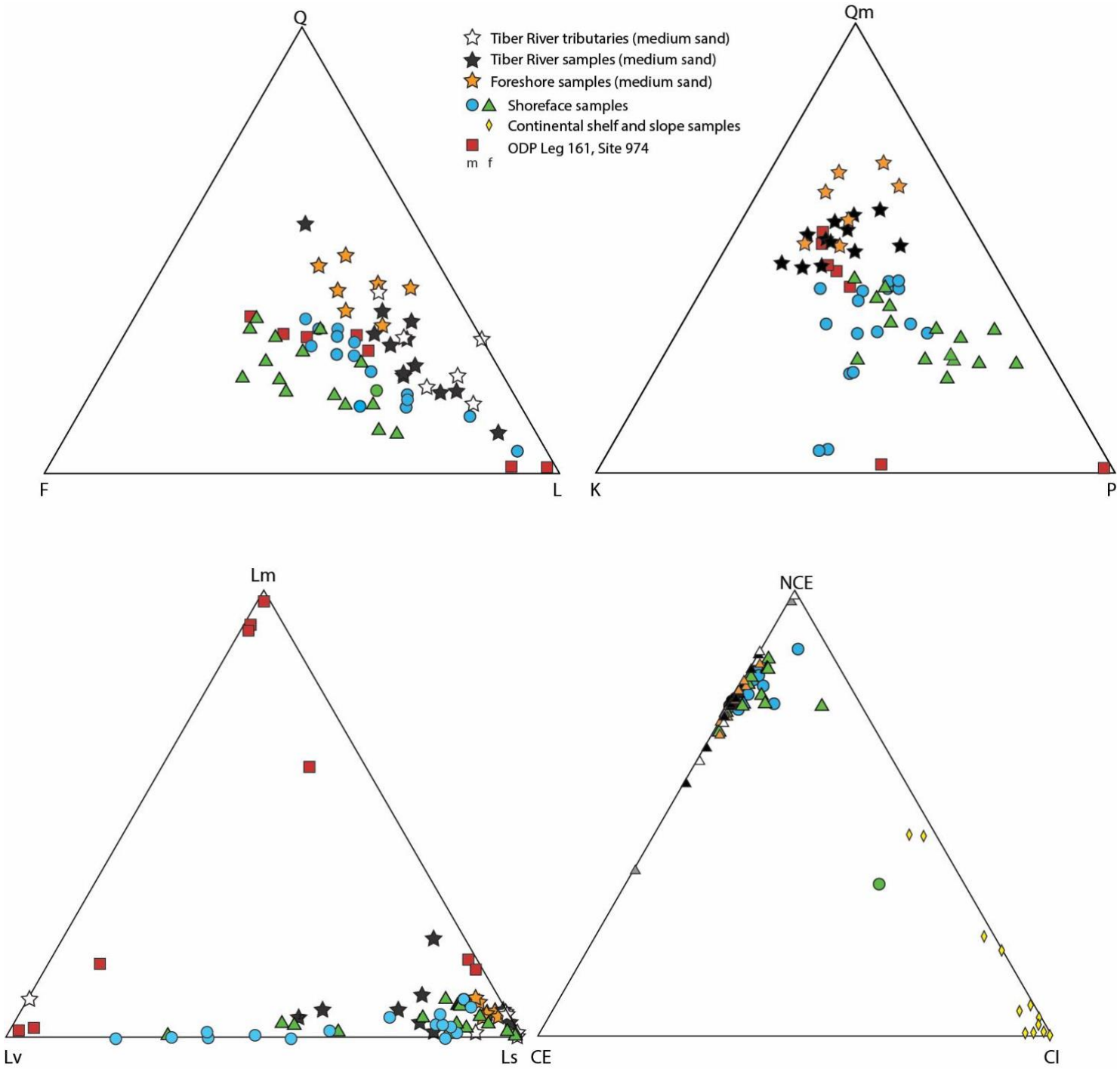

FIG. 3.11 —QFL, QmKP, LmLvLs, and NCE, CE, and CI ternary plots for fluvial, coastal (m, medium-grained sand and f, fine-grained sand) and continental shelf and slope petrofacies of the TDS for ODP Leg 161, Site 974 (data from Marsaglia et al. 1999).

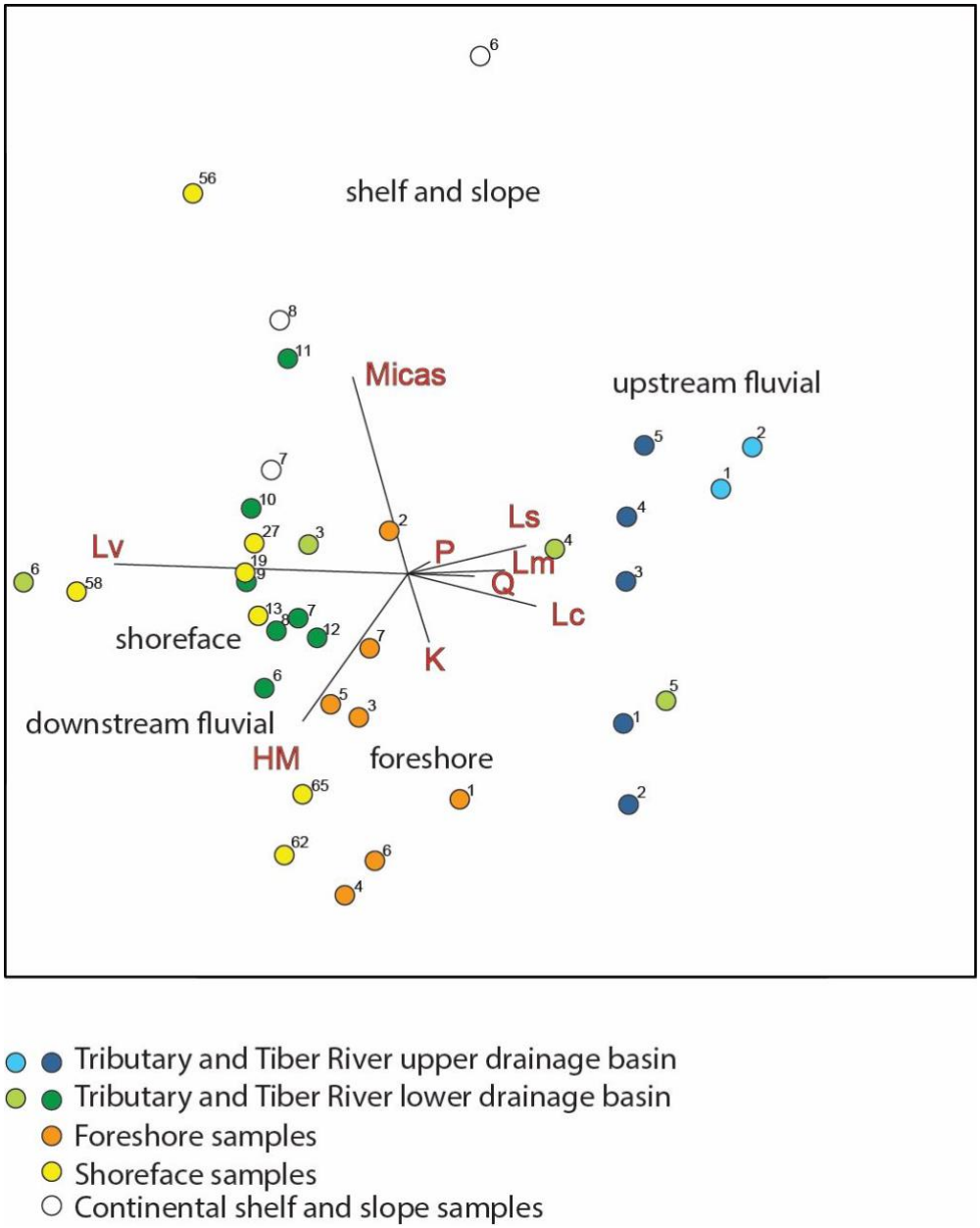

FIG. 3.12 —This compositional biplot (Gabriel 1971) displays both data (samples) and parameters (rays; Q, total quartz; K, K-feldpsar; P, plag; Lc, carbonate lithics; Lm, metamorphic lithics; Lv, volcanics; Hm, dense minerals). The length of each ray is proportional to the variability of the parameter in the data set; the angle between two rays reveals whether the corresponding parameters are well correlated (08), uncorrelated (908), or inversely correlated (1808) (from Veermesch et al. 2016). Note that downstream fluvial samples cluster with marine sand.

Tiber River drainage basin can be divided into two sub-basins hydrographically separated by the Corbara dam, each with distinct lithic- fragment signature (Figs. 3.12, 3.13). Detrital modes from the upstream Tiber River drainage basin down to the Corbara dam show abundant quartz and feldspar grains derived from multi-stage recycling of quartzo-feldspathic Miocene turbidites and common siliciclastic and carbonate lithic fragments. In the lower drainage basin, lithic-fragment composition changes abruptly, with carbonate and volcaniclastic rock fragments derived from the erosion of

Mesozoic carbonate succession and Quaternary volcaniclastic rocks of the Roman Magmatic Province, respectively (Figs. 3.12, 3.13) and additional quartz, feldspar, and dense minerals produced by multistage reworking of volcaniclastic rocks. The two main tributaries of the lower reaches of the Tiber River, which contribute with the highest values of flow rate and sediment discharge, drain carbonate successions (Nera River), lavas, and pyroclastic-flow deposits (Aniene River), resulting in mixed provenance and downstream decrease in the mineralogical maturity index (MI=Qt/Qt+F+Lt) (see Fig. 3.14; see also Garzanti 2017).

The ultimate Tiber River sediment input to the marine basin mainly reflects multistage reworking of siliciclastic units (monomineralic grain contribution) and erosion of carbonate and volcanic source rocks (monomineralic grain and lithic fragment contribution) of the lower Tiber River drainage basin.

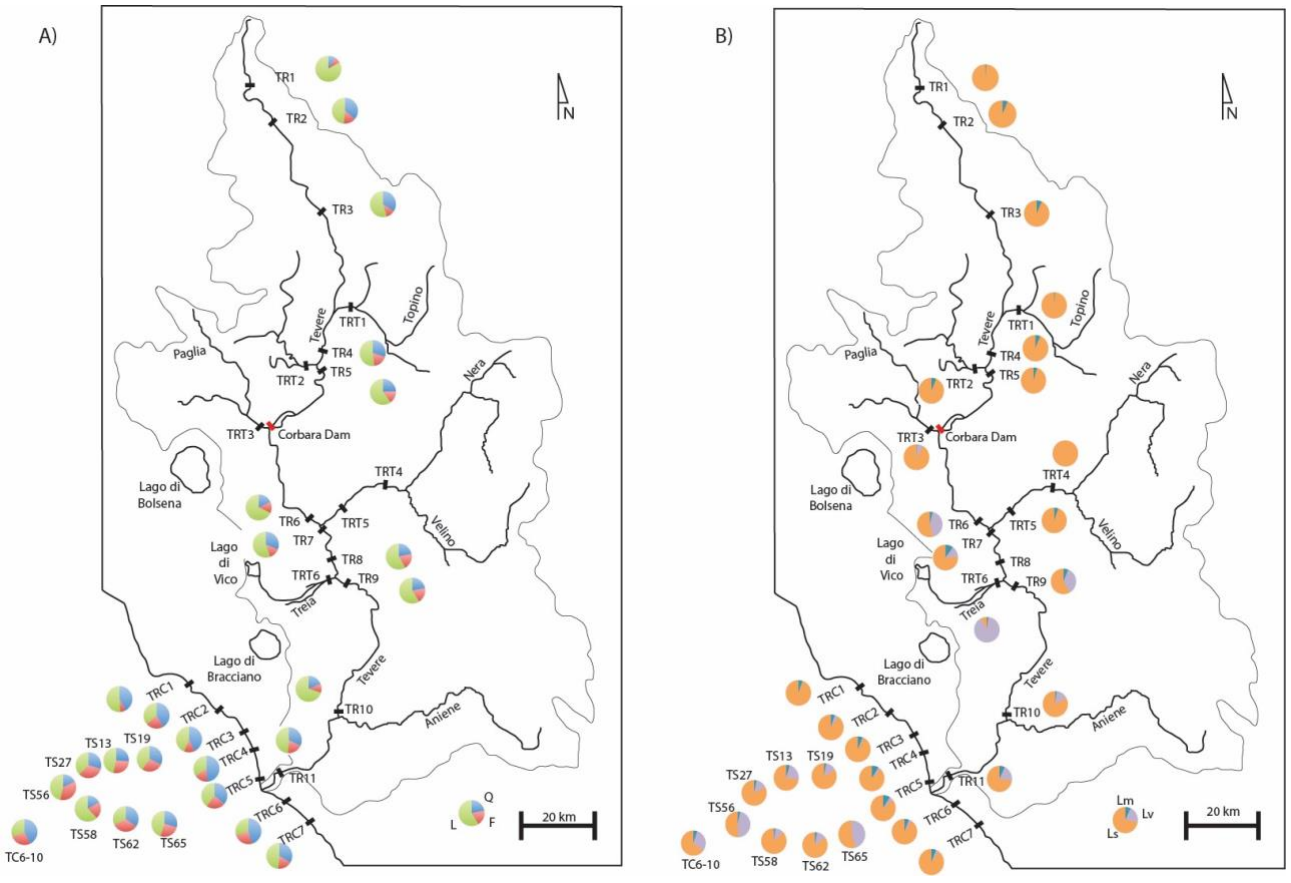

FIG. 3.13 —Sand petrography and provenance mixing from onshore source to offshore sink. A) Q, quartz; F, feldspar; L, lithic fragments; B) Lm, metamorphic lithic fragments; Ls, sedimentary lithic fragments; Lv, volcanic lithic fragments). The keys to the colors used on pie diagrams are located in the lower right corners of each plot to the left of the map scale.

3.7.2 Coastal-Sand Petrofacies (C)

The recent coastal petrofacies signature reflects, in part, long-distance multistage transport from siliciclastic units of the northern Apennines, but mostly recycling from the carbonate sedimentary successions of the central Apennines and the volcaniclastic units of the Roman Magmatic Province. Since construction of the Corbara dam, the main provenance of the Tiber coastal sand is the sum of the Paglia River and the lower reaches of the Tiber River from the intersection with the Paglia River up to the river mouth, as suggested by clustering of samples in Figure 3.12. Continental and marine deposits show slightly different trends in lithic-fragment proportions and in Q/F. River medium sand has intermediate Q/F with respect to quartz-rich foreshore and feldspar-rich shoreface medium sand on the QmKP ternary diagram of Figure 3.11, reflecting the effect of coastal reworking (hydraulic sorting and eolian reworking) on river sand. The LmLvLs ternary plot defines one main group having dominant sedimentary lithic fragments and few fluvial and coastal samples with abundant volcanic lithics. The presence of volcanic grains suggests important contributions from a volcaniclastic source cropping out along the Tiber River downstream drainage basin. Physical controls on sand petrography in the coastal depositional environments that modify the provenance signal include hydraulic sorting, mechanical breakdown, and reworking of coastal dune sand and volcaniclastic detritus (e.g., phenocrysts, vitric pyroclastic and/or epiclastic lithic fragments). These processes produce further compositional variation and discrepancies between foreshore and shoreface sand. The dominant components of the foreshore samples are quartz, feldspar, and pyroxene grains, and carbonate lithic fragments, whereas shoreface samples are generally richer in feldspar grains and volcanic lithic fragments.

Pyroxene grains (phenocrysts) accumulate in the foreshore sand, indicating reworking of debris from chemically altered volcaniclastic paleosols in the floodplain and eolian dune fields near the coast and/or hydraulic sorting and enhanced coastal erosion in the beaches adjacent the Tiber River mouth. Pyroxene phenocrysts are liberated in the coastal environment owing to grain-to-grain collisions of pyroclastic debris during eolian transport and marine reworking in the swash zone, as seen elsewhere along the coast by Morrone et al. (2017). Nearshore marine processes and coastal reworking in the swash zone, in turn, modify sand composition by increasing the mineralogical maturity index (MI) and Q/F of foreshore sand (Figs. 3.11, 3.14). Feldspar grains are preferentially concentrated in the shoreface facies due to their hydraulic behavior (Figs. 3.11, 3.13) (see also Bellotti et al. 1994; Garzanti et al. 2002). Volcanic lithic fragments also accumulate in the shoreface facies, where volcaniclastic sediment is partially protected from eolian reworking and coastal-dune

contamination. Carbonate biogenic intrabasinal production is minimal along the coast and highly inhibited by clastic material delivered by rivers, with the exception of sample TS65D, which is located below the parasequence boundary (PSB) representing a flooding surface (see Fig. 3.7).

Coastal Grain-Size Variability.—Based on the above discussion, other considerations should account for coastal grain-size variation and relationships with sediment composition. The coastline profile of the Tiber Delta system shows a grain-size zonation that corresponds with morphodynamic zones of the submarine delta, in turn influenced by coastal hydrodynamics (see Bellotti et al. 1993; Bellotti and Tortora 1996; Zaghloul et al. 2009; Reddad et al. 2016) (Fig. 3.6). In general, sediment distribution shows a decrease in grain size (from coarse to very-fine sand and silt) away from the coastline, which is a direct consequence of the hydrodynamic conditions along the coast. In detail, medium to coarse sand dominates the exposed sectors of the delta and foreshore and shoreface sand above water depths of 5 meters, whereas fine and very fine sand and silt accumulate in water deeper than 5 m. These grain-size zonations are subparallel to the coastline and are reflected in sediment compositions of subaerial, proximal foreshore, and shoreface facies (Fig. 3.6). Foreshore coarse to medium sands are compositionally more mature than finer- grained shoreface sand: reworking of well-sorted medium-grained eolian dunes might contribute to the compositional maturity of the proximal beach samples (Figs. 3.13, 3.14). In contrast, shoreface sand shows a wider range of QFL values and a higher percentage of feldspar grains and lithic fragments owing to mixing of detrital populations with different provenance and contrasting grain sizes derived from different sources (volcanic rocks, soils, and coastal dunes). This trend of enrichment in feldspar and lithic fragments in finer-grained facies has been seen elsewhere in shelf environments (e.g., Parra et al. 2012; Bender-Whitaker et al. in press). Feldspars break into fragments along cleavage planes and are hydraulically selected in the finer fraction and in lower-energy environments.

Intrasample grain-size variability of shoreface samples shows a decrease in quartz and an increase in feldspar content (especially plagioclase) in the fine-sand fraction, a trend similar to that observed in Tiber fluvial samples (Tentori et al. 2016). Also, pyroxene grains liberated from volcanic lithic fragments decrease abruptly in the fine-sand fraction, suggesting that reworking of lithic fragments produces at least two grain-size populations with distinct compositional signatures and hydraulic behavior (e.g., volcanic lithic fragments and phenocrysts phases).

Compositional Variability of Coastal Deposits through Time.— Compositional changes within different shoreface core intervals reflect short-term Holocene climate cyclicity, which resulted in phases of high sediment supply. In particular, climatic oscillations over the last 3000 yr characterized

the last parasequence of the HST (Fig. 3.7), which developed in response to periodic events of Tiber Delta progradation and river runoff (Bellotti et al. 1994; Di Rita and Magri 2009; Di Bella et al. 2013; Milli et al. 2013; Margaritelli et al. 2016). In particular, two main humid phases characterized the parasequence development: from 2700 to 1900 yr BP the Tiber River delta prograded with a rate of 5–6 m/yr, and over the last 500 yr when historically documented Tiber River flood events became more frequent and intense (Bellotti et al. 2011; Milli et al. 2016). These events, in some cases, were recorded in the Tiber system shoreface deposits in their compositional signatures and sediment age reversal. During times of increased precipitation, following the onset of humid conditions in the Tiber River drainage basin, major floods eroded and cannibalized sediments from the Tiber River floodplain and volcaniclastic source rocks of the lower drainage basin, depositing them in the marine environment. Freshly delivered sediment contained high concentrations of volcanic lithic fragments and older material with respect to the coastal deposits, providing radiocarbon ages that are ‘‘virtually’’ older than the effective depositional age. As a result, younger volcaniclastic-rich sediments yield older ages relative to the underlying deposits. Shoreface sand shows systematic high concentration of volcaniclastic material in the lower-shoreface facies.

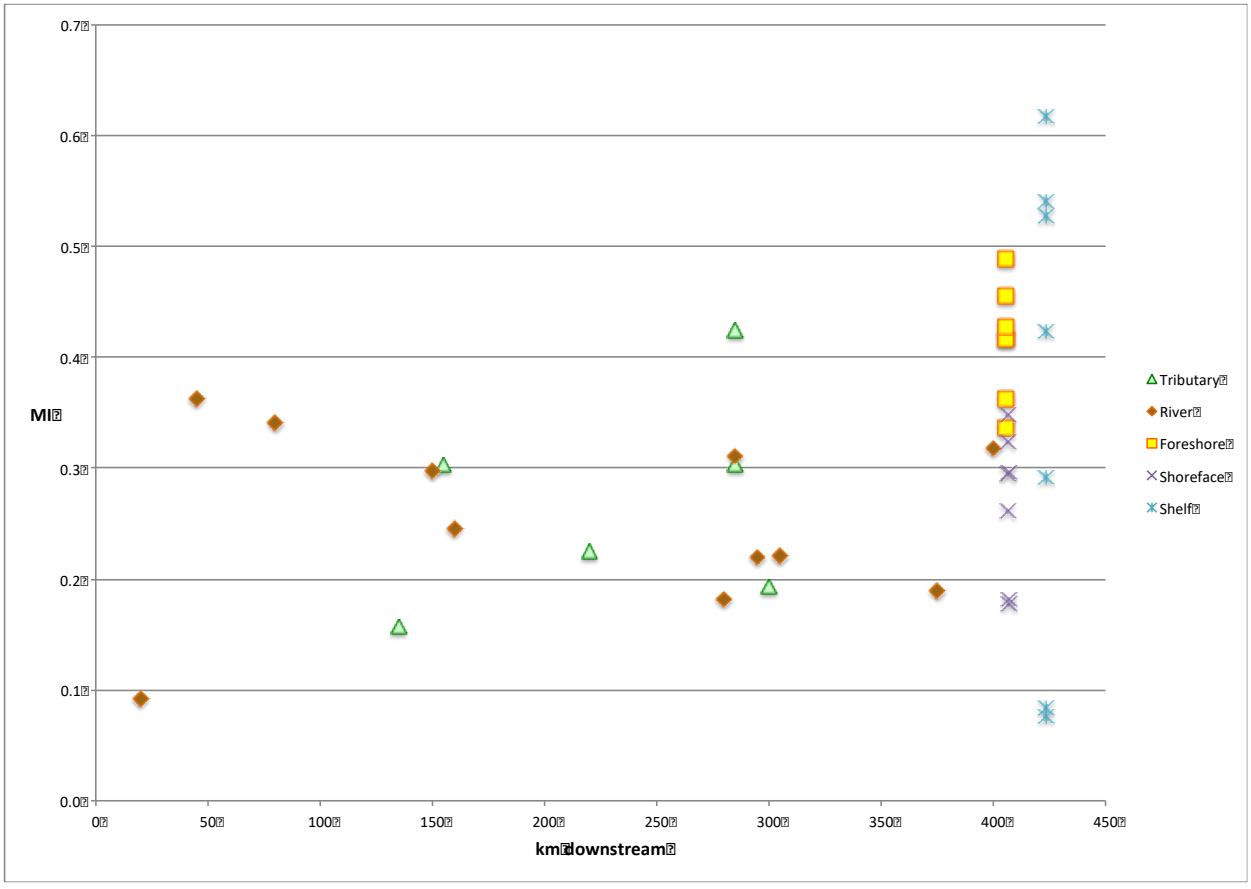

FIG. 3.14.—Mineralogical maturity index (MI=Q/Q+F+L) (after Picard and McBride 2007) vs. kilometers (km) downstream for river, coast, tributary, delta front, and prodelta samples.

3.7.3 Continental Shelf and Slope Sand Petrofacies (S)

Intrabasinal allochems (mainly bioclasts) represent the most significant differences between river and marine offshore sand (Fig. 3.11). Intrabasinal carbonate production is highly inhibited by the clastic input along the proximal coast; they are more stable offshore. Also, the NCE-CE-CI ternary plot shows a decrease in the noncarbonate-extrabasinal and carbonate-extrabasinal fractions from proximal to distal marine sand due to dilution and sedimentary mixing. The continental shelf and slope petrofacies can be easily differentiated from fluvial and coastal sand in the NCE-CE-CI ternary diagram, because they plot near the CI end member (Fig. 3.11). Intrabasinal allochems are, in fact, the dominant components of these sand deposits (~ 100%), although all the core samples show some degree of riverine influence. In particular, sand samples from the TC6 core (located in an incised gully) show a significant proportion of noncarbonate extrabasinal grains (mostly quartz and mica), which probably record a major riverine influence with respect to sand samples of the TC7 and TC8 cores. Platy micas, due to their hydraulic behavior, tend to concentrate in distal lower-energy environments (Fig. 3.12).

3.7.4 Comparison with Ancient Deep-Marine Facies in the Tyrrhenian Basin

Marsaglia et al. (1999) proposed that the ultimate sink of the Tiber River sediment was the Tyrrhenian Basin, and that this sediment was potentially cored at Ocean Drilling Program Site 974. The sandy turbidites of Pleistocene age recovered at Site 974 show QFL and QmKP proportions similar to modern Tiber shoreface and fluvial sand, respectively, but different lithic compositions (Fig. 3.11). In particular, sedimentary lithic fragments, which dominate the modern Tiber River coastal system, are almost absent in the metamorphic- and volcanic-rich Pleistocene sand (see Fig. 3.11). If sourced by the paleo-Tiber system, as proposed by Marsaglia et al. (1999), softer sedimentary lithic components from a paleo-Tiber source could have been selectively removed by abrasion during long-distance submarine transport to Site 974 or have been removed via climatic overprinting in the source area.

The Site 974 sand compositions also include volcaniclastic intervals, suggesting that there were at least two sources for the deep-water deposits. The most important sources of Pliocene–Pleistocene tephra deposits at Site 974 were the high-potassic volcanic province of the Tuscan, Roman, and Campanian domains, as determined by glass geochemistry of volcanic sand (McCoy and Cornell 1990), whereas a possible source for significant quantities of metamorphic lithic fragments

at Site 974 could have been input from the east coast of Sardinia. In that area, rivers of the east Sardinian margin (e.g., Flumendosa and Cedrino Rivers), drain Variscan metamorphic basement rocks and feed several submarine canyons which transition downslope into the Sardinia Valley feeding the Vavilov Basin (Gamberi and Marani 2009; Gamberi et al. 2009).

During the current HST, Tiber sand deposition is mostly confined to coastal and inner shelf, and sediment input is minimal in the shelf margin and deepwater environments of the Tyrrhenian Sea. The Pleistocene Site 974 sand is coeval with the older Tiber River succession, and in particular, with LST and TST sand of the Ponte Galeria Sequence analyzed in Tentori et al. (2016), which shows trends of metamorphic and volcanic lithic fragments similar to those of modern sand. The Pleistocene Ponte Galeria sand records rapid and abrupt introduction of coeval volcaniclastic detritus to the system that left a distinct volcaniclastic signature, and very low percentages of metamorphic lithic fragments. Thus, we suggest that Pleistocene sedimentation in the Tyrrhenian Sea basin plain at Site 974 was mainly driven by a relative sea-level lowstand, which determined a close connection between river entry points draining Variscan metamorphic basement, the heads of slope channels along the eastern Sardinian margin, and the Plio-Pleistocene volcanism of the Latium and Campanian margin.

3.7.5 Sand Compositional Changes among Systems Tracts

Sediment composition of siliciclastic fluvial to marginal-marine successions can be predicted using a sequence-stratigraphic approach (see Amorosi and Zuffa 2011; Tentori et al. 2016 and references therein). Sand petrography can vary according to changes in relative sea level, sediment supply, and sedimentation rate in response to climatic and tectonic forcing. Thus, variation in detrital composition might be recorded at predictable intervals in a sequence, reflecting changes in sediment supply that characterizes systems tracts of a depositional sequence. In the case of TDS, relative sea-level fall during deposition of the early lowstand systems tract leads to increased river erosion and shelf incision, which results in bypass of large amounts of sediment with heterogeneous compositions directly into the basin. When sea level was stable or began to rise during the late lowstand systems tract, sediment was partially deposited in the incised valleys, off the river mouth, and on the shelf. Sediment composition of the cores located on the shelf and slope records, in fact, a riverine influence, as displayed by the benthic foraminiferal record (Di Bella et al. 2013) and by the textural and compositional characteristics of the sediments. In particular, we observe a trend of enrichment in the extrabasinal fraction (mostly siliciclastic) in the samples attributable to LST (TC6-

4/TC6-10/TC6-18) and HST (TC6-31) phases of the TC6 core. Enrichment in the lithic fraction in the early LST deposits (TC6-4/TC6-10) also reflects increased sediment supply and grain-size variations attributable to seaward migration (forestepping and down- stepping) of the Tiber Delta at the end of the sea-level fall that followed the last highstand phase correlated with the MIS 5.5 (see Milli et al. 2016).

Relative sea-level rise during deposition of the transgressive system tract resulted in increased accommodation space as sediment was rapidly trapped in the continental areas following fluvial aggradation. This process caused a progressive decrease in river runoff recorded in the marine environment in terms of lower percentages of extrabasinal grains and relative abundance of characteristic foraminiferal assemblages (see also Di Bella et al. 2013; Milli et al. 2016). In particular, most of the samples from the TST and HST in the TC6–TC7–TC8 cores are composed almost 100% of carbonate intrabasinal grains, suggesting a general decrease in terrigenous input on the continental shelf and shelf break during development of these systems tracts (Fig. 3.11).

During the HST, as accommodation decreased, lateral migration of the fluvial channel belts caused reworking of floodplain and paleosol deposits, which are currently redistributed along the coast as the delta continues to prograde. Major sediment influx occurs during floods, which carry material to the coastline, where it is reworked by local sedimentary processes (e.g., eolian and wave reworking, alongshore transport, rip-current reworking, hydraulic sorting). Sedimentary mixing of multiple detrital populations such as freshly delivered river sediment, material weathered from paleosols, and reworked deltaic sediment produce compositional variability in the highstand deposits of the Tiber Depositional Sequence.

Alluvial, delta-plain, delta-front, and prodelta detrital signatures and compositional indices (e.g., Q/F, MI, QFL%) can be interpreted and their vertical trends used to evaluate the role of autogenic factors and sedimentary processes in controlling sediment composition of high- frequency depositional sequences (see also Tentori et al. 2016). Sand compositional signatures from the Tiber River systems can help decipher other wave-dominated delta successions deposited over the last high- stand.

3.8 CONCLUSIONS

Study of the modern Tiber River sedimentary system from source to sink illustrates the complexity of defining variables, such as source-rock lithologies, fluvial transport, and coastal reworking, in controlling sediment composition along the Tyrrhenian margin of Italy. However,

some important considerations can be made when reconstructing sediment compositional variations from source to sink in the Tiber River sedimentary system:

1. Fluvial sand composition reflects significant mixing of detritus from siliciclastic (~ 50–70%) and carbonate (~ 10–30%) sedimentary and volcanic source rocks (~ 15%). The upper and lower reaches of the Tiber River show similar Q/F, which represent recycling of siliciclastic and volcaniclastic source rock. In contrast, lithic- fragment proportions identify two sub-basins: an upstream drainage basin, where siliciclastic sedimentary lithics dominate, and Tiber lower reaches, below the Corbara Dam, where carbonate and volcaniclastic lithic fragments prevail. The presence of artificial dams along the Tiber River course simulates the effects of abrupt natural changes in the river drainage basin (tectonic and/or depositional events), which affect composition from source to sink.
2. Hydraulic sorting and recycling of coastal dune sand and volcaniclastic detritus from paleosols produce further compositional variability in the coastal environment. Foreshore sand is dominated by the monomineralic fraction (e.g., quartz and pyroxene grains) sorted by wave and wind action whereas shoreface deposits show higher percentages of cleavable feldspar grains hydraulically selected by alongshore currents and dispersed in the shoreface environment. Volcanic lithic fragments carried by periodic flood events in the marine basin are also preferentially stored in the lower shoreface facies and carried along the coast by alongshore currents.
3. Continental shelf and slope deposits off the Tiber River mouth show very little correlation with coastal and fluvial petrofacies. Sediment is made of ~ 100% intrabasinal bioclastic material; terrigenous sand bypasses directly into the basin or is sporadically deposited in incised shelf gullies. The extrabasinal sand signature is limited to occasional events of riverine influence.
4. The modern fluvial and marine petrofacies in the Tiber River System have compositions different from Pleistocene sand recovered at ODP Site 974, suggesting multiple sources for Pleistocene deep-water sand and different forcing mechanisms for sediment dispersal, volcanic activity, and relative sea-level change.

In the Tiber River system, during the last highstand, autogenic factors are the dominant controls on sediment composition. Petrofacies trends are linked, and intimately controlled by, sedimentary processes operating in each depositional environment.

The study of spatial sand compositional variations in the present highstand of the Tiber River system provide a model for interpreting a source-to-sink fluvial to marine system and an ideal stacking-pattern evolution of a clastic progradational deltaic succession. An upward- shallowing succession of shelfal, prodelta, delta-front (shoreface, fore- shore), delta-plain, and alluvial facies associations can be seen in terms of vertical petrofacies changes. A direct linkage between actualistic petrofacies and sand depositional environments provides key elements to interpret sedimentary successions with fixed detrital provenances and compositional variations of ancient marginal-marine successions.

SUPPLEMENTARY MATERIAL - See Appendix B -

ACKNOWLEDGMENTS

Several organizations have supported this study, which was funded by MIUR (Ministero dell'Istruzione, dell'Università e della Ricerca), SAPIENZA University of Rome, CNR (Consiglio Nazionale delle Ricerche), CARG Project–Geological Map of Italy 1:50000, and Autorità Portuale di Civitavecchia Fiumicino e Gaeta. We also would like to thank José Arribas and anonymous reviewer, JSR Associate Editor, Ray Ingersoll, and Editor, Gary Hampson, for their helpful and constructive comments, which improved the paper, and John Southard for his thorough copy editing.

REFERENCES

AMOROSI, A., AND ZUFFA, G.G., 2011, Sand composition changes across key boundaries of siliciclastic and hybrid depositional sequences: Sedimentary Geology, v. 236, p. 153– 163.

AMOROSI, A., MASELLI, V., AND TRINCARDI, F., 2016, Onshore to offshore anatomy of a late Quaternary source-to-sink system (Po Plain–Adriatic Sea, Italy): Earth-Science Reviews, v. 153, p. 212–237.

ANDERSON, J.B., WALLACE, D.J., SIMMS, A.R., RODRIGUEZ, A.B., WEIGHT, R.W., AND TAHA, Z.P., 2016, Recycling sediments between source and sink during a eustatic cycle: systems of late Quaternary northwestern Gulf of Mexico Basin: Earth-Science Reviews, v. 153, p. 111–138.

ANDO`, S., GARZANTI, E., PADOAN, M., AND LIMONTA, M., 2012, Corrosion of heavy minerals during weathering and diagenesis: a catalog for optical analysis: Sedimentary Geology, v. 280, p. 165–178.

BARBERI, F., BUANASORTE, G., CIONI, R., FIORDELISI, A., FORESI, L., IACCARINO, S., LAURENZI, M.A., SBRANA, A., VERNIA, L., AND VILLA, I.M., 1994, Plio-Pleistocene geological evolution of the geothermal area of Tuscany and Lazio: Memorie Descrittive della Carta Geologica d'Italia, v. 49, p. 77–134.

BELFIORE, A., BELLOTTI, P., CARBONI, M.G., CHIARI, R., EVANGELISTA, S., TORTORA, P., AND VALERI, P., 1987, Il delta del Tevere le facies sedimentarie della conoide sommersa: un'analisi statistica dei caratteri tessiturali, microfaunistici e mineralogici: Societa` Geologica Italiana, Bollettino, v. 106, p. 425–445.

BELLOTTI, P., AND TORTORA, P., 1996, I sedimenti sul fondale del delta del Fiume Tevere: Societa` Geologica Italiana, Bollettino, v. 115, p. 449–458.

BELLOTTI, P., CHIOCCI, F.L., MILLI, S., AND TORTORA, P., 1993, Variabilita` nel tempo della distribuzione granulometrica sui fondali del Delta del Tevere: Societa` Geologica Italiana, Bollettino, v. 112, p. 143–153.

BELLOTTI, P., CHIOCCI, F.L., MILLI, S., TORTORA, P., AND VALERI, P., 1994, Sequence stratigraphy and depositional setting of the Tiber delta: integration of high-resolution seismics, well logs, and archeological data: Journal of Sedimentary Research, v. 64, p. 416–432.

BELLOTTI, P., CALDERONI, G., DI RITA, F., D'OREFICE, M., D'AMICO, C., ESU, D., MAGRI, D., PREITE MARTINEZ, M., TORTORA, P., AND VALERI, P., 2011, The Tiber river delta plain (central Italy): coastal evolution and implications for the ancient Ostia Roman settlement: The Holocene, v. 21, p. 1105–1116.

BENCIVENGA, M., DI LORETO, E., AND LIPERI, L., 1995, Il regime idrologico del Tevere, con particolareriguardoallepienenellacitta`di Roma:Memorie Descrittive della Carta Geologica d'Italia, v. 50, p. 125–172.

BENDER-WHITAKER, C., MARSAGLIA, K.M., BROWNE, G.H., AND JAEGER, J.M., in press, Sedimentary processes and sequence stratigraphy of a Quaternary siliciclastic shelf– slope system: insights from sand provenance studies, Canterbury Basin, New Zealand, in Ingersoll, R.V., Lawton, T.F., and Graham, S.A., eds., Tectonics, Sedimentary Basins, and Provenance: A Celebration of the Career of William R. Dickinson: Geological Society of America, Special Paper 540. https://doi.org/10.1130/SPE540

BENTLEY, S.J., BLUM, M.D., MALONEY, J., POND, L., AND PAULSELL, R., 2016, The Mississippi River source-to-sink system: perspectives on tectonic, climatic, and anthropogenic influences, Miocene to Anthropocene: Earth-Science Reviews, v. 153, p. 139–174.

BERSANI, P., AND BENCIVENGA, M., 2001, Le piene del Tevere a Roma dal V secolo A.C. all'anno 2000: Presidenza del Consiglio dei Ministri, Dipartimento per i Servizi Tecnici Nazionali, 100 p.

BLUM, M., MARTIN, J., MILLIKEN, K., AND GARVIN, M., 2013, Paleovalley systems: insights from Quaternary analogs and experiments: Earth-Science Reviews, v. 116, p. 128–169.

BOND, G., SHOWERS, W., CHESEBY, M., LOTTI, R., ALMASI, P., DE-MENOCAL, P., PRIORE, P., CULLEN, H., HAJDAS, I., AND BONANI, G., 1997, A pervasive millennial-scale cycle in North Atlantic Holocene and glacial climates: Science, v. 278, p. 1257–1266.

BONI, C., PETITTA, M., PREZIOSI, E., AND SERENI, M., 1993, Genesi e regime di portata delle acque continentali del Lazio: Consiglio Nazionale delle Ricerche, 79 p.

BORDONI, P., AND VALENSISE, G., 1998, Deformation of the 125 ka marine terrace in Italy: tectonic implications, in Stewart, I.S., and Vita-Finzi, C., eds., Coastal Tectonics: Geological Society of London, Special Publication 146, p. 71–110.

BORTOLUZZI, G., FRASCARI, F., GUERZONI, S., INCREMONA, N., RAVAIOLI, M., AND ROVATTI, G., 1982, Some sedimentological and chemical features of the seafloor in front of the Tiber River: Geografia Fisica e Dinamica Quaternaria, v. 5, p. 120–128.

BROMMER, M.B., WELTJE, G.J., AND TRINCARDI, F., 2009, Reconstruction of sediment supply from mass accumulation rates in the Northern Adriatic Basin (Italy) over the past 19,000 years: Journal of Geophysical Research: Earth Surface, v. 114 (F2). doi:10.1029/2008JF000987

CAPUTO, C., LA MONICA, G.B., LUPIA PALMIERI, E., AND PUGLIESE, F., 1987, Physiographic characteristics and dynamics of the shores of Rome (Italy), in Proceedings of the First International Conference on Geomorphology, Part I: London, J. Wiley & Sons, p. 1185– 1198.

CARTER, L., MANIGHETTI, B., ELLIOT, M., TRUSTRUM, N., AND GOMEZ, B., 2002, Source, sea level and circulation effects on the sediment flux to the deep ocean over the past 15 ka off eastern New Zealand: Global and Planetary Change, v. 33, p. 339–355.

CARTER, L., ORPIN, A.R., AND KUEHL, S.A., 2010, From mountain source to ocean sink: the passage of sediment across an active margin, Waipaoa Sedimentary System, New Zealand: Marine Geology, v. 270, p. 1–10.

CATUNEANU, O., ABREU, V., BHATTACHARYA, J.P., BLUM, M.D., DALRYMPLE, R.W., ERIKSSON, P.G., FIELDING, C.R., FISHER, W.L., GALLOWAY, W.E., GIBLING, M.R., GILES, K.A., HOLBROOK, J.M.,

JORDAN, R., KENDALL, C.G.ST.C., MACURDA, B., MARTINSEN, O.J., MIALL, A.D., NEAL, J.E., NUMMEDAL, D., POMAR, L., POSAMENTIER, H.W., PRATT, B.R., SARG, J.F., SHANLEY, K.W., STEEL, R.J., STRASSER, A., TUCKER, M.E., AND WINKER, C., 2009, Towards the standardization of sequence stratigraphy: Earth-Science Reviews, v. 92, p. 1–33.

CATUNEANU, O., GALLOWAY, W.E., KENDALL, C.G.ST.C., MIALL, A.D., POSAMENTIER, H.W., STRASSER, A., AND TUCKER, M.E., 2011, Sequence stratigraphy: methodology and nomenclature: Newsletters on Stratigraphy, v. 44, p. 173–245.

CAVINATO, G., DE RITA, D., MILLI, S., AND ZARLENGA, F., 1992, Correlazione tra i principali eventi tettonici, sedimentari, vulcanici ed eustatici che hanno interessato l'entroterra (conche intrappenniniche) ed il margine costiero tirrenico laziale durante il Pliocene superiore ed il Pleistocene: Studi Geologici Camerti, Volume Speciale, 1992/1, p. 109– 114.

CHIOCCI, F.L., AND LA MONICA, G.B., 1996, Analisi sismostratigrafica della piattaforma continentale, in Il Mare del Lazio: Universita` degli Studi di Roma ''La Sapienza,'' Regione Lazio Assessorato Opere e Reti di Sevizi e Mobilita`, p. 41–61.

CIONI, R., LAURENZI, M.A., SBRANA, A., AND VILLA, I.M., 1993, 40Ar/39Ar chronostratig- raphy of the initial activity in the Sabatini Volcanic Complex (Italy): Societa Geologica Italiana, Bollettino, v. 112, p. 251–263.

COVAULT, J.A., FILDANI, A., ROMANS, B.W., AND MCHARGUE, T., 2011, The natural range of submarine canyon-and-channel longitudinal profiles: Geosphere, v. 7, p. 313–332.

CRITELLI, S., AND LE PERA, E., 1994, Detrital modes and provenance of Miocene sandstones and modern sands of the southern Appennines thrust-top Basins (Italy): Journal of Sedimentary Research, v. 64, p. 824–835.

CRITELLI, S., AND LE PERA, E., 2002, Provenance relations and modern sand petrofacies in an uplifted thrust-belt, northern Calabria, Italy, in Basu, A., and Vallone, R., eds., Quantitative Provenance Studies in Italy: Memorie Descrittive della Carta Geologica Italia, v. 61, p. 25–38.

CRITELLI, S., LE PERA, E., AND INGERSOLL, R.V., 1997, The effects of source lithology, transport, deposition and sampling scale on the composition of southern California sand: Sedimentology, v. 44, p. 653–671.

CRITELLI, S., ARRIBAS, J., LE PERA, E., TORTOSA, A., MARSAGLIA, K.M., AND LATTER, K.K., 2003, The recycled orogenic sand provenance from an uplifted thrust belt, Betic Cordillera, southern Spain: Journal of Sedimentary Research, v. 73, p. 72–81.

CROOK, K.A.W., 1960, Classification of arenites: American Journal of Science, v. 258, p. 419–428.

DICKINSON, W.R., 1970, Interpreting detrital modes of graywacke and arkose: Journal of Sedimentary Petrology, v. 40, p. 695–707.

DE RITA, D., FUNICIELLO, R., CORDA, L., SPOSATO, A., AND ROSSI, U., 1993, Volcanic Unit, in Di Filippo, M., ed., Sabatini Volcanic Complex: Consiglio Nazionale Delle Ricerche, Progetto Finalizzato ‘‘Geodinamica’’ Monografie Finali, v. 11, p. 33–79.

DE RITA, D., MILLI, S., ROSA, C., ZARLENGA, F., AND CAVINATO, G.P., 1994, Catastrophic eruptions and eustatic cycles: example of Lazio volcanoes: Atti dei Convegni Lincei, v. 112, p. 135–142.

DE RITA, D., FACCENNA, C., FUNICIELLO, R., AND ROSA, C., 1995, Stratigraphy and volcano- tectonics, in Trigila, R., ed., The Volcano of the Albani Hills: Tipografia S.G.S., p. 33– 71.

DE RITA, D., FABBRI, M., MAZZINI, I., PACCARA, P., SPOSATO, A., AND TRIGARI, A., 2002, Volcaniclastic sedimentation in coastal environments: the interplay between volcanism and Quaternary sea level changes (central Italy): Quaternary International, v. 95–96, p. 141–154.

DI BELLA, L., BELLOTTI, P., AND MILLI, S., 2013, The role of foraminifera as indicators of the Late Pleistocene–Holocene palaeoclimatic fluctuations on the deltaic environment: the example of Tiber delta succession (Tyrrhenian margin, Italy): Quaternary International, v. 303, p. 191–209.

DI RITA, F., AND MAGRI, D., 2009, Holocene drought, deforestation and evergreen vegetation development in the central Mediterranean: a 5500 year record from Lago Alimini Piccolo, Apulia, southeast Italy: The Holocene, v. 19, p. 295–306.

DOGLIONI, C., INNOCENTI, F., MORELLATO, C., PROCACCIANTI, D., AND SCROCCA, D., 2004, On the Tyrrhenian sea opening: Memorie Descrittive della Carta Geologica d’Italia, v. 64, p. 147–164.

FERRANTE, A., FRANCO, L., AND BOER, S., 1992, Modelling and monitoring of a perched beach at Lido di Ostia (Rome), in Edge, B.L., ed., Coastal Engineering, Proceedings, p. 3305–3318.

GABRIEL, K.R., 1971, The biplot graphic display of matrices with application to principal component analysis: Biometrika, v. 58, p. 453–467.

GAMBERI, F., AND MARANI, M., 2009, Control of regional geology on the style of basin-plain depositional systems in the Tyrrhenian Sea, in Kneller, B., Martinsen, O.J., and McCaffrey, B., eds., External Controls on Deep-Water Depositional Systems: SEPM, Special Publication 92, p. 221–232.

GAMBERI, F., DALLA VALLE, G., AND KNELLER, B., 2009, The impact of margin-shaping processes on the architecture of the Sardinian and Sicilian margin submarine depositional systems within the Tyrrhenian sea, in Kneller, B., Martinsen, O.J., and McCaffrey, B., eds., External Controls on Deep-Water Depositional Systems: SEPM, Special Publication 92, p. 207–219.

GARZANTI, E., 1986, Source rock versus sedimentary control on the mineralogy of deltaic volcanic arenites (Upper Triassic, northern Italy): Journal of Sedimentary Petrology, v. 56, p. 267–275.

GARZANTI, E., 2016, From static to dynamic provenance analysis: sedimentary petrology upgraded: Sedimentary Geology, v. 336, p. 3–13.

GARZANTI, E., 2017, The Maturity myth in sedimentology and provenance analysis: Journal of Sedimentary Research, v. 87, p. 353–365. doi: 10.2110/jsr.2017.17

GARZANTI, E., CANCLINI, S., FOGGIA, F.M., AND PETRELLA, N., 2002, Unraveling magmatic and orogenic provenance in modern sand: the back-arc side of the Appennine thrust belt, Italy: Journal of Sedimentary Research, v. 72, p. 2–17.

GARZANTI, E., ANDO`, S., AND VEZZOLI, G., 2009, Grain-size dependence of sediment composition and environmental bias in provenance studies: Earth and Planetary Science Letters, v. 277, p. 422–432.

GARZANTI, E., VEZZOLI, G., AND ANDO`, S., 2011, Paleogeographic and paleodrainage changes during Pleistocene glaciations (Po Plain, northern Italy): Earth-Science Reviews, v. 105, p. 25–48.

GARZANTI, E., ANDO`, S., PADOAN, M., VEZZOLI, G., AND EL KAMMAR, A., 2015, The modern Nile sediment system: processes and products: Quaternary Science Reviews, v. 130, p. 9–56.

GIORDANO, G., ESPOSITO, A., DE RITA, D., FABBRI, M., MAZZINI, I., TRIGARI, A., ROSA, C., AND FUNICIELLO, R., 2003, The sedimentation along the roman coast between Middle and Upper Pleistocene: the interplay of eustatism, tectonics and volcanism–new data and review: Il Quaternario, v. 16, p. 121–129.

GIRAUDI, C., 2011, The sediments of the ‘‘Stagno di Maccarese’’ marsh (Tiber river delta, central Italy): a late Holocene record of natural and human-induced environmental changes: The Holocene, v. 21, p. 1233–1243.

GUILLOCHEAU, F., ROUBY, D., ROBIN, C., HELM, C., ROLLAND, N., LE CARLIER DE VESLUD, C., AND BRAUN, J., 2012, Quantification and causes of the terrigeneous sediment budget at the scale of a continental margin: a new method applied to the Namibia–South Africa margin: Basin Research, v. 24, p. 3–30.

HANSON, H., BRAMPTON, A., CAPOBIANCO, M., DETTE, H.H., HAMM, L., LAUSTRUP, C., LECHUGA, A., AND SPANHOFF, R., 2002, Beach nourishment projects, practices, and objectives: a European overview: Coastal Engineering, v. 47, p. 81–111.

INCARBONA, A., DI STEFANO, E., SPROVIERI, R., BONOMO, S., PELOSI, N., AND SPROVIERI, M., 2010, Millennial-scale paleoenvironmental changes in the central Mediterranean during the last interglacial: comparison with European and North Atlantic records: Geobios, v. 43, p. 111–122.

INGERSOLL, R.V., BULLARD, T.F., FORD, R.L., GRIMM, J.P., PICKLE, J.D., AND SARES, S.W., 1984, The effect of grain size on detrital modes: a test of the Gazzi-Dickinson point counting method: Journal of Sedimentary Petrology, v. 54, p. 103–116.

JOHNSSON, M.J., 1990, Overlooked sedimentary particles from tropical weathering environments: Geology, v. 18, p. 107–110.

KARNER, D.B., MARRA, F., AND RENNE, P.R., 2001, The history of the Monti Sabatini and Alban Hills volcanoes: groundwork for assessing volcanic–tectonic hazards for Rome: Journal of Volcanology and Geothermal Research, v. 107, p. 185–219.

KUEHL, S.A., ALEXANDER, C.R., BLAIR, N.E., HARRIS, C.K., MARSAGLIA, K.M., OGSTON, A.S., AND CARTER, L., 2016, A source-to-sink perspective of the Waipaoa River margin: Earth-Science Reviews, v. 153, p. 301–334.

LECHI, G.M., AND TODISCO, A., 1980, Prospettive dell'impiego del telerilevamento nello studio della dispersione a mare di scarichi idrici inquinanti: Collana Progetto Finalizzato, Promozione della Qualità dell'Ambiente, AQ/6/2, 141 p.

LE PERA, E., AND ARRIBAS, J., 2004, Sand composition in an Iberian passive-margin fluvial course: the Tajo River: Sedimentary Geology, v. 171, p. 261–281.

LE PERA, E., AND CRITELLI, S., 1997, Sourceland controls on the composition of beach and fluvial sand of the northern Tyrrhenian coast of Calabria, Italy: implications for actualistic petrofacies: Sedimentary Geology, v. 110, p. 81–97.

LOCARDI, E., LOMBARDI, G., FUNICIELLO, R., AND PAROTTO, M., 1976, The main volcanic group of Lazio (Italy): relations between structural evolution and petrogenesis: Geologica Romana, v. 15, p. 279–300.

MALINVERNO, A., AND RYAN, W.B.F., 1986, Extension in the Tyrrhenian Sea and shortening in the Apennines as result of arc migration driven by sinking of the lithosphere: Tectonics, v. 5, p. 227–245.

MANCINI M., AND CAVINATO, G.P., 2005, The Middle Valley of the Tiber River, central Italy: Plio-Pleistocene fluvial and coastal sedimentation, extensional tectonics and volcanism, in Blum, M., Marriot, S., and Leclair, S., eds., Fluvial Sedimentology VII: International Association of Sedimentologists, Special Publication 35, p. 373–396.

MARCHESINI, L., AMOROSI, A., CIBIN, U., SPADAFORA, E., ZUFFA, G.G., AND PRETI, D., 2000, Detrital supply versus facies architecture in the late Quaternary deposits of the southeastern Po Plain (Italy): Journal of Sedimentary Research, v. 70, p. 829–838.

MARGARITELLI, G., VALLEFUOCO, M., DI RITA, F., CAPOTONDI, L., BELLUCCI, L.G., INSINGA, D.D., PETROSINO, P., BONOMO, S., CACHOF, I., CASCELLA, A., FERRAROA, L., FLORINDO, F., LUBRITTO, C., LURCOCK, P.C., MAGRI, D., PELOSI, N., RETTORI, R., AND LIRER, F., 2016, Marine response to climate changes during the last five millennia in the central Mediterranean Sea: Global and Planetary Change, v. 142, p. 53–72.

MARIANI, M., AND PRATO, R., 1988, I bacini Neogenici costieri del margine tirrenico: approccio sismico-stratigrafico: Societa` Geologica Italiana, Memorie, v. 41, p. 519–531. MARSAGLIA, K.M., 1992, Petrography and provenance of volcaniclastic sands recovered from the Izu–Bonin Arc, Leg 126: Proceedings of the Ocean Drilling Program, Scientific Results, v. 126, p. 139–154.

MARSAGLIA, K.M., AND TAZAKI, K., 1992, Diagenetic trends in ODP Leg 126 sandstone: Proceedings of the Ocean Drilling Program, Scientific Results, v. 126, p. 125–138.

MARSAGLIA K.M., LATTER, K.K., AND CLINE, V., 1999, Sand provenance in the Alborian and Tyrrhenian basins: Proceedings of the Ocean Drilling Program, Scientific Results, v. 161, p. 37–56.

MARSAGLIA, K.M., DAWSON, S., PARRA, J., RIVERA, K., DEVAUGHN, A., JAMES, D., AND KUEHL, S., 2007, Tracing sand from source to sink across eastern North Island, New Zealand. Insights from the shelf segment of the system [Abstract]: American Association of Petroleum Geologists, Annual Meeting, Long Beach, California, 1–4 April.

MARSAGLIA, K.M., DEVAUGHN, A.M., JAMES, D.E., AND MARDEN, M., 2010, Provenance of fluvial terrace sediments within the Waipaoa sedimentary system and their importance to New Zealand source-to-sink studies: Marine Geology, v. 270, p. 84–93.

MCBRIDE, E.F., 1985, Diagenetic processes that effects provenance determination in sandstone, in Zuffa, G.G., ed., Provenance of Arenites: Dordecht, Reidel, p. 95–114. MCBRIDE, E.F., AND PICARD, M.D., 1987, Downstream changes in sand composition, roundness, and gravel size in a short-headed, high-gradient stream, northwestern Italy: Journal of Sedimentary Petrology, v. 57, p. 1018–1026.

MCCOY, F.W., AND CORNELL, W., 1990, Volcaniclastic sediments in the Tyrrhenian Basin: Proceedings of the Ocean Drilling Program, Scientific Results, v. 107, p. 291–305.

MIKHAILOVA, M.V., BELLOTTI, P., VALERI, P., AND TORTORA, P., 1999, Intrusion of seawater into the river Part of the Tiber mouth: Water Resources, v. 26, p. 679–686.

MILLI, S., 1994, High-frequency sequence stratigraphy of the middle–late Pleistocene to Holocene deposits of the Roman Basin (Rome, Italy): relationships among high frequency eustatic cycles, tectonics and volcanism, in Posamentier, H.W., and Mutti E., eds., Second High-Resolution Sequence Stratigraphy Conference: Tremp, Spain, 20–27 June.

MILLI, S., 1997, Depositional setting and high-frequency sequence stratigraphy of the Middle–Upper Pleistocene to Holocene deposits of the Roman Basin: Geologica Romana, v. 33, p. 99–136.

MILLI, S., MOSCATELLI, M., PALOMBO, M.R., PARLAGRECO, L., AND PACIUCCI, M., 2008, Incised valleys, their filling and mammal fossil record: a case study from Middle–Upper Pleistocene deposits of the Roman Basin (Latium, Italy), in Amorosi, A., Haq, B.U., and Sabato, L., eds, Advances in Application of Sequence Stratigraphy in Italy: GeoActa, Special Publication 1, p. 67–87.

MILLI, S., D'AMBROGI, C., BELLOTTI, P., CALDERONI, G., CARBONI, M.G., CELANT, A., DI BELLA, L., DI RITA, F., FREZZA, V., MAGRI, D., PICHEZZI, R.M., AND RICCI, V., 2013, The transition from wave-dominated estuary to wave-dominated delta: the Late Quaternary stratigraphic architecture of Tiber River deltaic succession (Italy): Sedimentary Geology, v. 284–285, p. 159–180.

MILLI, S., MANCINI, M., MOSCATELLI, M., STIGLIANO, F., MARINI, M., AND CAVINATO, G.P., 2016, From river to shelf, anatomy of a high-frequency depositional sequence: the Late Pleistocene to Holocene Tiber depositional sequence: Sedimentology, v. 63, p. 1886– 1928.

MITCHUM, R.M., JR., AND VAN WAGONER, J.C., 1991, High-frequency sequences and their stacking pattern: sequence stratigraphy evidence of high-frequency eustatic cycles: Sedimentary Geology, v. 70, p. 131–170.

MORRONE, C., DE ROSA, R., LE PERA, E., AND MARSAGLIA, K.M., 2017, Provenance of volcaniclastic beach sand in a magmatic-arc setting: an example from Lipari island (Aeolian archipelago, Tyrrhenian Sea): Geological Magazine, v. 154, p. 804–828.

NOLI, A., DE GIROLAMO, P., AND SAMMARCO, P., 1996, Parameteri meteomarini e dinamica costiera, in Il Mare del Lazio: Università degli Studi di Roma ''La Sapienza,'' Regione Lazio Assessorato Opere e Reti di Sevizi e Mobilità, p. 285–315.

PARRA, J.G., MARSAGLIA, K.M., RIVERA, K.S., DAWSON, S.T., AND WALSH, J.P., 2012, Provenance of sand on the Poverty Bay shelf, the link between source and sink sectors of the Waipaoa River sedimentary system: Sedimentary Geology, v. 280, p. 208–233.

PATACCA, E., SARTORI R., AND SCANDONE P., 1990, Tyrrhenian basin and Appenninic arc: kinematic relations since late Tortonian times: Societa Geologica d'Italia, Memorie, v. 45, p. 425–451.

PECCERILLO, A., 2005, Plio-Quaternary Volcanism in Italy; Petrology, Geochemistry, Geodynamics: Heidelberg, Springer, 365 p.

PERRI, F., CRITELLI, S., DOMINICI, R., MUTO, F., TRIPODI, V., AND CERAMICOLA, S., 2012, Provenance and accomodation pathways of late Quaternary sediments in the deep-water northern Ionian Basin, southern Italy: Sedimentary Geology, v. 280, p. 244–259.

PEYRON, O., MAGNY, M., GORING, S., JOANNIN, S., BEAULIEU, J.L.D., BRUGIAPAGLIA, E., SADORI L., GARFI, G., KOULI, K., IOAKIM, C., AND COMBOURIEU-NEBOUT, N., 2013, Contrasting patterns of climatic changes during the Holocene across the Italian Peninsula reconstructed from pollen data: Climate of the Past, v. 9, p. 1233–1252.

PICARD, M.D., AND MCBRIDE, E.F., 2007, Comparison of river and beach sand composition with source rocks, Dolomite Alps drainage basins, northeastern Italy, in Arribas, J., Johnsson, M.J., and Critelli, S., eds., Sedimentary Provenance and Petrogenesis: Perspectives from Petrography and Geochemistry: Geological Society of America, Special Paper 420, p. 1–12.

REDDAD, H., EL TALIBI, H., PERRI, F., EL MOUSSAOUI, S., ZERDEB, M.A., ZAGHLOUL, M.N., AND CRITELLI, S., 2016, Textural and compositional controls on modern fluvial and beach sands of Mediterranean coastal Rif belt (Northern Rif, Morocco): Italian Journal of Geoscience, v. 135, p. 336–349.

SADORI, L., BERTINI, A., COMBOURIEU-NEBOUT, N., KOULI, K., MARIOTTI LIPPI, M., ROBERTS, N., AND MERCURI, A.M., 2013, Palynology and Mediterranean vegetation history: Flora Mediterranea, v. 23, p. 141–156.

TENTORI, D., MARSAGLIA, K.M., AND MILLI, S., 2016, Sand compositional changes as a support for sequence-stratigraphic interpretation: the Middle Upper Pleistocene to Holocene deposits of the Roman Basin (Rome, Italy): Journal of Sedimentary Research, v. 86, p. 1208–1227. doi:10.2110/jsr.2016.75

TOMMASI, P., CHIOCCI, F.L., AND ESU, F., 1998, Geotechnical properties of soft clayey sediments from the submerged Tiber River delta, Italy: Marine Georesources & Geotechnology, v. 16, p. 221–242.

TORTORA, P., 1995, La superficie deposizionali del delta sottomarino del Tevere: zonazione del sediment e processi associati: Società GeologicaItaliana, Bollettino, v.114, p.89– 105.

TORTORA, P., 1999, Una classificazione ternaria su base granulometrica per la descrizione del sedimento sui fondali marini: Societa` Geologica Italiana, Bollettino, v. 118, p. 65–73.

VEERMESCH, P., RESENTINI, A., AND GARZANTI, E., 2016, An R package for statistical provenance analysis: Sedimentary Geology, v. 336, p. 14–25.

WELTJE, G.J., 2006, Ternary sandstone composition and provenance: an evaluation of the ‘‘Dickinson model,’’ in Buccianti, A., Mateu-Figueras, G., and Pawlowsky-Glahn, V., eds., Compositional Data Analysis: From Theory to Practice: Geological Society of London, Special Publication 264, p. 611–627.

WELTJE, G.J., AND BROMMER, M.B., 2011, Sediment-budget modelling of multi-sourced basin fills: application to recent deposits of the western Adriatic mud wedge (Italy): Basin Research, v. 23, p. 291–308.

ZAGHLOUL, M.N., REDDAD, H., AND CRITELLI, S., 2009, Source-area controls on the composition of beach and fluvial sands on the southern side of the Gibraltar Strait and Western Alboran Sea (Flysch Basin, Internal and External, Domains, Northern Rif Chain): Journal of African Earth Sciences, v. 55, p. 36–46.

ZUFFA, G.G., 1980, Hybrid arenites, their composition and classification: Journal of Sedimentary Petrology, v. 50, p. 21–29.

ZUFFA, G.G., 1985, Optical analyses of arenites: influence of methodology on compositional results, in Zuffa, G.G., ed., Provenance of Arenites: NATO-ASI, Dordrecht, Reidel, p. 165–189.

CHAPTER 4: SAND VARIABILITY IN THE MODERN PO RIVER SYSTEM AND SEDIMENT DISPERSAL PATHWAYS IN THE PO COASTAL PLAIN SINCE THE LAST GLACIAL MAXIMUM

DANIEL TENTORI[1], ALESSANDRO AMOROSI[2], SALVATORE MILLI[1], AND KATHLEEN M. MARSAGLIA[3]

[1]Dipartimento di Scienze della Terra, SAPIENZA Università di Roma, Piazzale Aldo Moro 5, 00185 Roma, Italy

[2]Dipartimento di Scienze Biologiche, Geologiche e Naturali, Università di Bologna, Via Zamboni 67, 40126 Bologna, Italy

[3]Department of Geological Sciences, California State University Northridge, 18111 Nordhoff Street, Northridge, California 91330, U.S.A.

ABSTRACT: We examined downstream trends in sediment composition within the modern Po River system and defined provenance changes within a selected sector of the Upper Pleistocene to Holocene coastal plain in response to paleogeographic reorganization during the last glacial-interglacial cycle. The upper Po River and its western Alpine tributaries release plutoniclastic and metamorphiclastic detritus which is diluted downstream by sedimentary-lithic-rich sand supplied by Central Alpine and Northern Apennines tributaries. Sediment composition of the Upper Pleistocene to Holocene alluvial and coastal plain succession overlaps with the modern petrofacies, suggesting that ancient fluvial sand was sourced from a dynamic river system attributable to a distal paleo-Po. Ancient marine sand reflects an additional sediment contribution from a paleo-river network that drained the sedimentary cover of the Southern Alps and Northern Apennines and fed the coastal system, where sediment was redistributed by marine processes (e.g., waves and alongshore currents). Secondary controls on sand composition include downstream hydrodynamic sorting by size and sedimentary mixing by alongshore currents. Provenance changes during the last glacial-interglacial cycle record the effect of glacio-eustasy in controlling sediment generation and dispersal throughout the sequence development. Proximal South Alpine glaciofluvial fans and transverse Apennine rivers supplied the lowstand alluvial plain deposits during the Last Glacial Maximum and glacial covers likely contributed to the storage of detrital material sourced from the Alpine upland catchments. Additional input of sand rich in sedimentary lithics is recorded in the transgressive and highstand systems tracts of the coastal plain and marginal marine succession,

which document rapid paleodrainage shifts and stream captures and alongshore mixing of sand with Southern Alpine and Apennine provenance.

4.1 INTRODUCTION

Alluvial and marginal marine deposits include a wide variety of coexisting depositional systems whose lithofacies, facies associations and geometries, as well as their stratigraphic relationships, reflect the complex interaction between external forcing (climate, tectonics, and glacio-eustasy) and intrinsic autogenic processes. In this light, the stratigraphic architecture of continental to marine Upper Pleistocene and Holocene deposits, for which high-frequency sea-level changes and climate fluctuations are well known, can be investigated in detail to interpret the evolving paleogeography in response to allogenic and autogenic forcing factors. The generally high preservation of Quaternary depositional systems allows for their good spatial and temporal characterization, making it possible to investigate their complexity with multiple techniques that provide diverse pieces of information and high-resolution analyses.

Sand composition is highly sensitive to a suite of factors operating from grain production to final deposition and may provide valuable insights to decipher physical and chemical modifications occurring during the entire life cycle of sediments (Garzanti, 2016). In particular, tectonics and climate influence, at various scale, detrital grains production from hinterland source rocks, whereas eustasy and local autogenic factors control transport and dispersal mechanisms from source to sink (Amorosi and Zuffa, 2011; Garzanti, 2016). The composition of detrital grains has also proven to be an effective tool to support sequence-stratigraphic interpretation and to define provenance changes across key stratigraphic surfaces (Zuffa et al. 2015; Amorosi and Zuffa, 2011; Tentori et al., 2016, 2018). Sand compositional changes may reflect abrupt provenance modifications, which result from paleodrainage reorganization induced by external driving mechanisms and intrinsic autogenic factors. Sand petrography, thus, can help unravel the complex relationships among the main driving mechanisms.

The Po River, the longest in Italy, flows eastward for 652 km and empties into the Adriatic Sea, creating a fluvial-dominated delta plain with minor tidal and wave influence. The Upper Pleistocene to Holocene alluvial and coastal sedimentary successions of the Po Plain have been largely described in terms of sedimentology, facies architecture, paleontology, geochemistry, and sequence stratigraphy (Amorosi, 2012; Amorosi et al., 2014; 2016; 2017a; Bruno et al., 2017; Campo et al., 2017; Scarponi et al., 2017; Amorosi and Sammartino 2018). These studies have shown that

continuous accommodation (i.e., tectonic subsidence) was a major depositional control of Upper Pleistocene fluvial architecture, whereas glacio-eustatic fluctuations significantly influenced changes in sediment dispersal of Holocene coastal deposits. However, detailed petrographic characterization of Upper Pleistocene to Holocene Po Plain deposits is lacking, except for few locations on the Po Plain (Marchesini et al., 2000; Garzanti et al., 2012; Di Giulio et al., 2003).

In this study, we aim to reconstruct sediment provenance of the Upper Pleistocene to Holocene alluvial and coastal succession from the subsurface sedimentary record of the modern Po coastal plain. Actualistic petrographic analysis of a large dataset, that includes the modern Po drainage basin sand, will be combined with high-resolution stratigraphic, sedimentologic and chronologic data (Amorosi et al., 2017a). In particular, we aim to: i) investigate changes in sediment provenance and sediment dispersal pathways during the last 30 ky, across the last glacial/interglacial transition, ii) clarify the effects of sedimentary differentiation and hydrodynamic sorting in controlling the final composition of sand, and iii) define sand compositional variability across the lowstand, transgressive and highstand systems tracts of the Po Plain depositional sequence.

4.2 GEOLOGICAL SETTING

The Po River originates in the Western Alps and flows into the Adriatic Sea, receiving sediment from a great number of tributaries that drain the Apennine and Alpine chains (Fig. 4.1). The Po Plain represents both the Alpine retroforeland basin and the Apennines foredeep. The Alps and Apennines are very distinct mountain belts developed during the closure of the Mesozoic Tethyan basin (Carminati and Doglioni, 2012) and each bears distinct source-rock signatures (Fig. 4.1). The Alps are significantly more elevated (ranging from ~1000 to 4800 m a.s.l) than the Apennines (ranging from ~500 to 1300 m a.s.l.) and underwent higher rates of uplift and erosion removing sedimentary cover rocks and exhuming deeper structural levels, which provide diagnostic detrital signatures (Garzanti et al., 2004, 2006, 2008, 2010; Carminati and Doglioni, 2012). The Alpine belt was formed during the Cretaceous to present convergence of the Adriatic continental upper plate and subduction of the Mesozoic ocean and European passive continental margin (Dal Piaz et al., 2003; Carminati and Doglioni, 2012). The principal tectonic domains from the internal to the external side of the Alps are the Austroalpine composite nappe system, the Penninic zone, and the Helvetic zone. The Australpine-Southalpine system derives from the passive Adriatic continental margin and developed during the Cretaceous orogeny. The Pennides are mainly constituted by ophiolites scraped off the oceanic lithosphere and metamorphic units of the European continental

passive margin. The Helvetides derive from the deformation of the European continental margin and consist of basement and cover units. The Austroalpine and Penninic units are made of continental and minor oceanic nappes belonging to three structural levels which record increasing thermobaric conditions (Frey et al., 1999; Garzanti et al., 2006; Berger and Bousquet, 2008; Beltrando et al., 2010; Garzanti et al., 2010). The deep level of the Alpine belt mainly consists of eclogitic units (eclogite-facies metasediments and metabasites) that yield high-grade metamorphic source-rocks, locally associated with granitoid gneisses and metaophiolites. These units are exposed in the Western and Ligurian Alps. The intermediate level consists of granitoids, low- to medium-grade basement and metasedimentary rocks that underwent blueschist-facies, greenschist-facies, and amphibolite-facies metamorphism associated with ophiolite bodies that are exposed in the Western and Central Alps. The shallow structural level crops out in the Ligurian, Central and Eastern Alps and includes Mesozoic to early Eocene clastic turbidites and carbonate sequences (Di Giulio, 1992; Cibin et al., 2001; Bosellini et al., 2003). Carbonate platform sedimentary successions of Mesozoic age and volcanic products related to the Permian and Triassic magmatism are exposed in the Eastern (Dolomites) and Southern Alps (Bosellini et al., 2003).

South of the Po Plain, clastic sedimentary successions in the Northern Apennines record deep-marine sedimentation of Paleogene to Neogene age. In the Northern Apennines, the Ligurian units consisting of ophiolites, shales and Jurassic to Eocene carbonate turbidites overlie the Oligocene to late Miocene foredeep turbidite successions of the Macigno, Cervarola, and Marnoso-arenacea formations (Ricci Lucchi, 1986; Boccaletti et al., 1990; Dinelli et al., 1999). The epi-Ligurian succession consisting of marine sedimentary deposits rests unconformably on deformed Upper Jurassic-lower Eocene Ligurian Units (Ricci Lucchi, 1986; Cibin et al. 2001).

The Apennines and Alpine chains represent two distinct sources of sediment for the Pliocene-Quaternary Po Plain succession (Garzanti et al., 2011). The 7-km thick sedimentary succession of the Po Basin has been investigated in detail through subsurface stratigraphic logs, seismic profiles and magnetostratigraphic studies, and this allowed previous workers to subdivide the entire succession into several depositional sequences separated by regional unconformities, and internally organized into eccentricity-driven - 100 ky transgressive-regressive cycles (Ghielmi et al. 2013; Rossi et al., 2015; Amadori et al., 2019). In the Po Basin fill, the lower boundary of the youngest depositional sequence influenced by tectonics is dated to 0.87 Ma (Muttoni et al., 2003). The overlying succession records relatively continuous sedimentation and includes a distinctive alternation of coastal and alluvial deposits in a rapidly subsiding region, which promoted aggradationally-stacked

channel belt deposition and prevented valley incision during phases of sea-level fall (Amorosi et al., 1999, 2004, 2007, 2008; Scarponi and Kowalewski, 2004; Scarponi et al., 2013, Amorosi et al., 2017b).

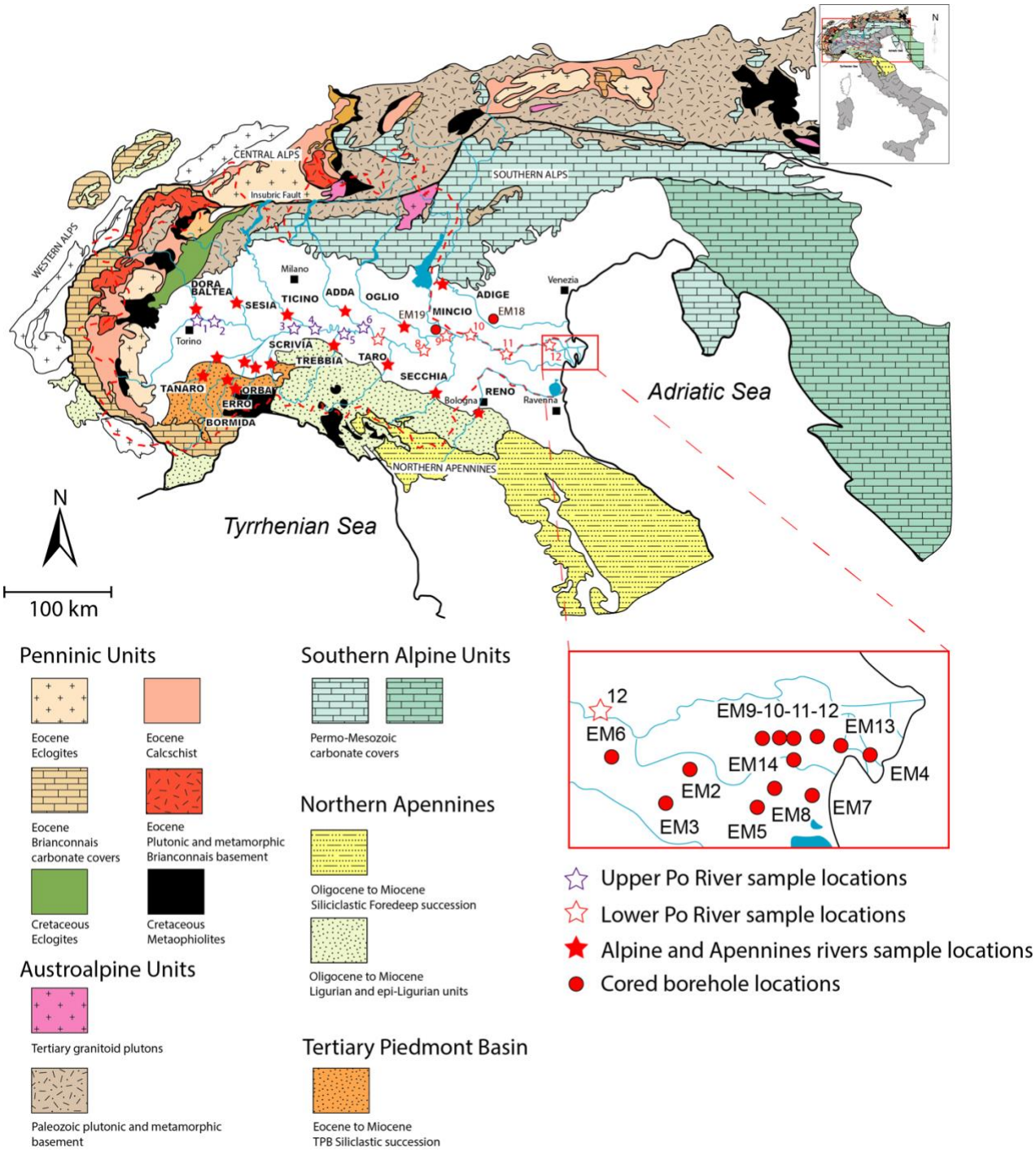

FIG. 4.1 — Geological map of the Po drainage basin with stream samples and cored borehole locations. Geology of the Alps and Apennines belts is after Dal Piaz et al. (2003) and Schmid et al. (2004).

In this study, we focus on sedimentation that occurred in the Po alluvial and coastal areas over the last glacial-interglacial cycle, with a particular emphasis on the Last Glacial Maximum (LGM) and post-glacial depositional sequence. In the Po coastal area, Upper Pleistocene alluvial deposits

(lowstand systems tract or LST) are separated by a pronounced transgressive surface from overlying barrier-lagoon systems (transgressive systems tract or TST) and prograding delta front deposits (highstand system tract or HST) (Fig. 4.2). The stepwise, post-18 kyr sea-level rise promoted the rapid landward migration of a wave-dominated estuarine depositional system on top of an alluvial system, resulting in a retrogradational stacking pattern of millennial-scale parasequences, whereas HST includes an aggradational to progradational stacking pattern of delta-front and prodelta-transition depositional systems encompassing the modern delta (Amorosi et al., 2017a; Bruno et al., 2017; Campo et al., 2017).

4.3 METHODS

Sampling was conducted between 2015 and 2019 on 18 modern streams and 13 cored boreholes (Fig. 1). Modern sand was collected from active bars in the Po and Alpine and Apennines rivers. Nine Po tributaries, including Dora Baltea, Sesia, Ticino, Adda, Oglio, Mincio, Tanaro, Bormida, Scrivia, Trebbia, Taro, and Secchia rivers and Erro, Orba, Reno and Adige rivers were sampled to represent the main source-rock types of the Po River drainage basin and catchments potentially similar to those that fed the late Pleistocene to Holocene alluvial, deltaic and coastal plain deposits (Fig. 4.1). Twelve stream-sand samples were also collected from the Po River downstream the confluence with the main tributaries to evaluate downstream changes in sediment composition.

Cores from fifteen boreholes, 13 penetrating the modern Po Delta (EM acronyms in Fig. 4.1 – see also Amorosi et al., 2017a; Bruno et al., 2017) and two in the alluvial plain at the confluence between Mincio and Po rivers (EM19) and near the Adige lower reaches (EM18), were sampled at various intervals to represent Upper Pleistocene alluvial (LST) and Holocene coastal (TST and HST) sand. Subsurface samples include medium- to fine-grained alluvial (fluvial channel, crevasse splays) and coastal (bay-head delta, transgressive barrier, delta front, prodelta-transition) depositional environments.

Quantitative petrographic analysis was conducted on a total of 88 samples. Thin sections from 30 modern sand and 56 ancient sand samples were stained with alizarine red to distinguish calcite and dolomite. Samples were sieved with a broad sand-size-range (125-500 μm) so that most of the size distribution of modern and ancient sand was considered. Modern samples are mostly medium-grained well-sorted sand (250-500 μm) whereas ancient sand is mostly finer-grained and range from fine to medium-grained (125-500 μm). Sand composition was quantified using the Gazzi-Dickinson point-count method (Ingersoll et al., 1984) which assign the sand-sized crystals within coarse-

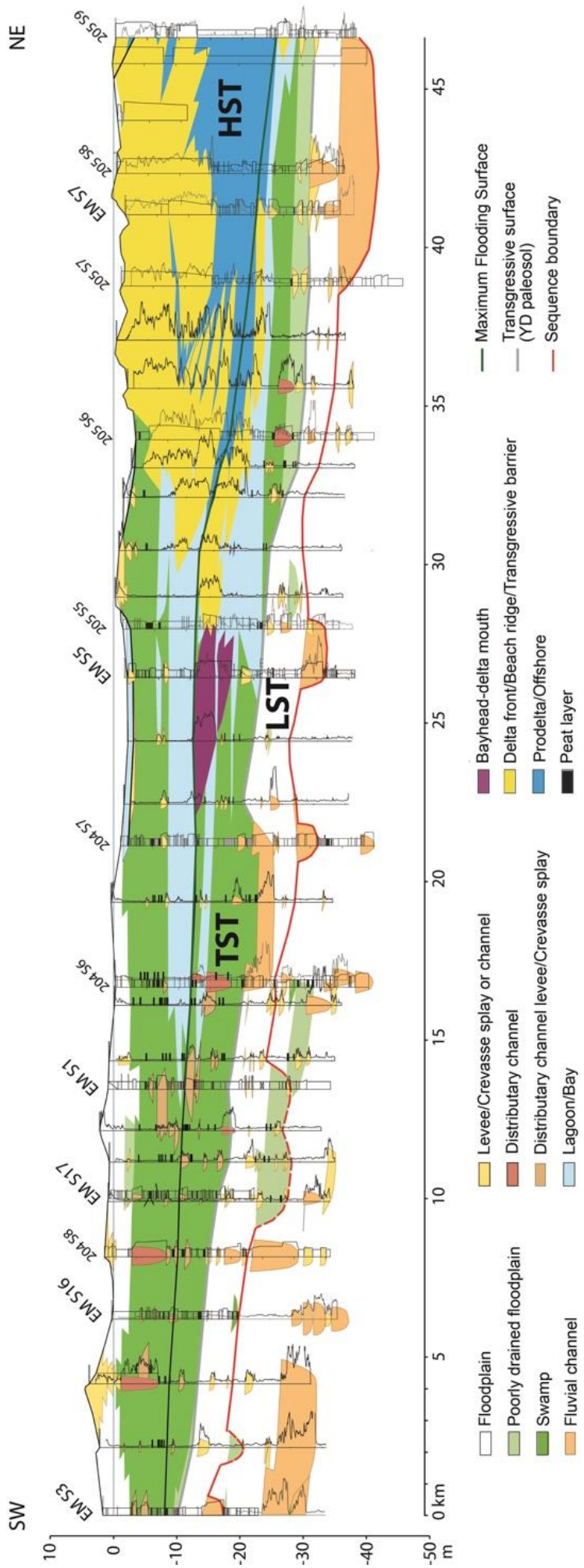

FIG. 4.2 —Stratigraphic architecture and sequence-stratigraphic interpretation of the late Quaternary succession of the Po Plain (after Amorosi et al., 2017a). LST: lowstand systems tract, TST: transgressive systems tract; HST: highstand systems tract.

grained rock fragments to the category of the grain, rather than to the category of the larger fragments. Counted grains were grouped into monomineralic and polymineralic categories (see Table C1 in Appendix C), including the metamorphic rock classification scheme based on Garzanti and Vezzoli (2003). Metamorphic lithic fragments were distinguished based on their protolith composition and metamorphic rank according to Winkler (1976), which assign ranks 1-2 to grains corresponding to the very-low grade field, ranks 3-4 to the low-grade, and rank 5 to medium/high-grade metamorphic fields. For sand classification, we used the descriptive nomenclature based on the Q:F:L relative abundance and prevailing rock fragment types, as proposed by Garzanti (2018). Various parameters were calculated to determine trends in compositional data (see Table C1 in Appendix C) and plotted on ternary diagrams proposed by Zuffa (1980, 1985) and Garzanti (2016). Ellipses of confidence regions at 95% were calculated on the entire and average compositions (Weltje, 2002; 2006) using the "R package for statistical provenance analysis" developed by Vermeesch et al. (2016). Confidence regions of the population mean, located with 95% of probability, were used to enhance data visualization and investigate compositional trends of large samples populations.

Sediment mineralogy was also investigated using X-ray powder diffraction on 6 modern and 16 ancient samples (bulk and <63 μm fractions) to define intrasample and inter-samples mineralogical variability and improve petrographic characterization. Identification of crystalline compounds was obtained using "X powder" software and the PDF2.DAT database of the International Center of Diffraction Data (ICDD).

4.4 DATA AND RESULTS

4.4.1 Modern sand petrography

Composition of modern Po River sand reflects sediment contribution from the Western, Central and Ligurian Alps, and Northern Apennine source rocks. The analysis of Alpine and Apennines river sands helped us identify signatures of source areas and describe the main sand components that, in different percentages, were recognized in the modern Po. In general, the monomineralic composition is quite homogeneous across our modern dataset and dominated by quartz and feldspar grains, whereas lithic fragment signatures range from sedimentaclastic to metamorphiclastic and testify sediment supply from a variety of sources, including metamorphic and plutonic source terranes of the Western Alps, 2nd cycle alpine detritus of the Ligurian Units, and surficial sedimentary covers of the Central/Eastern Alpine belts (Figs. 4.2, 4.3). The lithic fragments

composition of modern rivers samples allowed us to identify three main petrofacies that testify sediment supplied from a variety of sources, including metamorphic and plutonic source terranes of the Western and Ligurian Alps and surficial sedimentary covers of the Tertiary Piedmont Basin (TPB) and Central/Eastern Alpine and Northern Apennines belts (Fig. 4.2). In particular, three petrofacies with diagnostic Lm:Lv:Ls proportions (Fig. 3) reflect sediment contribution from: 1) the upper Po drainage basin, fed among other rivers by Dora Baltea, Sesia, and Ticino Alpine rivers and the Ligurian Alpine rivers including the Tanaro, Bormida, Orba, and Erro rivers (Petrofacies WLA); 2) the middle/lower Po drainage basin, fed by Central Alpine (Adda, Oglio) rivers and the Adige River, which at present flows from the Eastern Alps into the Adriatic Sea (downstream Petrofacies CA – Central/Eastern Alps), and 3) Trebbia, Taro, and Secchia Apennines rivers (Petrofacies AP - Apennines).

Western and Ligurian alpine rivers bear an almost identical lithic fragment signature. However, the WLA Petrofacies can be differentiated in two sub-petrofacies considering the Lm:Ls(silic):Lsc relative proportion that allow to discriminate 1st cycle (Penninic and Australpine domain source rock of the Western Alps, WA - Petrofaceis) from 2nd cycle alpine detritus (Ligurian Alps petrofacies - LA), the latter being mainly recycled from the TPB sedimentary succession (Fig. 4.3).

Here we provide a description of the main detrital components recognized in the modern petrofacies through petrographic observations on sand-sized sediment and mineralogical identification of bulk and fine-grained sediment (<63 micron) through XRD powder diffraction.

4.4.1.1 Petrofacies WLA – Western and Ligurian Alps rivers and upper Po River

Dora Baltea, Sesia, and Ticino rivers drain the Western Alps (Penninic domain and Australpine basement units) and Tanaro, Bormida e Orba drain the Ligurian Alps and supply the upper Po River (Po1-6) with feldspatho-quartzose and feldspatho-litho-quartzose sands (Figs. 4.3, 4.4). Monomineralic components include quartz, feldspar, micas (muscovite, biotite, chloritoid) and heavy-mineral minerals rich assemblages with pyroxene (clinopyroxene), amphibole (glaucophane, actinolite, hornblende), epidote, garnet, staurolite, titanite, kyanite, and fibrous sillimanite as single monomineralic grains and accessory minerals in metamorphic, plutonic and volcanic lithic fragments (Figs. 4.2, 4.3). Western Alpine and Ligurian Alps rivers and upper Po sand have a characteristic metamorphiclastic signature and carry low-rank to high-rank metapsammite (quartz-mica lithic fragments, muscovite and biotite gneiss rock fragments), metapelite (micaschist, phyllite) and metaigneous (with greenschist, blueschist and amphibolite facies minerals associations) grains

with schistose, gneissic and granofels textures. Ultramafic serpentinite grains (with cellular and schistose texture), siliciclastic (siltstone and shale) and carbonate rock fragments and felsic to mafic volcanic rock fragments (with felsitic, microlithic and lathwork texture) are minor components in the modern upper Po drainage basin.

4.4.1.2 Sub-petrofacies LA – Ligurian Alps rivers

The overall monomineralic and lithic fragment compositions of the Western and Ligurian Alps rivers sand are similar owing to reworking of 1st and 2nd cycle alpine sourced from the Western and Ligurian Alps respectively. However two sub-petrofacies can be distinguished based on the relative proportion of Lm:Ls(silic):Lsc and amount of serpentinite grains (Fig. 4.3). In particular, Ligurian Alps river sand shows higher amount of siliciclastic sedimentary lithic fragments bearing metamorphic detritus sourced in the Penninic and Australpine domains. Moreover, serpentinite grains with schistose texture are more abundant in the Erro, Orba and Bormida di Spigno rivers sourced from ophiolitic sequences of the Ligurian oceanic units.

4.4.1.3 Petrofacies AP - Northern Apennines rivers

Apennines (Trebbia, Secchia, Reno, and Scrivia rivers) sands have a sedimentaclastic feldspatho-quartzo-lithic to feldspatho-lithic signature (Figs. 4.3, 4.4). Monomineralic grains include quartz and feldspar grains, micas (muscovite, biotite), pyroxene (augite) and amphibole. Sedimentary lithic fragments (including carbonate rock fragments with micritic and sparitic texture, chert and arenaceous grains, siltstone and shale lithic fragments) are dominant, with minor volcanic (with felsitic, microlithic and lathwork textures) and low-rank metasedimentary (metapelite) and metavolcanic (chloriteschist) lithic fragments. Ultramafic rock fragments include serpentinite grains with cellular and schistose textures.

4.4.1.4 Petrofacies CA – Central/Eastern Alpine rivers and lower Po River

Central alpine tributaries (Adda, Oglio), the easternmost Adige River draining the Southalpine and Austroalpine domains, and the lower Po River (Po7-12) carry feldspatho-litho-quartzose to feldspatho-quartzo-lithic sand (Figs. 4.3, 4.4). Monomineralic grains include abundant quartz and feldspar grains and minor accessory minerals, such as micas (muscovite and biotite) and heavy-mineral assemblages (pyroxene, amphibole, garnet, epidote, sillimanite). Rocks fragments include abundant sedimentary lithic grains and variable amounts of metamorphic and volcanic lithic

fragments. Sedimentaclastic detritus is represented by common limestone (sparitic and micritic carbonate grains) and dolostone rock fragments with minor siliciclastic (pelitic and arenaceous) lithics. Metamorphic detritus is characterized by low- to high-rank metasedimentary and metapsammite grains (slate, phyllite, micaschist, and muscovite and biotite gneiss amphibolite-facies metasediment) and metavolcanic (metariolite, metadacite and metabasite grains) types. Volcanic lithic fragments include felsic, intermediate and mafic grains with felsitic, microlithic and lathwork textures. Ultramafic serpentinite grains are a minor component. Central and Eastern Alpine tributary sand is particularly enriched in carbonate lithic fragments. With respect to the lower Po composition, it shows a lower contribution from the metamorphic and basement source rocks of the upland catchments.

4.4.1.5 X-Ray powder diffraction

X-ray powder diffraction analysis of modern sand shows mineralogical differences among tributary samples and between upper and lower Po fluvial sand (Fig. C1 in Appendix C). We note an overall dominance of quartz, feldspar and mica in sediment sourced from the Western Alps (Sesia River sample) compared to dolomite- and calcite-rich sand supplied by rivers draining carbonate successions of the Central/Eastern Alps and Apennines (Adige and Secchia, respectively). Po River sand also shows a predominance of quartz and feldspar, with a downstream increase in calcite and dolomite. Finer-grained sediment fractions (<63 μm) show systematically higher peaks of intensity for calcite and dolomite compared to bulk analyses.

4.4.2 Modern sand composition: downstream trends

The modern Po River sand shows little QFL variability and affinity with the feldspatho-litho-quartzose composition of the Western Alpine tributary rivers that drain plutonic and metamorphic basement units in the Western Alps (Fig. 4.3).

The modern upper and lower Po river sands show very narrow compositions on the QFL diagram of Figure 4.3. The relative QFL abundances remain constant downstream, owing to reworking of 2nd cycle alpine detritus and progressive recycling of quartzofeldspathic foredeep turbidites from the northern Apennines. The Apennine turbidites were sourced or indirectly derived from the Alps in the old Alpine foreland and possibly sourced from the crystalline massifs of the Leopontine Dome (Garzanti and Malusà, 2008) and the Ivrea crustal block (Di Giulio, 1999) which shed abundant monomineralic quartz and feldspar grains. Thus, recycling of first- and second-cycle western Alpine

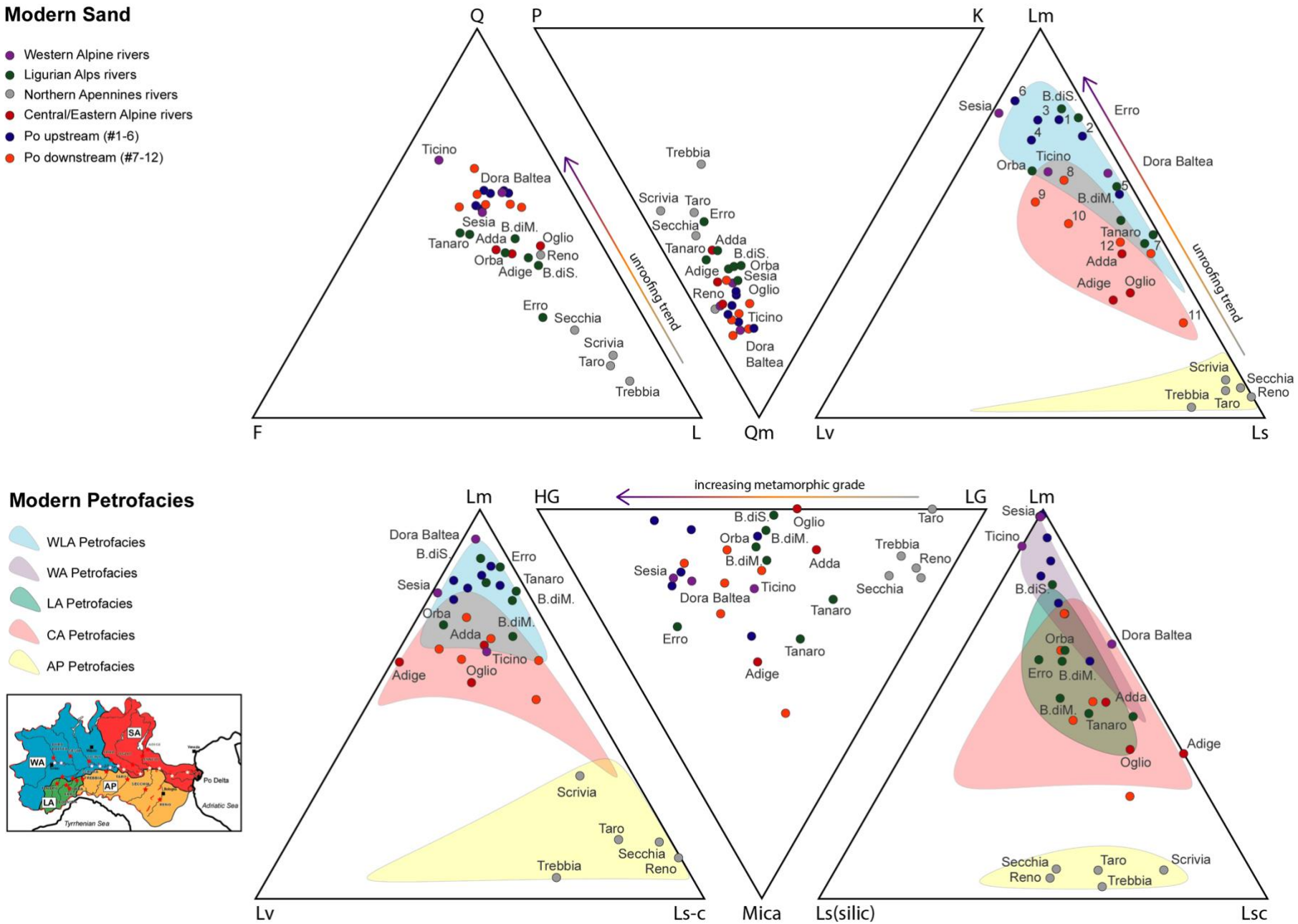

FIG. 4.3 — QFL, QmKP, LmLvLs, LmLvLs-c, MicaLGHG, LmLs(silic)Lsc ternary plots for modern Po, Apennine and Alpine river sand and WLA, WA, LA, CA and AP petrofacies identified in this work. Compositional fields on the LmLvLs, LmLvLs-c and LmLs-cLsc ternary diagrams are confidence regions at 95% calculated for Petrofacies WLA, WA, LA, CA, and AP. In the LmLvLs and LmLvLs-c ternary diagrams, note the lithic fragment compositional affinity between upper Po (1-6) sand and sand supplied by the Western and Ligurian Alps tributaries, and between lower Po (7-12) sand and sand from the Central/Eastern Alps rivers. Arrows highlight petrofacies successions from sedimentaclastic (Apennines and Central/Eastern Alpine rivers and lower Po sand) to metamorphiclastic and plutoniclastic sand (Western and Ligurian Alpine rivers and upper Po sand) and increasing metamorphic grade associated to unroofing of deeper tectonostratigraphic levels.

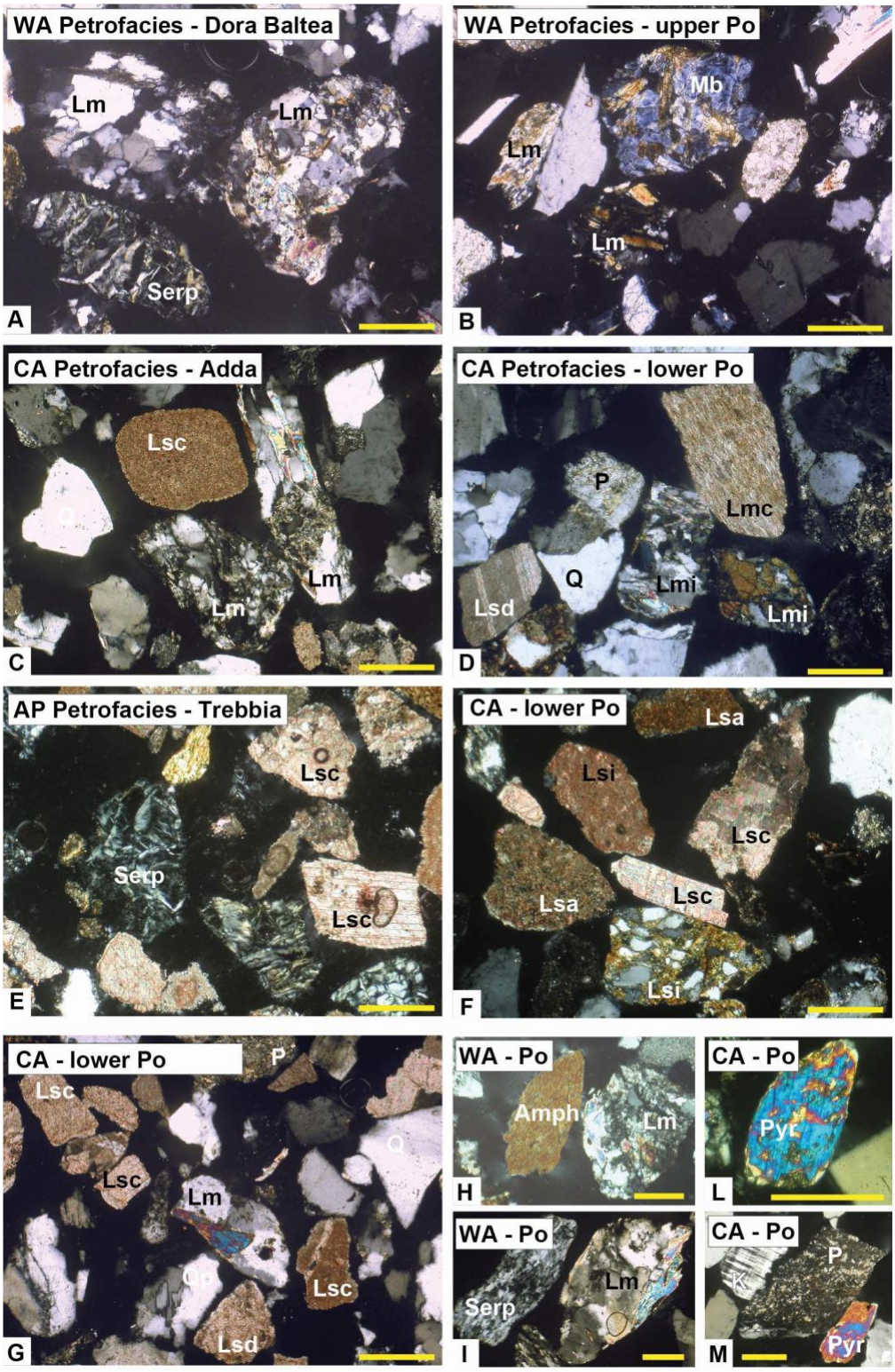

FIG. 4.4 — Main grain types in the modern petrofacies including Po and tributary rivers. Dora Baltea (A) and upper Po Sample #3 (B) metamorphiclastic sand (Lm=metatmorphic lithic fragment; Serp=serpentinite lithic fragment; Mb= metabasite grain). Adda (C) and Po mixed sedimentaclastic and metamorphiclastic Sample #7 (D) (Q=quartz; P=plagioclase feldspar; Lm=metamorphic lithic fragment; Lmc=metacarbonate lithic fragment; Lsc=carbonate lithic fragment; Lsd=dolostone rock fragment). Trebbia river sand (C) sourced from ophiolitic sequences of the Ligurian Units and carbonate turbidites sources (Serp=serpentinite; Lsc=carbonate lithic fragment). Sedimentaclastic sand (F, G) from the lower Po (#11, #12) (Lsi=siltstone lithic fragment). H-M) Other monomineralic grains (K= K-feldspar; Amph=Amphibole; Pyr= Pyroxene) and lithic fragments (Serp= serpentinite schist) from upstream and downstream Po River sand. Scale bars are 250 µm.

detritus yields an almost identical signature and results in the progressive dilution of carbonaticlastic sand fed by the middle course and downstream Alpine tributaries.

The QmKP ternary plot of Figure 4.3 shows a good correspondence between Po and Alpine tributaries compositions, but lower Q/F ratios compared to sand from the Ligurian Alps and Apennine rivers. Abundant detrital feldspars in Tertiary Piedmont Basin and Apennine siliciclastic turbidite sandstones were derived directly or indirectly from the Alps, suggesting that there was a major supply from granitoid and metagranitoid rocks during the Miocene, as well as a relatively higher sediment supply from the metamorphic source terrane rocks of the modern Alpine catchment.

The Po River system and its tributaries drain the sedimentary cover of the Ligurian Alps, Apennine belt and of South Alpine domains, as well as the deep and the intermediate structural levels of the western Alpine axial belt, providing an ideal compositional unroofing trend with diagnostic lithic signatures ranging from sedimentaclastic to metamorphiclastic (see also Garzanti et al., 2010) (Fig. 4.3). In particular, Apennine tributaries (Trebbia, Taro, Secchia and Scrivia rivers) and rivers draining the TPB carry sedimentaclastic sand derived from recycling of calcareous and siliciclastic turbidites covers (Fig. 4.1), whereas Central and Eastern Alpine rivers (Adda, Oglio and Adige) drain the basement units and the sedimentary cover of the South Alpine domain, carrying sedimentary lithic (limestone and dolostone rock fragments)-rich sand with intermediate values of metamorphic lithic fragments content compared to Apennines and Western Alpine rivers. These latter (Ticino, Sesia and Dora Baltea rivers), sourced in deeper tectonostratigraphic levels of the Alpine axial belt (ophiolites and basement of the Penninic domain – Fig. 4.1), mainly release plutoniclastic and metamorphiclastic detritus (Figs. 4.3, 4.4). The Ticino modern sand, however, overlaps with the CA petrofacies on the LmLvLs ternary diagram suggesting recycling from the Quaternary alluvial terrains of the Po plain. The Lago Maggiore could in fact represent an extremely efficient sediment trap of modern sand and reduce the Ticino downstream connectivity. A similar scenario was envisaged to interpret the Mincio sand composition which show unexpected high values (almost 100%) of sedimentary lithic fragment and very little metamorphic and plutonic detritus sourced from the upland catchments (see Table C2 in Appendix C). The artificial dam associated to its lower course and the natural Garda Lake, might function as sedimentary traps making the upland catchment detrital signature undetectable and reducing the tributary sediment discharge. Similarly, the present-day catchments of the Adda and Oglio rivers are divided downstream by the Lecco arm of the Como Lake and Iseo Lake, respectively, and result in enhanced downstream erosion of the

sedimentary cover of the South Alpine domain and reworking of Quaternary alluvial sediment with limited input from the upland source rocks.

The metamorphic grade of lithic fragments increases from the Apennines to the Central and Western Alps, where deeper tectono-stratigraphic levels are exposed (see MicaLGHG in Fig. 4.3). In the modern Po River, sedimentary lithic fragments (carbonate and siliciclastic grains) progressively increase downstream, from upper to lower Po River (see LmLvLs-c and LmLs-cLsc in Fig. 4.3). This trend reflects contribution from sedimentary source rocks of the South Alpine domain (Central and Eastern Alps) and northern Apennines and results from a continuous dilution of the western Alpine metamorphic signature. This downstream trend allowed us to create a compositional model to constrain sediment provenance of the Upper Pleistocene to Holocene Po coastal plain succession.

The diffraction patterns (Fig. C1 in Appendix C) of bulk and fine-grained (<63µm,) sediment fit the petrographic trends and suggest: (i) contribution of quartz, feldspar, micas and serpentine minerals from the Western Alps and Ligurian units of the Northern Apennines, and (ii) downstream increase of calcite and dolomite minerals derived from erosion of sedimentary units of the northern Apennines and Southern Alpine domains. In particular, Western Alpine (Sesia River), Eastern Alpine (Adige River) and northern Apennine (Secchia River) sediments suggest progressively increasing detrital contribution downstream from sedimentary (calcite- and dolomite-bearing) rocks in the Po drainage basin.

4.4.3 Sand petrography of cored samples

Upper Pleistocene to Holocene cored sand belongs to a variety of depositional environments, from lowstand fluvial (channel and levee) deposits, to transgressive estuarine (bay-head delta) and nearshore (transgressive barrier) facies associations, to highstand deltaic (delta front, prodelta-transition) deposits as interpreted by previous workers (Fig. 4.2). In general, terrigenous compositions are similar to those from the modern Po River system and the Apennines and Alpine tributaries, ranging from feldspatho-litho-quartzose to litho-quartzo-feldspathic. The marine facies associations show variable concentration in carbonate intrabasinal fraction which increase progressively in delta front ($NCE_{83}CE_{10}CI_{7}$), transgressive barrier ($NCE_{77}CE_{7}CI_{16}$) and prodelta ($NCE_{65}CE_{7}CI_{28}$) deposits.

The main extrabasinal grain types (Fig. 4.5) include dominant quartz, abundant feldspar, minor micas and heavy-mineral grains, common sedimentary (limestone and dolostone), subordinate metamorphic lithic fragments, and minor volcanic lithic fragments with felsic, intermediate, and

mafic compositions. Metamorphic lithic fragments include low- to high-rank metasedimentary (phyllite, quartz-mica schist, muscovite schist) and metaigneous (epidosite, amphibolite) rock fragments and ultramafic grain types (serpentineschist and cellular serpentine). In general, Upper Pleistocene to Holocene sand shows a wide range of lithic fragment proportions (Figs. 4.5, 4.6). Channel belt sand shows an overall higher metamorphic lithic content relative to more sedimentaclastic marine sand.

4.4.3.1 X-Ray powder diffraction

Diffraction patterns of cored sand and fine-grained (<63 μm) sediment samples from EM4, EM7, EM11, EM13 cores (Figs. C2, C3, C4, C5 in Appendix C) show a dominance of quartz, feldspar and variable amounts of calcite and dolomite**.** Minor components include mica, chlorite, amphibole and serpentine. Intrasample variability shows higher peaks of intensity for calcite and dolomite minerals in the finer-grained fractions (<63 μm).

4.4.4 Ancient sand compositional trends

Petrography of the Upper Pleistocene to Holocene alluvial and marine sand, and comparison with modern petrofacies from the Po River system, allow for identification of provenance changes in the study area as a function of depositional environments and their evolution through time. The LmLvLs ternary diagram of Figure 4.6 shows that fluvial (channel belt and crevasse channel deposits) sand composition overlaps almost entirely the modern CA Petrofacies (e.g., lower Po River), recording episodic sediment input from Western Alpine (e.g., paleoDora Baltea and paleoTicino compositions; Petrofacies WA) and Apennine (e.g., paleoSecchia and paleReno compositions; Petrofacies AP) source rocks. Bay-head delta and transgressive barrier sands show a narrow composition consistent with sediment provenance from the Central/Eastern Alps (Petrofacies CA). Delta front sand shows three distinct compositional groups that suggest provenance from the Po main trunk sourced in the western Alps (Petrofacies WA), the lower Po River and its downstream tributaries (Petrofacies CA), and Apennine rivers (Petrofacies AP), respectively. Prodelta-transition sedimentaclastic sand suggests significant sediment contribution from the South Alpine domain (Petrofacies CA).

In summary, lithic fragment composition of ancient marine sand suggests dilution of the western Alpine source rocks metamorphic signature and a major detrital supply from the Central/Eastern Alps and Apennines alongside with increased contribution from intrabasinal sources. This trend of

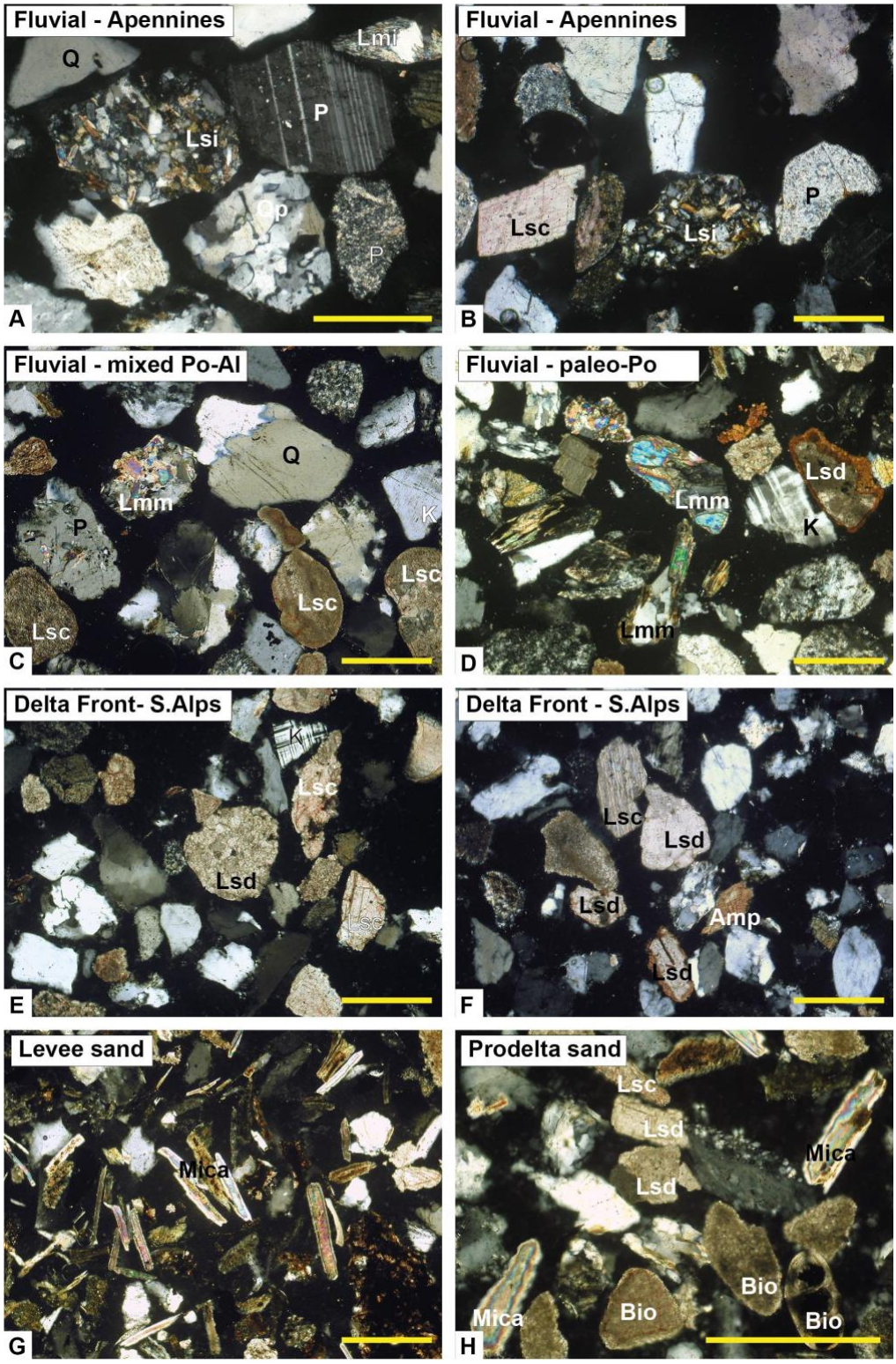

FIG. 4.5 — Main grain types in the Upper Pleistocene to Holocene fluvial and marine sand. (A, B) Ancient fluvial sand with Apennine provenance (Q=quartz; P=plagioclase feldspar; K=K-feldspar; Qp= polycrystalline sand; Lmi= metarhyolite lithic fragment; Lsi= siltstone lithic fragment). C) Ancient fluvial sand with mixed Po-Alpine provenance (Lsc= carbonate lithic fragment; Lmm= metapsammite lithic fragment). D) Ancient fluvial sand with paleo-Po provenance (Lsd=dolostone rock fragment). E, F) Sedimentaclastic ancient marine sand with Central/Eastern Alpine provenance. G) Mica-rich channel-levee sand. H) Bioclastic and carbonate-rich (limestone (Lsc) and dolostone (Lsd) lithic fragment) prodelta-transition sand. Scale bars are 250 µm.

enrichment of sedimentaclastic detrital material and biogenic intrabasinal fraction reflect a change in paleogeography and sediment dispersal paths following marine transgression and relative sea-level rise.

4.5 DISCUSSION

4.5.1 Paleoenvironmental evolution

Petrographic results record that the Upper Pleistocene to Holocene cored deposits analyzed in this study were sourced from a dynamic river system mainly attributable to the paleo-Po river system, with a significant contribution from Apennine and Alpine sources and locally significant sediment mixing as interpreted by previous workers. Terrigenous and intrabasinal grains defines abrupt vertical changes which reflect changes in facies association and dispersal paths following marine transgression.

Most fluvial-channel samples fall within the compositional range of the modern lower Po River, which is consistent with the downstream location of the study cores (Fig. 4.6). During the LGM, the fluvial channel belt was supplied predominantly by the paleo-Po main trunk, with its Alpine and Apennines tributaries, sourced in the metamorphic and plutonic basements of the Western Alps and sedimentary covers of the Central/Eastern Alps and Apennines, defining metamorphiclastic, sedimentaclastic and mixed compositions (Fig. 4.6).

During the early to middle Holocene transgression, the alluvial plain evolved into a wave-dominated estuarine system (Amorosi et al., 2017a; Bruno et al., 2017), and sediment delivered by the paleo-Po to the coastal area was deposited in small bay-head deltas and mixed and reworked in the marine environment, with sediment sourced from the Central/Eastern Alps (transgressive barrier deposits). This mixed composition reflects additional sediment contribution from a paleo-river network draining the sedimentary covers of the Central/Eastern Alps (Fig. 4.6). In this coastal system, sediment was redistributed by marine processes (e.g., waves and alongshore currents) and/or transported landwards from older transgressive barriers (Marchesini et al., 2000).

Finally, the mixed sediment composition of deltaic deposits in the upper cored intervals testifies to a late phase of sediment dispersal controlled by coastal progradation and alongshore reworking. Sediment compositions similar to those of the modern Po River (Fig. 4.6) likely reflect prograding delta systems very close to the river mouth, whereas enrichments in sedimentaclastic detrital material are interpreted to reflect progradation of adjacent strandplains, where along-strike sediment transport was significant.

Our findings fit sedimentological observations (Amorosi et al. 2017a) and sediment provenance characterization through heavy-metal contents by Bruno et al. (2017), who defined facies and provenance changes in the study area during the Holocene transgression. Petrography of the early Holocene sedimentaclastic marine sand, in particular, confirm the heavy-metal signatures from Amorosi et al. (2019), and suggests the significant role of south-directed alongshore currents in transporting sedimentary lithic-rich sand from the Alpine region.

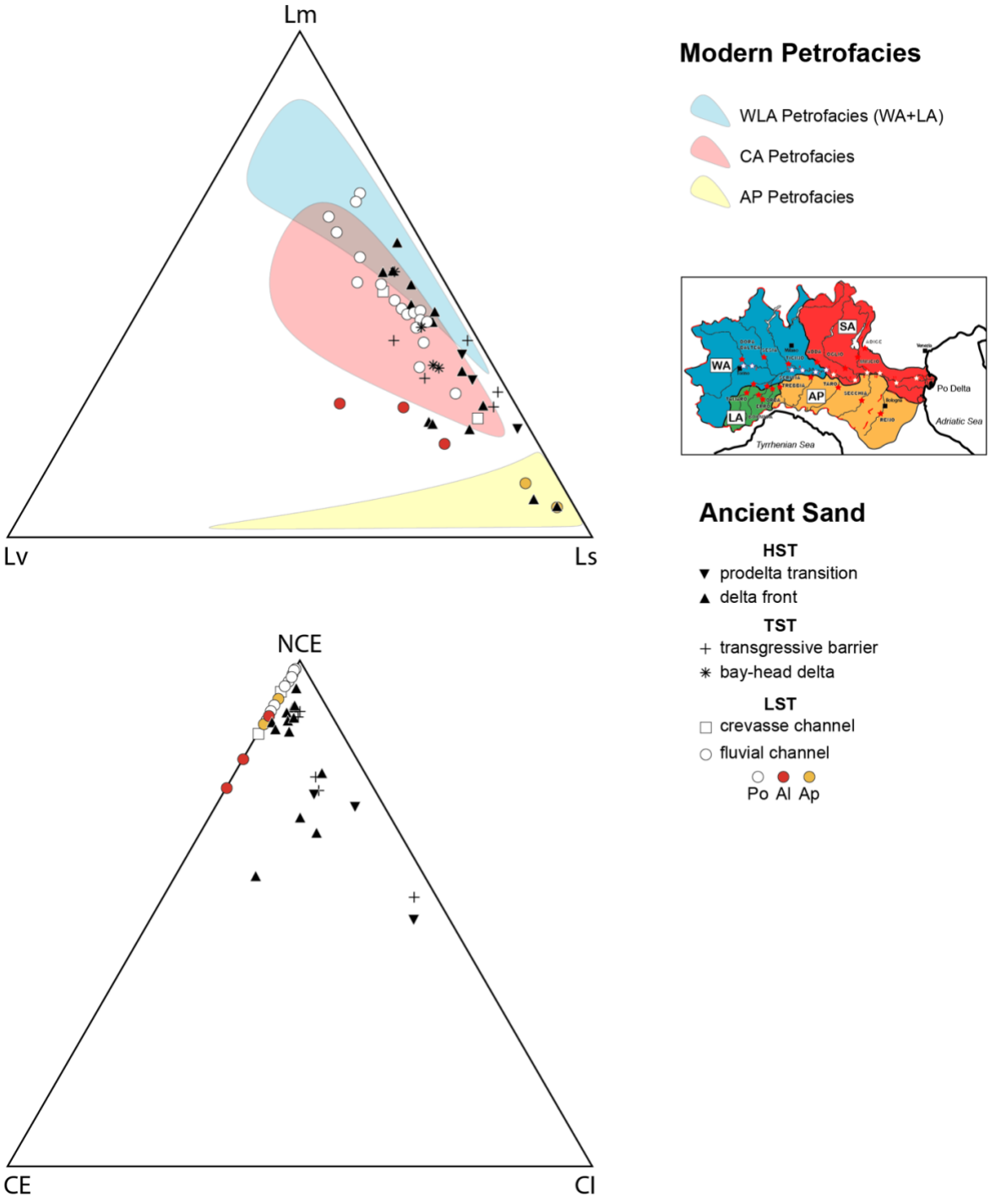

FIG. 4.6 —LmLvLs ternary plots of Holocene to Pleistocene sand, which include fluvial channel, crevasse channel, bay-head delta, delta front, transgressive barrier, and prodelta-transition deposits; these are compared with modern WLA, CA, and AP Petrofacies.

4.5.2 Compositional variability across systems tracts and key boundaries

Three systems tracts characterize the LGM and post-glacial succession of the Po Basin beneath the modern coastal plain (Amorosi et al., 2016; 2017a) (Fig. 4.2). A thick package of fluvial channel-belt deposits represents the lowstand systems tract, whereas the Holocene, transgressive-regressive coastal wedge forms the transgressive and highstand systems tracts.

Here, we analyze compositional trends across the LGM depositional sequence and explore the effect of glacio-eustatic fluctuations in controlling the sand compositional variability. Average lithic fragment compositions in the LST, TST and HST sand define three main petrofacies that show a progressive increasing contribution from sedimentary source rocks of the Central/Eastern Alps and Northern Apennines during the last interglacial (Fig. 4.7).

The Upper Pleistocene aggradational alluvial succession of the Po basin consists of distinct channel-belt sand bodies attributable to the lowstand systems tract and supplied by the paleo-Po river system (LST Po compositions in Fig. 4.7) or by its Alpine and Apennines tributaries (LST tributaries compositions in Fig. 4.7) depending on geographic location. The LST Po lithic fragment compositions are consistent with the downstream location of the study cores (lower Po River) and suggest that, at LGM, Alpine glaciers likely stored detrital material sourced from the upland catchments (e.g., metamorphic and basement units; see also Vittori and Ventura, 1995) and, while advancing many times during the last glaciations (Seguinot et al. 2018), fed glaciofluvial fans with abundant sedimentary lithic clasts eroded from the more proximal sources of the Southern Alps.

A significant change in sediment flux following the early Holocene transgression documents a major paleodrainage rearrangement, which is recorded in terms of changes in the Lm:Lv:Ls and Lm:Ls(silic):Lsc relative proportions. Average Lm/Ls and Lm/Lsc ratios reveal a notable change in lithic composition across the transgressive surface (TS), associated with the transition from an alluvial (LST) to an estuarine (TST) depositional system and reflecting enhanced supply via coastal processes from sedimentary sources in the Southern Alps (TST in Fig. 4.7). In contrast, no remarkable changes in sediment dispersal occurred between TST and HST deposits across the maximum flooding surface (MFS), at the turnaround from retrogradation to progradation (overlapping TST and HST compositions in Fig. 4.7). Contrasting LST vs TST compositional signatures, and little variability between TST and HST lithic fragment compositions confirm recent results from bulk-sediment geochemistry characterization in the Po coastal plain (Amorosi and Sammartino, 2018) which

showed significant changes in heavy metal contents and sediment dispersal pattern across the TS, but similar compositions across the MFS.

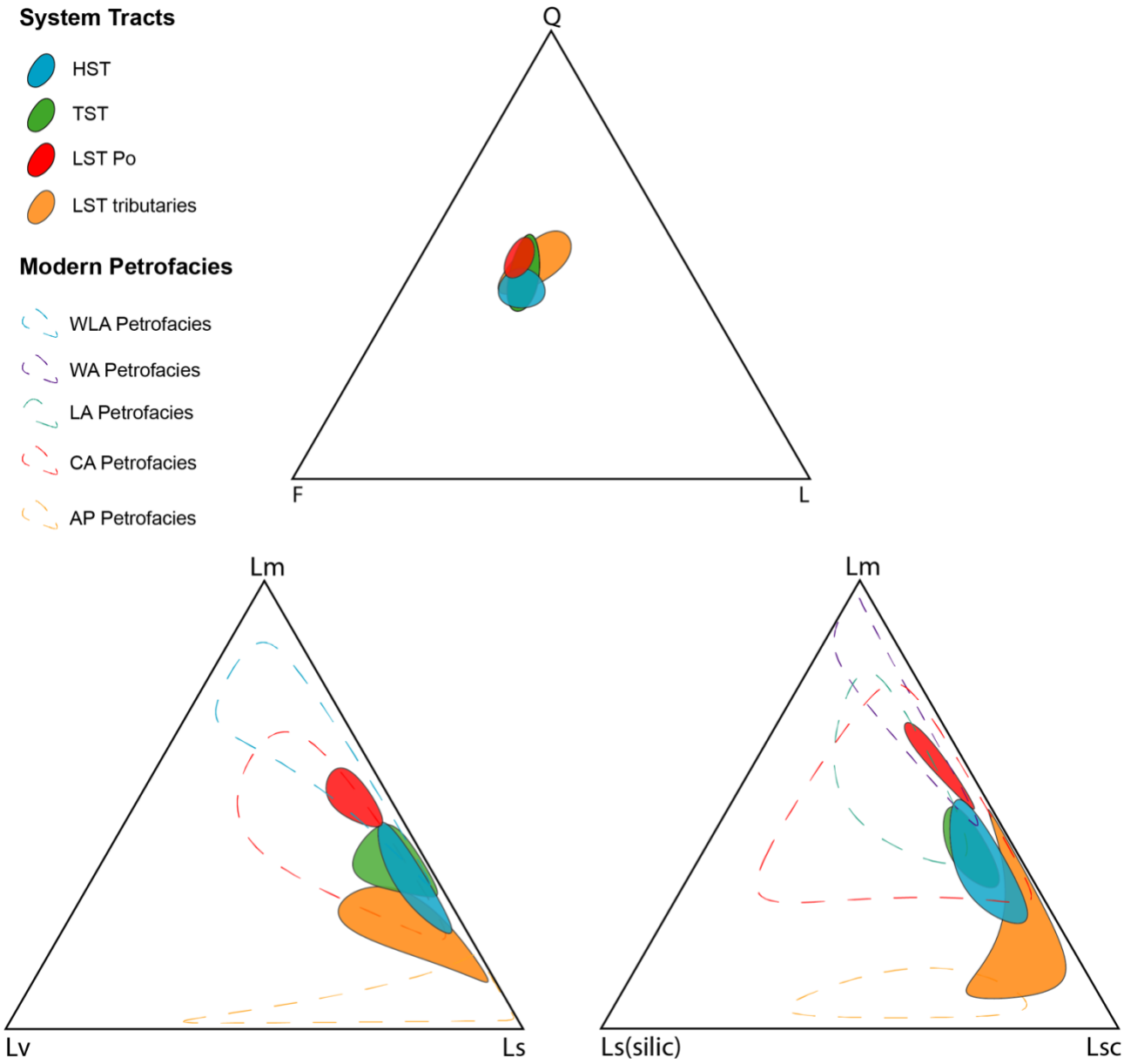

FIG 4.7 — QFL, LmLvLs and LmLs(silic)Lsc ternary plots of fluvial and marine sand corresponding to the lowstand (Po and Alpine and Apennines tributaries), transgressive and highstand systems tracts of the studied succession. Confidence regions calculated at 95% about the mean.

Alongside with increased extrabasinal carbonate fragment supply at the transition between LST and the TST and HST systems tracts deposits, we observe an enhanced contribution from intrabasinal carbonate sources which reflect changing paleogeographic condition during marine transgression and sea-level rise (Fig. 4.8). The compositional biplot in Figure 4.8 suggests that intrabasinal production reached is climax during the HST of the sequence whereas the TST deposits shows higher degree of riverine influence and lithic fragment proportion. In particular, the

sedimentaclastic signature of the TST deposits suggests that LST Po river sediment was partially trapped in the back-barrier environment during the configuration of the wave dominate estuary and mixed with sediment with south Alpine and Apennines signature or derived from reworking of older barriers with Po, Alpine and Apennines composition. The late phase of sediment dispersal regulated by coastal progradation during HST, defines lithic fragment compositions with an overall higher Lm to Ls ratio similar to those of the LST Po metamorphiclastic sand.

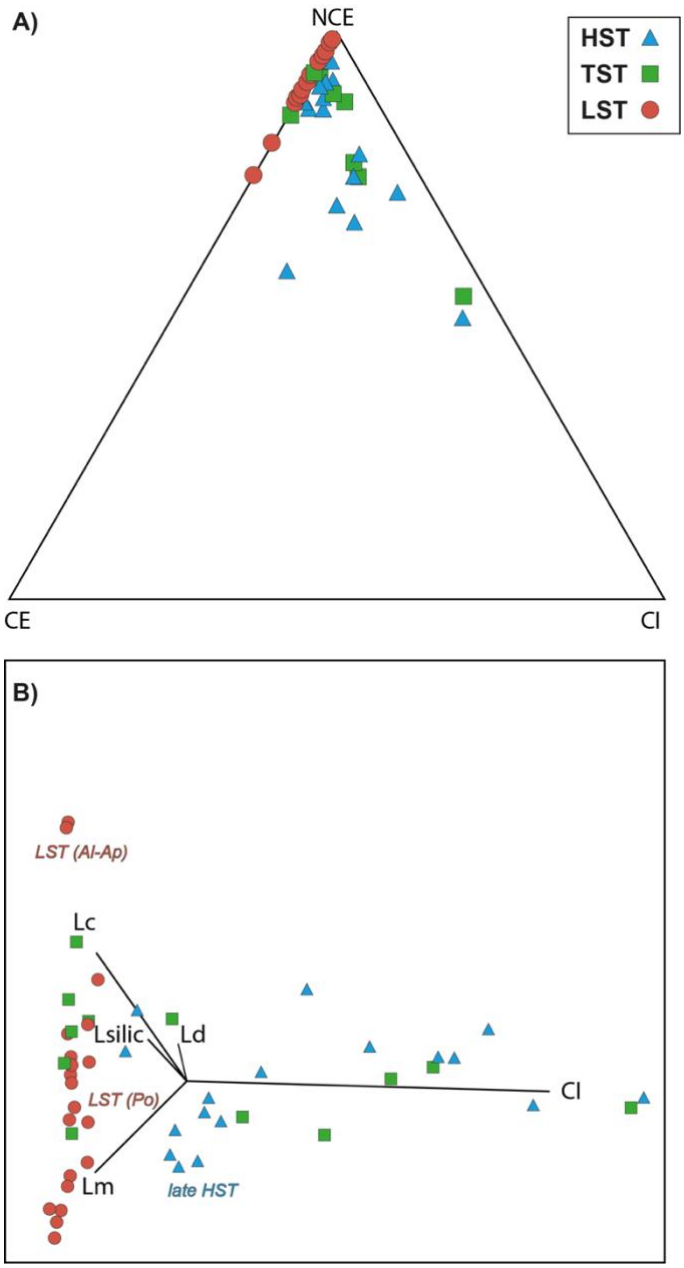

FIG. 4.8 — A) NCECECI ternary plot of LST, TST, and HST sand. B) Compositional biplot where the main extrabasinal (Lm= metamorphic lithic, Lc= limestone lithic, Lsilic= siliciclastic lithic, Ld= dolostone lithic fragments) and intrabasinal (CI= carbonate bioclasts) grains identify major changes in sediment dispersal and relative influence of river vs. marine related transport within the LST, TST and HST systems tracts. The length of each ray is proportional to the variability of the parameter in the data set; the angle between two rays reveals whether the corresponding parameters are well correlated (0°), uncorrelated (90°), or inversely correlated (180°) (from Veermesch et al. 2016).

4.5.3 Sedimentary differentiation and hydrodynamic sorting

In this study we provide a preliminary attempt to explain the QFL variability between the modern and ancient sand based on the compositional dependence by grain-size. Modern sediment sampled from the active fluvial bar is consistently coarser grained with respect to ancient fluvial and marine sand. Thus, the primary signal imparted by source-rock lithologies in modern and ancient sands could be affected by size-dependent compositional variability. In particular, different mechanisms of transport (e.g., suspended load vs. bedload) regulate hydrodynamic sorting by size and may control compositional variability between modern and ancient sand and between fluvial and marine sand. In the case of the modern Po and ancient coastal plain deposits, these grain-size-controlled trends might reflect mixing of finer second-cycle detritus reworked from the northern Apennines feldspathic turbidites with coarser and basement-derived sand sourced from the upland Alpine catchments. Relatively coarser-grained sand sampled from modern, active fluvial bars (e.g. modern river bedload) shows an overall higher quartz to feldspar content compared with fine-grained ancient sand, which likely includes higher volumes of suspended load deposited in the ancient channel-belt system (Fig. 4.9). Thus, progressive enrichment of fine-grained feldspar grains and dilution of coarser quartz grains result from hydrodynamic grain-size fractionation, which is controlled by different mechanism of transport (e.g., suspended load vs. bedload) and that has been described in several depositional environments (see also Odom et al., 1970; Parra et al. 2012; Garzanti et al. 2015; Tentori et al., 2018). Downstream, hydrodynamic sorting likely controlled intersample variability between ancient fluvial and marine sand and progressively concentrated the fine and very-fine grained feldspar-rich sand transporting detrital material as suspended load in the marine environments, where it further mixed with feldspar-rich detritus supplied by the Apennines rivers along the coast.

A quantitative estimation of grain-size classes of modern and ancient detrital populations is necessary to further constrain the role of hydrodynamic sorting by size and mechanism of transport in regulating compositional trends and variability between modern and ancient fluvial and marine sand.

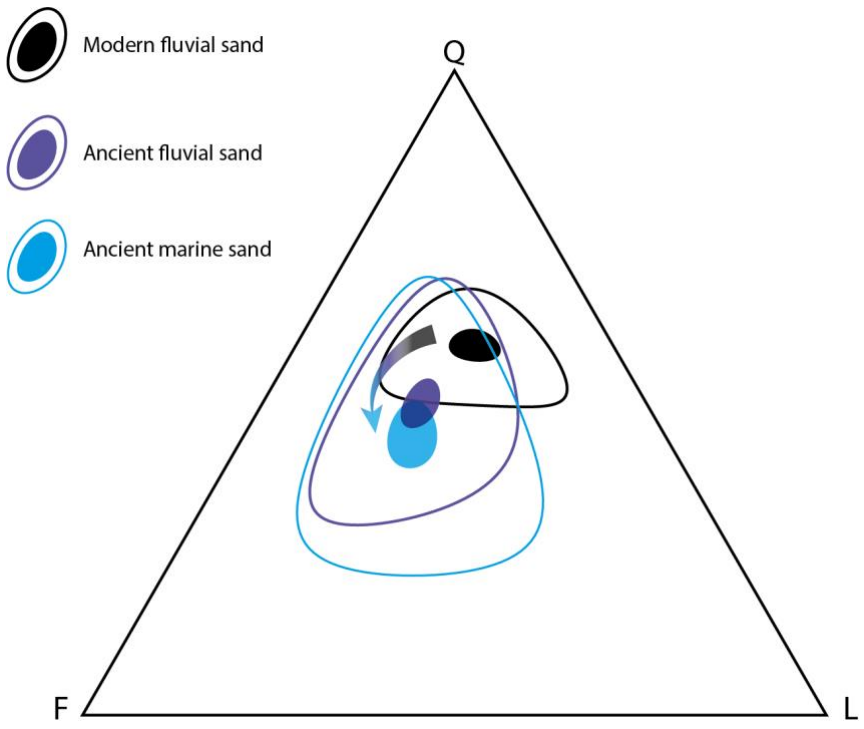

FIG. 4.9 — QFL ternary diagrams of modern fluvial (medium-grained sand) and ancient (medium to fine-grained fluvial and marine sand) sand. Ellipses of confidence regions at 95% were calculated on the entire sample set (empty fields) and average (filled fields) compositions. The arrow indicates a decrease in grain size. Note that finer-grained marine sand is relatively enriched in feldspar grains.

4.6 CONCLUSIONS

Sand petrography and XRD data in the modern Po River watershed allowed for the characterization of sand provided from different source-rock lithologies exposed in the adjacent Alpine and Apennines mountain belts and the definition of modern fluvial sand composition on a basin scale. The upper Po River catchment, and especially its Western Alpine tributaries, release characteristic plutoniclastic and metamorphiclastic detritus. This is diluted downstream by sedimentary-lithic-rich sand supplied by Central Alpine and Apennines tributaries that drain carbonate platform covers and thick siliciclastic and calcareous turbidite successions, respectively. Percentages of metamorphic vs. sedimentary lithic fragments, thus, can be used to discriminate the relative influence of upstream vs. downstream catchment source rocks.

Comparison between modern detrital signatures and sand composition of Upper Pleistocene-Holocene cored successions of the modern coastal plain suggests that alluvial sand during the Last Glacial Maximum was sourced by distinct fluvial sources, which included the main trunk of the Po river, with a minor contribution from rivers draining the Apennines and south Alpine (Central/Eastern Alps) domains.

The paleoenvironmental evolution in the study area following the early Holocene transgression documents a significant paleodrainage rearrangement which is recorded in sand deposits by

distinctive changes in Lm:Lv:Ls relative proportions. In the wave-dominated estuarine depositional system that developed during the last interglacial, following relative sea-level rise, Po-derived detritus mixed in the coastal system with sediment fed by Central/Eastern Alpine rivers, which was redistributed southwards by alongshore currents. The similar, mixed composition of late Holocene depositional systems reflects progradation of Po delta lobes (similar in composition to Po River sands) and adjacent strandplains (typified by sediment mixing due to alongshore transport).

Detrital modes were also used to define changes in sediment dispersal pathways within a sequence stratigraphic framework. Compositional signatures of sand deposits record the effect of glacio-eustatic forcing in controlling sediment generation and transport throughout the sequence development. The transgressive surface marks a major change in lithic fragment composition that reflects the abrupt transition from an alluvial (LST) to an estuarine (TST) depositional system. In contrast, no significant change at the MFS is captured in the sand petrographic record. The relative power of river related transport versus along-shore and coastal processes among the LST, TST, HST can be read as a function of lithic fragment composition and increasing contribution from the sedimentary sources in the Southern Alps (Lm to Ls ratio). The ratio between extrabasinal and intrabasinal grains proportion within the LST, TST and HST systems tracts defines major changes in facies associations that occur across transgressive and maximum flooding surfaces and can be used to investigate the relative influence of river related transport (e.g, terrigenous input) versus intrabasinal carbonate production throughout the sequence development.

SUPPLEMENTARY MATERIAL - See Appendix C -

ACKNOWLEDGEMENTS

We wish to thank Irene Sammartino for the collection of modern stream sediment samples. This work greatly benefitted from comments and suggestion on a previous version of the manuscript by Andrea Di Giulio and Salvatore Critelli. This work was partially funded by SAPIENZA, University of Rome (Progetto di Ateneo).

REFERENCES

AMADORI, C., TOSCANI, G., DI GIULIO, A., MAESANO, F.E., D'AMBROGI, C., GHIELMI, M. AND FANTONI, R., 2019, From cylindrical to non-cylindrical foreland basin: Pliocene–Pleistocene evolution of the Po Plain–Northern Adriatic basin (Italy): Basin Research, v. 31, p. 991-1015.

AMOROSI, A. AND SAMMARTINO, I., 2011, Assessing natural contents of hazardous metals in soils by different analytical methods and its impact on environmental legislative measures: International Journal of Environment and Pollution, v. 46, p. 164-177.

AMOROSI, A. AND ZUFFA, G.G., 2011, Sand composition changes across key boundaries of siliciclastic and hybrid depositional sequences: Sedimentary Geology, v. 236, p. 153-163.

AMOROSI, A. AND SAMMARTINO, I., 2018, Shifts in sediment provenance across a hierarchy of bounding surfaces: A sequence-stratigraphic perspective from bulk-sediment geochemistry: Sedimentary Geology, v. 375, p.145-156.

AMOROSI, A., COLALONGO, M.L., PASINI, G., PRETI, D., 1999, Sedimentary response to late Quaternary sea-level changes in the Romagna coastal plain (northern Italy): Sedimentology, v. 46, p. 99-121. http://dx.doi.org/10.1046/j.1365-3091.1999.00205.x.

AMOROSI, A., COLALONGO, M.L., FIORINI, F., FUSCO, F., PASINI, G., VAIANI, S.C., SARTI, G., 2004, Palaeogeographic and palaeoclimatic evolution of the Po Plain from 150-ky core records: Global Planetary Change, v. 40, p. 55-78. http://dx.doi.org/10.1016/ S0921-8181(03)00098-5.

AMOROSI, A., COLALONGO, M.L., DINELLI, E., LUCCHINI, F., VAIANI, S.C., 2007, Cyclic variations in sediment provenance from late Pleistocene deposits of the eastern Po Plain, Italy. In: Arribas, J., Critelli, S., Johnsson, M.J., (Eds.), Sedimentary Provenance and Petrogenesis: Perspectives from Petrography and Geochemistry: Geological Society of America Special Paper 420, p. 13–24.

AMOROSI, A., PAVESI, M., RICCI LUCCHI, M., SARTI, G., PICCIN, A., 2008, Climatic signature of cyclic fluvial architecture from the Quaternary of the central Po Plain, Italy: Sedimentary Geology, v. 209, p. 58-68. http://dx.doi.org/10.1016/j.sedgeo.2008.06.010.

AMOROSI, A., BRUNO, L., ROSSI, V., SEVERI, P. AND HAJDAS, I., 2014, Paleosol architecture of a late Quaternary basin–margin sequence and its implications for high-resolution, non-marine sequence stratigraphy: Global Planetary Change, v. 112, p. 12–25.

AMOROSI, A., MASELLI, V. AND TRINCARDI, F., 2016, Onshore to offshore anatomy of a late Quaternary source-to-sink system (Po Plain–Adriatic Sea, Italy): Earth-Science Reviews, v. 153, p. 212-237.

AMOROSI, A., BRUNO, L., CAMPO, B., MORELLI, A., ROSSI, V., SCARPONI, D., HONG, W., BOHACS, K.M. AND DREXLER, T.M., 2017a, Global sea-level control on local parasequence architecture from the Holocene record of the Po Plain, Italy: Marine and Petroleum Geology, v. 87, p. 99-111.

AMOROSI, A., BRUNO, L., CLEVELAND, D.M., MORELLI, A., HONG, W., 2017b, Paleosols and associated channel-belt sand bodies from a continuously subsiding late Quaternary system (Po

Basin, Italy): New insights into continental sequence stratigraphy: Geological Society of America Bulletin, v. 129, p. 449-463.

AMOROSI, A., BRUNO, L., CAMPO, B., COSTAGLI, B., DINELLI, E., HONG, W., SAMMARTINO, I. AND VAIANI, S.C., 2019, Tracing clinothem geometry and sediment pathways in the prograding Holocene Po Delta system through integrated core stratigraphy: Basin Research, in print.

BELTRANDO, M., COMPAGNONI, R., AND LOMBARDO, B., 2010, Ultra-high-pressure metamorphism and orogenesis: an Alpine perspective: Gondwana Research, v. 18, p. 147–166. doi:10.1016/j.gr.2010.01.009.

BERGER, A., AND BOUSQUET, R., 2008, Subduction related metamorphism in the Alps: Review of isotopic ages based on petrology and their geodynamic consequences, *in* Siegesmund, S., Fuegenschuh, B., Froitzheim, N. (Eds.), Tectonic Aspects of the Alpine-Dinaride-Carpathian-Geological Society, London, Special Publication 298, p. 117–144.

BOCCALETTI, M., CALAMITA, F., DEIANA, G., GELATI, R., MASSARI, F., MORATTI, G. AND LUCCHI, F.R., 1990, Migrating foredeep-thrust belt systems in the northern Apennines and southern Alps: Palaeogeography, Palaeoclimatology, Palaeoecology, v. 77, p. 3-14.

BOSELLINI, A., GIANOLLA, P., & STEFANI, M., 2003, Geology of the Dolomites: Episodes, v. 26, p. 181-185.

BRUNO, L., BOHACS, K.M., CAMPO, B., DREXLER, T.M., ROSSI, V., SAMMARTINO, I., SCARPONI, D., HONG, W. AND AMOROSI, A., 2017, Early Holocene transgressive palaeogeography in the Po coastal plain (northern Italy): Sedimentology, v. 64, p. 1792-1816.

CAMPO, B., AMOROSI, A. AND VAIANI, S.C., 2017, Sequence stratigraphy and late Quaternary paleoenvironmental evolution of the Northern Adriatic coastal plain (Italy): Palaeogeography, Palaeoclimatology, Palaeoecology, v. 466, 265-278.

CARMINATI, E. AND DOGLIONI, C., 2012, Alps vs. Apennines: the paradigm of a tectonically asymmetric Earth: Earth-Science Reviews, v. 112, p. 67-96.

CIBIN, U., SPADAFORA, E., ZUFFA, G.G., AND CASTELLARIN, A., 2001, Continental collision history from arenites of episutural basins in the northern Apennine, Italy: Geological Society of America Bulletin, v. 113, p. 4-19.

DAL PIAZ, G.V., BISTACCHI, A. AND MASSIRONI, M., 2003, Geological outline of the Alps: Episodes, v. 26, p. 175-180.

DINELLI, E., LUCCHINI, F., MORDENTI, A. AND PAGANELLI, L., 1999, Geochemistry of Oligocene–Miocene sandstones of the northern Apennines (Italy) and evolution of chemical features in relation to provenance changes: Sedimentary Geology, v. 127, p. 193-207.

DI GIULIO, A., 1992, The evolution of the Western Ligurian Flysch Units and the role of mud diapirism in ancient accretionary prisms (Maritime Alps, Northwestern Italy): Geologische Rundschau, v. 81, p. 655-668.

DI GIULIO, A., 1999, Mass transfer from the Alps to the Apennines: volumetric constraints in the provenance study of the Macigno–Modino source–basin system, Chattian–Aquitanian, northwestern Italy: Sedimentary Geology, v. 124, p. 69-80.

DI GIULIO A., CERIANI A., GHIA E. & ZUCCA F., 2003, Composition of modern stream sands derived from sedimentary source rocks in a temperate climate (northern Apennines, Italy): Sedimentary Geology, v. 158, p. 145–161.

FREY, M., DESMONS, J., AND NEUBAUER, F., 1999, The new metamorphic map of the Alps: Schweizerische Mineralogische und Petrographische Mitteilungen, v. 79, p. 1–209.

GARZANTI, E., 2016. From static to dynamic provenance analysis—Sedimentary petrology upgraded: Sedimentary Geology, v. 336, p. 3-13.

GARZANTI, E., 2018, Petrographic classification of sand and sandstone: Earth-Science Reviews, v. 192, p. 545-563.

GARZANTI, E. AND VEZZOLI, G., 2003, A classification of metamorphic grains in sands based on their composition and grade: Journal of Sedimentary Research, v. 73, p. 830-837.

GARZANTI, E., VEZZOLI, G., LOMBARDO, B., ANDÒ, S., MAURI, E., MONGUZZI, S., RUSSO, M., 2004, Collision-orogen provenance (Western and Central Alps): detrital signatures and unroofing trends: Journal of Geology, v. 112, p. 145–164.

GARZANTI, E., ANDÒ, S., VEZZOLI, G., 2006, The continental crust as a source of sand (Southern Alps cross-section, Northern Italy): Journal of Geology, v. 114, p. 533–554.

GARZANTI, E., DOGLIONI, C., VEZZOLI, G., ANDÒ, S., 2007, Orogenic belts and orogenic sediment provenances: Journal of Geology, v. 115, p. 315–334.

GARZANTI, E. AND MALUSÀ, M.G., 2008, The Oligocene Alps: Domal unroofing and drainage development during early orogenic growth: Earth and Planetary Science Letters, v. 268, p. 487-500.

GARZANTI, E., RESENTINI, A., VEZZOLI, G., ANDO, S., MALUSA, M.G., PADOAN, M. AND PAPARELLA, P., 2010, Detrital fingerprints of fossil continental-subduction zones (Axial Belt Provenance, European Alps), The Journal of Geology, v. 118, p. 341-362.

GARZANTI, E., VEZZOLI, G. AND ANDÒ, S., 2011, Paleogeographic and paleodrainage changes during Pleistocene glaciations (Po Plain, northern Italy): Earth-Science Reviews, v. 105, p. 25-48.

GARZANTI, E., ANDŌ, S., PADOAN, M., VEZZOLI, G. AND EL KAMMAR, A., 2015, The modern Nile sediment system: Processes and products: Quaternary Science Reviews, v. 130, p. 9-56.

GHIELMI, M., MINERVINI, M., NINI, C., ROGLEDI, S. AND ROSSI, M., 2013, Late Miocene–Middle Pleistocene sequences in the Po Plain–Northern Adriatic Sea (Italy): the stratigraphic record of modification phases affecting a complex foreland basin: Marine and Petroleum Geology, v. 42, p.50-81.

INGERSOLL, R.V., BULLARD, T.F., FORD, R.L., GRIMM, J.P., PICKLE, J.D. AND SARES, S.W., 1984, The effect of grain size on detrital modes: a test of the Gazzi-Dickinson point-counting method: Journal of Sedimentary Research, v. 54, p. 103-116.

ODOM, I.E., DOE, T.W. AND DOTT, R.H., 1976, Nature of feldspar-grain size relations in some quartz-rich sandstones: Journal of Sedimentary Research, v. 46, p. 862-870.

PARRA, J.G., MARSAGLIA, K.M., RIVERA, K.S., DAWSON, S.T., AND WALSH, J.P., 2012, Provenance of sand on the Poverty Bay shelf, the link between source and sink sectors of the Waipaoa River sedimentary system: Sedimentary Geology, v. 280, p. 208–233.

RICCI LUCCHI, F., 1986, The Oligocene to recent foreland basins of the northern Apennines, *in* Allen, P., and Homewood, P., (Eds.), Foreland basins: International Association of Sedimentologist Special Publication 8, p. 105–139.

ROSSI, M., MINERVINI, M., GHIELMI, M. AND ROGLEDI, S., 2015, Messinian and Pliocene erosional surfaces in the Po Plain-Adriatic Basin: Insights from allostratigraphy and sequence stratigraphy in assessing play concepts related to accommodation and gateway turnarounds in tectonically active margins: Marine and Petroleum Geology, v. 66, p.192-216.

SEGUINOT, J., IVY-OCHS, S., JOUVET, G., HUSS, M., FUNK, M. AND PREUSSER, F., 2018, Modelling last glacial cycle ice dynamics in the Alps: The Cryosphere, v. 12, p. 3265-3285.

SCHMID, S.M., FÜGENSCHUH, B., KISSLING, E. AND SCHUSTER, R., 2004, Tectonic map and overall architecture of the Alpine orogen: Eclogae Geologicae Helvetiae, v. 97, p. 93-117.

SCARPONI, D., KOWALEWSKI, M., 2004, Stratigraphic paleoecology: bathymetric signatures and sequence overprint of mollusk associations from upper Quaternary sequences of the Po Plain, Italy: Geology, v. 32, p. 989-992. http://dx.doi.org/10.1130/ G20808.1.

SCARPONI, D., KAUFMAN, D., AMOROSI, A., KOWALEWSKI, M., 2013, Sequence stratigraphy and the resolution of the fossil record: Geology, v. 41, p. 239-242.

SCARPONI, D., AZZARONE, M., KUSNERIK, K., AMOROSI, A., BOHACS, K.M., DREXLER, T.M. AND KOWALEWSKI, M., 2017, Systematic vertical and lateral changes in quality and time resolution of the macrofossil record: insights from Holocene transgressive deposits, Po coastal plain, Italy: Marine and Petroleum Geology, v. 87, p. 128-136.

TENTORI, D., MARSAGLIA, K.M. AND MILLI, S., 2016. Sand compositional changes as a support for sequence-stratigraphic interpretation: the Middle Upper Pleistocene to Holocene deposits of the Roman Basin (Rome, Italy): Journal of Sedimentary Research, v. 86, p. 1208-1227.

TENTORI, D., MILLI, S. AND MARSAGLIA, K.M., 2018, A Source-to-Sink Compositional Model of a Present Highstand: An Example in the Low-Rank Tiber Depositional Sequence (Latium Tyrrhenian Margin, Italy): Journal of Sedimentary Research, v. 88, p. 1238-1259.

VERMEESCH, P., RESENTINI, A. AND GARZANTI, E., 2016, An R package for statistical provenance analysis: Sedimentary Geology, v. 336, p. 14-25. doi:10.1016/j.sedgeo.2016.01.009.

VITTORI, E. AND VENTURA, G., 1995, Grain size of fluvial deposits and late Quaternary climate: A case study in the Po River valley (Italy): Geolog, v. 23, p. 735-738.

WELTJE, G.J., 2002. Quantitative analysis of detrital modes: statistically rigorous confidence regions in ternary diagrams and their use in sedimentary petrology: Earth-Science Reviews, v. 57, p. 211-253.

WELTJE, G. J., 2006, Ternary sandstone composition and provenance: an evaluation of the 'Dickinson model': Geological Society, London, Special Publications, v. 264, p. 79-99.

ZUFFA, G.G., 1980, Hybrid arenites, their composition and classification: Journal of Sedimentary Petrology, v. 50, p. 21–29.

ZUFFA, G.G., 1985, Optical analyses of arenites: influence of methodology on compositional results *in* Zuffa, G.G., (Eds.), Provenance of Arenites: NATO-ASI, Dordrecht, Reidel, p. 165–189.

ZUFFA G.G., CIBIN U. & DI GIULIO A. 1995, Arenite petrography in sequence stratigraphy: Journal of Geology, v. 103, p. 451-459.

CHAPTER 5: DISCUSSION

In Chapters 2, 3, and 4 sand variability in the Tevere and Po sedimentary successions is described in the context of well constrained depositional sequences in order to investigate the relationships between sequence-stratigraphy and sediment composition. The stratigraphic architecture in the Po and Tevere alluvial and deltaic successions reflect the sedimentary responses to allogenic forcing mechanisms and intrinsic autogenic factors. These processes affected sedimentation in both areas and resulted in major compositional changes across high- and low-rank stratigraphic surfaces. Sand variability across the systems tracts constituting high- to low-rank depositional sequences defines major provenance changes across key-boundaries surfaces, reflecting the interaction of several forcing mechanism. The key information to discriminate major provenance changes related to allogenic and time-dependent factors lies in lithic fragments composition (reflecting contribution from different source rocks) and their time relationships (e.g., coeval vs non-coeval grains). Moreover, the presence and abundance of the carbonate intrabasinal grains contribute to define vertical facies changes in response to relative sea-level fluctuations.

In the following sections, I will first summarize the main results and discuss the effects of the main forcing mechanisms in controlling the sand variability within the sedimentary record in the Roman and Po basin, and secondly investigate how physical and chemical processes affected the downstream sedimentary differentiation in the two river systems causing a distortion in the provenance signal. Sand petrography in the modern Tevere and Po river systems helped identify signatures of source areas and describe the downstream variability of the main sand components that, in different percentages, were recognized in the ancient sedimentary successions.

5.1 SAND COMPOSITIONAL CHANGES ACROSS HIGH-RANK AND LOW-RANK SEQUENCES, SYSTEMS TRACTS, AND KEY-BOUNDARIES SURFACES

5.1.1 The Roman Basin

In the high-rank Ponte Galeria sequence (PGS) sourced by the paleo-Tevere, the effects of glacio-eustacy, volcanism, and tectonic uplift influenced sediment supply and basin physiography as recorded by the stratal architecture of its depositional units (Milli 1997; Milli et al. 2008). In particular, the stratigraphic reorganization of the low-rank sequences constituting the PGS, show a progressive seaward stacking pattern, and suggests that tectonic uplift played a major role in controlling the sequence-stratigraphic evolution of the high-rank sequence. Differently, the analysis of petrofacies changes among the system tracts of the PGS, suggests that volcanic activity regulated

sand compositional variability and defined pre- syn- and post-volcanic composition which have a good correspondence with the LST, TST and HST. In other words, sand petrography suggests that petrofacies trends are intimately linked to volcanic paroxysm and reworking of volcanoclastic material while the stratigraphic architecture suggests that the sequence stacking pattern evolution is controlled by the interplay of tectonic uplift and glacio-eustatic sea-level changes. These findings suggest that the relative contribution of each forcing mechanism might be recorded differently by the stratigraphic architecture and sediment compositional variability. Another important implication of our results is that improper classification of grain types based on time relationships (e.g., coeval versus non coeval volcanic grains) may lead to ambiguous interpretation of the relative of influence of coeval volcanic activity versus changes in source lithology (reworking of non-coeval detritus).

Of the most recent low-rank depositional sequence of the PGS (see **Chapter 3** for details), a detailed depositional architecture of the Tiber Depositional Sequence (TDS) (Milli et al., 2016), allowed to investigate compositional changes among the LST, TST, and HST of the continental shelf and slope deposits in response to high-frequency sea-level changes and variation in sediment supply related to Holocene climatic cyclicity. The transitional shelf deposits of the LST of TDS record a higher riverine influence and relative enrichment in extrabasinal fraction with respect to TST composition. Decrease in river runoff across the TST surface resulted in a decrease of extrabasinal grains and simultaneous increase of the carbonate intrabasinal fraction. During the HST, as accommodation decreased, lateral migration of the fluvial channel belts caused reworking of floodplain and altered volcaniclastic deposits, which are currently redistributed along the coast as the delta continues to prograde. Increased precipitation at the onset of humid conditions in the Tiber River drainage basin during the HST, resulted in phases of high sediment supply, and major floods eroded and cannibalized sediments from the Tiber River floodplain and volcaniclastic source rocks of the lower drainage basin, depositing them in the marine environment. Sediment mixing of detritus from separate sources (e.g., Tevere River input, coastal plain reworking, and alongshore transport) can thus be considered the main autogenic factor controlling sand composition in the TDS.

5.1.2 The Po Basin

Sequence-stratigraphic interpretation of the Pleistocene to Holocene Po alluvial and coastal sedimentary successions shows that continuous accommodation (i.e. tectonic subsidence) and

glacio-eustatic fluctuation were the major depositional control regulating alluvial and marine stratigraphic architecture of the low-rank Po depositional sequence (Amorosi et al. 2016). Although the analysis of the sand detrital modes among the systems tracts of the Po sequence suggests that relative sea-level rise following the Holocene transgression triggered a significant paleodrainage rearrangement and resulted in major provenance shifts, the relative influence of tectonism and eustasy is difficult to disentangle. Within the three systems tracts characterizing the Po sequence, the average lithic fragment compositions in the LST, TST and HST sand define three main petrofacies that show a progressive increasing contribution from sedimentary source rocks of the Central/Eastern Alps and Northern Apennines. Average Lm/Ls and Lm/Lsc ratios reveal a notable change in lithic composition across the transgressive surface (TS), associated with the transition from an alluvial (LST) to an estuarine (TST) depositional system and enhanced supply via coastal processes from sedimentary sources in the Southern Alps during relative sea-level rise. Alongside with increased recycling from the sedimentary sources of the Southern Alps at the transition between LST and the TST and HST systems tracts deposits, we observe an enhanced contribution from intrabasinal carbonate sources which reflect changing paleogeographic condition during marine transgression. Lithic fragment types and spatial relationships between extrabasinal versus intrabasinal grain types in the Po coastal plain succession record source to basin dynamics under the effect of relative sea level fluctuations.

5.2 THE MODERN PO AND TEVERE SEDIMENTARY SYSTEMS - PHYSICAL PROCESSES AND DOWNSTREAM SEDIMENTARY DIFFERENTIATION

Some general considerations can be made regarding the physical processes acting in the modern Tevere and Po river systems that govern sediment transport and deposition. The understanding of physical effects on composition which distort the provenance signal may be converted in crucial pieces of information that can be predicted in source-to-sink compositional analyses and help the interpretation of ancient detrital modes. This thesis work, in particular, emphasizes the role and hydrodynamic fractionation by size and hydraulic sorting in controlling compositional trends of fluvial and marine sand. Along the modern river streams and shorelines off the river mouth we interpreted sand compositional changes as a result of sedimentary mixing of detrital populations with different provenance, grain-sizes, and hydraulic behavior. Moreover, the most labile grains (volcanic and limestone grains) undergo some modification in terms of percentages and textures owing to mechanical breakdown and grain abrasion by fluvial, coastal and eolian processes, and

hydraulic sorting concentrate high-density phenocrysts phases in the high-energy depositional environment.

5.2.1 Hydrodynamic fractionation and size sorting in fluvial and marine depositional systems

In **Chapter 4** the QFL compositional variability between the modern Po and Pleistocene to Holocene sand is explained with the compositional dependence by grain-size. A preliminary attempt is made to investigate grain-size-controlled trends considering mixing of detrital population with similar density but different grain sizes (e.g., quartz and feldspar) and hydraulic behavior. Relatively coarser-grained sand sampled from modern, active fluvial bars (e.g., river bedload), shows an overall higher quartz to feldspar content compared to finer-grained recent marine sand which progressively concentrated the fine and very-fine grained feldspar-rich sand transported as suspended load in the marine environments where it further mixed with feldspar-rich detritus supplied by the Apennines rivers along the coast. In the Po river system relative enrichment in fine-grained feldspar grains and decrease of coarser quartz grains results from progressive mixing of fine-grained second-cycles detritus reworked from the northern Apennines feldspathic turbidites with coarser and basement-derived sand sourced from the upland Alpine catchments. Although downstream signatures in the Po sedimentary systems suggests that hydrodynamic fractionation affects compositional variability, a quantitative estimation of grain-size classes of modern and ancient detrital populations is necessary.

In the modern Tevere delta, grain-size distribution in the emerged and submerged sectors of the delta plain and delta front reflects the action of several erosional and depositional processes that are active at the Tiber mouth and surrounding beaches. In particular, grain-size distribution along the subaerial beaches and the submarine portion of the delta reflects the response to fluvial, eolian, and wave dynamics which in turn concentrate grains with different density and hydraulic behavior. Heavy mineral grains (e.g. pyroxene) are liberated during eolian transport owing to grain to grain collision in the coastal dunes and sorted by wave reworking in the adjacent foreshore depositional environment. In the submerged part of the Tiber delta, the coastline profile of the Tiber Delta system shows a grain-size zonation that corresponds with morphodynamics zones of the submarine delta, in turn influenced by coastal hydrodynamics (Bellotti et al. 1993; Bellotti and Tortora 1996; Tortora, 1995; see Chapter 2 for details). In general, sediment distribution shows a decrease in grain size (from coarse to very-fine sand and silt) away from the coastline, which is a direct consequence of the hydrodynamic conditions along the coast. If on one hand, medium sand dominates the

exposed sectors of the delta and foreshore and shoreface sand above water depths of 5 meters, fine and very fine sand and silt accumulate in water deeper than 5 m. These grain-size zonations are subparallel to the coastline and control sediment compositions in the foreshore and proximal and distal shoreface facies. Foreshore sand is dominated by the monomineralic fraction (e.g., quartz and pyroxene grains) sorted by wave and wind action whereas shoreface deposits show higher percentages of cleavable and finer grained feldspar grains hydraulically selected by alongshore currents and dispersed in the shoreface environment.

5.2.2 Mechanical Abrasion and Rounding

Several studies in modern fluvial sedimentary systems have proven that long-distance transport is unable to substantially modify sand composition through mechanical breakdown (Nesbitt and Young, 1996). However, abrasion may affect selectively the most labile rock fragments (e.g., shale, carbonate, and volcanic rock fragments) in high energy environments modifying their texture and relative abundances (Garzanti et al., 2013; Garzanti et al. 2017; McBride and Picard, 1987).

Detrital grain shape properties such as roundness, can be assessed by comparison with sets of images, albeit obvious limitations concerning comparison with data collected from different operators (Resentini et al. 2018). However, consistency in data acquisition in this study allowed to investigate the effects of abrasion through the visual estimates of the degree of roundness along the modern Tevere river systems and associated coastal zone. Results show that softer carbonate grains are generally more rounded than quartz grains with fluvial sand roundness increasing from sub-angular to subrounded in the proximity of the river mouth and rounded to well-rounded along the beach. Rounding in the downstream alluvial sand is also interpreted as being related to mixing of fluvial sand with sediment reworked from ancient coastal sand. In the beach environments, grain to grain collisions derived from wave and wind reworking causes further mechanical abrasion resulting in higher roundness values and fluvial sand is mixed with sediment transported by wind winnowing from the adjacent coastal dune fields.

Regardless the effects of intrinsic reworking processes, our findings are similar to results from McBride and Picard (1987) and Garzanti et al. (2017) which found that limestone grains show a downstream increase in roundness in high-gradient stream and high-energy coastal environments. This study demonstrates that visual assessment of grain texture and rounding, has the advantage to provide a quick estimate that can assist petrographic investigation providing useful insight on the processes affecting grains textures.

5.2.3 Natural and Anthropogenic effects

Human intervention has a profound impact on the source-to-sink connectivity of modern sedimentary systems (Syvitski et al. 2005; Romans et al. 2016). Anthropogenic and natural exploitation factors (e.g., land use, dams) all concur in determining sediment yields and loads. Thus, the influence of anthropogenic factors must be assessed in order to predict the total sediment delivery to the basin-sinks. Artificial dams and lakes may simulate abrupt natural changes in the river drainage basins and sinking deltas contribute to modify the natural course of events enhancing the chance for catastrophic flooding (Syvitski et al. 2007). Sedimentary filling of natural and artificial lakes and associated dams built along lakes tributaries distort the provenance information provided by sand compositional analysis as demonstrated by sand petrography in the modern Tevere and Po river systems (**Chapter 3 and 4**). The Corbara Dam built in the middle course of the Tevere river system was responsible for a drastic reduction in sediment discharge following its construction in the 1950's and contribute to hydrographically separates the Tevere drainage basin into two sub-basins. This separation also contributes to determine two distinct compositional signatures in the upstream and downstream drainage basins and define the main provenance of the Tevere coastal sand. The downstream river samples composition cluster with the marine sand suggesting that modern source-to-sink composition is affected by the presence of artificial dams (see **Chapter 3**).

The effects of anthropogenic forcing are also displayed in the Alpine downstream tributaries and in particular in the Mincio sand composition which show unexpected high values (almost 100%) of sedimentary lithic fragment and very little metamorphic and plutonic detritus sourced from the upland catchments (see **Chapter 4** for details). The artificial dam associated to its lower course and the natural Garda Lake, function as sedimentary traps making the upland catchment detrital signature undetectable and reducing the tributary sediment discharge.

The study of river downstream composition highlights the influence of natural and artificial barrier in reducing the source-to-sink connectivity and emphasizes the problematic aspects of large-scale observation of sediment budgets and suggests that sediment sources of marine sinks can be often regarded as the lower downstream drainage basins in modern river systems.

CHAPTER 6: CONCLUSIONS

Sequence stratigraphy describes the spatial and temporal relationships among stratigraphic units bounded by unconformities surfaces and potentially identify the forcing mechanisms which produce systematic cyclicity in the rock record. In this regard, sediment compositional changes across key boundaries surfaces and within depositional sequences have proven to help detecting major paleogeographic changes in relation to relative sea-level changes and to investigate the dominant driving mechanism controlling the sedimentary successions evolution. Stratigraphic units deposited during specific phases of relative sea-level cycles (e.g., systems tracts) are associated with petrofacies that reflect paleogeographic rearrangement and changes in sediment dispersal paths. However, the main controls mechanisms that govern changes in relative sea-level cannot always be disentangled when looking at sediment petrography alone. The analysis of the forcing mechanisms regulating compositional trends within the Po and Tevere sedimentary successions show, in fact, that limitations occur when more processes occur simultaneously (e.g., tectonic vs. volcanic activity and tectonism vs. eustatic fluctuations). Moreover, when unconformity surfaces are not associated to major compositional changes (e.g. variability in the lithic fragment composition) it is very challenging to disentangle the superposed effects of intrinsic and local factors that add to the time-dependent petrographic signals. Another important limitation inherent the study of compositional signatures within high-frequency depositional sequences, is that the relatively short time span covered by low-rank sequences and their high preservation potential, results in high facies variability and superposition of local and intrinsic facies-related trend which makes the interpretation of detrital modes very difficult.

The two case studies presented in this thesis, not only provide a better understanding on the potential use and limitations of sand petrography as a tool to support the sequence-stratigraphic interpretations but add some insights on the effect of autogenic factors and local sedimentary processes governing sand composition. A detailed knowledge of the geology of the drainage basin and a good understanding of the sedimentary processes operating in the modern Tevere and Po sedimentary routing system have proven to be crucial aspects for a correct comprehension of the effects of physical and chemical processes that modified the primary provenance signals imparted by source-rock lithologies in the two river systems. Source-rock lithology and downstream sand dilution can be regarded, in fact, as the primary control on sand composition. However, all the physical processes acting during transport (e.g., mechanical abrasion, hydraulic sorting, and hydrodynamic grain-size fractionation) as well as chemical alteration (weathering during temporary

storage) have a profound impact in controlling downstream sediment compositional variability. Only by exploring the modern earth we can reduce the uncertainties associated to the interpretation of ancient compositional trends and identify how environmental bias and post-depositional changes may play a role in controlling sediment compositional changes throughout ancient sedimentary succession development.

Although this work illustrates the complexity of defining all the variables controlling sediment composition in the context of the sequence stratigraphic framework, it proves that a direct linkage between petrofacies, depositional environments, and systems tracts can be used to predict lithological and textural properties away from the control points and support the sequence-stratigraphic methodology. Sand petrography could, indeed, be very useful for applied purposes, because textural and compositional analysis has an important economic impact for the characterization of physical characteristic of petroleum reservoirs and aquifers.

By looking at the results from the case studies presented in this work, we can conclude that a combination between qualitative petrographic analysis and quantitative mass balance estimations (how much sediment is generated from a certain land) is necessary to discriminate and better define all the forcing mechanisms regulating sediment generation and dispersal. To achieve such a goal, data from different research fields (i.e. sedimentology, geomorphology, climatology, geophysics) and information from modern similar settings must be put together in a more comprehensive approach.

REFERENCES

AMOROSI, A., MASELLI, V. AND TRINCARDI, F., 2016, Onshore to offshore anatomy of a late Quaternary source-to-sink system (Po Plain–Adriatic Sea, Italy): Earth-Science Reviews, v. 153, p. 212-237.

BELLOTTI, P., CHIOCCI, F.L., MILLI, S. AND TORTORA, P., 1993, Variabilità nel tempo della distribuzione granulometrica sui fondali del Delta del Tevere: Bollettino Società Geologica Italiana, v. 112, p. 143–153.

BELLOTTI, P. AND TORTORA, P., 1996, I sedimenti sul fondale del delta del Fiume Tevere: Bollettino Società Geoligica Italiana, v. 115, p. 449–458.

GARZANTI, E., PADOAN, M., ANDÒ, S., RESENTINI, A., VEZZOLI, G., LUSTRINO, M., 2013, Weathering and relative durability of detrital minerals in equatorial climate: sand petrology and geochemistry in the East African Rift: The Journal of Geology, v. 121, p. 547–580.

GARZANTI E., VERMEESCH, P., AL-RAMADAN, K.A., ANDÒ, S., LIMO'NTA, M., PETERS, G., RITTNER, M., AND VEZZOLI, G., 2017, Tracing transcontinental sand transport from the Anatolia–Zagros orogen to beyond the Gulf foreland-basin into the Rub' al Khali sand sea: Journal of Sedimentary Research, v. 87, p. 1196–1213.

MCBRIDE, E.F. AND PICARD, M.D., 1987, Downstream changes in sand composition, roundness, and gravel size in a short-headed, high-gradient stream, northwestern Italy: Journal of Sedimentary Research, v. 57, p. 1018-1026.

MILLI, S., 1997, Depositional setting and high-frequency sequence stratigraphy of the middle-upper Pleistocene to Holocene deposits of the Roman basin: Geologica Romana, v. 33, p. 99–136.

MILLI, S., MOSCATELLI, M., PALOMBO, M.R., PARLAGRECO, L. AND PACIUCCI, M., 2008, Incised valleys, their filling and mammal fossil record: a case study from Middle-Upper Pleistocene deposits of the Roman Basin (Latium, Italy), *in* Advances in Application of Sequence Stratigraphy in Italy (Eds A. Amorosi, B.U. Haq and L. Sabato): GeoActa Special Publication, v. 1, p. 67–87.

MILLI, S., MANCINI, M., MOSCATELLI, M., STIGLIANO, F., MARINI, M., AND CAVINATO, G.P., 2016, From river to shelf, anatomy of a high-frequency depositional sequence: The Late Pleistocene to Holocene Tiber depositional sequence: Sedimentology, v. 63, p. 1886-1928.

NESBITT, H.W. AND YOUNG, G.M., 1989, Formation and diagenesis of weathering profiles: The Journal of Geology, v. 97, p. 129-147.

RESENTINI, A., ANDÒ, S. AND GARZANTI, E., 2018, Quantifying roundness of detrital minerals by image analysis: Sediment transport, shape effects, and provenance implications: Journal of Sedimentary Research, v. 88, p. 276-289.

ROMANS, B.W., CASTELLTORT, S., COVAULT, J. A., FILDANI, A., AND WALSH, J.P., 2016, Environmental signal propagation in sedimentary systems across timescales: Earth-Science Reviews, v. 153, p. 7-29.

SYVITSKI, J.P.M., VOROSMARTY, C.J., KETTNER, A.J., AND GREEN, P., 2005, Impact of humans on the flux of terrestrial sediment to the global coastal ocean: Science, v. 308, p. 376–380.

SYVITSKI, J.P. AND MILLIMAN, J.D., 2007, Geology, geography, and humans battle for dominance over the delivery of fluvial sediment to the coastal ocean: The Journal of Geology, v. 115, p. 1-19.

TORTORA, P., 1995, La superficie deposizionale del delta sottomarino del Tevere: zonazione del sedimento e processi associate: Bollettino Società Geologica Italiana, v. 113, p. 89–105.

AKNOWLEDGEMENTS

This thesis work is the result of an intense collaboration among high-level scientists. All the people involved contributed actively to make the three years of the Ph.D. program an incredible and successful journey. I would like to first thank my advisor Salvatore Milli. My relationship with Salvatore goes way beyond his academic mentorship; he's been a friend when things got tough and strong motivator when the work demanded it. He was and will always be a guide through life and academia. I owe a debt of gratitude to Kathie Marsaglia who introduced me to the world of research, thought me the secrets of scientific writing and disseminations, and encourage me to overcome my insecurities. Thanks to Alessandro Amorosi whose dedication to research and student mentorships has been very inspiring for my future career. I would like to also thank him for providing his expertise in developing a chapter of my thesis. A special thanks to Domenico "Mimmo" Mannetta for his effort in preparing hundreds, high-quality thin sections, and without whom my work could not be possible.

Thanks to Andrea Di Giulio and Salvatore Critelli for reviewing a previous version of the thesis and for their helpful and constructive comments which substantially improved the thesis. Thanks to all the reviewers and editors who helped me during papers publication.

Last but not least, thanks to all my family members, Erica, friends and colleagues for the moral support over the three years. This thesis is dedicated to Angela.

APPENDIX A

(Supplementary Material of Chapter 2)

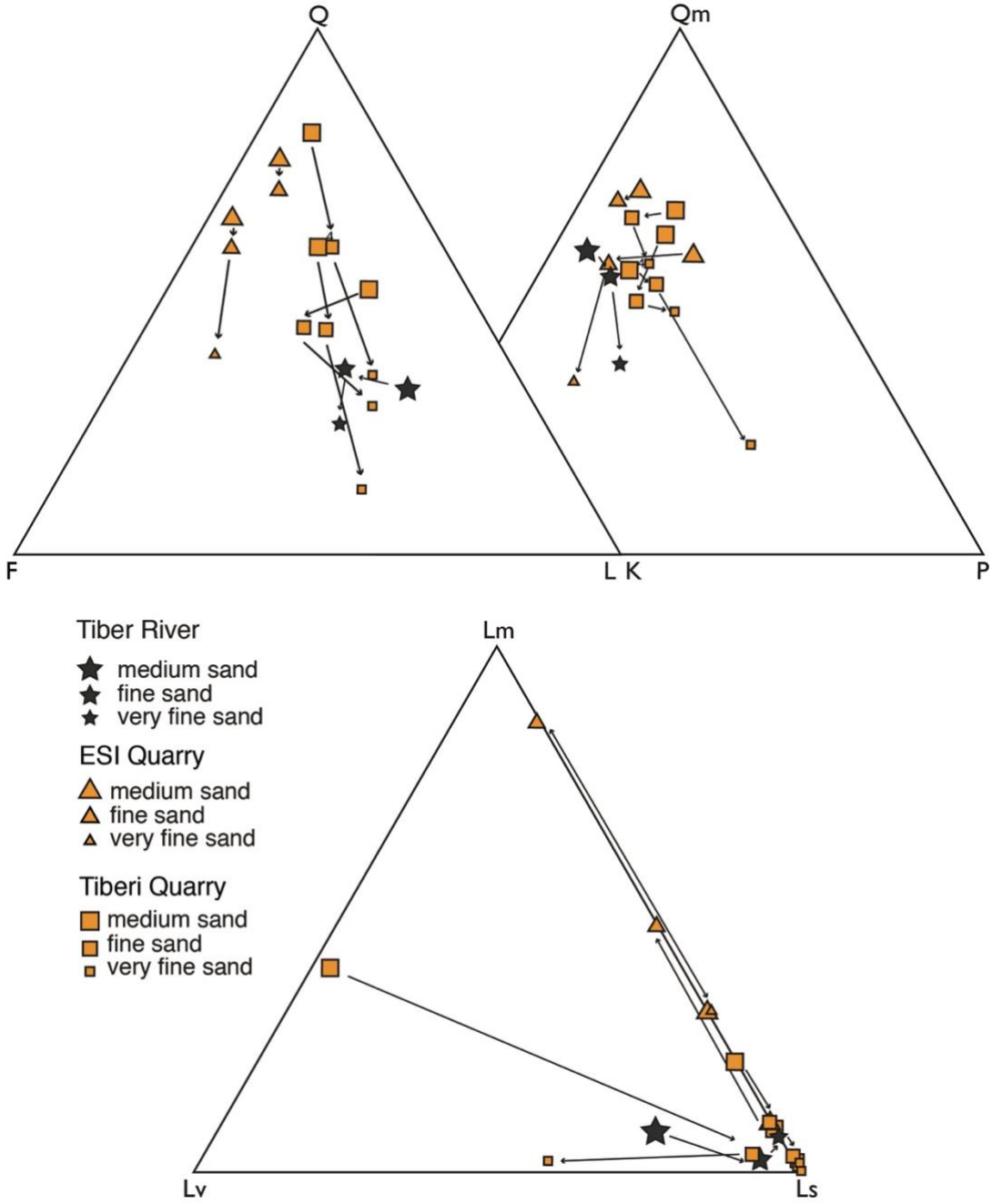

FIG. A1 – Grain-size compositional variability in the modern Tiber River and ancient sand (ESI and Tiberi quarries).

Table A1. – Counted and Recalculated Parameters

NCE
- Qpt = polycrystalline quartz with tectonite fabric
- Qpw = polycrystalline quartz
- Qm in Qp = monocrystalline quartz in polycrystalline quartz
- Q(chert) = chert
- Qm= monocrystalline quartz
- Qm in Ls = monocrystalline quartz in sedimentary lithic
- Qm in other = monocrystalline quartz in other lithic
- P = plagioclase feldspar
- Palt = altered plagioclase feldspar
- P in Lv = plagioclase feldspar in volcanic lithic
- P in Ls = plagioclase feldspar in sedimentary lithic
- P in other = plagioclase feldspar in other lithic
- K = potassium feldspar
- Kalt = altered potassium feldspar
- K in Lv = potassium feldspar in volcanic lithic
- K in Ls = potassium feldspar in sedimentary lithic
- K in other = potassium feldspar in other lithic
- Lvv = vitric volcanic lithic
  - pugl = pumice
  - brgl = brown glass
  - clgl = colorless glass
  - blgl = black glass
  - algl = altered glass
- Lvml = volcanic lithic with microlitic texture
  - brgl = brown glass
  - clgl = colorless glass
  - blgl = black glass
  - algl = altered glass
- Lvl = volcanic lithic with lathwork texture
  - brgl = brown glass
  - clgl = colorless glass
  - blgl = black glass
  - algl = altered glass
- Lvf = volcanic lithic with felsitic texture
- Lvp = pyroclastic tuff
- Lma = quartz-feldspar-mica aggregate lithic
- Lmt = quartz-mica aggregate with tectonite fabric
- Lsa = claystone lithic
- Lsi = siltstone lithic
- Lss = sandstone lithic
- M = muscovite
- B = biotite
- D opaque = opaque dense mineral
- D non-opaque = non-opaque dense mineral
- Pyr = pyroxene
- Serp = serpentine
- Flds = feldspathoids

Table A1. – Counted and Recalculated Parameters (continued)

FeOx = Fe oxides Unkn = Unknown grain CE Lsc(mic) = micritic carbonate lithic Lsc(cry) = carbonate crystal lithic Lsc(sil+carb) = silt and carbonate lithic fragment CI Foram = foraminifer Carb bio = carbonate bioclast Total Pts= total points counted
Qm total = Qm+Qm in Qp+Qm in Ls+Q in other K total = K+Kalt+K in Lv+K in Ls+K in other P total = P+Palt+P in Lv+P in Ls+P in other Q = Qpt+Qpw+Qp(chert)+Qm total F = P total +K total Lm = Lma+Lmt Lv = Lvv+Lvml+Lvl+Lvf+Lvp Ls = Lsa+Lsi+Lss+Lsc(mic)+Lsc(cry)+Lsc(sil+carb) L = Lm+Lv+Ls Ls-c = Lsa+Lsi+Lss L-c = Lm+Lv+Ls-c QFL%Q= 100*Q/(Q + F+ L) QFL%F= 100*F/(Q + F+ L) QFL%L= 100*L/(Q + F+ L) QmKP%Qm= 100*Qm/(Qm total+F) QmKP%K= 100*K/(Qm total+F) QmKP%P= 100*P/(Qm total+F) LmLvLs%Lm= 100*Lm/(Lm+Lv+Ls) LmLvLs%Lv= 100*Lv/(Lm+Lv+Ls) LmLvLs%Ls= 100*Ls/(Lm+Lv+Ls) QFL-c%Q= 100*Q/(Q + F+ L-c) QFL-c%F= 100*F/(Q + F+ L-c) QFL-c%L-c= 100*L-c/(Q + F+ L-c) LmLvLs-c%Lm= 100*Lm/(Lm+Lv+Ls-c) LmLvLs-c%Lv= 100*Lv/(Lm+Lv+Ls-c) LmLvLs-c%Ls-c= 100*Ls-c/(Lm+Lv+Ls-c) NCE-CE-CI%NCE= 100*NCE/(NCE+CE+CI) NCE-CE-CI%CE= 100*CE/(NCE+CE+CI) NCE-CE-CI%CI= 100*CI/(NCE+CE+CI)

Table A2. – Point Count Data

MODERN SAND

Sample#	Stream and Beach Sample Location	Grain Size	km downstream	Qpt	Qpw	Qm in Qp	Qp chert	Qm	Qm in Ls	Qm other	P	Palt	P in Lv	P in Ls	P other	K	Kalt	K in Lv	K in Ls	K other	Lvv	Lvv pugl	Lvv brgl	Lvv clgl	Lvv blgl	Lvv algl	Lvml brgl	Lvml clgl	Lvml blgl	Lvml algl	Lvl brgl	Lvl clgl	Lvl blgl	Lvl algl	Lvf	Lvp	Lma	Lmt	Lsa	Lsi	Lss	Lsc mic	Lsc cry	Lsc sil+carb	M	B	D opaq	D nonop	Pyr	Serp	Flds	Foram	Carb bio	FeOx	Unkn	Total pts
TR1	PIEVE S. STEFANO	medium	20		4		30			11	11				6																					1	3	81	50	6	28	100	37				1	15			14	2		400
TR2	PIOSINA	medium	45	2	23		1	103	5	9	13		1		26	7																			2	9	14	33	5	14	78	24			4	5		18			4				400
TR3	PIERANTONIO	medium	80	4	22			88	17	2	9		4		23	5																			4	10	34	53	12	34	40	23		1	2	3	2	8						400
TR4	CASALINA	medium	150		16		5	88	6	5	11		4		40	9		1																	2	10	22	28	1	56	74	8	1	1	2	6				4			400
TR5	PANTALLA	medium	160	2	13		6	43	30	3	16		9		20	9		2																	4	7	25	81	20	24	38	31	1	1		3	1			11			400
TR6	ORTE	medium	280	1	14		6	50	1	9	5		1		38	1	1				6	13	1	1	1	38	25	18		3	1		1	4	2	8	19	23	2	39	60	3				5							400
TR7	ORTE SCALO	medium	285		18		3	87	3	4	12		1		22	10				2						14		7		2	2		1		3	17	22	17		30	61	20		1	1	4	29		6		1			400
TR8	MAGLIANO SABINA	medium	295	1	4		8	61	6	2	3				53	12	2			8	2			2		15		8					2	3	7	26	40		29	47	24		1	2	2	24		3		3			400
TR9	STIMIGLIANO	medium	305		6		13	65		11	14				38	9						18				32	10	10		1		5		3	8	6	32	32		18	30	18		1	1	5	13				1			400
TR10	ROMA-TOR DI QUINTO	medium	375		5		14	43	9	2	6		3		22	7		1		11	3	1		2		20		4							2	3	16	140	6	20	20	14		2	1	1	17		4		1			400
TR11	DRAGONA	medium	400	2	10		13	94	3		11				38	23		1		4	2			2		17	1	9		2		1			8	5	32	44		20	30	11	3	3		1	3		6		1			400
TR11F	DRAGONA	fine	400	1	11	1	4	93		7	15			1	40	21										4		2								2	19	1		19	49	18		4	12	1	59		1		15			400
TR11V	DRAGONA	very fine	400		9		8	67		22	19				70	8																			4	5	11			52	63	6	1	2	3		43				7			400
TR12	FIUMICINO	medium	403	1	43		20	117	6	7	16				34	9		4		2						1		1				1			6	11	13	26	7	1	5	2	1		1	2	59		3		1			400
TRT1	BASTIA UMBRA – FIUME CHIASC	medium	135		7		5	45	3		7		1		10	13		1																	1	2	9	39	2	96	104	37								18			400
TRT2	MARSCIANO - FIUME NESTORE	medium	155	2	30		5	76	8	12	17		6		17	6		1																	7	7	52	92	5	20	20	15								2			400
TRT3	CICONIA - FIUME PAGLIA	medium	220		15		4	63	4	8	7				10	3				7						9	3			3					2		63	58	11	30	64	17	1		1	5	10			2			400
TRT4	CASCATE MARMORE - FIUME NEI	medium	285	1	1		119																														11	12	1	59	72	122					2						400
TRT5	RECENTINO - FIUME NERA	medium	285	4	34		20	109	1	8	14				28	9																			3	6	15	24	4	28	52	36					4		1				400
TRT6	CIVITA CASTELLANA-FIUME TREI	medium	300		1		4	48		12	4				25	3				60	1					51	13	19		8		4		1	2	1	2	6	3		1	1	3		3	10	1	113							400
TRC1	S.SEVERA	medium	406	2	31		36	84		1			1		20	5				1						1									2	8	53	11		20	57	33			1		26		4		3			400
TRC2	PASSO OSCURO	medium	406	1	12		9	138	1	8	19				42	15										2	1	4							4	3	33	13	2	10	32	37		1			6		7				400
TRC3	FREGENE	medium	406		9		5	95	1	5	11				9	8		1										2							3	4	9			12	50	33	1			1	136		3		2			400
TRC4	FOCENE	medium	406		16		10	89		1	20				8	9		1						2				1								7	8	2		24	23	14					159		2		4			400
TRC5	FIUMICINO	medium	406	3	23		5	79		2	21				39	9						4		1				1							5	6	9	6		19	50	21		1			93		3					400
TRC6	OSTIA	medium	406	1	24		31	102		9	10				58	7										2	1	1							2	4	8	7		8	33	39				1	48				4			400
TRC7	OSTIA - CANCELLO 2	medium	406	3	20		6	92		1	19				36	7										1	1	3		1					4	7	21	12		17	72	36		1			37		1		2			400

ANCIENT SAND

Sample#	Sampled Sequence in Measured Section	Grain size	Stratigraphic Height (m)	Qpt	Qpw	Qm in Qp	Qp chert	Qm	Qm in Ls	Qm other	P	Palt	P in Lv	P in Ls	P other	K	Kalt	K in Lv	K in Ls	K other	Lvv	Lvv pugl	Lvv brgl	Lvv clgl	Lvv blgl	Lvv algl	Lvml brgl	Lvml clgl	Lvml blgl	Lvml algl	Lvl brgl	Lvl clgl	Lvl blgl	Lvl algl	Lvf	Lvp	Lma	Lmt	Lsa	Lsi	Lss	Lsc mic	Lsc cry	Lsc sil+carb	M	B	D opaq	D nonop	Pyr	Serp	Flds	Foram	Carb bio	FeOx	Unkn	Total pts
TQ1	PG1-fluvial	medium	0.50	1	20	10	142	78		2	4	30			1	28	9			2																6	4	2	4		38	9	6								3		1	400
TQ2	PG1-fluvial	medium	1.90	3	31	5	80	100	3		5	38				38	15			1							3									16	3		3		18	15	22		1										400
TQ3	PG1-fluvial	medium	3.00	1	35	10	86	102	1		8	34				33	4			1							3									8	5				48	13	6								2			400
TQ4	PG1-fluvial	medium	4.00	1	25	2	110	93			2	25				33	20																			12	6	2	4		28	15	17	1	2						2				400
TQ4F	PG1-fluvial	fine	4.00	4	21		26	114			9	37				41	19																			11		1	3		23	35	47		6						1		2	400
TQ4V	PG1-fluvial	very fine	4.00				11	36			24	23				77	14																			1					120	73	4	3	5	3			2	4					400
TQ5	PG1-fluvial	medium	5.00	2	34	2	132	113			1	16				14	4																			3	1	13			25	14	14		2			1		1	3	2	3		400
TQ6	PG1-fluvial	medium	6.00	3	30	6	20	150	2		7	37			2	31	15																			9	1	1			45	23	16		1						1				400
TQ7	PG1-lower shoreface	medium	6.25	3	29	6	210	75				20				15	7																			2	1		1		22	5	4												400
TQ7F	PG1-lower shoreface	fine	6.25	3	16		82	132			10	11				39	14																			3		5	2		22	21	35								4		1	400
TQ7V	PG1-lower shoreface	very fine	6.25		1		18	114			23	13				35	20																					5	2		30	71	50		3		9	2			1	3			400
TQ8	PG1-lower shoreface	medium	7.25		19	5	201	86			1	9				14	5																			2	2	14	1		13	11	16		1										400
TQ9	PG1-lower shoreface	medium	8.15	3	22	12	87	114			2	26				43	9																			7	1	17	1		23	25	5						2		1				400
TQ10	PG2-upper shoreface	medium	9.00		9		15	38			4	6				25	1	2			7	3	1		3		25	176	15			5	3			4					10	6	2		12			23		5				400
TQ11	PG2-upper shoreface	medium	10.50		2		16	8			1	3				22		4									16	280	8			1				1		2				6	2	1	21	1	1	1		2				1	400
TQ12	PG2-beachface	medium	12.75	2	25		73	96			9	17				32	2				1	2		3			2	69							2	1	6	3		30	8	5		8			2			2			400
TQ12F	PG2-beachface	fine	12.75	1	29		26	111			10	33				56	18										6									4		4	1		23	35	29		2	1	1	8			2			400
TQ12V	PG2-beachface	very fine	12.75		3		13	76			27	15				37	7						2				45	15							2		7			8	45	22	3	4	4		60		3		2			400
TQ13	PG2-lower shoreface	medium	14.50	1	18		94	99			5	25				26	8																			4	2	11	12		57	18	7	2	1	2	3				4		1	400
TQ14	PG2-upper shoreface	medium	17.90		30	8	98	110	1		5	30				30	5			2																4	3	16	1		29	16	1		4					7				400
TQ15	PG3-transition shelf	fine	20.25		7		31	87			14	19				48	33																			2		22	3		40	47	29		1						5	12		400
TQ15V	PG3-transition shelf	very fine	20.25		10		29	119			26	25				46	10																			4		1			46	50	13	5	5			1			2	5		397
TO1	PG6-fluvial	medium	1.00	1	14		12	82			4	12				39	5						40		12												1	4			9	5	3			6		148		3					400
TO2	PG6-palustrine-lacustrine	medium	4.50		only for description																																																		
TO3	PG7-fluvial	medium	8.00	10	7	2		20				6				26	3	1			4			5			18	17	9							3		8	3		2	9	5		1	20		215		5		1			400
EQ1	PG2-beachface	fine	2.10		39	13	43	198			8	37				23	9																			1	2	5	1		15	3			1		1				1			400
EQ2	PG2-beachface	fine	5.00	1	30	10	104	157			4	18				39	14																				2	6			11		4												400
EQ2F	PG2-beachface	fine	5.00		29		76	174			9	8				46	21																			15	2	6			8	5									1			400
EQ3	PG2- beachface	medium	7.25		33	17	59	229			3	16				32	4																			1	1	4							1									400
EQ4	PG2-washover	medium	9.50		38	8	40	190			7	44				57	8																			3		5																400
EQ5	PG3-lower shoreface	fine	17.00	1	32	19	51	156			12	61				48	7																			1	3	7	2															400
EQ5	PG3-lower shoreface	fine	17.00	3	36		27	171			14	31				68	24																			16	3	2	1					2	2								400
EQ5F	PG3-lower shoreface	very fine	17.00	1	7		47	88			16	26				60	79																			10	5	32	3					5	3	2	5	10	1					400
EQ6	PG3-lower shoreface	fine	19.20	1	41	15	31	187			6	40				60	5																			3		3	5								2						1	400
EQ7	PG4-fluviopalustrine	medium	20.00	2	68	5	26	187			9	16				67	12																			5	1	2																400
EQ8	PG4-fluviopalustrine	fine	21.00	2	44	6	25	258			2	15				38	1																			2	1	3																400
EQ9	PG5-fluvio-palustrine	medium	25.00			1		12			11	3				71	5										8	4	2							1		13																400
EQ10	PG5-fluvio-palustrine	medium	27.00					14			65	2				##	12					3																	1																400
EQ11	PG5-fluvio-palustrine	medium	28.25		1			3			29	2				##	3					20				5	3	3							2			1																400

Table A2. – Point Count Data (continued)

MODERN SAND

Sample#	QFL%Q	QFL%F	QFL%L	LmLvLs%Lm	LmLvLs%Lv	LmLvLs%Ls	QmKP%Qm	QmKP%P	QmKP%K	QFL-c%Q	QFL-c%F	QFL-c%L-c	LmLvLs-c%Lm	LmLvLs-c%Lv	LmLvLs-c%Ls	NCE-CE-CI%NCE	NCE-CE-CI%CE	NCE-CE-CI%CI
TR1	9.2	7.6	83.2	1.3	0.0	98.7	51.7	37.9	10.3	16.7	13.8	69.5	2.8	0.0	97.2	96	4	0
TR2	36.3	15.2	48.5	6.1	0.0	93.9	65.9	14.0	20.1	53.0	22.1	24.9	17.5	0.0	82.5	59	41	0
TR3	34.1	11.2	54.7	6.7	0.0	93.3	70.9	10.1	18.9	45.6	15.0	39.4	12.4	0.0	87.6	76	24	0
TR4	29.8	18.1	52.1	6.0	0.0	94.0	57.3	12.2	30.5	46.4	27.8	25.4	19.0	0.0	81.0	57	43	0
TR5	24.5	15.4	60.1	4.8	0.0	95.2	55.3	21.2	23.5	32.4	19.7	47.2	8.0	0.0	92.0	85	15	0
TR6	18.2	13.9	67.8	3.7	41.8	54.5	48.1	14.2	37.7	24.6	18.4	56.7	6.0	67.5	26.5	44	5	52
TR7	31.0	13.7	55.3	10.1	14.1	75.8	64.7	12.2	23.0	44.9	19.8	35.2	23.0	32.2	44.8	39	25	36
TR8	21.9	19.7	58.4	4.7	17.4	77.9	48.2	3.6	48.2	30.2	26.4	42.6	8.8	32.7	58.4	51	11	39
TR9	22.2	19.0	58.8	6.3	35.4	58.3	47.4	18.2	34.3	26.8	23.0	50.2	8.9	50.3	40.8	46	8	46
TR10	19.0	11.0	70.1	1.9	15.6	82.4	55.9	11.8	32.3	22.2	12.5	65.0	2.4	19.7	77.9	75	3	23
TR11	31.9	19.1	49.1	6.9	20.2	72.9	57.1	6.5	36.5	37.9	22.4	39.4	10.2	29.9	59.8	50	13	38
TR11F	35.7	27.3	37.0	1.8	5.3	93.0	52.8	12.9	34.3	49.5	37.8	12.6	7.1	21.4	71.4	31	17	52
TR11V	24.4	34.6	41.0	6.4	0.0	93.6	36.0	22.0	41.9	37.7	53.4	9.0	45.0	0.0	55.0	17	83	0
TR12	56.2	21.0	22.8	22.4	6.6	71.1	63.7	11.9	24.4	57.5	20.3	20.9	25.0	7.4	67.6	39	47	14
TRT1	15.7	8.4	75.9	1.0	0.0	99.0	60.0	10.0	30.0	41.4	21.4	36.6	5.7	0.0	94.3	87	13	0
TRT2	30.4	14.8	54.8	6.4	0.0	93.6	58.7	24.5	16.8	35.3	16.9	47.5	8.6	0.0	91.4	85	15	0
TRT3	22.6	7.3	70.1	0.7	8.2	91.0	70.5	15.8	13.7	31.9	10.4	57.8	1.3	14.1	84.6	79	2	19
TRT4	30.4	0.0	69.6	0.0	0.0	100.0	0.0	0.0	0.0	83.4	0.0	16.6	0.0	0.0	100.0	100	0	0
TRT5	42.5	14.9	42.5	5.4	0.0	94.6	65.1	13.0	21.9	60.2	21.1	18.6	17.3	0.0	82.7	52	48	0
TRT6	19.4	16.1	64.5	1.7	90.3	8.0	52.2	17.4	30.4	19.8	16.4	63.8	1.8	93.0	5.3	40	1	59
TRC1	41.8	7.4	50.8	5.4	1.1	93.5	75.7	1.8	22.5	59.8	10.5	29.7	13.2	2.6	84.2	65	29	6
TRC2	41.7	21.8	36.5	5.0	5.0	90.1	62.3	12.1	25.6	52.4	27.4	20.2	11.3	11.3	77.4	47	26	26
TRC3	42.8	13.2	44.0	6.2	1.8	92.0	73.8	12.3	13.8	67.9	20.4	11.1	38.9	11.1	50.0	18	64	18
TRC4	48.9	16.6	34.5	8.6	3.7	87.7	69.5	16.4	14.1	66.1	21.8	11.5	35.0	15.0	50.0	19	57	24
TRC5	36.3	23.4	40.3	9.0	4.9	86.1	52.7	15.3	32.0	51.6	33.3	15.0	34.4	18.8	46.9	22	50	28
TRC6	45.5	24.2	30.3	5.7	3.8	90.5	54.8	10.2	34.9	59.2	31.5	9.4	24.0	16.0	60.0	19	49	32
TRC7	33.7	17.5	48.7	6.3	3.4	90.3	59.4	12.9	27.7	51.7	26.9	21.4	22.0	12.0	66.0	39	40	22

ANCIENT SAND

Sample#	QFL%Q	QFL%F	QFL%L	LmLvLs%Lm	LmLvLs%Lv	LmLvLs%Ls	QmKP%Qm	QmKP%P	QmKP%K	QFL-c%Q	QFL-c%F	QFL-c%L-c	LmLvLs-c%Lm	LmLvLs-c%Lv	LmLvLs-c%Ls	NCE-CE-CI%NCE	NCE-CE-CI%CE	NCE-CE-CI%CI
TQ1	63.9	18.7	17.4	14.5	0.0	85.5	54.9	21.3	23.8	73.8	21.0	4.7	62.5	0.0	37.5	7	93	0
TQ2	55.6	24.3	20.1	23.8	3.8	72.5	52.7	21.0	26.3	64.5	27.9	7.3	76.0	12.0	12.0	8	80	13
TQ3	59.0	20.1	20.9	15.7	3.6	80.7	58.5	21.8	19.7	71.0	23.9	4.8	81.3	18.8	0.0	5	78	18
TQ4	58.5	20.3	21.3	21.4	0.0	78.6	54.3	15.4	30.3	69.0	23.9	7.2	75.0	0.0	25.0	9	91	0
TQ4F	42.2	27.1	30.7	9.2	0.0	90.8	51.8	20.9	27.3	57.7	37.1	5.2	73.3	0.0	26.7	7	93	0
TQ4V	12.3	36.0	51.7	0.5	0.0	99.5	20.7	27.0	52.3	25.3	74.2	0.5	100.0	0.0	0.0	1	99	0
TQ5	72.9	9.0	18.0	5.7	0.0	94.3	76.7	11.3	12.0	84.5	10.4	5.1	23.5	0.0	76.5	18	82	0
TQ6	53.0	23.1	23.9	10.5	0.0	89.5	63.2	18.4	18.4	67.2	29.3	3.5	90.9	0.0	9.1	4	96	0
TQ7	80.8	10.5	8.8	8.6	0.0	91.4	65.9	16.3	17.9	87.5	11.4	1.1	75.0	0.0	25.0	1	99	0
TQ7F	59.0	18.7	22.3	3.4	0.0	96.6	64.1	10.2	25.7	73.5	23.3	3.2	30.0	0.0	70.0	10	90	0
TQ7V	34.8	23.8	41.4	0.0	0.0	100.0	55.6	17.6	26.8	57.6	39.4	3.0	0.0	0.0	100.0	100	0	0
TQ8	77.9	7.3	14.8	6.8	0.0	93.2	75.8	8.3	15.8	86.6	8.1	5.3	21.1	0.0	78.9	20	80	0
TQ9	59.9	20.2	19.9	10.1	0.0	89.9	61.2	13.6	25.2	69.2	23.3	7.6	30.8	0.0	69.2	20	80	0
TQ10	17.2	10.6	72.2	1.5	91.5	6.9	50.0	13.2	36.8	18.1	10.5	70.8	1.7	98.3	0.0	41	1	58
TQ11	7.0	8.1	84.9	0.3	96.5	3.2	21.1	10.5	68.4	7.1	7.1	84.6	0.3	99.0	0.6	46	0	54
TQ12	50.5	15.5	34.0	2.3	58.3	39.4	61.5	16.7	21.8	56.8	17.4	25.8	3.4	86.5	10.1	22	3	75
TQ12F	43.3	30.3	26.4	3.9	5.9	90.2	48.7	18.9	32.5	55.9	39.1	5.0	26.7	40.0	33.3	7	37	56
TQ12V	28.4	26.5	45.1	1.4	42.5	56.2	46.9	25.9	27.2	36.9	34.5	28.5	2.8	87.3	9.9	24	2	74
TQ13	54.8	16.5	28.7	5.4	0.0	94.6	60.7	18.4	20.9	69.5	21.0	9.5	20.7	0.0	79.3	31	69	0
TQ14	63.5	18.5	18.0	10.0	0.0	90.0	62.3	18.3	19.4	72.0	20.4	7.0	29.2	0.0	70.8	19	81	0
TQ15	32.7	29.8	37.4	1.4	0.0	98.6	43.3	16.4	40.3	47.0	42.9	10.2	7.4	0.0	92.6	58	42	0
TQ15V	41.7	28.2	30.1	3.5	0.0	96.5	52.7	22.6	24.8	58.5	39.6	1.9	80.0	0.0	20.0		98	0
TO1	44.9	24.7	30.5	1.4	70.3	28.4	57.7	11.3	31.0	48.2	26.5	25.2	1.8	91.2	7.0	96	1	77
TO2	only for description																	
TO3	24.7	22.8	52.5	3.6	63.9	32.5	37.9	10.3	51.7	27.5	24.6	47.2	4.5	79.1	16.4	96	4	0
EQ1	73.8	19.4	6.8	11.1	0.0	88.9	73.3	15.6	11.1	77.3	20.3	2.4	33.3	0.0	66.7	7	93	0
EQ2	75.5	18.8	5.8	8.7	0.0	91.3	69.0	9.1	21.9	78.4	19.5	2.1	25.0	0.0	75.0	8	92	0
EQ2F	69.9	21.1	9.0	47.2	0.0	52.8	67.4	6.6	26.0	72.3	21.8	6.0	73.9	0.0	26.1	7	93	0
EQ3	84.7	13.8	1.5	33.3	0.0	66.7	81.7	6.3	12.0	84.7	13.8	1.5	33.3	0.0	66.7	4	96	0
EQ4	69.0	29.0	2.0	37.5	0.0	62.5	63.1	16.2	20.7	69.0	29.0	2.0	37.5	0.0	62.5	5	95	0
EQ5	64.8	32.0	3.3	30.8	0.0	69.2	57.8	24.1	18.2	64.8	32.0	3.3	30.8	0.0	69.2	10	90	0
EQ5	59.8	34.6	5.6	86.4	0.0	13.6	55.5	14.6	29.9	59.8	34.6	5.6	86.4	0.0	13.6	100	0	0
EQ5F	38.2	48.4	13.4	30.0	0.0	70.0	32.7	15.6	51.7	38.2	48.4	13.4	30.0	0.0	70.0	100	0	0
EQ6	69.3	28.0	2.8	27.3	0.0	72.7	64.5	14.7	20.8	69.3	28.0	2.8	27.3	0.0	72.7	100	0	0
EQ7	72.0	26.0	2.0	75.0	0.0	25.0	64.9	8.4	26.7	72.0	26.0	2.0	75.0	0.0	25.0	100	0	0
EQ8	84.4	14.1	1.5	50.0	0.0	50.0	82.5	5.3	12.2	84.4	14.1	1.5	50.0	0.0	50.0	100	0	0
EQ9	9.9	68.7	21.4	3.6	50.0	46.4	12.6	13.6	73.8	9.9	68.7	21.4	3.6	50.0	46.4	100	0	0
EQ10	4.6	93.8	1.6	0.0	60.0	40.0	4.7	22.4	72.9	4.6	94.1	1.3	0.0	75.0	25.0	100	0	0
EQ11	1.4	87.0	11.6	0.0	97.1	2.9	1.2	12.1	86.8	1.4	87.0	11.6	0.0	97.1	2.9	100	0	0

Table A3. – Roundness

MODERN SAND

Sample#	Stream and Beach Sample Location	km downstream	Qtz Grains* 1	2	3	4	5	6	Qtz tot grains	Carb Grains* 1	2	3	4	5	6	Carb tot grains	Qtz Mean Roundness	Carb lithic Mean Roundness
TR1	PIEVE S. STEFANO	20	11	13	5	0	1	0	30	3	6	5				14	1.9	2.1
TR2	PIOSINA	45	3	17	9	1			30		19	11				30	2.3	2.4
TR3	PIERANTONIO	80	4	15	11				30	1	16	11	2			30	2.2	2.5
TR4	CASALINA	150	4	17	7	2			30	2	10	13	2	3		30	2.2	2.8
TR5	PANTALLA	160	1	17	11	1			30		9	16	5			30	2.4	2.9
TR6	ORTE	280		12	15	3			30		6	19	5			30	2.7	3.0
TR7	ORTE SCALO	285		12	14	4			30		6	17	5	1	1	30	2.7	3.1
TR8	MAGLIANO SABINA	295		10	19	1			30		4	17	9			30	2.7	3.2
TR9	STIMIGLIANO	305		9	14	7			30		8	9	6	7		30	2.9	3.4
TR10	ROMA-TOR DI QUINTO	375		6	17	7			30		3	12	13	2		30	3.0	3.5
TR11	DRAGONA	400		9	14	6	1		30		4	12	10	4		30	3.0	3.5
TR12	FIUMICINO	403		12	12	6			30		1	6	4			11	2.8	3.3
TRT1	BASTIA UMBRA – FIUME CHIASCIO	135	1	16	10	3			30		5	16	9			30	2.5	3.1
TRT2	MARSCIANO - FIUME NESTORE	155	1	15	14				30		11	17	2			30	2.4	2.7
TRT3	CICONIA - FIUME PAGLIA	220	2	12	15	1			30	1	14	12	3			30	2.5	2.6
TRT4	CASCATE MARMORE - FIUME NERA	285		9	13	8			30		5	13	11	1		30	3.0	3.3
TRT5	RECENTINO - FIUME NERA	285		18	12				30		6	17	6	1		30	2.4	3.1
TRT6	CIVITA CASTELLANA-FIUME TREIA	300	5	17	8				30		3	2				5	2.1	2.4
TRC1	S.SEVERA	406		11	16	2	1		30		5	14	9	2		30	2.8	3.3
TRC2	PASSO OSCURO	406		6	13	9	2		30		4	9	9	7	1	30	3.2	3.7
TRC3	FREGENE	406		5	14	7	3	1	30			10	11	6	3	30	3.4	4.1
TRC4	FOCENE	406		4	8	12	6		30		2	9	10	4	5	30	3.7	4.0
TRC5	FIUMICINO	406		5	13	9	3		30			1	8	15	6	30	3.3	4.9
TRC6	OSTIA	406		6	12		3	2	23			7	5	15	3	30	3.3	4.5
TRC7	OSTIA - CANCELLO 2	406		8	5	9	6	2	30		2	4	12	10	2	30	3.6	4.2

ANCIENT SAND

Sample#	Sampled Sequence in Measured Section	Stratigraphic Height (m)	Qtz Grains* 1	2	3	4	5	6	Qtz tot grains	Carb Grains* 1	2	3	4	5	6	Carb tot grains	Qtz Mean Roundness	Carb lithic Mean Roundness
TQ1	PG1-fluvial	0.50		2	10	11	5	2	30			6	8	6	10	30	3.8	4.7
TQ2	PG1-fluvial	1.90		10	17	3			30			12		18		30	2.8	4.2
TQ3	PG1-fluvial	3.00		6	12	11	1		30			5	11	8	6	30	3.2	4.5
TQ4	PG1-fluvial	4.00	1	3	15	8	3		30		3	8	15	4		30	3.3	3.7
TQ5	PG1-fluvial	5.00	1	6	16	5	2		30		2	13	8	5	2	30	3.0	3.7
TQ6	PG1-fluvial	6.00		3	15	7	3	2	30		2	12	7	8	1	30	3.5	3.8
TQ7	PG1-lower shoreface	6.25		10	13	6	1		30		1	6	15	6	2	30	2.9	4.1
TQ8	PG1-lower shoreface	7.25		6	11	13			30		2	14	11	3		30	3.2	3.5
TQ9	PG1-lower shoreface	8.15	2	12	10	6			30		3	16	6	5		30	2.7	3.4
TQ10	PG2-upper shoreface	9.00		7	15	7		1	30		3	14	11	2		30	3.1	3.4
TQ11	PG2-upper shoreface	10.50							0							0		
TQ12	PG2-upper shoreface	12.75			17	12	1		30		3	5	12	6	4	30	3.5	4.1
TQ13	PG2-lower shoreface	14.50		6	15	9			30		1	13	10	4	2	30	3.1	3.8
TQ14	PG2-upper shoreface	17.90		7	16	7			30	1	1	10	10	3	5	30	3.0	3.9
TO1	PG6-fluvial	1.00																
TO2	PG6-palustrine-lacustrine	4.50																
TO3	PG7-fluvial	8.00		1	10	16	1	2	30		1	13	13	2	1	30	3.8	3.6
EQ1	PG2-beachface	2.10		3	12	9	3	3	30				12	11	7	30	3.7	4.8
EQ2	PG2-beachface	5.00		3	15	10	1	1	30			9	8	10	3	30	3.4	4.2
EQ3	PG2- beachface	7.25		7	11	9	3		30							0	3.3	
EQ4	PG2-washover	9.50		4	13	9	4		30							0	3.4	
EQ5	PG3-lower shoreface	17.00	1	2	17	10			30							0	3.2	
EQ6	PG3-lower shoreface	19.20		4	13	13			30							0	3.3	
EQ7	PG4-fluviopalustrine	20.00	2	6	15	7			30							0	2.9	
EQ8	PG4-fluviopalustrine	21.00		6	14	5	5		30							0	3.3	

*** Key to Grain Shape Categories**
1 = very angular
2 = angular
3 = sub angular
4 = sub rounded
5 = rounded
6 = well rounded

Table A4. – Geology of the Tiber Drainage Basin

% Drainage Basin	Age	Formations, Succession or Units	Description	References	Source signature (Tributary and grain types)
>30%	Triassic to Miocene	Umbria-Marche succession	Pelagic to shallow water limestone (wackestone to packstone), chert, cherty mudstone, shale, evaporites, and bioclasts	Marino and Santantonio, 2010	**Chiascio River (TRT1)** - high percentage of lithic fragments (>80%), mostly micritic (Lsc(mic)) and sparitic (Lsc(cry))
~25%	Oligocene to Miocene	Macigno Cervarola, and Marnoso-Arenacea	Calcareous, marly, sandstone and pelitic turbidites	Van de Kamp and Leake, 1995; Dunkl et al., 2001; Gandolfi et al., 1983	**Nestore River (TRT2)** - drains arenaceous turbidite units, and siliclastic lithic grains (Lsa+Lsi+Lss)
~20%	Quaternary	Volcanic rock units of the Roman Magmatic province	Potassic lavas and pyroclastic rocks, leucite is the most characteristic phenocryst phase	Thompson, 1977; Peccerillo, 1985; Freda et al., 2006; Gaeta et al., 2011	**Treia River (TRT6)** - Volcanic lithic fragments dominate over monomineralic grains (Lvv+Lvml+Lvl)
15%	Jurassic to Miocene	Lazio-Abruzzi succession	Neritic shallow water limestone (packstone to grainstone), chert, shale and bioclasts	Brandano and Corda, 2002	**Nera River (TRT4/TRT5) -** lithic fragments dominate over monomineralic grains Lsc(sil+carb) Lsc(cry)+Lsc(mic))
<5%	Jurassic to Oligocene	Basinal and slope units	Basinal and slope micritic limestone, shale, sandstone, conglomerate, and breccia	Damiani, 1991	**Paglia River (TRT3)** - most diverse composition **(**Qm+Q, in Ls+P+P alt+K and K alt+Pyr+D+M+Lsa+Lsi+Lss)
<5%	Jurassic	Liguride and Sicilide successions	Ophiolites - rock assemblages include peridotite, gabbro, basalt (diabase), serpentine, and chert	Elter et al., 2003	**(TR1)** - Potential contribution of Qm+Lsa+Lsi+Lsc(cry)+Serp
<5%	Quaternary	Continental and marine units	Deltaic, alluvial and coastal plain deposits (mud, sand, and gravel)	Bellotti et al., 1993a, 1994, 1995	**Tiber River** – this study

APPENDIX B

(Supplementary Material of Chapter 3)

Table B1. – Counted and Recalculated Parameters

NCE = non carbonate extrabasinal grains
- Qpt = polycrystalline quartz with tectonite fabric
- Qpw = polycrystalline quartz
- Qm in Qp = monocrystalline quartz in polycrystalline quartz
- Q(chert) = chert
- Qm= monocrystalline quartz
- Qm in Ls = monocrystalline quartz in sedimentary lithic
- Qm in other = monocrystalline quartz in other lithic
- P = plagioclase feldspar
- Palt = altered plagioclase feldspar
- P in Lv = plagioclase feldspar in volcanic lithic
- P in Ls = plagioclase feldspar in sedimentary lithic
- P in other = plagioclase feldspar in other lithic
- K = potassium feldspar
- Kalt = altered potassium feldspar
- K in Lv = potassium feldspar in volcanic lithic
- K in Ls = potassium feldspar in sedimentary lithic
- K in other = potassium feldspar in other lithic
- Lvv = vitric volcanic lithic
  - pugl = pumice
  - brgl = brown glass
  - clgl = colorless glass
  - blgl = black glass
  - algl = altered glass
- Lvml = volcanic lithic with microlitic texture
  - brgl = brown glass
  - clgl = colorless glass
  - blgl = black glass
  - algl = altered glass
- Lvl = volcanic lithic with lathwork texture
  - brgl = brown glass
  - clgl = colorless glass
  - blgl = black glass
  - algl = altered glass
- Lvf = volcanic lithic with felsitic texture
- Lvp = pyroclastic tuff
- Lmp = metapelite lithic fragment and degree of metamorphism (I-IV)
- Lmm = metapsammite lithic fragment and degree of metamorphism (I-IV)
- Lsa = claystone lithic
- Lsi = siltstone lithic
- Lss = sandstone lithic
- M = muscovite
- B = biotite
- Chl = chlorite

Table B1. – Counted and Recalculated Parameters (continued)

D opaque = opaque dense mineral
D non-opaque = non-opaque dense mineral
Pyr = pyroxene
Serp = serpentine
alterites = altered unknown lithic fragment
alt n.n. = non identifiable alterite grain
saltati n.n. = unknown mashed grain
CI = carbonate intraclast
CE = carbonate extrabasinal grains
Lsc(mic) = micritic carbonate lithic
Lsc(cry) = carbonate crystal lithic
Lsc(sil+carb) = silt and carbonate lithic fragment

Total Pts= total points counted

Qm total = Qm+Qm in Qp+Qm in Ls+Q in other
K total = K+Kalt+K in Lv+K in Ls+K in other
P total = P+Palt+P in Lv+P in Ls+P in other
Q = Qpt+Qpw+Qp(chert)+Qm total
F = P total +K total
Lm = Lmp+Lmm
Lv = Lvv+Lvml+Lvl+Lvf+Lvp
Ls = Lsa+Lsi+Lss+Lsc(mic)+Lsc(cry)+Lsc(sil+carb)
L = Lm+Lv+Ls+alterites

QFL%Q= 100*Q/(Q + F+ L)
QFL%F= 100*F/(Q + F+ L)
QFL%L= 100*L/(Q + F+ L)

QmKP%Qm= 100*Qm/(Qm total+F)
QmKP%K= 100*K/(Qm total+F)
QmKP%P= 100*P/(Qm total+F)

LmLvLs%Lm= 100*Lm/(Lm+Lv+Ls)
LmLvLs%Lv= 100*Lv/(Lm+Lv+Ls)
LmLvLs%Ls= 100*Ls/(Lm+Lv+Ls)

NCE-CE-CI%NCE= 100*NCE/(NCE+CE+CI)
NCE-CE-CI%CE= 100*CE/(NCE+CE+CI)
NCE-CE-CI%CI= 100*CI/(NCE+CE+CI)

Table B2. – Point Count Data

TENTORI ET AL. 2016			NCE									CE	CI		QFL%			LmLvLs%			QmKP%			NCE-CE-CI%			MI
Sample#	Sample Location	Grain Size*	km downstream	Q	K	P	Lm	Lv	Lsi	Lsc	Micas	Heavy Minerals	CE bio	CI bio	Others	Total pts	Q	F	L	Lm	Lv	Ls	Qm	P	K	NCE	CE	CI	(Q/Q+F+L)
TR1	PIEVE S. STEFANO	m	20	34	6	22	4	0	137	165	0	16	14		2	400	9.2	7.6	83.2	1.3	0.0	98.7	51.7	37.9	10.3	55.0	41.5	3.5	0.1
TR2	PIOSINA	m	45	134	33	23	11	0	52	116	0	27	4		0	400	36.3	15.2	48.5	6.1	0.0	93.9	65.9	14.0	20.1	70.0	29.0	1.0	0.4
TR3	PIERANTONIO	m	80	131	28	15	14	0	99	97	1	15	0		0	400	34.1	11.2	54.7	6.7	0.0	93.3	70.9	10.1	18.9	75.8	24.3	0.0	0.3
TR4	CASALINA	m	150	115	50	20	12	0	51	138	2	8	4		0	400	29.8	18.1	52.1	6.0	0.0	94.0	57.3	12.2	30.5	64.5	34.5	1.0	0.3
TR5	PANTALLA	m	160	94	31	28	11	0	126	93	2	4	11		0	400	24.5	15.4	60.1	4.8	0.0	95.2	55.3	21.2	23.5	74.0	23.3	2.8	0.2
TR6	ORTE	m	280	72	40	15	10	112	44	102	0	5	0		0	400	18.2	13.9	67.8	3.7	41.8	54.5	48.1	14.2	37.7	74.5	25.5	0.0	0.2
TR7	ORTE SCALO	m	285	111	32	17	20	28	39	111	1	34	1		6	400	31.0	13.7	55.3	10.1	14.1	75.8	64.7	12.2	23.0	72.0	27.8	0.3	0.3
TR8	MAGLIANO SABINA	m	295	80	67	5	10	37	66	100	1	28	3		3	400	21.9	19.7	58.4	4.7	17.4	77.9	48.2	3.6	48.2	74.3	25.0	0.8	0.2
TR9	STIMIGLIANO	m	305	84	47	25	14	79	64	66	1	19	1		0	400	22.2	19.0	58.8	6.3	35.4	58.3	47.4	18.2	34.3	83.3	16.5	0.3	0.2
TR10	ROMA-TOR DI QUINTO	m	375	71	30	11	5	41	162	54	2	19	1		4	400	19.0	11.0	70.1	1.9	15.6	82.4	55.9	11.8	32.3	86.3	13.5	0.3	0.2
TR11	DRAGONA	m	400	122	62	11	13	38	76	61	6	4	1		6	400	31.9	19.1	49.1	6.9	20.2	72.9	57.1	6.5	36.5	84.5	15.3	0.3	0.3
TR12	FIUMICINO	m	403	187	47	23	17	5	46	8	1	62	1		3	400	56.2	21.0	22.8	22.4	6.6	71.1	63.7	11.9	24.4	97.8	2.0	0.3	0.6
TRT1	BASTIA UMBRA - FIUME CHIASCIO	m	135	60	24	8	3	0	50	237	0	0	18		0	400	15.7	8.4	75.9	1.0	0.0	99.0	60.0	10.0	30.0	36.3	59.3	4.5	0.2
TRT2	MARSCIANO - FIUME NESTORE	m	155	121	24	35	14	0	149	55	0	0	2		0	400	30.4	14.8	54.8	6.4	0.0	93.6	58.7	24.5	16.8	85.8	13.8	0.5	0.3
TRT3	CICONIA - FIUME PAGLIA	m	220	86	13	15	2	22	132	111	1	16	2		0	400	22.6	7.3	70.1	0.7	8.2	91.0	70.5	15.8	13.7	71.8	27.8	0.5	0.2
TRT4	CASCATE - MARMORE - FIUME NERA	m	285	121	0	0	0	0	24	253	0	2	0		0	400	30.4	0.0	69.6	0.0	0.0	100.0	0.0	0.0	0.0	36.8	63.3	0.0	0.3
TRT5	RECENTINO - FIUME NERA	m	285	168	37	22	9	0	43	116	0	4	0		1	400	42.5	14.9	42.5	5.4	0.0	94.6	65.1	13.0	21.9	71.0	29.0	0.0	0.4
TRT6	CIVITA CASTELLANA - FIUME TREIA	m	300	53	28	16	3	159	9	5	3	124	0		0	400	19.4	16.1	64.5	1.7	90.3	8.0	52.2	17.4	30.4	98.8	1.3	0.0	0.2
TRC1	S.SEVERA	m	406	153	25	2	10	2	64	110	0	27		3	4	400	41.8	7.4	50.8	5.4	1.1	93.5	75.7	1.8	22.5	71.8	27.5	0.8	0.4
TRC2	PASSO OSCURO	m	406	161	57	27	7	7	48	79	1	6		0	7	400	41.7	21.8	36.5	5.0	5.0	90.1	62.3	12.1	25.6	80.3	19.8	0.0	0.4
TRC3	FREGENE	m	406	110	18	16	7	2	9	95	1	137		2	3	400	42.8	13.2	44.0	6.2	1.8	92.0	73.8	12.3	13.8	75.8	23.8	0.5	0.4
TRC4	FOCENE	m	406	115	18	21	7	3	10	61	0	159		4	2	400	48.9	16.6	34.5	8.6	3.7	87.7	69.5	16.4	14.1	83.8	15.3	1.0	0.5
TRC5	FIUMICINO	m	406	110	48	23	11	6	15	90	1	93		0	3	400	36.3	23.4	40.3	9.0	4.9	86.1	52.7	15.3	32.0	77.5	22.5	0.0	0.4
TRC6	OSTIA	m	406	158	65	19	6	4	15	80	0	49		4	0	400	45.5	24.2	30.3	5.7	3.8	90.5	54.8	10.2	34.9	79.0	20.0	1.0	0.5
TRC7	OSTIA CANCELLO 2	m	406	121	43	20	11	6	33	125	1	37		2	1	400	33.7	17.5	48.7	6.3	3.4	90.3	59.4	12.9	27.7	68.3	31.3	0.5	0.3
THIS STUDY			NCE									CE	CI		QFL%			LmLvLs%			QmKP%			NCE-CE-CI%			MI
Sample#	Sample Location	Grain Size*	km downstream	Q	K	P	Lm	Lv	Lsi	Lsc	Micas	Heavy Minerals	CE bio	CI bio	Others	Total pts	Q	F	L	Lm	Lv	Ls	Qm	P	K	NCE	CE	CI	(Q/Q+F+L)
TS65A	FIUMICINO	m	406.237	108	38	56	4	21	40	100	0	29	0	1	3	400	29.3	25.5	45.1	2.4	12.7	84.8	42.7	23.2	34.1	74.6	25.1	0.3	0.3
TS65A	FIUMICINO	f		123	60	58	11	12	31	89	2	9	2	2	1	400	32.0	30.7	37.2	7.7	8.4	83.9	43.0	29.0	28.0	76.7	22.8	0.5	0.3
TS65B	FIUMICINO	m		56	43	40	0	138	22	65	2	10	1	17	6	400	15.1	22.4	62.4	0.0	61.3	38.7	21.0	41.0	38.1	79.3	16.5	4.3	0.2
TS65B	FIUMICINO	f		83	48	147	0	2	13	89	0	4	1	12	1	400	21.7	50.9	27.4	0.0	1.9	98.1	25.3	18.4	56.3	74.7	22.6	2.8	0.2
TS65C	FIUMICINO	m		45	23	18	0	200	31	23	7	2	0	32	19	400	12.5	11.4	76.0	0.0	78.7	21.3	4.7	53.5	41.9	86.7	5.8	7.5	0.1
TS62A	FIUMICINO	m	406.625	113	38	67	2	12	22	70	0	73	0	3	0	400	34.9	32.4	32.7	1.9	11.3	86.8	41.3	21.2	37.4	81.8	17.5	0.8	0.3
TS62A	FIUMICINO	f		96	30	139	5	7	14	90	2	9	0	8	0	400	25.2	44.4	30.4	4.3	6.0	89.7	30.7	12.3	57.0	75.5	22.5	2.0	0.3
TS62B	FIUMICINO	m		111	39	65	8	8	19	90	0	54	2	2	2	400	32.5	30.4	37.1	6.4	6.4	87.2	42.9	21.4	35.7	76.5	23.0	0.5	0.3
TS58A	FIUMICINO	m	407	50	36	25	0	77	15	78	3	74	0	25	17	400	17.1	20.9	62.0	0.0	45.3	54.7	33.0	39.6	27.5	77.0	20.6	2.4	0.2
TS58A	FIUMICINO	f		35	16	68	2	44	24	56	68	4	7	75	1	400	14.3	34.3	51.4	1.6	34.9	63.5	24.3	14.4	61.3	76.1	18.4	5.5	0.1
TS58B	FIUMICINO	f		68	39	109	9	11	26	70	25	5	1	36	1	400	20.4	44.4	35.1	7.8	9.5	82.8	26.0	19.5	54.5	75.3	18.3	6.4	0.2
TS56A	FIUMICINO	f	407.237	62	16	109	5	70	27	51	30	4	0	13	13	400	17.7	35.7	46.6	3.3	45.8	51.0	30.9	8.8	60.2	84.7	13.0	2.3	0.2
TS56B	FIUMICINO	f		59	53	54	3	26	47	116	6	4	1	12	19	400	15.8	28.7	55.5	1.6	13.5	84.9	25.2	37.1	37.8	68.8	30.2	1.0	0.2
TS56D	FIUMICINO	m		24	15	34	0	12	12	56	14	1	0	227	5	400	15.6	31.8	52.6	0.0	15.0	85.0	31.0	21.1	47.9	34.3	17.0	48.6	0.2
TS56D	FIUMICINO	f		26	8	73	1	115	22	30	20	0	0	87	18	400	8.9	27.7	63.4	0.6	68.5	31.0	24.3	7.5	68.2	74.6	7.9	17.5	0.1
														0		400													
TS19A	FIUMICINO	m	406.262	84	36	52	4	22	30	94	3	67	1	5	2	400	26.1	27.3	46.6	2.7	14.7	82.7	41.7	23.8	34.4	74.9	23.9	1.3	0.3
TS19A	FIUMICINO	f		94	40	58	9	31	53	86	9	4	4	10	2	400	25.3	26.4	48.2	5.0	17.3	77.7	41.0	24.1	34.9	74.9	22.6	2.5	0.3
TS19B	FIUMICINO	m		79	45	46	1	86	19	61	1	31	2	12	17	400	22.3	25.7	52.0	0.6	51.5	47.9	30.5	34.4	35.1	82.3	15.9	1.8	0.2
TS19C	FIUMICINO	m		63	40	38	3	133	17	68	0	23	0	10	5	400	17.2	21.3	61.6	1.4	60.2	38.5	22.0	40.0	38.0	80.7	17.0	2.3	0.2
TS19D	FIUMICINO	m		66	37	47	3	65	19	89	1	42	5	17	9	400	19.7	25.1	55.2	1.7	36.9	61.4	31.7	30.1	38.2	73.9	24.0	2.0	0.2
TS19D	FIUMICINO	f		118	62	96	2	2	9	99	1	1	4	3	3	400	30.3	40.5	29.2	1.8	1.8	96.4	36.5	24.9	38.6	73.4	25.8	0.8	0.3
TS13A	FIUMICINO	m	406.662	119	61	38	7	34	25	84	1	25	1	4	1	400	32.3	26.9	40.8	4.7	22.7	72.7	40.4	36.7	22.9	77.7	21.3	1.0	0.3
TS13A	FIUMICINO	f		131	73	85	9	10	21	56	1	1	2	11	0	400	34.0	41.0	24.9	9.4	10.4	80.2	39.0	28.2	32.8	82.8	14.5	2.8	0.3
TS13B	FIUMICINO	m		102	59	57	9	23	38	98	0	8	1	5	0	400	26.4	30.1	43.5	5.4	13.7	81.0	38.6	31.2	30.2	74.0	24.8	1.3	0.3
TS13C	FIUMICINO	m		18	12	9	0	178	19	64	0	6	2	39	53	400	5.1	6.0	88.9	0.0	68.2	31.8	4.5	54.5	40.9	74.3	16.8	8.9	0.1
TS13D	FIUMICINO	f		124	69	103	3	5	11	71	0	2	0	8	4	400	32.0	44.3	23.7	3.3	5.6	91.1	33.1	26.8	40.1	81.4	18.1	0.5	0.3
TS27A	FIUMICINO	m	407.175	103	40	76	4	19	31	74	3	44	0	3	3	400	29.4	33.1	37.4	3.1	14.8	82.0	33.3	23.0	43.7	80.8	18.5	0.8	0.3
TS27A	FIUMICINO	f		75	55	116	3	14	39	81	2	5	0	5	5	400	19.3	44.1	36.6	2.2	10.2	87.6	24.7	24.2	51.1	78.5	20.3	1.3	0.2
TS27B	FIUMICINO	m		104	46	51	11	13	16	102	1	50	0	4	2	400	30.1	28.1	41.7	7.7	9.2	83.1	40.1	28.4	31.5	73.9	25.6	0.5	0.3
TS27C	FIUMICINO	f		107	37	102	5	15	27	91	3	1	0	9	3	400	27.8	36.1	36.1	3.6	10.9	85.5	32.2	18.0	49.8	74.9	22.9	2.3	0.3
TS27D	FIUMICINO	f		36	33	82	5	67	29	56	7	0	0	17	68	400	9.6	30.6	59.8	3.2	42.7	54.1	20.1	22.9	56.9	82.4	14.1	3.5	0.1
																400													
TC6-4	OFF-SHORE	f	423.5	34	4	11	0	1	4	1	12	3	0	325	5	400	61.8	27.3	10.9	0.0	16.7	83.3	68.8	8.3	22.9	18.6	0.3	81.1	0.6
TC6-10	OFF-SHORE	f		40	4	10	1	6	6	7	9	0	0	314	3	400	54.1	18.9	27.0	5.0	30.0	65.0	69.6	8.7	21.7	21.3	2.0	76.7	0.5
TC6-18	OFF-SHORE	f		84	19	19	8	6	5	18	15	1	0	217	8	400	52.8	23.9	23.3	21.6	16.2	62.2	61.2	19.4	19.4	44.5	5.1	50.4	0.5
TC6-24	OFF-SHORE	f		1	0	1	0	0	1	10	0	0	5	382	0	400	7.7	7.7	84.6	0.0	0.0	100.0	0.0	0.0	100.0	0.8	3.8	95.5	0.1
TC6-25	OFF-SHORE	f		1	0	0	0	0	0	11	0	0	0	388	0	400	8.3	0.0	91.7	0.0	0.0	100.0	0.0	0.0	0.0	0.3	2.8	97.0	0.1
TC6-31	OFF-SHORE	f		67	8	34	17	0	26	6	10	2	0	227	3	400	42.4	26.6	31.0	34.7	0.0	65.3	56.7	8.2	35.1	44.8	1.6	53.6	0.4
TC6-33	OFF-SHORE	f		7	0	2	1	0	6	8	3	0	0	313	2	400	29.2	8.3	62.5	6.7	0.0	93.3	66.7	0.0	33.3	5.7	2.4	91.9	0.3
TC7-3	OFF-SHORE	f		14	1	5	0	0	0	0	4	1	0	375	0	400	70.0	30.0	0.0	0.0	0.0	0.0	66.7	5.6	27.8	6.3	0.0	93.8	0.7
TC7-18	OFF-SHORE	f		0	0	0	0	0	0	0	0	0	0	400	0	400	0.0	0.0	0.0	0.0	0.0	0.0	0.0	0.0	0.0	0.0	0.0	100.0	0.0
TC7-24	OFF-SHORE	f		0	0	0	0	0	0	0	0	0	0	400	0	400	0.0	0.0	0.0	0.0	0.0	0.0	0.0	0.0	0.0	0.0	0.0	100.0	0.0
TC7-26	OFF-SHORE	f		0	0	0	0	0	0	1	0	0	0	399	0	400	0.0	0.0	100.0	0.0	0.0	100.0	0.0	0.0	0.0	0.0	0.3	99.8	0.0
TC7-27	OFF-SHORE	f		8	0	5	0	0	0	0	0	2	0	384	1	400	61.5	38.5	0.0	0.0	0.0	0.0	61.5	0.0	38.5	3.8	0.0	96.2	0.6
TC7-29	OFF-SHORE	f		3	0	1	0	1	0	1	0	0	0	394	0	400	50.0	16.7	33.3	0.0	50.0	50.0	75.0	0.0	25.0	1.3	0.3	98.5	0.5
TC7-41	OFF-SHORE	f		5	0	0	0	0	2	0	0	2	1	388	2	400	71.4	0.0	28.6	0.0	0.0	100.0	100.0	0.0	0.0	2.3	0.3	97.5	0.7
TC8-6	OFF-SHORE	f		4	0	0	0	0	0	0	1	0	0	360	35	400	100.0	0.0	0.0	0.0	0.0	0.0	100.0	0.0	0.0	1.4	0.0	98.6	1.0
TC8-16	OFF-SHORE	f		1	0	0	0	0	0	0	1	0	0	397	1	400	100.0	0.0	0.0	0.0	0.0	0.0	0.0	0.0	0.0	0.5	0.0	99.5	1.0
TC8-20	OFF-SHORE	f		0	0	0	0	0	0	0	0	0	0	388	12	400	0.0	0.0	0.0	0.0	0.0	0.0	0.0	0.0	0.0	0.0	0.0	100.0	0.0
TC8-22	OFF-SHORE	f		3	0	0	0	0	0	0	0	0	0	397	0	400	100.0	0.0	0.0	0.0	0.0	0.0	100.0	0.0	0.0	0.8	0.0	99.3	1.0
TC8-23	OFF-SHORE	f		1	0	0	0	0	0	0	0	0	0	399	0	400	100.0	0.0	0.0	0.0	0.0	0.0	100.0	0.0	0.0	0.3	0.0	99.8	1.0
TC8-26	OFF-SHORE	f		7	0	0	0	0	1	0	0	1	0	391	0	400	87.5	0.0	12.5	0.0	0.0	100.0	100.0	0.0	0.0	2.3	0.0	97.8	0.9
TC8-42	OFF-SHORE	f		9	0	1	0	0	0	0	0	0	0	390	0	400	90.0	10.0	0.0	0.0	0.0	0.0	90.0	0.0	10.0	2.5	0.0	97.5	0.9

For acronym description see Table 2 in the Supplementary material. *m=medium sand; f=fine sand

Table B3. - Table of Tiber River main grain types from source-to-sink

SOURCE ↓ SINK	FLUVIAL	TRIBUTARIES	**Chiascio River (TRT1)** - high percentage of lithic fragments (>80%), mostly micritic (Lsc(mic)) and sparitic (Lsc(cry)) **Nestore River (TRT2)** - drains arenaceous metamorphic–lithic bearing turbidite units, and siliclastic lithic grains (Lsa+Lsi+Lss) **Paglia River (TRT3)** - most diverse composition **(**Qm+Q, in Ls+P+P alt+K and K alt+Pyr+D+M+Lsa+Lsi+Lss) **Nera River (TRT4/TRT5) -** lithic fragments dominate over monomineralic grains Lsc(sil+carb) Lsc(cry)+Lsc(mic)) **Treia River (TRT6)** - Volcanic lithic fragments dominate over monomineralic grains (Lvv+Lvml+Lvl)
		TIBER RIVER	**Upstream samples** **TR1/TR2/TR3/TR4/TR5 –** dominant quartz (Q+Qpw+Qpt), significant feldspar (K+P), minor micas (M+B) and heavy minerals(Serp); siliciclastic (15-50%), carbonate (Lsc(cry)+Lsc(mic)+Lsc(sil+carb) ~20-70%) and low grade metamorphic (Lmp+Lmm <10%) lithic fragments proportion are variable depending on tributaries input. **Downstream samples** **TR6/TR7/TR8/TR9/TR10/TR11/TR12 –** dominant quartz (Q+Qpw+Qpt), significant feldspar (K+P), minor feldspathoids (Fldsp) micas (M+B) and heavy (Pyr+Dopaque+Dnonop); dominant carbonate (Lsc(cry)+Lsc(mic)+Lsc(sil+carb) and minor siliciclastic (Lsa+Lsi+Lss) sedimentary lithic and significant volcanic lithic (Lvv+Lvml+Lvl) fragments
	COASTAL	FORESHORE	**Samples TRC1/TRC2/TRC3/TRC4/TRC5/TRC6-** dominant quartz (Q+Qpw+Qpt) and pyroxene (Pyr), common feldspar (K+P), and minor dense mineral (Dopaque+Dnonop); dominant carbonate (Lsc(cry)+Lsc(mic)), and significant volcanic lithic (Lvv+Lvml+Lvl) fragments; common bioclasts (CI+CE)
		SHOREFACE	**Cores TS27/TS13/TS19/TS56/TS58/TS62/TS65 –** dominant quartz (Q+Qpw+Qpt) and feldspar (K+P), minor micas (M+B+Chl) and heavy (Pyr+Dopaque+Dnonop); common carbonate (Lsc(cry)+Lsc(mic)+Lsc(sil+carb) and siliciclastic (Lsa+Lsi+Lss) sedimentary lithic, significant volcanic lithic (Lvv+Lvml+Lvl) fragments and minor low grade metamorphic (Lmp+Lmm <10%); common bioclasts (CI+CE)
	DEEP MARINE	SHELF	**Core TC6 –** dominant bioclasts (CI) with common quartz (20-40%) and feldspar (K+P) and minor micas (B+M+Chl) and dense minerals (Pyr+Amph) and minor carbonate (Lsc(cry)+Lsc(mic)) and volcanic (Lvv+Lvml+Lvl) and metamotphic lithic fragments (Lmp+Lmm) **Cores TC7/TC8 –** mostly composed of carbonate bioclast (CI ~100%)
		ABYSSAL PLAIN	**ODP Site 794-** dominant quartz (Q+Qpw+Qpt) and pyroxene (Pyr), common feldspar (K+P), minor dense mineral; significant low and medium grade metamorphic (Lmp+Lmm <10%) and volcanic lithic (Lvv+Lvml+Lvl) fragments and minor carbonate (Lsc(cry)+Lsc(mic)+Lsc(sil+carb) and siliciclastic (Lsa+Lsi+Lss) sedimentary lithic

APPENDIX C

(Supplementary Material of Chapter 4)

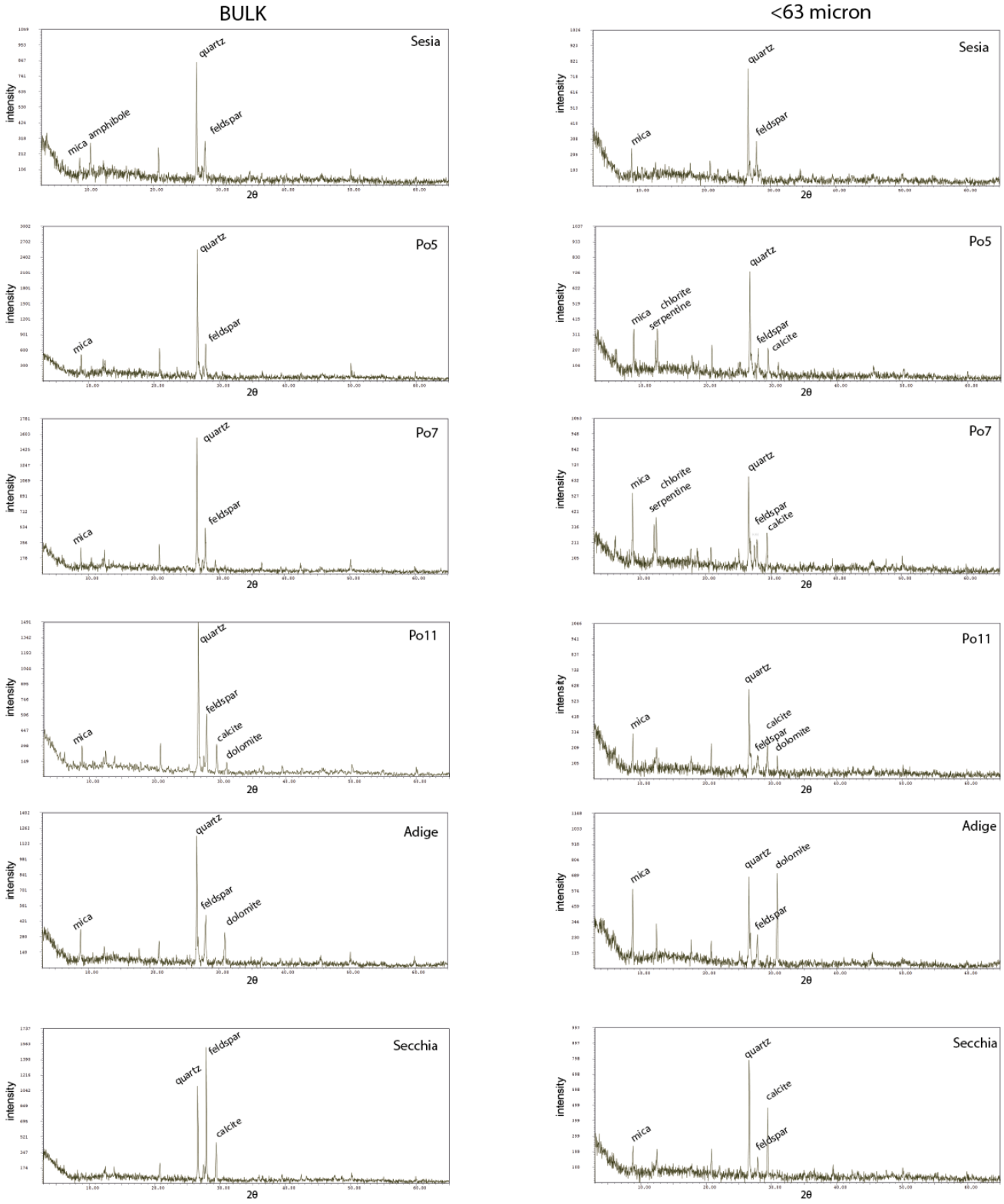

FIG. C1 – XRD powder diffraction of modern Po river and tributary samples for bulk and fine-grained (<63 microns) sediment.

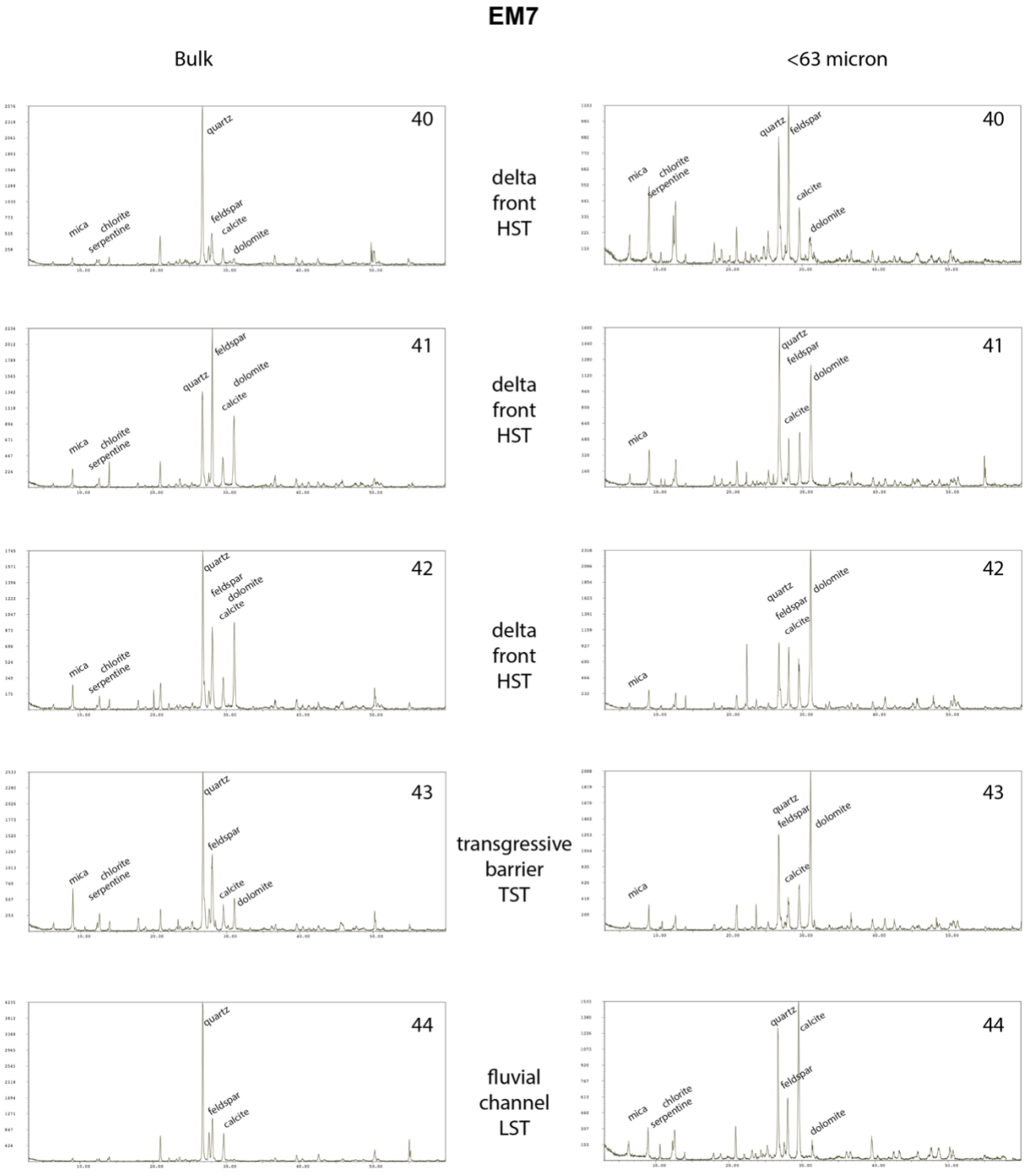

FIG. C2 – XRD powder diffraction of samples from core EM7 for bulk and fine-grained (<63 microns) sediment.

EM4

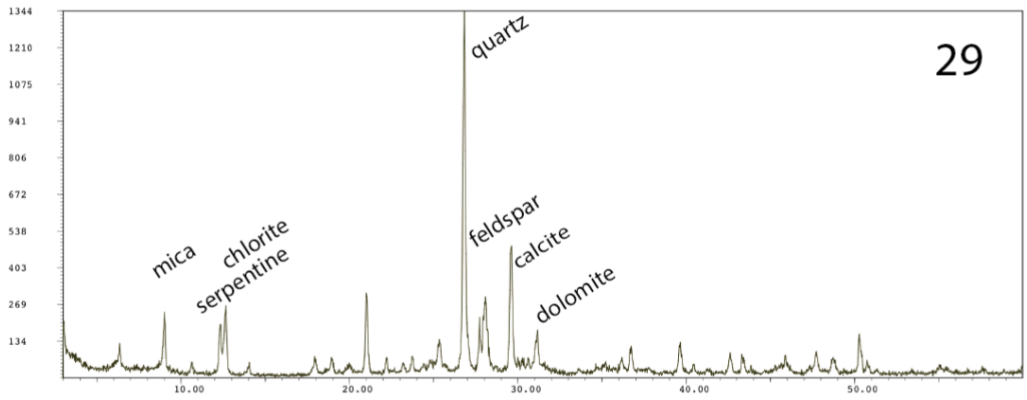

delta front
HST

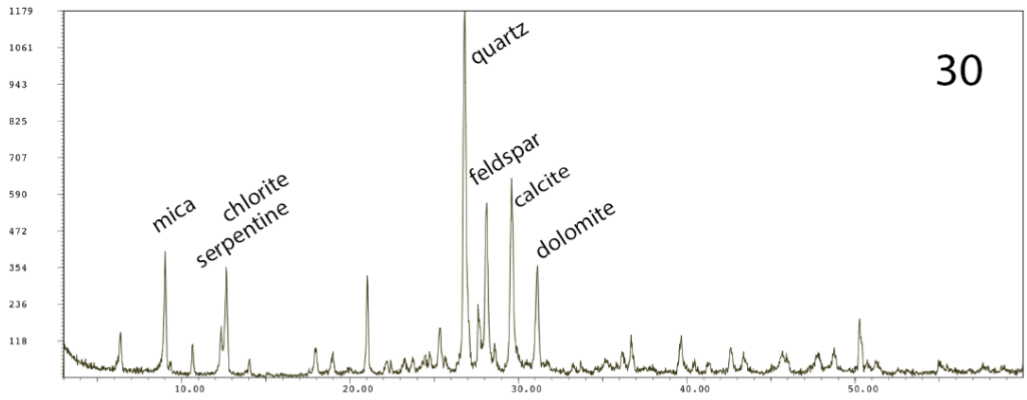

transgressive
barrier
TST

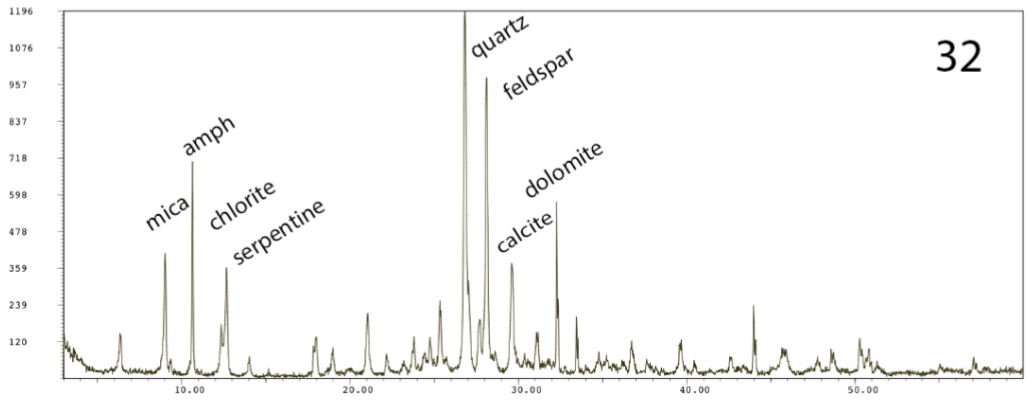

fluvial
channel
LST

FIG. C3 – XRD powder diffraction of fine-grained samples (<63 microns) from cores EM4.

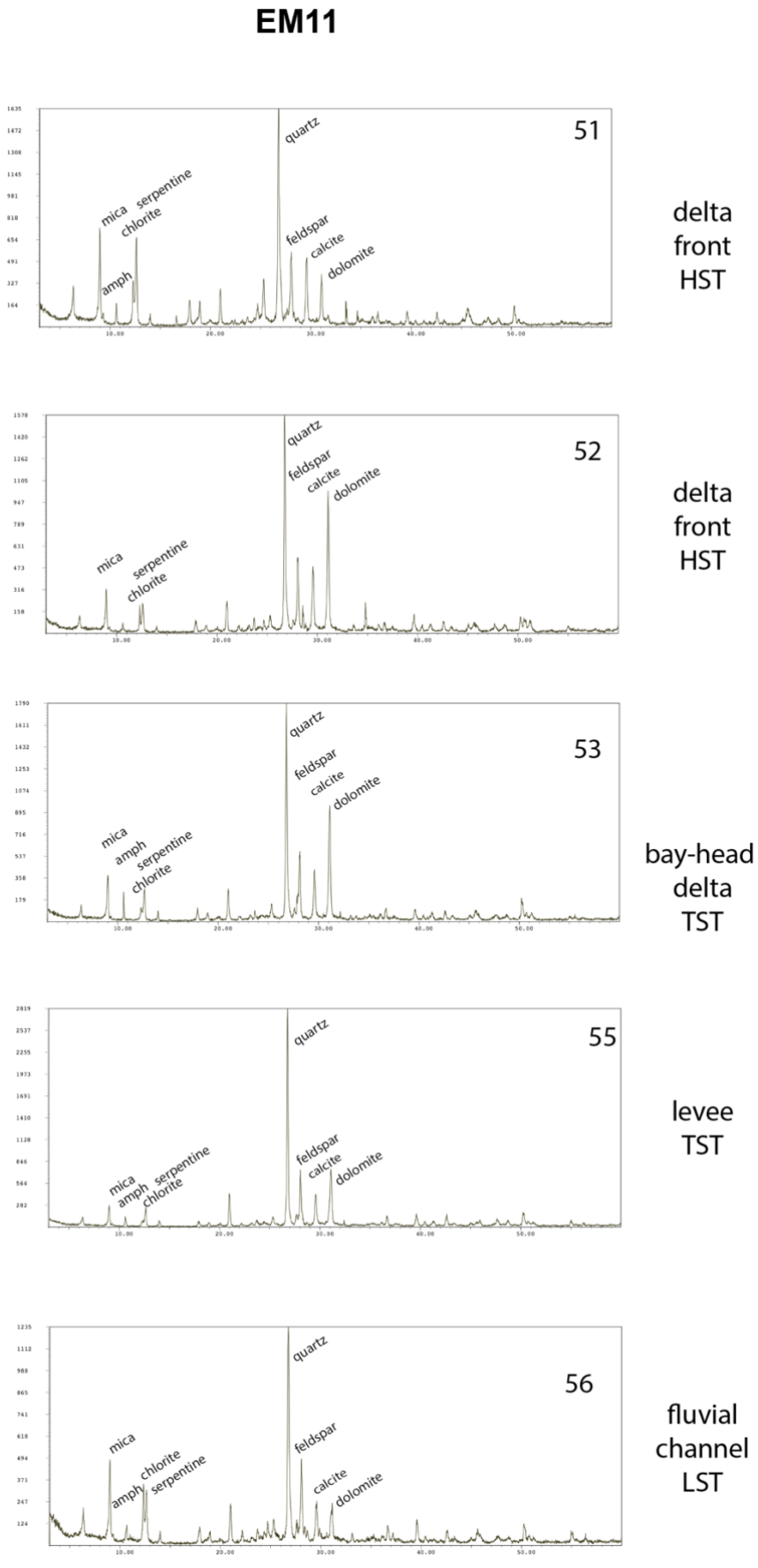

FIG. C4 – XRD powder diffraction of fine-grained samples (<63 microns) from cores EM11.

EM13

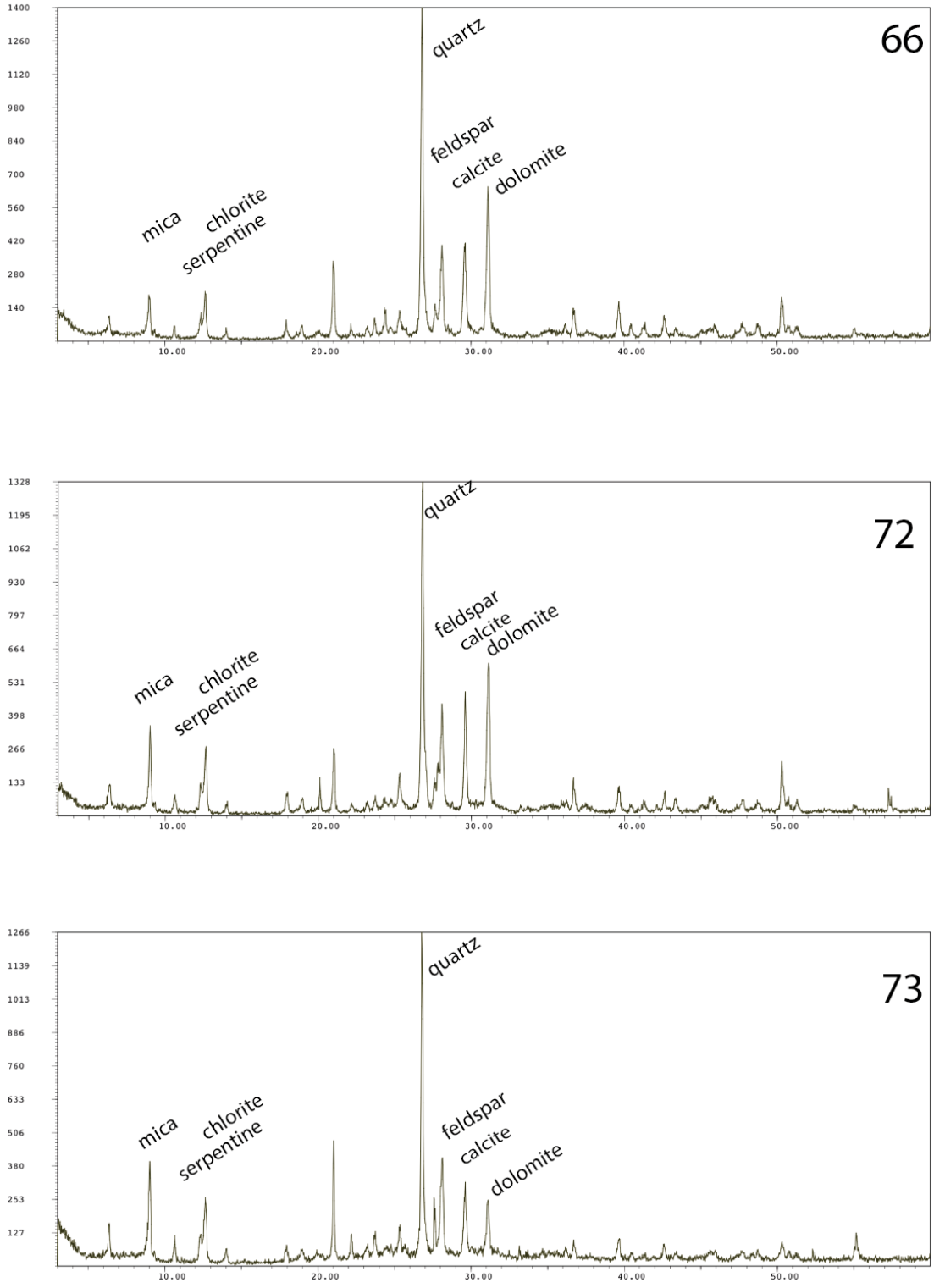

FIG. C5 – XRD powder diffraction of fine-grained samples (<63 microns) from cores EM11.

Table C1. – Counted and recalculated parameters

NCE
- Qm= monocrystalline quartz
- Qpt = polycrystalline quartz with tectonite fabric
- Qpw = polycrystalline quartz
- P = plagioclase feldspar
- Pser = seriticized plagioclase feldspar
- K = potassium feldspar
- Kalt = altered potassium feldspar
- Lsa = claystone lithic
- Lsi = siltstone lithic
- Lvf = volcanic lithic with felsitic texture
- porph. quartz: felsic volcanic lithic with porphyritic texture
- Lvml = volcanic lithic with microlitic texture
- porph. plagioclase: intermediate volcanic lithic with porphyritic texture
- Lvl = volcanic lithic with lathwork texture
- porph. pyroxene: mafic volcanic lithic with porphyritic texture
- Serp cell = volcanic cellular serpentinite
- Lmp = metapelite lithic fragment and degree of metamorphism (I-IV)
- Lmm = metapsammite lithic fragment and degree of metamorphism (I-IV)
- Lmi = metaigneous lithic fragment and degree of metamorphism (I-IV)
- Lmc = metacarbonate lithic fragment and degree of metamorphism (I-IV)
- Serp schist = foliated serpentinite schist

ACC= accessory grains
- M = muscovite
- B = biotite
- Chl = chlorite
- D opaque = opaque dense mineral
- D non-opaque = non-opaque dense mineral
- Pyr = pyroxene
- Amph: Amphibole
- Sp: spinel
- Gt: garnet
- Ep: epidote
- Z: zircon
- T: titanite
- R: rutile
- Alt = non identifiable altered grain
- Unkn = unknown grain or lithic fragment

CI = carbonate intraclast

CE = carbonate extrabasinal bioclast
- Lsc(mic) = micritic carbonate lithic
- Lsc(spar) = sparitic carbonate lithic
- Lsc(dolo) = dolomite lithic fragment

Total Pts= total points counted

Table C1. – Counted and recalculated parameters (continued)

Qm = Qm
K total = K+Kalt
P total = P+Pser
Q= Qpt+Qpw+ Qm
F = P total +K total
Mica = M+B
Lm = Lmp+Lmm
LG = low-grade metamorphic lithic fragments (ranks I-II)
HG = medium to high-grade metamorphic lithic fragments (ranks III-IV)
Lv = Lvf+Lvml+Lvl + porph. quartz+ porph. plagioclase+ porph. pyroxene
Lsc = Lsc(mic)+Lsc(cry)+Lsc(dol)
Ls(silic) = Lsa+Lsi
Ls = Ls(silic)+Lsc
Ls-c = Ls-Lsc
L = Lm+Lv+Ls

QFL%Qt= 100*Q/(Q+ F+ L)
QFL%F= 100*F/(Q + F+ L)
QFL%L= 100*L/(Q + F+ L)

QmKP%Qm= 100*Qm/(Qm total+F)
QmKP%K= 100*K/(Qm total+F)
QmKP%P= 100*P/(Qm total+F)

LmLvLs%Lm= 100*Lm/(Lm+Lv+Ls)
LmLvLs%Lv= 100*Lv/(Lm+Lv+Ls)
LmLvLs%Ls= 100*Ls/(Lm+Lv+Ls)

LmLvLs-c%Lm= 100*Lm/(Lm+Lv+Ls-c)
LmLvLs-c%Lv= 100*Lv/(Lm+Lv+Ls-c)
LmLvLs-c%Ls-c= 100*Ls-c/(Lm+Lv+Ls-c)

LmLs(silc)Lsc%Lm= 100*Lm/(Lm+Lsc+Ls(silic))
LmLs(silic)Lsc%Ls-c= 100*Ls(silic)/(Lm+Lsc+ Ls(silic))
LmLs(silic)Lsc%Lsc= 100*Lsc/(Lm+Lsc+ Ls(silic))

MicaLGHG%Mica= 100*Mica/(Mica+LG+HG)
MicaLGHG%LG= 100*LG/(Mica+LG+HG)
MicaLGHG%HG= 100*HG/(Mica+LG+HG)

Table C2. – Point Count Data

Sample designation	Core	Sample depth (m)	FACIES	Systems Tract	Provenance	Qm	Qpw	Qpt	P	Pser	K
Dora Baltea	/	/	Fluvial channel	Modern	/	186	5	12	17	20	16
Sesia	/	/	Fluvial channel	Modern	/	112	5	23	22	18	19
Ticino	/	/	Fluvial channel	Modern	/	236	10	5	40	35	18
Adda	/	/	Fluvial channel	Modern	/	121	28	15	40	28	23
Cherio	/	/	Fluvial channel	Modern	/	41	6		11	7	5
Oglio	/	/	Fluvial channel	Modern	/	129	20	20	24	18	10
Mincio	/	/	Fluvial channel	Modern	/	130	19	10	33	9	19
Adige	/	/	Fluvial channel	Modern	/	138	8	4	20	37	17
Trebbia	/	/	Fluvial channel	Modern	/	25	8	4	20	9	6
Taro	/	/	Fluvial channel	Modern	/	49	4	1	20	22	11
Secchia	/	/	Fluvial channel	Modern	/	78	8	4	28	26	10
Reno	/	/	Fluvial channel	Modern	/	154	11	2	20	31	8
Scrivia	/	/	Fluvial channel	Modern	/	31	7	10	15	17	3
Bormida di Spigno	/	/	Fluvial channel	Modern	/	76	9	28	13	18	17
Orba	/	/	Fluvial channel	Modern	/	99	5	15	18	20	25
Tanaro (l.r.)	/	/	Fluvial channel	Modern	/	116	17	4	40	22	25
Tanaro (u.r.)	/	/	Fluvial channel	Modern	/	116	4	10	41	21	16
Bormida di Millesimo (u.r.)	/	/	Fluvial channel	Modern	/	86	22	11	25	11	17
Bormida di Millesimo (l.r.)	/	/	Fluvial channel	Modern	/	96	28	7	23	11	19
Erro	/	/	Fluvial channel	Modern	/	58	7	3	27	17	15
Po1	/	/	Fluvial channel	Modern	/	168	33	25	29	9	17
Po2	/	/	Fluvial channel	Modern	/	179	32		14	16	23
Po3	/	/	Fluvial channel	Modern	/	176	10	15	22	34	28
Po4	/	/	Fluvial channel	Modern	/	186	8	10	22	32	21
Po5	/	/	Fluvial channel	Modern	/	170	15	6	33	19	26
Po6	/	/	Fluvial channel	Modern	/	185	5	22	27	24	14
Po7	/	/	Fluvial channel	Modern	/	190	5	13	37	36	29
Po8	/	/	Fluvial channel	Modern	/	204	22		17	33	24
Po9	/	/	Fluvial channel	Modern	/	184	7	13	13	31	32
Po10	/	/	Fluvial channel	Modern	/	207	15	20	11	41	17
Po11	/	/	Fluvial channel	Modern	/	185	5	7	7	26	20
Po12	/	/	Fluvial channel	Modern	/	174	8	10	9	27	10
25	S2 EM2	27.30	Fluvial channel	LST	Po	181	9	14	13	34	35
26	EM2	31.10	Fluvial channel	LST	Po	210	6	15	14	28	44
27	EM2	34.80	Fluvial channel	LST	Po	213	10	10	17	28	33
28	S3 EM3	17.40	Fluvial channel	LST	Ap	154	20	3	8	39	52
29	S4 EM4	4.70	Delta front	HST	Al	165	12	3	14	25	30
30	EM4	27.15	Transgressive barrier	TST	Po/Ap	264	9	1	14	16	30
31	EM4	32.60	Fluvial channel	LST	Po/Al	191	22	4	16	36	18
32	EM4	35.80	Fluvial channel	LST	Po/Al	191	16	3	7	31	19
33	S5 EM5	11.30	Bay-head delta	TST	Po	174	5	6	44	22	34
34	EM5	15.50	Bay-head delta	TST	Po	162	10	8	44	20	32
35	EM5	28.80	Fluvial channel	LST	Ap	164	6	6	38	15	30
36	S6 EM6	26.40	Fluvial channel	LST	Po	184	11		48	19	37
37	EM6	34.80	Fluvial channel	LST	Po	166	5	11	50	18	50
38	EM6	42.90	Fluvial channel	LST	Po	198	6	8	39	10	57
39	EM6	47.70	Fluvial channel	LST	Po	163	5		60	7	64
40	S7 EM7	1.30	Delta front	HST	Po/Al	160	7	5	13	60	67
41	EM7	7.90	Delta front	HST	Al	107	3	2	29		34
42	EM7	13.70	Delta front	HST	Al	96		8	44	13	40
43	EM7	21.70	Transgressive barrier	TST	Ap	131		4	40	26	31
44	EM7	33.90	Fluvial channel	LST	Ap	150		5	70	14	62
45	S8 EM8	8.90	Delta front	HST	Al/Ap	158		13	46	28	56
46	EM8	9.80	Delta front	HST	Al/Ap	163	3	6	32	58	36
47	S9 EM9	12.60	Fluvial channel	TST	Ap	153	5		51	32	41
48	S10 EM10	20.20	Fluvial channel	TST?	Po/Al	162	20		12	55	45
49	EM10	25.80	Fluvial channel	TST?	Po/Al	138	16		64	27	47
50	EM10	31.80	Fluvial channel	LST	Po	140	26		68	25	29
51	S11 EM11	7.80	Delta front	HST	Po	155	12		50	37	44
52	EM11	11.40	Delta front	HST	Al	160	5	7	51	32	30
53	EM11	16.60	Bay-head delta	TST	Po	140		9	52	46	43
54	EM11	18.80	Crevasse channel	TST	Po	137	11	15	47	42	48
55	EM11	27.90	Levee	TST?	Po	108	7		60	27	34
56	EM11	33.20	Fluvial channel	LST	Po	117	8	13	58	54	33
57	S12 EM12	2.3	Delta front	HST	Al	160		16	51	48	54
58	EM12	4.8	Delta front	HST	Al	138	15		48	25	43
59	EM12	9.9	Delta front	HST	Al	159	8		57	10	33
60	EM12	12.8	Delta front	HST	Al	98	5	2	61	11	22
61	EM12	16.9	Delta front	HST	Al	70	1		40	9	9
62	EM12	20.6	Transgressive barrier	TST	Po/Al	41		2	30	14	13
63	EM12	22.3	Bay-head delta	TST	Po/Al	162	7	10	65	15	31
66	S13 EM13	12.1	Prodelta	HST	Al	83	6	2	90	4	22
67	EM13	16.7	Prodelta	HST	Al	87		5	58		24
70	EM13	24.4	Prodelta	HST	Al	42	4		58		12
71	EM13	26.3	Transgressive barrier	TST	Po/Al	136	5	5	61	19	33
72	EM13	29.6	Crevasse channel	TST	Po/Al	122		21	80	26	37
73	EM13	32.95	Fluvial channel	LST	Po/Al	157	3	20	62	27	29
74	S14 EM14	8.1	Delta front	HST	Po/Al	113	2	8	41	63	40
75	EM14	16.2	Transgressive barrier	TST	Po/Al	147	5	15	83	21	18
76	EM14	20.6	Fluvial channel	LST	Po	154	2	16	28	72	29
77	S18 EM18	20.3	Fluvial channel	LST	Al	177	10	10	83	14	23
78	EM18	22.8	Fluvial channel	LST	Al	166	10	1	43	45	36
79	EM18	31.8	Fluvial channel	LST	Po	171	16	2	70	14	21
80	S19 EM19	6.4	Fluvial channel???	TST?	Al	109		7	81		22
81	EM19	16.5	Fluvial channel	LST	Al	131	3	18	88	43	32
82	EM19	29.2	Fluvial channel	LST	Po	181	6	10	66	35	27

Sample designation	Kalt	Lsi	Lsa	Qp chert	Lvf	porph qz.	LvmL	porph pl.	Lvl	porph px.	Serp Cell	Lmp 1 2 3 4 5	Lmm 1 2 3 4 5	Lmi 1 2 3 4 5	Lmc 1 2 3 4 5	Serp schist	B	M	Chl	amph	pyx	sp	gt	ep	Z	T	R	D nonop	D opaque
Dora Baltea			2				1				1	2	11 23 10 3	1 2		7	4	8		4	15	1	2	3				10	2
Sesia			1		1	1	6		4		1	1 1	5 16 7 5	7 4 4		1	7	4		20	37		19	8			4	8	17
Ticino	3	1	1		2		3					2	2 7 11	1			5	1		4	7		3					1	2
Adda		3	8	3	1		5		2		1	4 2	25 18	4 2 2 1		2	4	3		4	5		2				1	4	
Cherio		2		7	10		15		3			2	1 2	8			2			2	1							1	
Oglio		8	7	1	2		9		7			1 6 2	3 15 13 3	4 4 1 5		2				6	2		5	2				3	1
Mincio	3	10	9	8	2		7		3			1 1	3 6 1	1			1		1	2	2		3					2	1
Adige					13	3	6		1			1 7 4	9 16 1	1 2			23	4		3	7		2	1					
Trebbia	8	54	34		5	2	6	1	4		26	8	2 2	1	1	4	1	1		3	4								
Taro	1	69	22		2		1		2		10	7 12	1 2 3			3													
Secchia	3	37	64		1		1				1	2 7	7 3			1	3	1											
Reno		25	51	3								2 7	1 1					2			1								
Scrivia		28	10		5		2	1				8	4	1 1		7	1		2	1	1								
Bormida di Spigno			7	1	3		1	1			1		37 19 3 2	1 3 # 2		22		1					2					2	3
Orba		6			10	2	1	4		1	1	3 2	6 4 2 1	1 4 3 3		34	1	2		3	9		1			1			7
Tanaro (l.r.)		3	4									3 1	3 19 6	1 1			7		3										
Tanaro (u.r.)		1	3					1				2 1 1	12 9	2 4 1			4	8	4	1	2			1					
Bormida di Millesimo (u.r.)			17		2							1 6 3	32 21 3	2 1 2			2	1	1	1								1	
Bormida di Millesimo (l.r.)		1	17		4						1	3	20 15 1	2 2 4		6	3	4			1		1	1					
Erro		12	1		2						2	1 1 3 2	3 9 3	5 8 9		61	5	12	2	1	3			3				7	2
Po1		8	1				2		2		2		19 20 10 3	2 2 5 7 1		16	1	3		3	2			1					
Po2		4	4		1						3	5	9 10 6 1	1 3 14 3	1 3	13	3	8		9	8		5	2			1	4	
Po3		2			1		3		3		1	3 3 1	1 11 15 4	2 5 1 5		18	3	1		6	7		1	4				5	
Po4		2	1		2		2		6		2	4 1 3	1 5 11 2 1	2 9 1		14	5	4	1	6	11	1	5	1		4	1	4	
Po5		3	4		1		2					1 2 2	1 15 17 1	3 1 3 1		4	10	9	4	3	9		1			1		5	2
Po6	1		1		3		3	1	3		3	1 2 1	1 7 12 3	4 2 19 7		14	1	1		2	11		6	6				5	
Po7	1	7	6		1						2	3 4	5 9 2	1 2		7	1	3	1	1	4		3	3		1			
Po8		2	4		3		3		4		2	2 1	2 8 17 5 1	2 1 6 2		7	4	4		3	3								
Po9		6			5	2	5	2	2		5	1 4	11 16 2	1 2 3 1		10	3	1	1	3	5		4	1		1		4	
Po10		5	2	1	7				2		3	1	7 12	4 2 3	1	3	3	4		2	4		1	2				4	
Po11	1	10	7		1		2		2		1	2	11 9	3 1		2	23	5	1	3	3			3		1		1	
Po12		5	9		5				3		1	1 2 2 1	9 18 2	2 4 2 3 1	1	7	6	6	6	3	14		2	2		2			2
25		6	2		3							1 1 1	3 15 15 4 2	1 6 3 8 1	1	6	1	6	2	6	5		1						
26		5	2		1				3				8 15 9	4 9		2	4	1		2	4							2	
27		4	4		3				1		3	1 2	9 12 3	3 2 2		6	7	3	1	3	3		1	2				2	
28	5	11	17		1							2	4 1 1	2						1									
29	3	4	10		3						2	2	11 17 5 1	5 1 3		2	13	4	3	2			1	1					
30	5	3	3						1			1 1	5 4 1			1	1		1	1	4								
31	1	3	1		2		1		1		1	2 1	8 13 2 2	6 2 2		2	6	3	2		5			1		2		3	1
32	4	1	3		2	1		1				4 2	12 8 1	2 2 6		5	5	2	1	3	13		7	3				1	
33		4			4			3				2 2	10 4 2 1	3 1 2		3	6	7	5	1	2					1		1	
34			3					1	4		1	2 2 2 1	7 11 2	4 1 4	2	5	4	2	2	1	8		1	5		1			
35		3	7		1			2			2		7 5	1 1		1	7		2										
36		1	3			1		2			1	1 1	4 19 5	2 3 1		1	4	5			2			1				1	
37	2	2	4		1			1			6	1 1	9 15 2 1	6 2 2		6	7	2		1	2		4	1				1	
38		1					1		2		2	4 1	2 8 6	1 2		5	20	10	3	1	2			1				1	
39		1	1				2				2	1 1	2 8 2	1 1		5	16	5	2		10		3	2		2		3	1
40		2	2					3				1	3 10 1	1 2 1			3	3	1		3			2				1	
41		1	10		2			4			1	1 1	1 8	1		1	10	9	4										
42		1	6		6	1	1	1				1	5 16 1				23	6			3							2	
43		3	3		2	3		2		1	1	2 2	7 10 3	1 1		1	20	5	1	1	5								
44		2		1	1							1	12 3 1	1			9	2	1		2								
45		3		1		1		1			1	3	12 12 2	3		5	1	3	1		7		1						
46					1		1					1 2	1 16 9 2	4 2		4	2	5			11		1						
47		6	4		1	1	1			1	3	2 4	3 9 6 2			5	8	3	2	1	4		1	1				2	
48		1	1	1	2	1		4	1		1	1 1 1 1	2 10 8 1	2 2		4	10	3	1	1	1		2					2	
49								3			1	1 1	2 13 6	3 3 5 2 1		9	4	2	1	3	5		1						
50		1	2		2			2		3		1 2	10 15 1	1 3 2	1	7	2	5	3	1	8							1	
51		2			2	1						1 1 3 1	10 8 1	1 2		5	3	3	2		7							5	
52		2	3		2							1 4 3	9 2	7		5	16	7	1	1	12							3	
53		1	2		1	1		1				1 1	15 8	1		3	7	8	1		4		1	2				3	
54		1	4		1	1		2	3			3 1	18 6 1	1 2 1		7	11	4			3					1		1	
55		4	2									1	11 4	1 1			74	23	1	1	1								
56		3	1		3	1		1	2	1		1 4 1	3 13 7 3	1 4 2		11	2	3		1	4		2	3		1		3	
57		1	3			1			1	1		1 2	1 5 11	1 3	1	2	1	3		1	5					1		3	
58		3	2		2							2 1	16 8 1	2 1		1	18	15	3	2	4							2	
59		3	3		2			1				1	14 4	1		2	24	21	1		1								
60		1	5	4	7			2				1	3 7	3			43	25	1		2								
61			1		1								4				88	37			1								
62		5	5									3 2	4 6			1	68	13			1						1		
63		2	2			1		7				4	2 18 6 1	1		3	3	4		1	5			1					
66		1	7									1 1	10 1			1	32	33			2								
67		2	9					1				3	12 3 1				42	37											
70		1	1		1							1	5 3	1	1		15	14			1				1				
71		1	3									1 3 1	5 7			2	4	3			4		1					3	
72		5	2					4		2		1 1	8 7			5	4	6		2	5			2			2		
73		1			1			4		1		1	14 13 2	2		1	3	5			10		1	1				2	
74		4	1					3		2	2	3 2	20 10 2	1 2		7	5	10	1	1	12		2	1			1	3	
75		4	2	1	4		1	2	1	1		3 1 2	10 7	2 2 2 1	1		5	4		3	7		1					2	
76		4	1	3	2			2		1	1	2	7 8	3 5 2 4 1	1 1	6	10	6	1	2	6		1	1				1	
77		1			2	2		6				2	2 8 3	1			3	3			2		1				1		
78		1			3			10				1	1 10 10	2 2			3	7			2							1	
79			1		2		1	1				2 3	5 10 2	1 1 2		3	18	13	1	2	11		2						
80			3		5			5					6				94	15	1										
81		1	1		5	1	3	6	2			4	8 6	2 1			7	3	1		3		1						
82			1	3	2			1				3	14 6				5	8			3		2					2	

Sample designation	CE Lsc mic	CE Lsc spar	CE Lsc dolo	CE bio	CI Bio	Unkn	Alt	Total pts	QFL Q%	F%	L%	LmLvLs Lm%	Lv%	Ls%	QmKP Qm%	K%	P%	NCE NCE%	CE%	CI%	MicaLGHG Mica%	LG%	HG%	LmLvLs-c Lm%	Lv%	Ls-c%	LmLs(silic)Lsc Lm%	Ls(silic)%	Lsc%
Dora Baltea	1	28					3	400	58.3	15.2	26.4	63.0	3.3	33.7	77.8	6.7	15.5	92.7	7.3	0.0	18.8	25.0	56.3	92.06	4.8	3.2	62.2	2.4	35.4
Sesia						12		400	53.0	22.3	24.6	78.5	20.0	1.5	65.5	11.1	23.4	100.0	0.0	0.0	18.0	21.3	60.7	78.46	20.0	1.5	98	2.0	0
Ticino								400	66.6	25.5	8.0	63.3	16.7	20.0	71.1	6.3	22.8	100.0	0.0	0.0	20.7	37.9	41.4	63.33	16.7	13.3	76	24.0	0
Adda	13	24	3					401	43.4	24.1	32.5	42.3	10.6	47.2	57.1	10.8	32.1	90.0	10.0	0.0	10.8	56.9	32.3	65	16.3	18.8	47.6	14.3	38.1
Cherio	86	20	162	3		3		400	12.1	5.9	82.0	0.9	11.3	87.7	64.1	7.8	28.1	31.7	68.3	0.0	13.3	73.3	13.3	6.977	83.7	9.3	1.09	1.5	97.5
Oglio	26	19	21			1		400	44.5	13.7	41.8	32.1	13.8	54.1	71.3	5.5	23.2	83.5	16.5	0.0	0.0	57.9	42.1	55.43	23.9	17.4	36.6	14.2	49.3
Mincio	28	55	29				1	400	41.1	16.5	42.4	7.3	7.3	85.4	67.0	11.3	22.0	71.9	28.1	0.0	13.3	33.3	53.3	27.27	27.3	45.5	8.33	13.9	77.8
Adige	15	33	17				7	400	42.5	21.0	36.5	30.2	18.6	51.2	65.1	8.0	26.9	83.5	16.5	0.0	39.7	29.4	30.9	60.94	37.5	1.6	37.1	1.0	61.9
Trebbia	95	59					4	397	9.6	11.2	79.2	2.6	14.8	82.6	36.8	20.6	48.3	60.8	39.2	0.0	12.5	75.0	12.5	5.333	30.0	64.0	1.57	37.6	60.4
Taro	89	68					1	400	13.5	13.5	72.9	6.9	5.2	88.0	47.6	11.7	41.2	60.7	39.3	0.0	0.0	88.0	12.0	14.93	11.2	73.1	6.23	36.3	57.5
Secchia	47	67					2	401	22.8	17.0	60.3	7.6	1.3	91.2	53.8	9.0	38.0	71.4	28.6	0.0	17.4	69.6	13.0	14.52	2.4	83.1	7.26	44.0	48.7
Reno	29	52						400	42.1	14.9	43.1	5.3	0.0	94.7	72.3	3.8	23.9	79.8	20.3	0.0	15.4	76.9	7.7	10.34	0.0	89.7	5.36	46.4	48.2
Scrivia	99	45					1	300	16.3	11.9	71.8	10.0	3.8	86.3	47.0	4.5	48.5	51.8	48.2	0	17.6	76.5	5.9	31.34	11.9	56.7	7.14	19.4	73.5
Bormida di Spigno	9	2				3	3	300	39.5	16.8	43.7	79.2	5.6	15.2	61.3	13.7	25.0	96.3	3.7	0	1.3	51.9	46.8	87.61	6.2	6.2	81.1	7.4	11.6
Orba	8	1	1				2	306	42.5	22.5	35.0	63.3	20.4	16.3	61.1	15.4	23.5	96.7	3.3	0	9.4	43.8	46.9	70.45	22.7	6.8	63.6	13.6	22.7
Tanaro (l.r.)	20	3		1			1	300	47.6	30.2	22.2	46.9	1.6	51.6	57.1	12.3	30.5	92.0	8.0	0	22.7	54.5	22.7	73.17	2.4	17.1	47.6	15.9	36.5
Tanaro (u.r.)	20	10		4		1		300	47.3	28.4	24.4	44.8	4.5	50.7	59.8	8.2	32.0	88.6	11.4	0	33.3	41.7	25.0	81.08	8.1	10.8	46.9	6.3	46.9
Bormida di Millesimo (u.r.)	15	12		3		2		300	41.2	18.3	40.5	59.0	3.4	37.6	61.9	12.2	25.9	89.9	10.1	0	5.3	48.0	46.7	76.67	4.4	18.9	61.1	15.0	23.9
Bormida di Millesimo (l.r.)	12	13		2		2	1	300	46.0	18.6	35.4	50.5	6.9	42.6	64.4	12.8	22.8	90.9	9.1	0	13.0	44.4	42.6	67.11	9.2	23.7	51.1	20.5	28.4
Erro	5	8					3	300	26.0	22.5	51.5	77.0	3.0	20.0	49.6	12.8	37.6	95.6	4.4	0	30.2	15.9	54.0	85.25	3.3	11.5	61.4	20.0	18.6
Po1	1	7					1	400	58.1	14.1	27.8	76.9	7.4	15.7	75.3	7.6	17.0	98.0	2.0	0.0	5.5	31.5	63.0	83	8.0	9.0	79.8	10.7	9.52
Po2	2	12					1	400	58.8	14.8	26.5	72.6	4.2	23.2	77.2	9.9	12.9	96.5	3.5	0.0	16.4	23.9	59.7	85.19	4.9	9.9	71.8	10.3	17.9
Po3		3				1	5	400	54.8	22.9	22.3	76.8	12.2	11.0	67.7	10.8	21.5	99.2	0.8	0.0	7.3	45.5	47.3	79.75	12.7	6.3	83.3	11.1	5.56
Po4	1	4					4	400	57.8	21.2	21.0	71.6	16.2	12.2	71.3	8.0	20.7	98.7	1.3	0.0	20.0	20.0	60.0	76.81	17.4	4.3	81.3	8.3	10.4
Po5	7	17				2		400	54.0	22.0	24.0	57.6	3.5	38.8	68.5	10.5	21.0	94.0	6.0	0.0	32.9	31.4	35.7	80.33	4.9	13.1	57.7	11.5	30.8
Po6							3	400	58.1	18.1	23.8	81.6	14.9	3.4	73.7	6.0	20.4	100.0	0.0	0.0	3.3	24.6	72.1	81.61	14.9	2.3	95	5.0	0
Po7	7	13	2	1			2	402	54.5	27.0	18.6	42.3	4.2	53.5	64.8	10.2	25.0	94.3	5.8	0.0	16.1	41.9	41.9	61.22	6.1	32.7	37.7	26.2	36.1
Po8	6	6	1				1	400	58.7	19.2	22.1	61.2	14.1	24.7	73.4	8.6	18.0	96.7	3.3	0.0	14.5	25.5	60.0	72.22	16.7	8.3	68.2	12.1	19.7
Po9	5	4	3			1	6	400	55.1	20.5	24.3	55.6	23.3	21.1	70.8	12.3	16.9	96.9	3.1	0.0	10.9	37.0	52.2	64.1	26.9	9.0	67.8	11.9	20.3
Po10	3	4	4			3	2	400	64.5	18.4	17.1	50.0	18.8	31.3	75.0	6.2	18.8	97.2	2.8	0.0	18.9	32.4	48.6	61.54	23.1	15.4	60.4	16.7	22.9
Po11	16	31	8	3			1	401	55.2	15.1	29.7	24.5	5.7	69.8	77.4	8.8	13.9	85.5	14.5	0.0	52.7	29.1	18.2	50.98	11.8	37.3	24.5	19.4	56.1
Po12	6	26	5				4	400	54.4	13.0	32.6	45.2	9.6	45.2	79.1	4.5	16.4	90.7	9.3	0.0	27.3	27.3	45.5	66.67	14.1	19.2	46.4	15.5	38.1
25	1	8	4				1	400	54.0	21.7	24.3	68.5	4.3	27.2	68.8	13.3	17.9	96.7	3.3	0.0	12.7	38.0	49.3	79.7	5.1	11.4	69.5	14.6	15.9
26	1	7	4					400	59.7	22.2	18.1	67.1	5.7	27.1	70.9	14.9	14.2	97.0	3.0	0.0	10.0	16.0	74.0	81.0	6.9	12.1	70.3	10.9	18.8
27	2	4	1			4	1	400	62.5	20.9	16.6	64.5	11.3	24.2	73.2	11.3	15.5	98.2	1.8	0.0	24.4	28.9	46.7	72.7	12.7	14.5	69.4	16.3	14.3
28	13	59	3	1		2	1	400	44.8	26.3	28.9	7.0	0.9	92.1	59.7	22.1	18.6	80.9	19.1	0.0	0.0	80.0	20.0	20.5	2.6	76.9	7.08	26.5	66.4
29	11	25	7		10	1	4	400	49.9	19.9	30.2	43.1	4.6	52.3	69.6	13.9	16.7	86.6	10.9	2.5	30.8	27.7	41.5	71.2	7.6	21.2	44.1	13.7	42.2
30	3	9	13		6		3	400	71.4	16.9	11.7	26.7	2.2	71.1	80.2	10.6	9.3	92.2	6.3	1.5	14.3	42.9	42.9	60.0	5.0	35.0	25.6	16.3	58.1
31	8	16	15				1	400	57.7	18.9	23.4	45.5	5.7	48.9	72.9	7.3	19.9	90.2	9.8	0.0	22.4	28.6	49.0	81.6	10.2	8.2	46.9	4.9	48.1
32	11	13	17				3	400	58.0	16.9	25.1	46.2	4.4	49.5	75.8	9.1	15.3	89.7	10.3	0.0	17.8	40.0	42.2	84.0	8.0	8.0	45.1	4.9	50
33	11	22	13	1			4	400	49.7	26.9	23.4	34.5	8.0	57.5	63.5	12.4	24.1	88.1	11.9	0.0	40.0	33.3	26.7	73.2	17.1	9.8	35.1	5.2	59.7
34	5	25	13			5		400	48.5	25.9	25.6	43.2	6.3	50.5	62.8	12.4	24.8	89.1	10.9	0.0	17.4	37.0	45.7	78.8	11.5	9.6	42.9	6.0	51.2
35	8	75	15	1		2	1	400	45.5	21.4	33.1	11.7	3.9	84.4	66.4	12.1	21.5	75.1	24.9	0.0	39.1	34.8	26.1	50.0	16.7	33.3	11.5	8.2	80.3
36	10	14	16	1			2	400	50.8	27.1	22.1	43.5	4.7	51.8	63.9	12.8	23.3	89.7	10.3	0.0	20.0	15.6	64.4	82.2	8.9	8.9	45	5.0	50
37	4	5	12					400	47.6	31.4	20.9	56.3	10.0	33.8	58.0	18.2	23.9	94.8	5.3	0.0	18.8	33.3	47.9	76.3	13.6	10.2	59.1	9.1	31.8
38	2	5	2					400	58.6	29.3	12.2	61.4	11.4	27.3	65.1	18.8	16.1	97.8	2.3	0.0	57.9	26.3	15.8	77.1	14.3	2.9	64.7	8.8	26.5
39	4	14	8			2	2	400	47.7	37.2	15.1	39.6	7.5	52.8	55.4	21.8	22.8	93.4	6.6	0.0	59.0	10.3	30.8	77.8	14.8	7.4	36.4	4.5	59.1
40	3	15	27		4			400	44.9	36.6	18.5	26.8	4.2	69.0	53.3	22.3	24.3	87.8	11.3	1.0	26.9	19.2	53.8	73.1	11.5	15.4	27.9	5.9	66.2
41	10	21	84		54		2	400	34.9	19.6	45.5	8.2	4.8	87.0	62.9	20.0	17.1	57.5	28.9	13.6	65.7	8.6	25.7	38.7	22.6	38.7	7.97	8.7	83.3
42	9	11	41		61	3	1	400	34.6	32.2	33.2	22.0	9.0	69.0	49.7	20.7	29.5	69.2	15.4	15.4	55.8	11.5	32.7	56.4	23.1	20.5	24.2	8.8	67
43	6	11	18		56	2	1	400	43.7	31.4	24.9	32.5	11.7	55.8	57.5	13.6	28.9	77.1	8.8	14.1	50.0	19.2	30.8	59.5	21.4	19.0	35.8	11.9	52.2
44	6	33	8	2	13		1	400	41.9	39.5	18.6	26.1	1.4	72.5	50.7	20.9	28.4	84.5	12.3	3.3	51.2	16.0	32.8	60.1	20.2	19.7	27.5	11.2	61.3
45	3	8	18		11		2	400	45.7	34.8	19.5	50.7	4.1	45.2	54.9	19.4	25.7	89.9	7.3	2.8	13.5	40.5	45.9	86.0	7.0	7.0	50	4.7	45.3
46	4	5	16		14	1		400	47.0	34.4	18.6	58.8	2.9	38.2	56.4	12.5	31.1	90.2	6.3	3.5	15.9	50.0	34.1	93.0	4.7	0.0	58.1	1.6	40.3
47	4	21	23					400	41.8	32.8	25.4	29.2	7.3	63.5	55.2	14.8	30.0	88.0	12.0	0.0	33.3	35.9	30.8	58.3	14.6	20.8	27.4	15.5	57.1
48	5	17	19					400	47.9	29.5	22.6	34.9	10.5	54.7	59.1	16.4	24.5	89.8	10.3	0.0	32.6	37.2	30.2	68.2	20.5	6.8	36.1	6.9	56.9
49	3	24	14			1		400	40.2	36.0	23.8	45.1	7.7	47.3	50.0	17.0	33.0	89.7	10.3	0.0	15.9	50.0	34.1	82.0	14.0	0.0	42.7	2.7	54.7
50	7	13	16			1	2	400	44.0	32.4	23.6	46.1	7.9	46.1	53.4	11.1	35.5	90.9	9.1	0.0	21.7	32.6	45.7	77.4	13.2	7.5	45.3	5.3	48
51	2	9	17		16			400	45.9	36.0	18.1	47.0	6.1	47.0	54.2	15.4	30.4	89.0	7.0	4.0	22.2	41.7	36.1	81.6	10.5	7.9	45.6	5.3	49.1
52	2	11	9		14		1	400	49.9	32.8	17.4	23.3	15.0	61.7	58.6	11.0	30.4	91.0	5.5	3.5	48.0	46.0	6.0	36.8	23.7	15.8	19.6	32.6	47.8
53	2	6	11		29	1		400	43.3	41.0	15.7	53.7	5.6	40.7	49.8	15.3	34.9	88.0	4.8	7.3	38.1	35.7	26.2	82.9	8.6	8.6	54.2	6.3	39.6
54	4	10	13				1	400	43.0	36.1	20.8	49.4	10.1	40.5	50.0	17.5	32.5	93.2	6.8	0.0	31.3	50.0	18.8	75.0	15.4	9.6	50	7.8	42.2
55	3	7	9	1	20			400	41.2	43.4	15.4	41.9	0.0	58.1	47.2	14.8	38.0	90.0	5.0	5.0	84.5	11.2	4.3	75.0	0.0	25.0	41.9	14.0	44.2
56	7	14	15					400	36.2	38.1	25.7	48.0	8.2	43.9	44.7	12.6	42.7	91.0	9.0	0.0	11.4	40.9	47.7	75.8	12.9	6.5	45.6	8.9	45.6
57	1	4	8		8		2	400	46.8	40.7	12.5	53.2	6.4	40.4	51.1	17.3	31.6	94.7	3.3	2.0	13.8	27.6	58.6	73.5	8.8	14.7	54.8	14.3	31
58	2	11	19		15	1		400	45.0	34.1	20.9	45.1	2.8	52.1	54.3	16.9	28.7	88.2	8.0	3.8	53.7	29.9	16.4	82.1	5.1	12.8	45.6	7.4	47.1
59	4	6	25		20			400	50.2	30.0	19.8	33.3	4.5	62.1	61.4	12.7	25.9	86.3	8.8	5.0	69.7	24.2	6.1	71.0	9.7	19.4	32.8	9.8	57.4
60	2	13	13		57	10	2	400	40.4	36.2	23.5	23.0	14.8	62.3	51.0	11.5	37.5	78.1	7.2	14.7	83.1	7.2	9.6	48.3	31.0	20.7	29.2	12.5	58.3
61	4	12	39		78	6		400	37.4	30.5	32.1	6.6	1.6	91.8	54.7	7.0	38.3	66.2	14.0	19.8	96.9	3.1	0.0	66.7	16.7	16.7	6.67	1.7	91.7
62	2	4	8		168	7	2	400	30.7	40.7	28.6	40.0	0.0	60.0	41.8	13.3	44.9	53.5	3.6	43.0	84.4	7.3	8.3	61.5	0.0	38.5	38.5	25.6	35.9
63	6	24	17				2	400	46.6	28.9	24.5	35.1	8.5	56.4	59.3	11.4	29.3	88.2	11.8	0.0	17.9	51.3	30.8	70.2	17.0	8.5	36.1	7.2	56.6
66		11	29		63		1	400	33.8	43.1	23.0	22.6	0.0	77.4	41.7	11.1	47.2	74.2	10.0	15.8	83.3	14.1	2.6	63.6	0.0	36.4	21.3	13.1	65.6
67	1	2	17		94		2	400	40.9	36.4	22.7	37.3	2.0	60.8	51.5	14.2	34.3	71.4	5.0	23.6	80.6	15.3	4.1	61.3	3.2	35.5	38	22.0	40
70	2	5	13		147		1	329	30.7	46.7	22.7	32.4	2.9	64.7	37.5	10.7	51.8	49.1	6.1	44.8	72.5	12.5	15.0	78.6	7.1	14.3	33.3	6.1	60.6
71	3	13	22		63		2	400	45.6	35.3	19.1	29.5	0.0	70.5	54.6	13.3	32.1	74.6	9.5	15.8	29.2	37.5	33.3	78.3	0.0	21.7	27.1	8.5	64.4
72	10	29	17	1			1	400	37.9	37.9	24.1	24.2	6.6	69.2	46.0	14.0	40.0	85.7	14.3	0.0	37.0	33.3	29.6	62.9	17.1	20.0	21.3	8.8	70
73	8	15	15				2	400	47.9	31.4	20.7	42.3	7.7	50.0	57.1	10.5	32.4	90.5	9.5	0.0	20.0	37.5	42.5	82.5	15.0	2.5	45.1	1.4	53.5
74	2	11	11		13	1		400	35.1	41.1	23.7	53.0	8.4	38.6	44.0	15.6	40.5	90.7	6.0	3.3	28.6	46.4	25.0	74.6	11.9	13.6	53.6	11.6	34.8
75	3	8	12		19			400	46.5	34.0	19.5	40.0	12.9	47.1	54.6	6.7	38.7	89.5	5.8	4.8	22.5	40.0	37.5	60.9	19.6	19.6	46.7	15.0	38.3
76	4	4	8				1	400	46.4	34.8	18.9	51.4	12.9	35.7	54.4	10.2	35.3	96.0	4.0	0.0	33.3	31.4	35.3	70.6	17.6	9.8	57.7	9.6	30.8
77	8	12	25			1		400	50.6	30.8	18.5	19.4	13.9	66.7	59.6	7.7	32.7	88.7	11.3	0.0	27.3	50.0	22.7	51.9	37.0	3.7	22.6	4.8	72.6
78	12	10	24					400	45.7	32.0	22.2	26.7	17.4	55.8	57.2	12.4	30.3	88.5	11.5	0.0	27.8	44.4	27.8	57.5	37.5	2.5	32.4	2.8	64.8
79	2	3	16			2	2	400	54.2	30.1	15.8	50.9	9.1	40.0	62.0	7.6	30.4	94.7	5.3	0.0	55.2	15.5	29.3	82.4	14.7	2.9	53.2	2.1	44.7
80	1	3	5		26	5	12	400	47.0	41.7	11.3	21.4	35.7	42.9	51.4	10.4	38.2	90.9	2.3	6.8	94.8	5.2	0.0	31.6	52.6	15.8	33.3	16.7	50
81	3	9	17			1		400	39.6	42.4	18.0	27.5	27.5	44.9	44.6	10.9	44.6	92.7	7.3	0.0	34.4	34.4	31.3	47.5	47.5	5.0	38	4.0	58
82	3	4	15				3	400	52.3	34.0	13.8	44.2	5.8	50.0	58.6	8.7	32.7	94.5	5.5	0.0	36.1	38.9	25.0	85.2	11.1	3.7	50	2.2	47.8